Mechanisms of Coenzyme Q_{10} Blood-Brain Barrier Transport

Luke Wainwright

University College London

Institute of Neurology

Thesis submitted for the degree of Doctor of Philosophy

August 2018

Supervisors:

Dr Iain Hargreaves, Dr Jane Preston & Prof Simon Heales

I, Luke Wainwright confirm that the work presented in this thesis is my own. Where information has been derived from other sources, I confirm that this has been indicated in the thesis.

Signed: ……

Date: ……

Abstract

Coenzyme Q_{10} (CoQ_{10}) deficiencies are unique among mitochondrial respiratory chain (MRC) disorders in that they are potentially treatable. While there is clear evidence, both clinically and biochemically, for the improvement of peripheral abnormalities associated with CoQ_{10} deficiency following CoQ_{10} supplementation, neurological symptoms are only partially ameliorated. The reasons for the refractory nature of the neurological sequelae associated with a CoQ_{10} deficiency are as yet unknown and may be a consequence of irreversible damage prior to CoQ_{10} supplementation, the retention of CoQ_{10} in the blood-brain barrier (BBB) itself, or simply reflect poor transport of CoQ_{10} across the BBB.
This thesis presents the first isolated investigations into the mechanisms that govern bi-directional BBB transport of CoQ_{10} and its synthetic analogue, idebenone, using normal and pathophysiological cell models relevant to disorders of CoQ_{10} biosynthesis.

The mouse BBB endothelial cell line bEnd.3 and porcine primary brain endothelial cells (PBECs) co-cultured with primary astrocytes were used to assess transcytosis from 'blood-to-brain' or 'brain-to-blood', revealing that although CoQ_{10} can traverse the BBB, CoQ_{10} is being effluxed back to the blood, which could explain the refractory nature of CoQ_{10} therapy, whereas, idebenone appeared to cross the BBB passively.
Using inhibitors of known transport systems for lipoproteins, the circulatory bio-carriers of CoQ_{10} *in vivo*, three systems mediating the BBB transport of lipoprotein-bound CoQ_{10} were identified. Inhibitors of the scavenger receptor class B type 1 (SR-B1), BLT-1, and the receptor for advanced glycation end products (RAGE), FPS-ZM1, reduced uptake of lipoprotein-bound CoQ_{10} towards the brain, implicating RAGE and SR-B1 as modes for CoQ_{10} brain uptake.. In the reverse direction, the low-density lipoprotein receptor-related protein-1 (LRP-1) inhibitor, RAP, reduced efflux of lipoprotein-bound CoQ_{10} towards the blood, implicating LRP-1 as a major impediment to brain entry of CoQ_{10}.

This study is the first to generate a BBB endothelial cell model of CoQ_{10} deficiency, using *para*-aminobenzoic acid (*p*ABA) to pharmacologically induce a depletion of cellular CoQ_{10} status, resulting in a global reduction of MRC enzyme activities. The CoQ_{10} deficient BBB

models were leakier to large permeability markers, with poor BBB tight-junction formation, and altered CoQ_{10} transport dynamics in favour of an increased net efflux towards the blood, suggesting BBB pathophysiology is key to the neurological presentation and refractory nature of CoQ_{10} supplementation in symptomatic patients.

In addition, the effects of vitamin E, a common clinical co-therapy in the 'mito-cocktail', and simvastatin were assessed. Interestingly, vitamin E co-administration reduced net efflux of CoQ_{10} from the brain. It is unknown why this occurs, but oxidative effects on the BBB transporters and/or carrier-lipoproteins may be factors to consider.
In-line with its deleterious effect on CoQ_{10} biosynthesis, simvastatin therapy appeared to disrupt BBB integrity, increasing the paracellular leak of the BBB. This would be detrimental to normal brain homeostasis, particularly given the BBBs major role in limiting brain entry of the small molecule plasma excitotoxins, calcium, and glutamate.

Throughout this study CoQ_{10} was quantified using a novel and rapid mass spectrometric method (ESI+ LC-MS/MS), which could potentially enable detection of CoQ_{10} in the CSF of patients presenting with neurological symptoms, perhaps providing a new analytical tool for the diagnosis of CoQ_{10} deficiencies in clinical laboratories.

In conclusion, this thesis has demonstrated for the first time the pathophysiological consequences of a CoQ_{10} deficiency on the BBB. It has highlighted the impact of a deficit in CoQ_{10} status on CoQ_{10} delivery to the brain parenchyma and has elucidated some of the mechanisms by which CoQ_{10} is transported across the BBB, which are ultimately dictated by lipoprotein interactions. Additionally, this thesis outlines the potential dangers of statin therapy in patients with an underlying or established MRC dysfunction.
Overall, this thesis provides insights into the limitations of CoQ_{10} supplementation as a therapy for neurological disorders associated with MRC dysfunction and indicates that further work will be required to improve the delivery of exogenous CoQ_{10} across the BBB, alongside a need for further investigations into the composition of the widely administered 'mito-cocktail'.

List of Abbreviations

α-toc	*RRR*-α-tocopherol (vitamin E)
ABC	ATP-binding cassette
ABL	aqueous boundary layer
ADME	absorption distribution metabolism and excretion
AJ	adherens junction
AMT	adsorptive-mediated transcytosis
APTX	encoding aprataxin
ATP	adenosine triphosphate
BBB	blood-brain barrier
BCSFB	blood-cerebral spinal fluid barrier
BDPS	bovine derived plasma serum
BLT-1	block lipid transport – 1
CBF	cerebral blood flow
CNS	central nervous system
CoQ_{10}	coenzyme Q_{10}
CP	choroid plexus
CSF	cerebrospinal fluid
CV	coefficient of variation
CVO	circumventricular organs
DMEM	Dulbecco's modified Eagle's medium
DNA	deoxyribonucleic acid
DTNB	5, 5'-dithio-bis (2-nitrobenzoic acid)
EDTA	ethylenediaminetetraacetic acid
EVOM	endothelial volt/ohm meter
FITC-40	fluorescein isothiocyanate – dextran (40 kDa)
FPP	farnesyl pyrophosphate
FPS-ZM1	4-chloro-N-cyclohexyl-N-(phenylmethyl)-benzamide
HBSS	Hank's balanced salt solution
HEPES	4-(2-hydroxyethyl)-1-piperazineethanesulfonic acid
HIV	human immunodeficiency virus

HMG-CoA	3-hydroxy-3-methyl-glutaryl-coA
HPLC	high performance liquid chromatography
IPP	isopentenyl pyrophosphate
IS	internal standard
ISF	interstitial fluid
JAM	junctional adhesion molecule
LC-MS/MS	liquid chromatography tandem mass spectrometry
LDL	low-density lipoprotein
LDLR	low-density lipoprotein receptor
LRP-1	lipoprotein receptor protein – 1
MELAS	mitochondrial encephalopathy with lactic acidosis and stroke-like episodes
MEM	minimum essential medium
MNC	blood mononuclear cell
MPP+	1-methyl-4-phenylpyridinium
MPTP	1-methyl-4-phenyl-1,2,3,6-tetrahydropyridine
MRC	mitochondrial respiratory chain
MRCE	mitochondrial respiratory chain enzyme
MS	Multiple Sclerosis
MTT	3-[4,5-dimethylthiazol-2-yl]-2,5-diphenyl tetrazolium bromide
MVK	mevalonate kinase
NAD(H)	nicotinamide adenine dinucleotide (reduced)
NPC1L1	Niemann-Pick C1-like 1
NVU	neurovascular unit
P-gp	P-glycoprotein receptor
***p*ABA**	*para*-aminobenzoic acid
PBEC	porcine-brain endothelial cell
PPAR-γ	peroxisome proliferator-activated receptor-γ
RAGE	receptor for advanced glycation endproducts
RAP	receptor associated protein
RMT	receptor-mediated transcytosis
RT	room temperature
SEM	standard error of the mean

SR-B1	scavenger receptor class B type 1
TEER	transendothelial electrical resistance
TJ	tight junction
TNB	5-thio-2-nitrobenzoic acid
Trolox	6-hydroxy-2,5,7,8-tetramethylchroman-2-carboxylic acid
TPP	triphenylphosphine
UK	United Kingdom
USA	Unites States of America
UV	ultra violet
ZO	zonula occluden

Acknowledgements

First and foremost I would like to thank my supervisors Dr Iain Hargreaves, Dr Jane Preston and Prof Simon Heales. In particular, I am sincerely grateful to Jane for her unwavering support and guidance through what has been a rather turbulent few years. I could not have wished for a better mentor throughout this process and I shall never forget the kindness that Jane has shown me.

In addition to my formal supervisors, I would like to extend a massive thank you to Dr Ana Georgian who taught me everything there is to know about the *in vitro* models of the blood-brain barrier. Her patience, resilience, humour and selflessness is truly admirable. Similarly, I would like to thank Prof R. Neil Dalton and Charles Turner of the WellChild Laboratory for their seemingly endless support throughout my career, both during this PhD and prior. They have been pivotal role-models in my life and I am indebted to them.

This PhD project has spanned various organisations and I am grateful to everyone who has helped me along the way, especially; Dr Kate Joseph (UCL), Dr Alex Dyson (UCL), Viruna Neergheen (National Hospital for Neurology and Neurosurgery), Prof Joan Abbott (KCL), Prof Alex Avdeef (KCL), Dr Liam Doonan (KCL), Dr Svetlana Drndarski (KCL), Jorgen Dam (PharmaNord), Bent Henriksen (PharmaNord), David Blundred (UCL), Dr Lee Stanyer (UCL), and Dr Alan Pittman (UCL).

Finally, my utmost gratitude goes to my friends and family who have unconditionally supported me during this very testing period of time. In particular, my dear friend Andrew Wilson for his help with proof-reading and general counsel, and my ever enduring partner, Carolyn Sharpe, who has been an absolute rock.

I acknowledge the support of Ataxia UK, University College London and PharmaNord for their generous sponsorship.

Contents

List of Figures and Tables

1. General Introduction

1.1. Coenzyme Q_{10}

Formerly recognised as the '275 mμ absorbing substance' at the start of World War II [1], it wasn't until the 1950s that 'quinone, Q-275' was isolated and characterised independently in the UK and USA by Festenstein *et al.* [2], studying fat-soluble vitamins at the University of Liverpool, and Crane *et al.* [3], studying enzymatic processes of the mitochondrial respiratory chain (MRC) at the University of Wisconsin–Madison Enzyme Institute. Following its discovery, Wolf *et al.* [4] determined the complex structure and proposed a chemical synthesis for 'coenzyme Q_{10}' at Merck & Co. Inc., New Jersey, USA.
During the 1960s Ernster *et al.* [5] substantiated the obligatory role of CoQ_{10} in the MRC by studying the interaction of succinate dehydrogenase, NADH dehydrogenase and Cytochrome *b*.
However, arguably, the most pioneering breakthrough came from the seminal work of Peter Mitchell. He received The Nobel Prize in Chemistry 1978 *"for his contribution to the understanding of biological energy transfer through the formulation of the chemiosmotic theory"* [6]. Mitchell revolutionised the concept of oxidative phosphorylation and the generally accepted phenomenon of the protonmotive Q cycle was introduced. This described the fundamental role of CoQ_{10} in the cyclic electron transfer pathway through complex III involving ubisemiquinone [7-9].
Ubiquinone became the 'official' name of the compound, established in 1975 by the IUPAC-IUB Commission on Biochemical Nomenclature [10].

1.1.1. Function of Coenzyme Q_{10}

Coenzyme Q (CoQ) is a naturally occurring compound with properties similar to vitamins. Due to its ubiquitous distribution in nature, CoQ is also known as ubiquinone. CoQ belongs to a homologous series of compounds. Each share a common benzoquinone core

with differing lengths of the repeating isoprenoid side chain. In humans, and higher mammalian species, the side chain is comprised of 10 isoprenoid units (Figure 1), hence, it is called CoQ_{10}.

CoQ_{10} has a similar chemical structure to vitamin K and shares some biochemical characteristics with vitamin E (α-toc). It is not considered a vitamin due to its *de novo* biosynthesis in virtually all cells of the body [11, 12]. The rate of CoQ_{10} *de novo* biosynthesis reaches a peak at the age of 20 years for most tissues in the body after which it declines, with the rate accelerating from the age of 40 years [13].

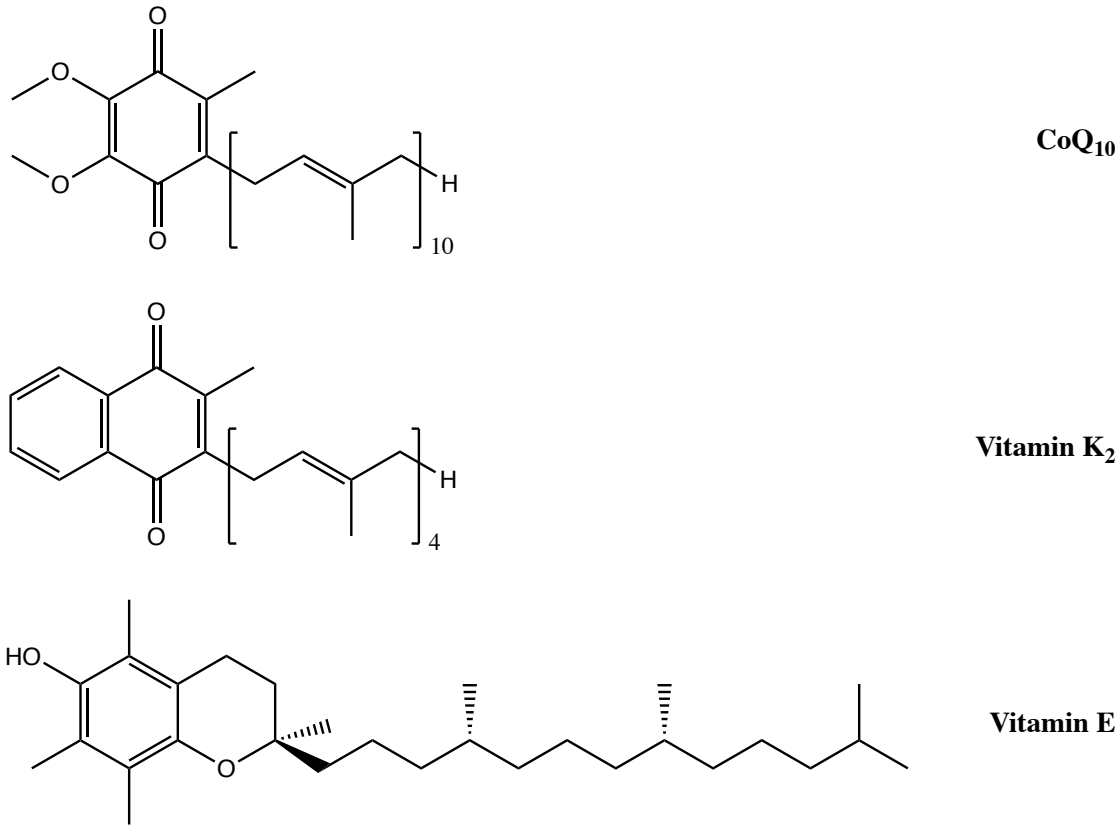

Figure 1: The skeletal structures of CoQ_{10}, vitamin K_2 and vitamin E, highlighting the similarities between the molecules.

CoQ_{10} has a fundamental role in cellular bioenergetics (Figure 2). It is a cofactor in the MRC where it shuttles electrons from complex I (NADH: ubiquinone reductase; EC 1.6.5.3) and complex II (succinate: ubiquinone reductase; EC 1.3.5.1) to complex III (ubiquinol: cytochrome c reductase; EC 1.10.2.2). It is, therefore, essential for the production of ATP [14, 15].

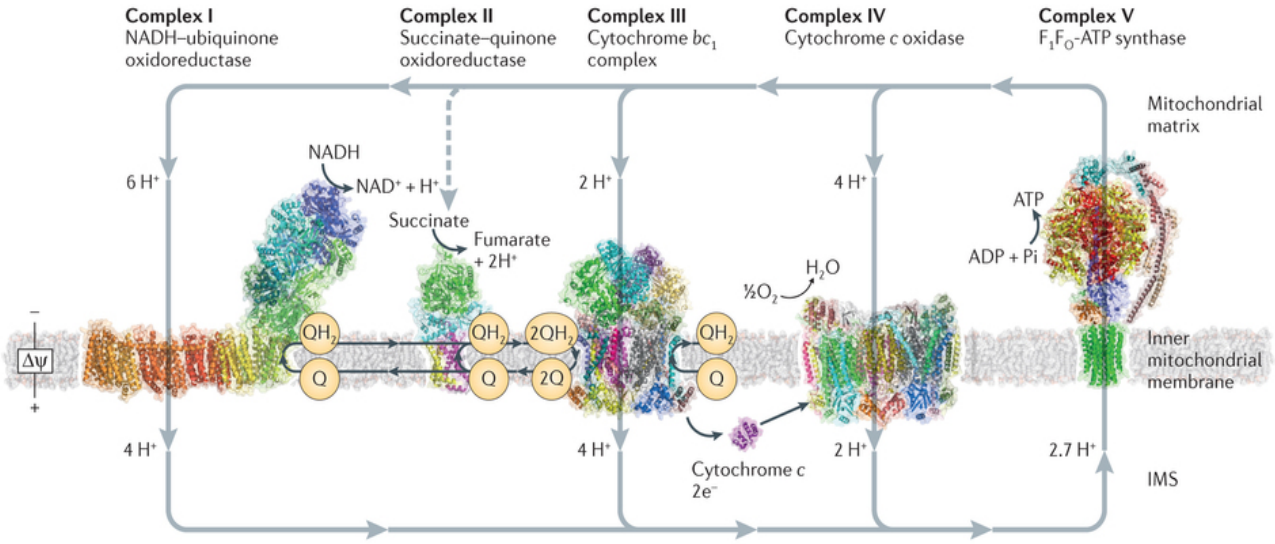

Figure 2: The mitochondrial respiratory chain, a series of complexes which undergo redox reactions, transferring electrons from donor to acceptor molecules, and generating a transmembrane proton gradient which ultimately drives the production of ATP through complex V.

Complex I oxidizes NADH, the product of glycolysis, the citric acid cycle and fatty acid oxidation. Electrons are transferred via the flavoprotein FMN and an Fe-S cluster to CoQ_{10} which is reduced. Complex II oxidizes succinate directly from the citric acid cycle. Electrons are transferred via the flavoprotein FAD and an Fe-S cluster to CoQ_{10}. Reduced CoQ_{10} (ubiquinol) from complexes I and II is the substrate for complex III, also known as the cytochrome bc1 complex. Ubiquinol is re-oxidized to CoQ_{10} and electrons are transferred via cytochrome b, c1, an Fe-S cluster and the 'Q cycle' to the water-soluble enzyme cytochrome c which transfers the electrons to complex IV. (Adapted from [16]).

In addition to existing as discrete entities, recent studies have indicated that the MRC enzymes can also exist as supercomplexes within the inner mitochondrial membrane consisting of aggregates of complexes I, III and IV, complexes I and III, and complexes III and IV [17]. CoQ_{10} is thought be an essential component of the functional superassembly of these structures in the so-called 'respirasome' [18], which serves to improve efficiency and prevent electron leakage to oxygen that results in the production of reactive oxygen species, and some authors suggest CoQ_{10} redox status acts as a metabolic sensor that fine-tunes the respirasome configuration in order to match the prevailing substrate profile, be that NAD- or FAD-dependent [19].

Interestingly, vitamin K_2 has also been shown to behave as a mitochondrial membrane bound electron carrier in bacteria, presumably as a result of the considerable likeness to

CoQ_{10}, as predicted by Crane *et al.* [20] and later corroborated by Vos *et al.* [21]. However, it is unknown if this remains true for higher organisms.

Importantly, the redox functions of CoQ_{10} extend beyond its role in the mitochondria, since it also serves as an electron acceptor for glycerol-3-phosphate, dihydroorotate, choline, sarcosine, sulfide and several amino acids and fatty acylCoA dehydrogenases [11, 22].

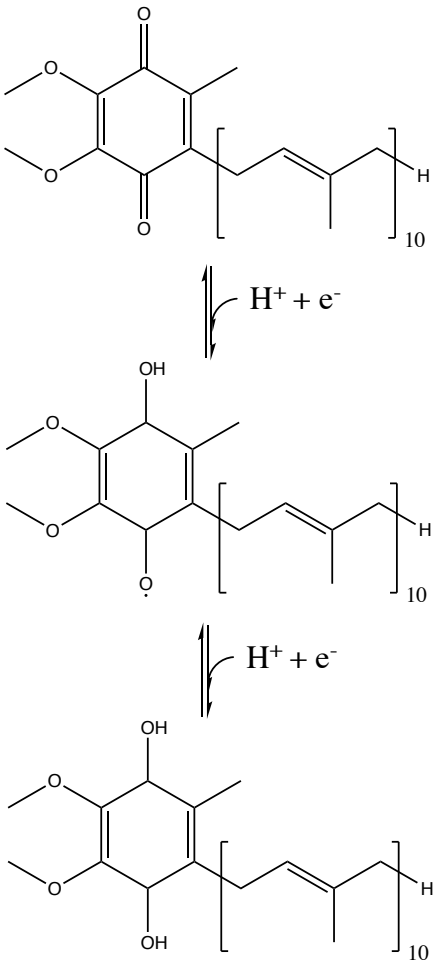

Ubiquinone (CoQ_{10})

Semi-quinone Radical ($CoQ_{10}H^*$)

Ubiquinol ($CoQ_{10}H_2$)

Figure 3: Skeletal structure of CoQ_{10} (oxidised) and $CoQ_{10}H_2$ (reduced) with the isoprenoid side chain shown in *trans*-configuration as is found *in vivo*.

In its fully-reduced form, $CoQ_{10}H_2$, often referred to as ubiquinol, is a potent lipophilic antioxidant (Figure 3) [23]. As well as protecting plasma membranes from oxidative damage, $CoQ_{10}H_2$ is capable of recycling and regenerating other antioxidants such as α-toc and ascorbate [24]. Effective enzymatic systems work continuously to maintain CoQ_{10} in its active reduced form. Other important functions of CoQ_{10} include cell signalling,

activation of mitochondrial uncoupling proteins, regulation of the mitochondrial permeability transition pore and gene expression [25-27].

1.1.2. Biosynthesis of Coenzyme Q_{10}

Knowledge of the biochemical pathway responsible for CoQ_{10} biosynthesis (Figure 4) is yet to be fully characterised. To date most investigations have focused on bacteria and yeast [28-30]. Relatively few have probed the pathway in mammals.

The precursor for the benzoquinone core in mammals, 4-hydroxybenzoic acid, is derived from tyrosine or phenylalanine in a cascade of uncharacterised reactions. Generally present in excess, 4-hydroxybenzoic acid undergoes a condensation reaction with the long isoprenoid side chain that is derived from acetyl-CoA.

The well-established mevalonate pathway is the route of biosynthesis for the isoprenoid side chain. This comprises the reactions starting from acetyl-CoA to produce farnesyl pyrophosphate (FPP), for which HMG-CoA reductase is considered to be the central regulatory enzyme. Condensation of the two components is catalyzed by polyprenyl-4-hydroxybenzoate transferase. Given that 4-hydroxybenzoic acid is generally in excess, the rate of this reaction is determined by the availability of the polyisoprenoid side chain [11, 27].

Following condensation, the benzoquinone core is iteratively modified by a sequence of C-hydroxylation, decarboxylation, O-methylation and C-methylation reactions. Mechanisms for these reactions have been examined primarily in bacteria and yeast, with the functions of several corresponding mammalian genes having been established through complementary recognition in yeast [31]. Incomplete details of CoQ_{10} biosynthesis in mammalian tissues is due to the difficulty associated with isolating the enzymes involved.

The terminal steps in CoQ_{10} biosynthesis are thought to be rate limiting for the process in eukaryotes and take place in the mitochondrial matrix, governed by Coq biosynthetic proteins (Table 1) [32]. In yeast, Coq proteins assemble in a multi-subunit complex and the presence of all its components are required for stability, [33]. This complex also seems to

be present in mammalian cells [34], however, the exact composition and organisation of this complex is not yet clear.

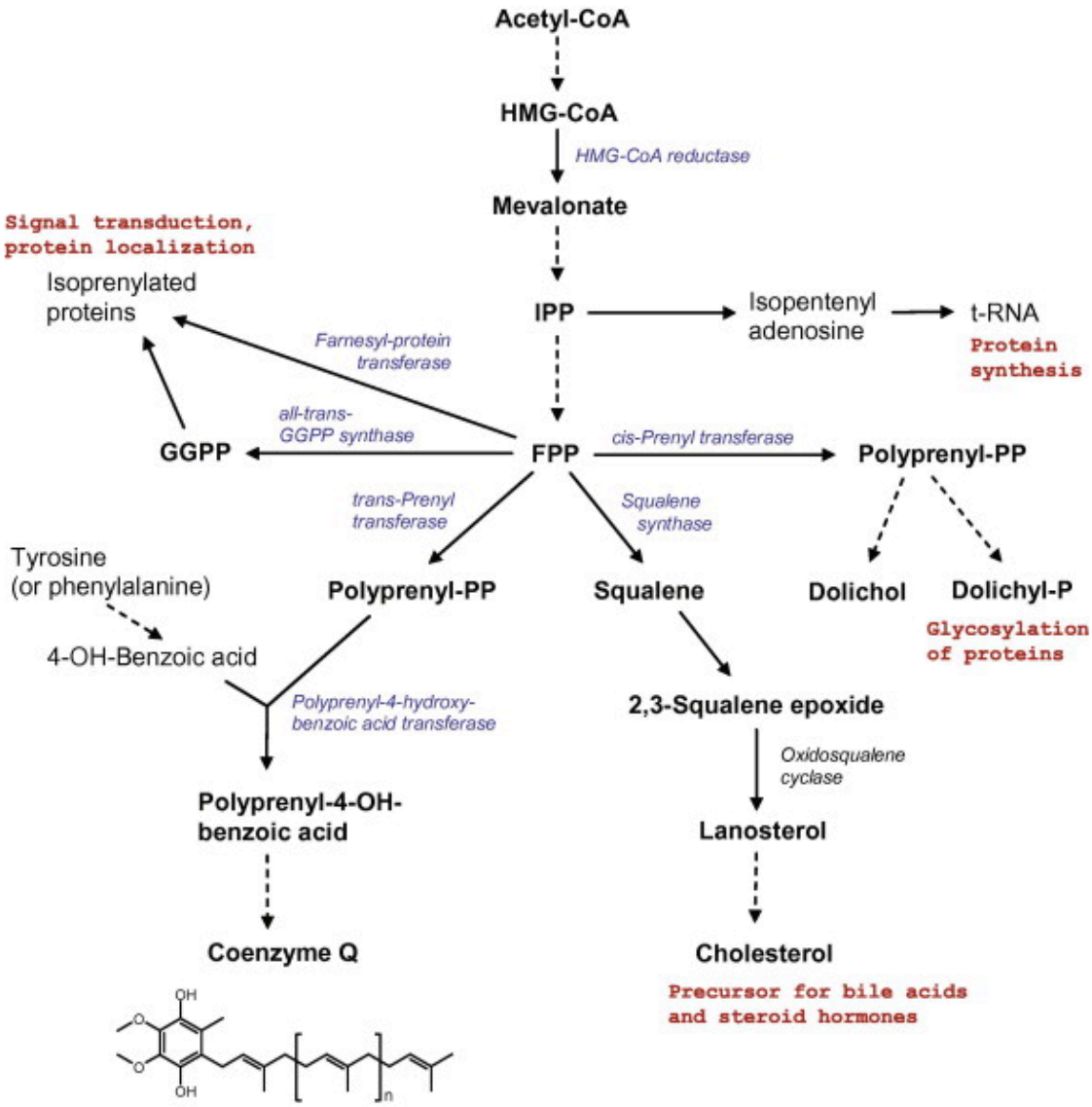

Figure 4: Schematic for the biosynthesis of CoQ_{10} (adapted from [27])., highlighting the end-point products that share the pathway. A perturbation of this pathway could cause a wide-spread downstream effect, for example in response to inhibition of HMG-CoA reductase by statins.

Table 1: Human genes encoding the Coq proteins that are responsible for CoQ_{10} biosynthesis in mammals.

Gene ***Homo Sapiens***	**Function**	**Number of Families w/Coenzyme Q_{10} Deficiency Attributed to Mutation of This Gene** [35]
Enzymes		
PDSS1/(COQ1A)	Prenyl diphosphate-	2
PDSS2/(COQ1B)	synthase	2
COQ2	Prenyltransferase	10
COQ3	O-methyltransferase	-
COQ5	C-methyltransferase	1
COQ6	Mono-oxygenase	5
COQ7	Hydroxylase	1
FDX1L	Electron transfer to-	-
FDXR	*COQ6*	-
Non-Enzymatic Role		
COQ4	Stabilisation of Q complex	9
ADCK3/(COQ8A)	Putative kinase	15
ADCK4/(COQ8B)	Phosphorylation of other Coq proteins?	34
COQ9	Lipid-binding protein. Co-factor of COQ7?	2
?	Decarboxylase?	-
Chaperone/Transporter		
COQ10A	Localisation of CoQ within inner	-
COQ10B	mitochondrial membrane	-

In addition to CoQ_{10}, FPP is also the common branch-point intermediate for cholesterol, dolichol and isoprenylated proteins (Figure 4). All are vital components of various important biological functions. This has been of interest recently since the most commonly prescribed lipid-lowering drug worldwide, statins, are HMG-CoA reductase inhibitors [36] which lead to down-stream inhibition of FPP, potentially leading to pathological consequences often associated with mitochondrial dysfunction [37-40].

1.1.3. Absorption and Distribution of Coenzyme Q_{10}

CoQ_{10} shares similar physicochemical properties to α-toc and appears to follow analogous uptake mechanisms *in vivo.* Gastric digestion releases dietary CoQ_{10} from the food matrix, secretions from the pancreas and bile then facilitate micelle formation leading to uptake of the solubilised lipid across the small intestine [41]. CoQ_{10} is then incorporated into chylomicrons and transported via the lymphatic system to the vascular circulation [41]. Somewhere between absorption and incorporation into the chylomicrons the molecule is reduced to its $CoQ_{10}H_2$ form [42]. After release into the vascular circulation, chylomicron remnants are readily taken up by the liver. Here $CoQ_{10}H_2$ is repackaged into lipoproteins, primarily low-density lipoprotein (LDL), and re-released into the systemic circulation [12].

Table 2: Summary of CoQ_{10} status in different tissues of the human body [43, 44]. The brain shows relatively low levels of total CoQ_{10}, which predominantly exists as CoQ_{10} (ox), due to high levels of oxidative stress associated with the tissue.

Tissue	CoQ_{10} (nmol/g)	Redox State (% reduced)
Heart	132.0	61.0
Kidney	77.0	75.0
Liver	63.6	95.0
Muscle	46.0	65.0
Brain	**15.5**	**23.0**
Intestine	13.3	95.0
Lungs	9.2	25.0
Plasma (μmol/L)	1.1	96.0

In general, tissues with a high-metabolic turnover or energy demand, such as the heart, kidney, liver, and muscle contain relatively high concentrations of CoQ_{10} (Table 2) with a significant proportion of CoQ_{10} in tissues being in the reduced form as $CoQ_{10}H_2$ [14]. The brain and lungs are exceptions, which appears to be a reflection of increased oxidative stress in these two tissues (Table 2).

In addition to variation between different species and organs, CoQ_{10} concentrations vary among cells and regions of the same organ. For example, the cerebellum has a notably low concentration of total CoQ_{10} relative to other regions of the brain [45]. This has been correlated with an ataxic presentation and multiple system atrophy in a recent study investigating CoQ_{10} deficiency and neurodegeneration [46]. Therefore, it could be said that the cerebellum has the narrowest safety margin and will be the first tissue to suffer from a pathological shortage of CoQ_{10} [47].

Perhaps more encouragingly, these findings may also suggest that, in the case of the cerebellum, only a small amount of CoQ_{10} is needed to restore tissue levels to a normal CoQ_{10} status.

At a subcellular level, CoQ_{10} is a component of virtually all cell membranes. In particular, the inner membrane of the mitochondria where more than 80 % of the endogenous lipid is found [48]. The long isoprenoid side chain of CoQ_{10} anchors the molecule in the middle of the membrane bilayer while the quinone core translocates from inside to the surface depending on its redox state, with the reduced form, $CoQ_{10}H_2$, moving to the surface due to an increased polarity [27, 31]. It can, therefore, be surmised that the 'active' part of the molecule is the quinone core with the isoprenoid side group behaving as a directing moiety. The remainder of cellular CoQ_{10} is found in the other organelles and also the cytosol.

CoQ_{10} is highly lipophilic (LogP > 10) with a cLogP of 19.4 – 20.2 [49, 50]. It also has a relatively large molecular weight (863.34 g/mol). Thus, absorption of dietary CoQ_{10} is slow and limited (2 – 4 %) [51]. In the case of dietary supplements, solubilised orally-administered CoQ_{10} formulations have shown enhanced bioavailability, an exemplary safety profile and are the preferred choice for therapeutic intervention [52, 53]. Intestinal absorption is three-fold faster if CoQ_{10} is administrated with food intake [54].

Gastrointestinal absorption of supplemented CoQ_{10} is non-linear, with increasing doses

absorbed to a decreasing degree. This behaviour may be a consequence of a carrier-mediated absorption, saturation of transporter protein and/or existence of absorption window [55, 56]. Higher daily doses of CoQ_{10} are, therefore, best taken in split doses.

Following administration, CoQ_{10} takes approximately 6 hours to reach its maximal plasma concentration. Subsequently, a second plasma CoQ_{10} peak is often observed at about 24 hours, which has been attributed to enterohepatic recycling as well as redistribution to the circulation [12, 57, 58]. Once administered, the circulatory half-life of CoQ_{10} has been reported to be approximately 36 hours requiring a 2 week period of cessation of treatment before it returns to its baseline level following 4 weeks of supplementation [59].

Opinion remains divided as to which is a more effective supplement, CoQ_{10} or $CoQ_{10}H_2$, with conflicting information being disseminated [52, 60-62]. Some have suggested this debate is likely driven by commercial entities who seek to expand their product portfolios by introducing 'biologically active' ubiquinol [63]. However, all forms of the quinone are biologically active and, to date, there has been no direct *in vivo* comparison of the compounds in formulation-matched or native form. Although, a recent paper by Lopez-Lluch *et al.* [64] compared the bioavailability of seven different formulations of CoQ_{10} in healthy volunteers, and concluded that the capsule matrix and preservatives used in the formulation affected absorption, but not whether CoQ_{10} was oxidised (ubiquinone) or reduced (ubiquinol).

Were the compounds to be administered in a matrix-matched or native form, it is likely the harsh conditions of gastric digestion would initiate redox reactions deeming both compounds analogous by the time they reach the point of uptake in the small intestine – most probably in the fully/semi-reduced form. This suggests that bioavailability is predominantly a function of formulation as opposed to an intrinsic difference between the physiochemical properties of the compounds. However, specific and better designed studies need to be performed before any definitive conclusions can be made on the topic.

1.2. Coenzyme Q_{10} and Pathology

CoQ_{10} deficiencies are defined by a decreased cellular CoQ_{10} content as is biochemically diagnosed in skeletal muscle and/or cultured skin fibroblasts [65]. Additionally, a reduction in MRC complex I-III and II-III activities has been shown in muscle tissue from severely affected patients, although these activities can be normal in muscle tissue from less severely affected patients [66].

Pathologies arising from a CoQ_{10} deficiency are clinically and genetically heterogeneous and are a result of impaired oxidative phosphorylation and compromised antioxidant status [11]. Manifestation of the disease ranges from fatal neonatal multisystem failure, to adult-onset encephalopathy [67]. However, there appears to be five distinct clinical phenotypes: encephalomyopathy; severe infantile multisystemic disease; nephropathy; cerebellar ataxia and isolated myopathy, with a clear preponderance of ataxic and neurological presentation [66, 68, 69], likely attributed to the innate susceptibility of the cerebellum to a decrease in CoQ_{10} status [47].

CoQ_{10} deficiency can be caused by mutations in *COQ* genes that encode proteins of the CoQ biosynthesis pathway [35], or as a secondary deficiency caused by defects in other mitochondrial functions that are indirectly involved in the biosynthesis of CoQ_{10} [70].

Primary deficiency of CoQ_{10} is attributed to mutations in enzymes involved in CoQ_{10} biosynthesis and is very rare. However, there are no precise epidemiological data to state overall incidence [67, 71]. In most cases, the family history suggests an autosomal recessive mode of inheritance. To date, mutations in 10 genes that encode proteins of the CoQ biosynthesis pathway have been identified (*PDSS1, PDSS2, COQ2, COQ4, COQ5, COQ6, COQ7, ADCK3, ADCK4,* and *COQ9*) (Table 3). The majority of symptoms reported are common to other mitochondrial disorders [11, 72].

Table 3: Primary CoQ_{10} deficiencies – an overview of the clinical phenotypes and associated defects in genes encoding the Coq proteins that are responsible for CoQ_{10} biosynthesis [11].

Tissue/Organ	Manifestation	Gene Defects
Central Nervous System	**Encephalomyopathy**	***PDSS2, COQ2, COQ4, COQ7, ADCK3, COQ9, COQ5***
	Cerebellar Ataxia	***PDSS2, COQ6, ADCK3, COQ5***
	Leigh Syndrome	***PDSS2, COQ2***
	Stroke-like episodes	***PDSS2, COQ2***
	Seizures	***PDSS2, COQ2, COQ6, ADCK3, ADCK4***
	Dystonia	***ADCK3***
	Spasticity	***ADCK3***
	Migraine	***COQ2***
	Mental retardation	***PDSS1, PDSS2, COQ2, COQ4, COQ6, ADCK3, ADCK4***
Kidney	Steroid Resistant Nephrotic Syndrome	*PDSS1, PDSS2, COQ2, COQ6, ADCK4*
	Tubulopathy	*COQ9*
Peripheral Nervous System & Sensory Organs	Sensorineural	*PDSS2, COQ2, COQ6*
	Optic atrophy	*PDSS1, COQ2*
	Retinitis pigmentosa	*PDSS2, COQ2*
	Peripheral neuropathy	*PDSS1, COQ4*
Muscle	Myopathy with lipid accumulation	*COQ2, COQ4*
Heart	Hypertrophic cardiomyopathy	*COQ2, COQ4*
Liver	Liver Failure	*COQ2*
Other	Lactic Acidosis	*PDSS1, COQ2, COQ4, COQ7, COQ9*
	Dicarboxylic aciduria	*COQ2*

Secondary deficiencies, defined by mutations in genes not involved in CoQ_{10} biosynthesis, are considerably more common than primary deficiencies [70]. This demonstrates how the CoQ_{10} biosynthetic pathway can be easily perturbed. Examples of secondary CoQ_{10} deficiency include mitochondrial myopathies [73] and mitochondrial DNA depletion

syndrome [74]. Additionally, mutations in the *APTX* (encoding aprataxin) [75] and *ETFA* (multiple acyl-CoA dehydrogenase deficiency caused by defects in electron transfer flavoprotein or ETF-ubiquinone oxidoreductase) [76] also result in CoQ_{10} deficiency. The *BRAF* gene has been shown to influence the MAPK (mitogen-activated protein kinase) pathway in such a way as to lead to the cardiofaciocutaneous syndrome [77]. Cardiofaciocutaneous syndrome is associated with a reduction in the muscle content of CoQ_{10} [27, 67].

CoQ_{10} is available over the counter as a dietary supplement in the UK and overseas. Supplementation is believed to benefit cardiovascular and neurodegenerative disorders [78-80]. As such, it has become an increasingly popular dietary supplement in recent years. The beneficial effects of CoQ_{10} supplementation have been attributed to its fundamental role in mitochondrial energy production.

Pathologies associated with CoQ_{10} deficiency can be successfully treated via oral supplementation of CoQ_{10}. These pathologies are, therefore, unique since other mitochondrial disorders are relatively untreatable. If, however, damage to the brain and kidneys is present at the time of diagnosis, such damage cannot be reversed completely. Therefore, early diagnosis is an absolute necessity. This is presently problematic since muscle biopsy and subsequent analysis of the mitochondria in this tissue are required. Plasma CoQ_{10} measurements are not useful for diagnosis due to the association of CoQ_{10} with circulating lipoproteins, meaning values are limited by, if not directly related to, the lipoidic deposit volume [81]. However, blood mononuclear cells have been suggested as a low invasive surrogate to assess endogenous CoQ_{10} status [82].

Uptake of exogenous CoQ_{10} supplements appears to be tissue-specific. The heart and skeletal muscle exhibit the most efficient uptake. In all peripheral tissues, plasma CoQ_{10} concentrations need to be high in order to promote uptake, particularly in the case of delivery across the blood-brain barrier [47, 52, 83].

The highest plasma CoQ_{10} concentrations and subsequent efficacy of treatment are achieved after chronic high dosing with an observed safe level of 1200 mg/day [53]. Plasma CoQ_{10} concentrations appear to plateau at 2400 mg using one specific chewable tablet formulation of CoQ_{10} [56]. The highest plasma CoQ_{10} concentration reported thus far is 10.7 µmol/L (*cf.* 'norm' 0.5–1.7 µmol/L) using a solubilised $CoQ_{10}H_2$ formulation [52, 84, 85].

In Parkinson's disease, plasma CoQ_{10} levels of 4.6 μmol/L were reported to be the most efficacious in slowing functional decline in patients [86]. In contrast, a plasma level of 2.8 μmol/L showed the highest therapeutic benefit in the treatment of congestive heart disease patients [87]. However, a recent study has indicated that 10.0 μmol/L CoQ_{10} is required to restore MRC enzyme activities in CoQ_{10} deficient cells [88, 89]. As such, efforts should be made to increase the bioavailability of oral-supplements to achieve this therapeutic concentration in the peripheral tissues and brain parenchyma. To date, there are no clinically available intravenous formulations of CoQ_{10}. These would, undoubtedly, increase plasma CoQ_{10} levels beyond those of oral-supplementation and could potentially prevent pathogenesis if administered at an acutely high dose in conjunction with an early diagnosis.

While there is clear evidence, both clinically and biochemically, for the improvement of peripheral abnormalities associated with CoQ_{10} deficiency following CoQ_{10} supplementation, neurological symptoms are only partially ameliorated [47, 90, 91]. This may be a result of irreversible damage prior to supplementation, retention of CoQ_{10} in the blood-brain barrier endothelial cells themselves, or simply poor transport across the barrier.

1.3. Barriers of the Central Nervous System

There are three main barriers that serve to selectively compartmentalise the CNS from the periphery; the blood-brain barrier (BBB); the blood-cerebrospinal fluid barrier (BCSFB); and the avascular arachnoid epithelium that completely encases the brain (Figure 5). The combined functions of these barriers are to regulate solute and cellular movement between brain fluids and blood. Selective transport processes are provided for essential nutrients, ions, and metabolic waste products [92]. The main sites of molecular exchange between systemic circulation and the brain occur at the vascular BBB and BCSFB.

However, the cellular basis and primary functions of the BBB and BCSFB differ. The BBB is comprised of a highly specialised network of brain microvascular endothelia. The main role of the BBB is to protect the brain from physiological fluctuations in plasma concentrations of various solutes and from blood-borne substances that could interfere with neurotransmission. Other unique features of the BBB are a lack of endothelial fenestrations [93] or pores, a very low rate of pinocytosis [94], and a high number of mitochondria associated with its high metabolic activity – over 50 % more than neuroglia [95]. In contrast to this, the BCSFB is created by a layer of a modified cuboidal epithelial cells, the choroid plexuses, that secrete cerebrospinal fluid (CSF) and this process could be considered as the main function of this epithelium [96, 97].

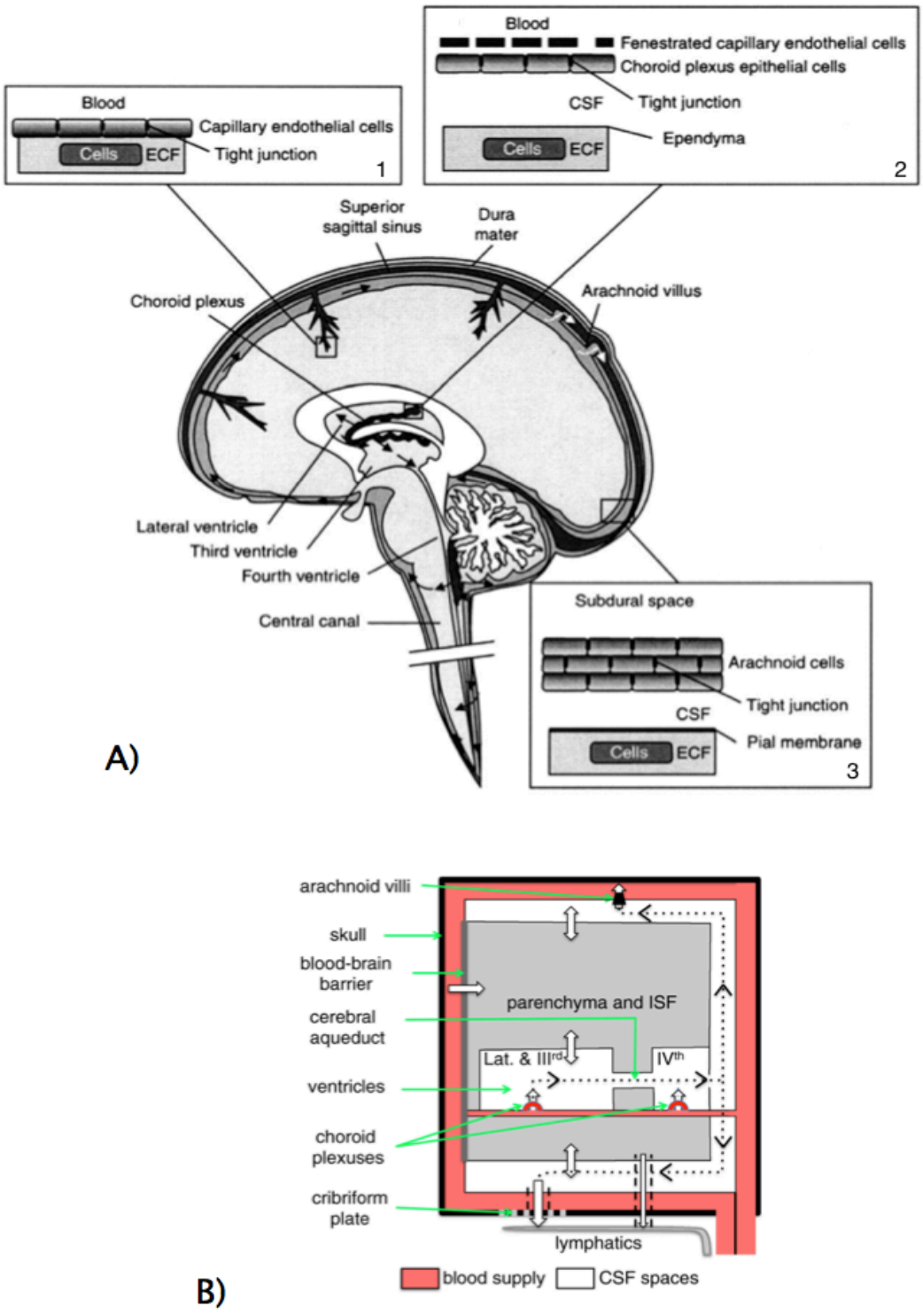

Figure 5: A) Illustration of the CNS barriers; 1 BBB; 2 BCSFB; and 3 Arachnoid barrier (adapted from [98]). B) The cerebral blood flow in relation to the barriers of the CNS [99].

Although constituting only 2 % of the weight of the body, the brain utilises roughly 20 % of its blood supply [100]. The BBB is large in relation to the other CNS barriers, making it the most important interface for blood-brain exchange. Blood flows through the brain via a complex microvasculature that spans approximately 20 m^2 and extends over 650 km [101-103], so the BBB ensures rapid distribution of small permeant molecules and ions throughout the brain, and subsequent exchange with the brain's interstitial space. There is a mean distance of ~ 40 μm between capillaries and a close proximity of 8-25 μm to individual neurons [100], effectively meaning each neuron is perfused by its own capillary. These qualities make permeation of the BBB a prime, yet underdeveloped, target for delivery of therapeutic molecules to the brain parenchyma, for example CoQ_{10} in the context of this study.

While the BBB is present throughout the majority of the brain, it is absent from the circumventricular organs (CVO). The CVO are highly specialised areas in the brain which require significant crosstalk between the brain and peripheral blood. For example, in the release and transport of hormones of the pituitary gland [104, 105].
The cerebral endothelia of the CVO are fenestrated and do not possess the typical properties associated with the BBB. That is not to say the CVO are a region of the brain lacking barrier properties, rather the barrier for the CVO lies in the epithelial cells known as tanycytes and ependymal cells. Therefore, circulating molecules can diffuse into the CVO but not beyond and into the general neural parenchyma.

1.4. The Blood–Brain Barrier

Arguably, the CNS is the most critical and sensitive system in the human body. Strict homeostasis of the local microenvironment, known as the *interior milieu* [106], is imperative for reliable neuronal signalling and a healthy life. This must be maintained during physiological and pathological conditions. A selective barrier between the changeable periphery and the CNS is formed to control movement of molecules into and out of the CNS. In doing so, the brain interstitial fluid (ISF) is formed [107]. This is a finely tuned reaction mixture that maintains a near perfect stoichiometry for all essential chemical

reactions and interactions. The composition of CSF and ISF are similar to that of plasma (Table 4), although, they have a much lower protein content, K^+ and Ca^{2+} concentrations. Levels of Mg^{2+}, however, are higher in comparison to plasma [107, 108].

Table 4: Molecular composition of the CSF in relation to the plasma (adapted from [101]).

Solute	Unit	Plasma	CSF
Na^+	mM	140.0	141.0
K^+	mM	4.6	2.9
Ca^{2+}	mM	2.5	1.25
Mg^{2+}	mM	0.85	1.2
Cl^-	mM	101.0	124.0
HCO_3^-	mM	23.0	21.0
Osmolarity	mOsmol	305.2	298.5
***p*H**		7.4	7.3
Glucose	mM	5.0	3.0
Total Amino Acid	µM	2890	890
Total Protein	mg/mL	70	0.43

The BBB provides a dynamic tri-functional barrier. Constantly adapting to its environment, it provides a physical, metabolic and transport interface between the CNS and the rest of the body, ensuring optimal conditions for normal physiological function [101].

1.1.4. Physical Barrier

Zonulae occludentes (ZOs) or 'tight junctions' (TJs) present between adjacent cerebral endothelia, in conjunction with the lack of fenestrae, are the foundations of the highly impermeable physical-barrier of the BBB. It severely restricts paracellular transport of polar molecules and effectively blocks the penetration of macromolecules into the brain parenchyma. Transcellular passage via specific carriers and/or receptor-mediated transporters on the luminal membrane of the brain endothelium is thereby enforced [101, 109]. Impediment of the paracellular pathway and subsequent ion movement results in a characteristically high *in vivo* transendothelial electrical resistance (TEER) of the BBB

(~1500–2000 $\Omega \cdot cm^2$) compared to the endothelium of other tissues in the body (~3–33 $\Omega \cdot cm^2$) [97, 101, 110, 111]. It is in this segregation of the luminal and abluminal domains of the brain endothelium that the TJs give rise to, resulting in the polarised properties of the BBB, analogous to the endothelium of the kidney and gastrointestinal tract [107].

The term 'tight junction' is often used to describe the physical barrier between adjacent endothelial cells of the BBB. In reality, the physical barrier is a combined intricate network of TJs, including junctional adhesion molecules (JAMs), and adherens junctions (AJs) (Figure 6).

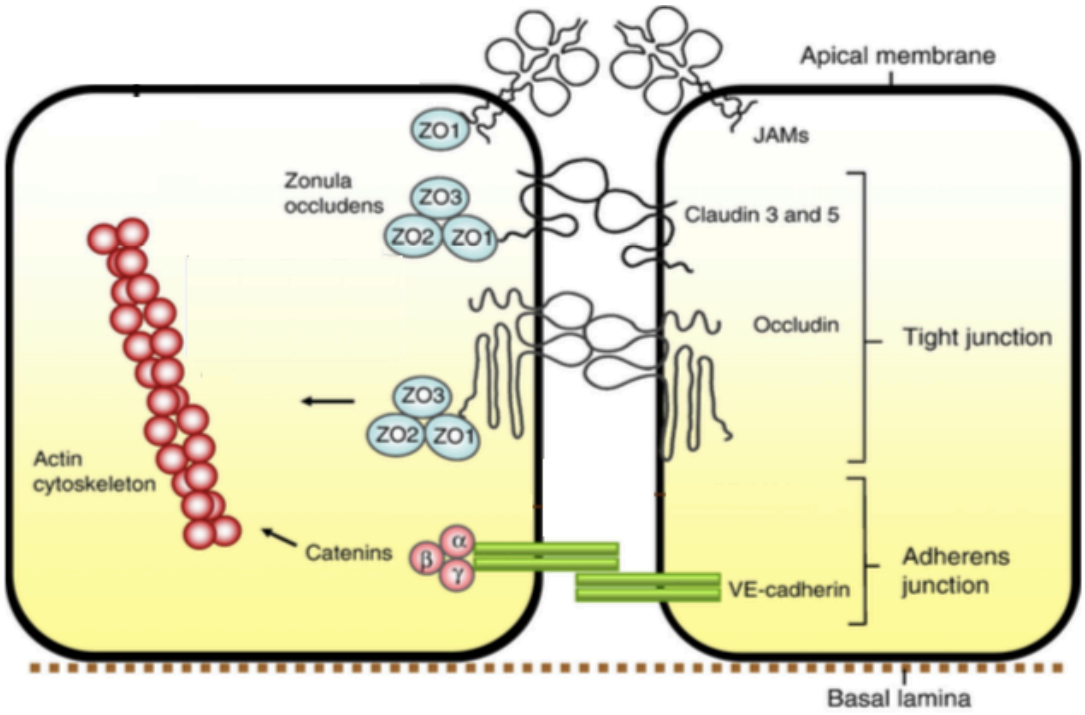

Figure 6: Structure of BBB tight junctions (adapted from [101]).
The tight junctional complex comprises occludin, claudins 3 and 5, and possibly other claudins. The claudins associate and bind to each other across the intercellular cleft forming a barrier to diffusion and a high electrical resistance. Occludin has similar associations across the cleft but does not form the restrictive pore to small ions. The claudins and occludin are linked to the scaffolding proteins ZO-1, ZO-2 and ZO-3, linked in turn via cingulin dimers to the actin/myosin cytoskeletal system within the cell. Cadherins of the adherens junctions provide structural integrity and attachment between the cells, and are necessary for formation of tight junctions.

The TJs are constructed from three integral membrane proteins; claudin, occludin, and JAMs, and a number of cytoplasmic accessory proteins: ZO-1, ZO-2, ZO-3, cingulin, and others (Table 5) [112].

Table 5: Components of the physical barrier and their function [113].

Cellular Junctions	Components	Abbreviation	Genes	Function
Tight Junctions	Occludin	Occludin	*OCLN*	Regulates permeability
	Claudins	Claudin-1	*CLDN1*	Sealing BBB
		Claudin-3	*CLDN3*	Unknown
		Claudin-5	*CLDN5*	Size-selective barrier to small molecules
		Claudin-12	*CLDN12*	Unknown
	Cytoplasmic Proteins	ZO-1	*TJP1*	Multi-domain scaffolding proteins, cytoskeleton anchorage for TJ proteins
		ZO-2	*TJP2*	
		ZO-3	*TJP3*	
Adherens Junctions	Adherens Junctions	Cadherins	*CDH5*	Cytoskeleton link, modulating receptor signalling, regulating transendothelial migration of lymphocytes
Other Junctional Molecules	JAMs	JAM-A	*F11R*	Modulating junctional tightness, regulating transendothelial migration of lymphocytes
		JAM-B	*JAM2*	
		JAM-C	*JAM3*	

Claudins are 22 kDa phosphoproteins and claudin-3 and claudin-5 comprise the major component of TJs [114]. The carboxy-(C)-terminal domain of the claudins bind to cytoplasmic proteins including ZO-1, ZO-2 and ZO-3 [115]. The zonula occludens proteins (ZO-1, ZO-2, and ZO-3) together with cingulin and several others are cytoplasmic proteins

involved in TJ formation [116]. This critical link provides for structural stability of the brain endothelial cell and is an important means of regulating paracellular permeability.
Occludin is a 60–65 kDa phosphoprotein with four transmembrane domains; a long (C)-terminal cytoplasmic domain, and a short amino-terminal cytoplasmic domain [107, 117]. Two extracellular loops of occludin and claudin originating in neighboring cells form the paracellular barrier of the TJ. Occludin is directly linked to the zonula occludens proteins and thereby regulates permeability through their association with the actin cytoskeleton [118].
JAMs (JAM-A, JAM-B and JAM-C) are 40 kDa membrane proteins within the TJs of brain endothelial cells that also bind with ZO-1. They are involved in the formation and maintenance of the TJs [47, 119-122].

AJs are composed of a cadherin-catenin complex and its associated proteins. Cytoplasmic proteins link membrane proteins to actin, which is the primary cytoskeleton protein in the maintenance of the structural and functional integrity of the brain endothelium [97, 105, 107, 123, 124].

1.1.5. Transport Barrier and Solute Uptake Overview

The majority of polar hydrophilic molecules and all macromolecules are prevented from paracellular transport across the BBB by the physical barrier imposed by the TJs. It is only gaseous molecules such as O_2 and CO_2 in addition to small lipophilic molecules (< 400-500 Da and < 8 H-bonds) that can move passively through the lipid membrane of the brain endothelia [100, 125-127]. Thus, a highly selective 'transport barrier' is formed from specific transporters distributed symmetrically or asymmetrically on the luminal and abluminal membranes of the brain endothelia. These selectively exclude potentially neurotoxic compounds, mainly via the ATP-binding cassette (ABC) efflux transport family, while facilitating the entry of required nutrients via solute carrier (SLC) uptake transporters or receptor-mediated transcytosis [96, 103, 107, 126].
Transcellular bidirectional transport across the BBB can be classified into five main categories: carrier-mediated transport, ion transport, active efflux transport, receptor-mediated transport, and adsorptive-mediated transport (Figure 7) [128].

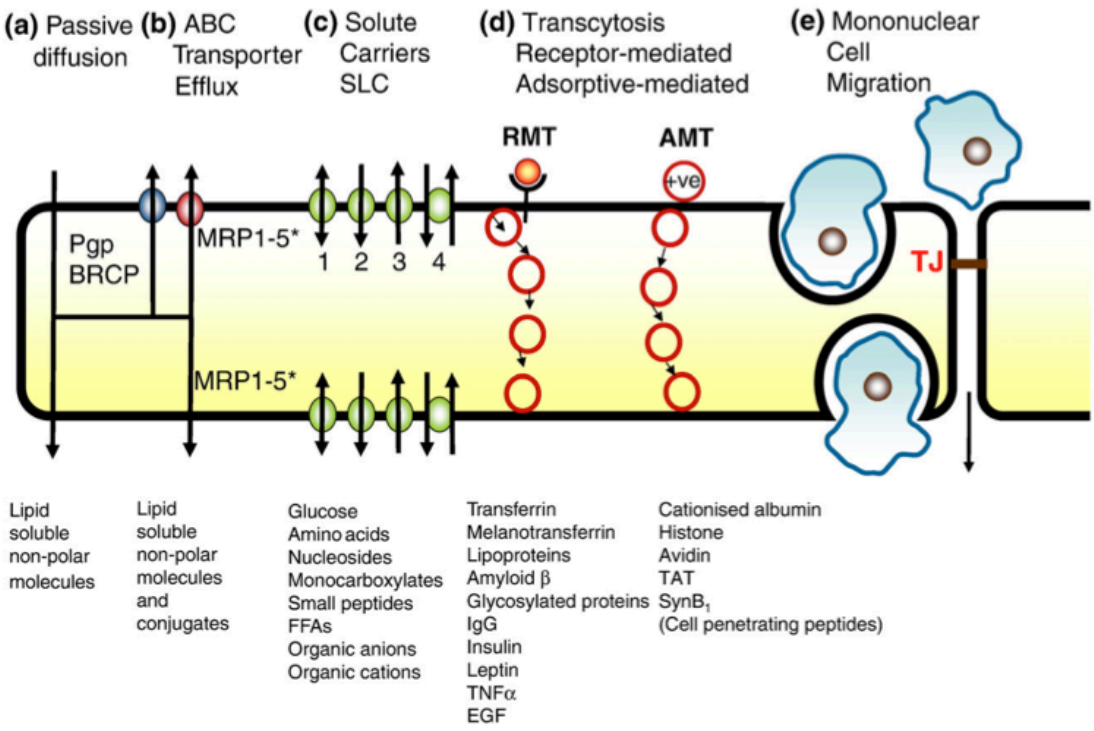

Figure 7: The transport barrier and bidirectional routes across the BBB [101]. ABC, ATP binding cassettes; SLC, solute carrier; RMT, receptor-mediated transcytosis; AMT, adsorptive-mediated transcytosis; Pgp, P-glycoprotein (ABCB1); BCRP, breast cancer resistance protein (ABCG2); MRP, multi-drug resistance protein (ABCC1-5).

Polar molecules such as glucose, amino acids, and several peptides have specific carriers. These highly selective transporters mediate transport into the endothelial cytosol and through to the brain parenchyma. Some macromolecules and also certain peptides cross the BBB through endocytic mechanisms involving receptor-mediated transcytosis (RMT) or adsorptive-mediated transcytosis (AMT). AMT is considered non-specific and comprises all vesicular transport mechanisms that do not involve protein receptors. In AMT, endocytosis is generally promoted by the interaction of the often positively-charged molecule with membrane phospholipids and the glycocalyx [127]. The two main trafficking routes for BBB transcytosis appear to involve clathrin-coated vesicles and caveolae. Macropinocytosis is implicated as a route for larger constructs such as nanoparticles [100, 129].

With restricted passage of haematogenous cells from blood-to-brain, the brain endothelium maintains the immune privilege status of the CNS under normal physiological conditions. Mononuclear leukocytes, monocytes and macrophages are able

to be recruited into the CNS during pathological conditions, providing support to the resident microglia [101, 130].

The BBB is thought to be intact for CoQ_{10} deficient patients. This has led to the assumption that a refractory response to CoQ_{10} supplementation is governed by transport mechanisms across the endothelia. Given its size, lipophilicity and transport within lipoproteins, CoQ_{10} is likely to experience receptor-mediated interactions at the barrier.
Some of the most exploited receptor-mediated transport systems for delivery across the BBB include the low density lipoprotein receptor (LDLR) superfamily, making them a promising candidate for CoQ_{10} [131, 132]. Moreover, some of them, particularly low-density lipoprotein receptor-related protein 1 (LRP-1), are well expressed in the brain [133]. Ligands targeting this family of receptors include the natural protein components of LDL and VLDL, ApoB and ApoE fragments [134].
A recent study in the Caco-2 epithelial-barrier model also indicates there may be a CoQ_{10} efflux mechanism operating via the P-glycoprotein efflux transporter (P-gp) [135], which may explain the apparently poor uptake of CoQ_{10} into the brain.

1.1.6. Metabolic Barrier

The final component of the dynamic tri-functional BBB is the metabolic barrier, where a range of Phase I and II metabolising enzymes are present in the cell membrane and in the cytosol of the brain endothelium [101].
The most prevalent Phase I (functionalisation) enzymes of the BBB are the cytochrome P450 enzymes which are responsible for the oxidative biotransformation of a variety of endogenous and xenobiotic substrates [136-139]. Phase I metabolites can then serve as substrates for Phase II enzymes, which conjugate the functional group with polar endogenous compounds, such as amino acids, sulphates, glutathione, or sugars.
Of the Phase II (conjugation) enzymes, the most prevalent in the BBB are UDP-glucuronyltransferases, glutathione *S*-transferases, sulphotransferases, and *N*-acetyltransferases [136-139]. However, relatively little characterisation of the BBB enzymes has been performed, with the presence of some Phase II enzymes being a topic of debate

since investigations have mainly focussed on brain homogenates instead of isolated brain microvessels.

Nevertheless, the metabolic barrier plays a prominent role in the restriction of endogenous and xenobiotic compounds to the brain and is a major consideration when designing drugs for neurological application [125, 140, 141].

1.5. The Neurovascular Unit

It is now widely accepted that the characteristics of the BBB are part of a complex local grouping of non-neuronal cells that work in concert to support vicinal neurons (Figure 8). In this ensemble, the brain endothelia are in close proximity to perivascular astrocytic end-feet, pericytes, and are closely associated with microglia that influence BBB permeability and collectively constitute a 'neurovascular unit' (NVU) [109, 142].

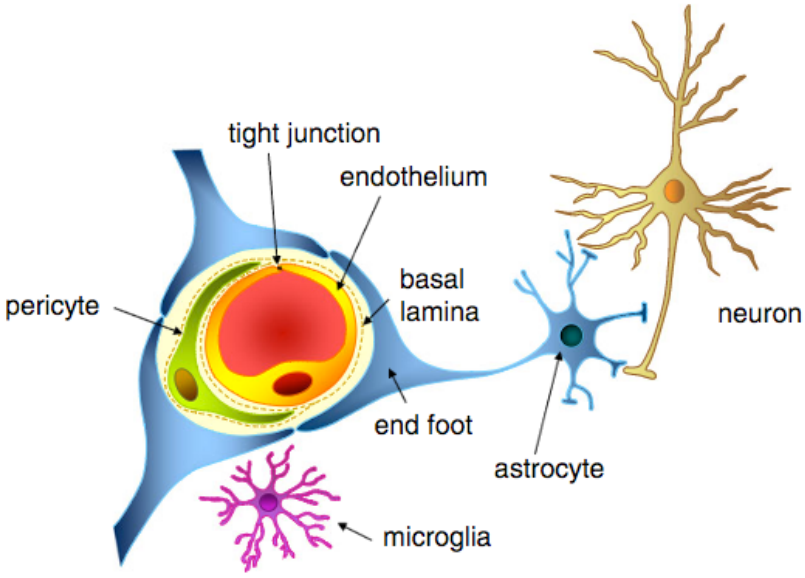

Figure 8: The neurovascular unit (NVU) - a finely tuned collection of specialised cells working in concert to ensure vicinal neurons are subject to optimal conditions [100].

Both pericytes and astrocytes regulate the phenotype of the endothelium. The mechanisms governing this are not yet fully understood, but involve cell–cell communication via soluble factors and possibly direct contact interactions [107, 143].

Proper structural and functional brain connectivity, synaptic activity, and information processing all require precise regulation of cerebral blood flow (CBF), oxygen delivery, and energy metabolite supply. It is in maintaining these key CNS functions for which the NVU is responsible [113].

Whilst the concept of the NVU widely is accepted, it is still developing and is an area of great interest [142, 144-146], with emerging research suggesting circulating leukocytes are part of this unique cellular structure, providing surveillance and immune protection of the CNS [147].

1.6. Blood-Brain Barrier and Pathology

Pathogenesis in the CNS often has a direct correlation with BBB dysfunction, either in a causative or exacerbating role. A breakdown of the 'physical-barrier' is the most prominent factor, although a change in transport and metabolic systems can also occur. Dysfunction can range from mild transient opening of the TJs to chronic barrier breakdown [148].

The pathophysiological 'leaky' barrier exposes the brain parenchyma to a flux of potentially neurotoxic molecules from the peripheral circulation. This can be a consequence of a lack of inductive factors due to astrocyte dysfunction, an increase in permeability factors, or a down-regulation of TJ proteins subsequent to an oxidative insult, for example [149]. In turn, this can contribute to a range of debilitating and/or progressive neuropathies such as; brain tumours [150]; multiple sclerosis [151, 152]; amyotrophic lateral sclerosis [153]; Alzheimer's disease [154, 155]; Parkinson's disease [156]; epilepsy [157, 158]; HIV encephalopathy [159]; lysosomal storage diseases [160]; stroke [161]; autism spectrum disorder [162]; and infectious or inflammatory processes [163].

Early diagnosis of regional defects in the BBB at onset could help long-term prognosis for a vast and increasing number of patients. Promising markers for the diagnosis of barrier dysfunction are associated with microglial activation and CNS inflammation. Thus, efforts should focus on developing these diagnostic methods [164].

1.7. *In Vitro* Models of the Blood-Brain Barrier

There are numerous methods to assess barrier transport *in vivo*, *ex vivo, in silico* and *in vitro* [165]. *In vitro* cell based BBB models provide the best compromise between cost, throughput and predictive value. Generally, they can produce good correlation with *in vivo* permeability values.

However, it is primary cell cultures, including the Porcine Brain Endothelial Cell (PBEC) BBB model, that exhibit the best *in vitro-in vivo* correlation [166]. In addition to forming very tight TJs with TEERs up to 1600 $\Omega \cdot cm^2$ [167], PBECs have been shown the express many of the transporters found within the human brain endothelia, including the well expressed LRP-1 and P-gp transporters. The PBEC BBB is therefore likely to yield the most clinically relevant results for the study of CoQ_{10} transport across the BBB [167].

Aims and Objectives

In view of the refractory nature of the neurological presentation of a CoQ_{10} deficiency to CoQ_{10} supplementation, the main aim of this project was to better understand the mechanisms of CoQ_{10} transport across the BBB. Additionally, it was important to understand how these transport mechanisms differed for clinical analogues of CoQ_{10}, in particular idebenone, with an overall aim to utilise this combined knowledge to suggest the most efficacious therapeutic strategy for the treatment of CoQ_{10} deficiencies.

Towards these aims, the following objectives were defined:

- To develop and validate new LC-MS/MS analytical methods for the measurement of CoQ_{10} and idebenone.
- To interrogate potential CoQ_{10} transport mechanisms at the BBB using *in vitro* models of the BBB, performing high-throughput apparent permeability assays in the immortalised bEnd.3 cell line and supporting this with focussed investigation in the gold-standard PBEC BBB.
- To develop an *in vitro* model of CoQ_{10} deficiency at the BBB and investigate its effect on CoQ_{10} transport mechanisms, using *para*-aminobenzoic acid to pharmacologically induce a CoQ_{10} deficiency.
- To comparatively assess the mechanisms of BBB transport for CoQ_{10} against the clinically relevant analogue, idebenone.
- To explore the effect of co-administered components of the mito-cocktail, specifically vitamin E, on CoQ_{10} BBB transport as a means to optimise the therapy.
- To measure the effect of statin therapy at the BBB and its overall effect on CoQ_{10} transport across the BBB *in vivo*.

2. Materials and Methods

2.1. Preparation of Rat-Tail Collagen

2.1.1. Materials

Rat tails; glacial acetic acid (109088, Sigma®, UK).

2.1.2. Method

Along with fibronectin, collagen is a key component of the extracellular matrix and basement membrane. It is widely accepted that for primary cells in particular, coating plates with collagen and fibronectin is conducive to a stable culture [168-170]. Additionally, the presence of a basement membrane has been shown to improve cell proliferation and differentiation in *in vitro* models of the BBB [171]. Collagen fibres in this project were sourced from the tendons of rat–tail vertebrae, in accordance to the method described by Strom *et al.* [172].

Rat tails were collected from experimental rats (6–8 tails), avoiding the use of animals that had been exposed to toxic substances, and a longitudinal incision made from the base to the tip of the tail. The skin was then removed. Starting at the tip of the tail, the distal 3 vertebrae were broken and gently pulled away with their associated collagen fibres attached. This process was repeated down the full length of the tail. Collagen fibres were then severed from their points of attachment on the vertebrae and left to dry (3 h; 25°C) before being weighed. The dried fibres were then subject to UV radiation (germicidal UV lamp; 48 h) and transferred to a sterile laminar flow hood for dissolution in acetic acid. Sterilised collagen fibres were dissolved in a solution of acetic acid (3.3 g/L in 0.1% (v/v) acetic acid) and continuously stirred (72 h) until dissolution was achieved. An intermediate stock solution (300 µg/mL in *dd*H_2O) was used throughout this project.

2.2. bEnd.3 Cell Culture

2.2.1. Materials

bEnd.3 cells (CRL-2299™, ATCC®, USA); rat tail collagen type I (Section 2.1); fibronectin from bovine plasma (F1141, Sigma®, UK); Hank's Balanced Salt Solution without Ca^{2+} and Mg^{2+} (HBSS; H9394, Sigma®, UK); Dulbecco's Modified Eagle's Medium (DMEM; 30-2002™, ATCC®, USA); Foetal Bovine Serum (FBS; F7524, Sigma®, UK); penicillin-streptomycin (P0781, Sigma®, UK); trypsin-EDTA solution (30-2101™, ATCC®, USA); dimethyl sulfoxide (DMSO; D5879, Sigma®, UK); Mr. Frosty™ freezing container (Thermo Scientific™, UK); Nunc™ 1.8 mL cryogenic tubes (Thermo Scientific™, UK); Nunc™ T-75 cell culture flasks with filter caps (Thermo Scientific™, UK); Costar® 12 mm Transwell® 0.4 μm pore polycarbonate inserts with 12-well plates (Corning® Inc., USA).

2.2.2. Method

bEnd.3s are an immortalised mouse brain endothelial cell line transformed with Polyoma virus middle T antigen [173, 174]. They are sensitive to *p*H changes and must be maintained between *p*H 7.35–7.45. Additionally, blood-brain barrier characteristics have been shown to degrade after passage 30 and, therefore, should not be used beyond this point [175]. bEnd.3s are a popular cell line for BBB permeability studies due to their low cost, speed and ease of use compared with the 'gold-standard' primary cell cultures. In the context of this project, bEnd.3s were used as a first-line platform for investigation prior to further experiments on the superior primary PBECs.

Initial Culture

Endothelial cells were thawed and re-suspended in culture medium as directed by the supplier (9 mL/vial; DMEM with 10 % (v/v) FBS, 100 U/mL penicillin, 100 μg/mL streptomycin). The cell suspension was then seeded onto a T-75 flask (1 vial/T-75 flask)

and grown to 90 % confluence in a humidified incubator at 37°C, 5 % CO_2 (Figure 9). An initial media change was performed at 24 h after seeding and every 2–3 days thereafter.

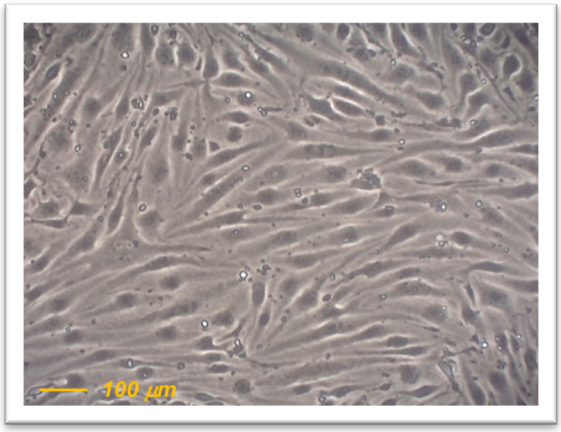

Figure 9: Fully confluent bEnd.3 cells after six days of growth. Images were captured using a Dino-Lite AM4023X eyepiece camera with DinoXcope software.

Cells thawed from liquid nitrogen were passaged at least once onto a new T-75 flask before being passaged again for bEnd.3 experiments: Cells were detached from the T-75 flask with trypsin-EDTA solution (2 mL/T-75 flask; 0.25 % trypsin, 0.53 mM EDTA in HBSS without Ca^{2+} and Mg^{2+}) at 37°C, 5 % CO_2, for 8-9 minutes. Trypsin was then quenched with culture medium (8 mL/T-75 flask), and the cell-suspension centrifuged at 125 × *g* for 7 minutes. The supernatant was aspirated, the pellet re-suspended in culture medium, and cells seeded onto T-75 flasks at a sub-cultivation ratio of 1:4.
Cultures from this passage were then taken forward for subsequent plating in bEnd.3 experiments or cryopreserved (2.5 × 10^5 cells/1 mL cryovial; DMEM, 10 % (v/v) FBS, 100 U/mL penicillin, 100 µg/mL streptomycin, 5 % DMSO) in liquid nitrogen.

Growth on Transwell®-Inserts

Cultures of bEnd.3 cells at 90 % confluence were detached from the T-75 flask with trypsin as described above. The resulting cell pellet was re-suspended in culture medium (1 mL) to be counted with a haemocytometer.

Cells were seeded in 0.5 mL medium into each 12-well Transwell®-insert coated with lab-prepared rat tail collagen type I (300 µg/mL) and fibronectin (7.5 µg/mL), at a density of 25000 cells/cm^2. The Transwell®-inserts were then carefully transferred to a 12-well plate containing culture medium (1.5 mL/well), and incubated at 37^{o}C, 5 % CO_2, for 3 days until confluent.

Stimulation of Differentiation Factors

After 3 days of growth on Transwell®-inserts, confluent bEnd.3 cells were differentiated to express a BBB phenotype. This was achieved by the addition of serum-free differentiation medium (1.5 mL/well; DMEM with 100 U/mL penicillin, 100 µg/mL streptomycin) to the basal compartments of the Transwell® apparatus. Apical chambers were replenished with standard culture medium (0.5 mL/insert). bEnd.3s were used in experiments 72 h after this medium change.

2.3. Porcine Brain Microvessel Isolation

2.3.1. Materials

IS89 multi-shelf shaker incubator (Wesbart Ltd., UK); Wheaton™ Dounce tissue grinders (Jencons Scientific Ltd., UK); Porcine brains (Cheale Meats Ltd., UK); Iscove's Modified Dulbecco's Medium (IMDM; Gibco™, UK); penicillin-streptomycin (P0781, Sigma®, UK); Dulbecco's Phosphate Buffered Saline (PBS; D8537, Sigma®, UK); Eagle's Minimum Essential Medium (MEM; Sigma®, UK); M199 medium (Sigma®, UK); nylon meshes (Plastok Associates Ltd., UK); trypsin-EDTA (Sigma®, UK); collagenase CLS3 (Lorne Laboratories Ltd., UK); DNase I (Lorne Laboratories Ltd., UK); Foetal Bovine Serum (FBS; F9665, Sigma®, UK); dimethyl sulfoxide (DMSO; D5879, Sigma®, UK); Mr. Frosty™ freezing container (Thermo Scientific™, UK); Nunc™ 1.8 mL cryogenic tubes (Thermo Scientific™, UK).

2.3.2. Method

Primary PBECs were isolated based on the method described by Abbott et al. [176]. Brains from domestic pigs (5-6 months-old) were obtained fresh as by-products from the abattoir and transported on ice in Iscove's Modified Dulbecco's Medium with added penicillin (100 U/mL) and streptomycin (100 µg/mL). Isolation proceeded within 2–3 h of brain harvesting.

In a sterile laminar flow hood, 6 – 8 brains were gently washed in cold PBS (1 L) with added penicillin (100 U/mL) and streptomycin (100 µg/mL). One brain at a time, the meninges were thoroughly peeled-off and discarded. White matter was then carefully removed and discarded. The isolated grey matter was collected in cooled isolation buffer (20 mL; MEM with 25 mmol/L HEPES, 10 % (v/v) FBS, 100 U/mL penicillin and 100 µg/mL streptomycin), stored on ice, and the procedure repeated for the remaining brains. The pooled grey matter was then forced through a 50 mL syringe, without a needle, to produce a slurry which was subsequently diluted in cooled isolation buffer (1:1, v/v) and stored on ice.

The grey matter material was gently homogenised in a hand-held Dounce glass tissue grinder (89–127 µm clearance, 15 strokes; 25–76 µm clearance, 15 strokes). The resulting homogenate was made up to 450 mL in cooled isolation buffer and sequentially filtered in 50 mL batches; first through a 150 µm nylon mesh, then through a 60 µm nylon mesh.

Microvessel fragments collected on the 150 µm and 60 µm meshes were kept separate and digested in Petri dishes (8.8 cm^2) at 37°C for 1 h in a digestion solution (20 mL; M199 medium with 10 % (v/v) FBS, 90 U/mL trypsin, 0.1 nM EDTA, 210 U/mL collagenase CLS3, 115 U/mL DNase I) with continuous orbital-agitation (180 rpm).

Keeping the fractions separate, the microvessels were then washed-off the meshes with the digestion solution, centrifuged for 5 minutes at 105 × g, 4°C, and the supernatant aspirated. Each pellet was then re-suspended in isolation buffer (20 mL) and centrifuged again. Finally, the separated '150s' and '60s' fractions were re-suspended in a freezing solution (~1 mL/brain isolated; 10 % (v/v) DMSO in FBS), triturated to ensure even distribution, aliquoted into cryovials (1 mL/vial), brought slowly to −80°C, and stored in liquid nitrogen. A 1:1 mixture ('150s'/'60s') was used for all experiments outlined in this project.

2.4. Porcine Brain Endothelial Cell Culture

2.4.1. Materials

Primary Porcine Brain Endothelial Cells (PBECs; Section 2.3); Dulbecco's Modified Eagle's Medium (DMEM; D5546, Sigma®, UK); Bovine Plasma Derived Serum (BPDS; First Link Ltd., UK); penicillin-streptomycin (P0781, Sigma®, UK); L-glutamine (G7513, Sigma®, UK); heparin (H3149, Sigma®, UK); hydrocortisone (H0135, Sigma®, UK); puromycin (P8833, Sigma®, UK); pCPT-cAMP (C3912, Sigma®, UK); RO-20-1724 (Calbiochem®, UK); trypsin-EDTA solution (T4299, Sigma®, UK); rat tail collagen type I (Section 2.1); fibronectin from bovine plasma (F1141, Sigma®, UK); Nunc™ T-75 cell culture flasks with filter caps (Thermo Scientific™, UK); Costar® 12 mm Transwell® 0.4 μm pore polycarbonate inserts with 12-well plates (Corning® Inc., USA).

2.4.2. Method

Initial Culture (P0)

Microvessel fragments were thawed and re-suspended in culture medium (9 mL/vial; DMEM with 10 % (v/v) BPDS, 100 U/mL penicillin, 100 μg/mL streptomycin, 2 mM glutamine, 125 μg/mL heparin) supplemented with puromycin (4 μg/mL) to kill contaminating cells, especially pericytes [177]. A 1:1 cell mixture (150s/60s) was seeded onto 2 × T-75 flasks coated with lab-prepared rat tail collagen type I (300 μg/mL) and fibronectin (7.5 μg/mL), and grown to 70 % confluence in a humidified incubator at 37°C, 5 % CO_2. Care was taken to avoid reaching 100 % confluence in order to prevent contact-inhibition that can halt further cell growth (Figure 10).

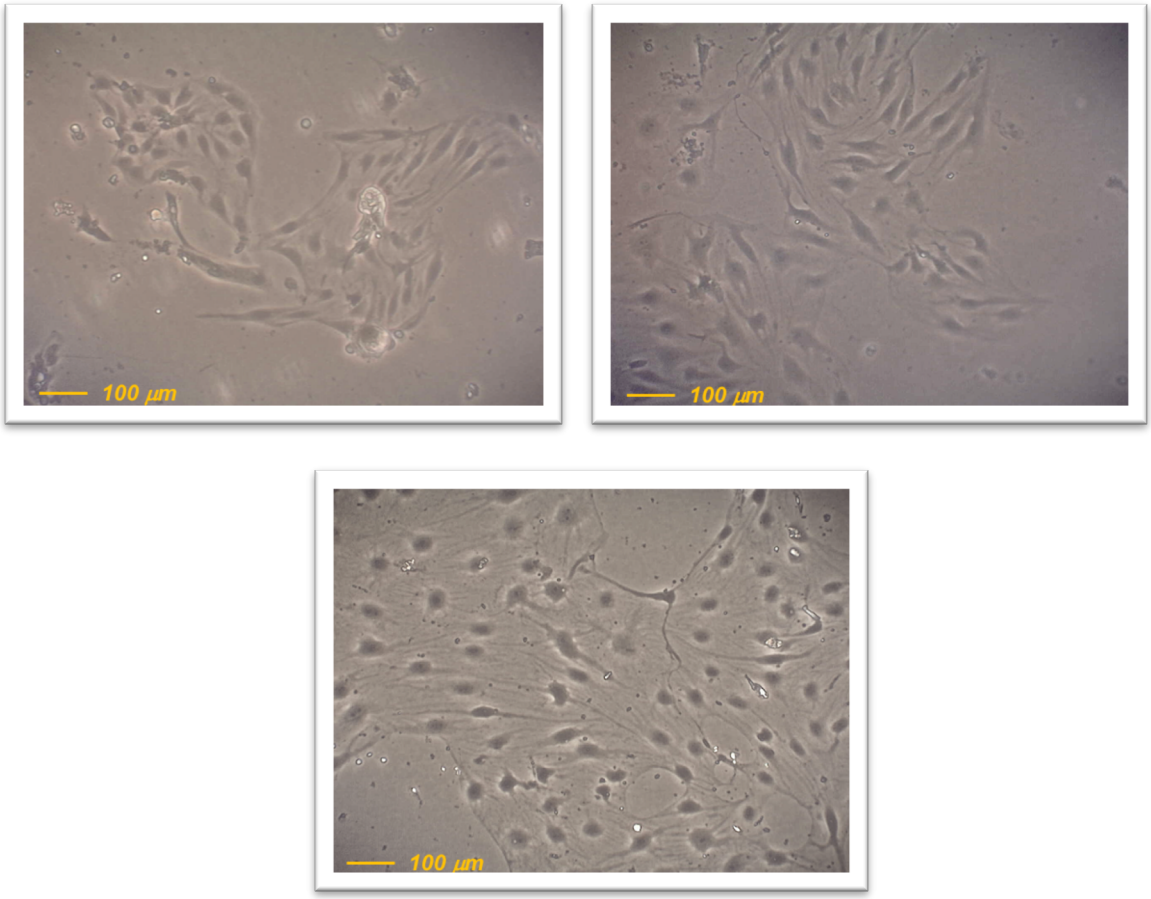

Figure 10: PBEC cells after 3 (top left image), 5 (top right image) and 7 (bottom image) days of growth. Images were captured using a Dino-Lite AM4023X eyepiece camera with DinoXcope software.

An initial media change was performed at 24 h after seeding (culture medium + puromycin) and every 2–3 days thereafter, with a maximum puromycin exposure of 5 days.

Growth of PBECs on Transwell® Inserts (P1)

Once 70 % confluence was achieved, the cells were detached from the T-75 flasks by incubating with trypsin-EDTA solution (2 mL/T-75 flask; 2.5 % trypsin, 0.1 nM EDTA in PBS), at 37°C, 5 % CO_2, for 8-10 minutes. Trypsin was then quenched with culture medium (8 mL/T-75 flask; DMEM with 10 % (v/v) BPDS, 100 U/mL penicillin, 100 µg/mL streptomycin, 2 mM glutamine, 125 µg/mL heparin), and the cell-suspension centrifuged at 360 × *g* for 5 minutes. The supernatant was aspirated and the pellet of first

passage (P1) cells re-suspended in culture medium (3 mL) to be counted with a haemocytometer.

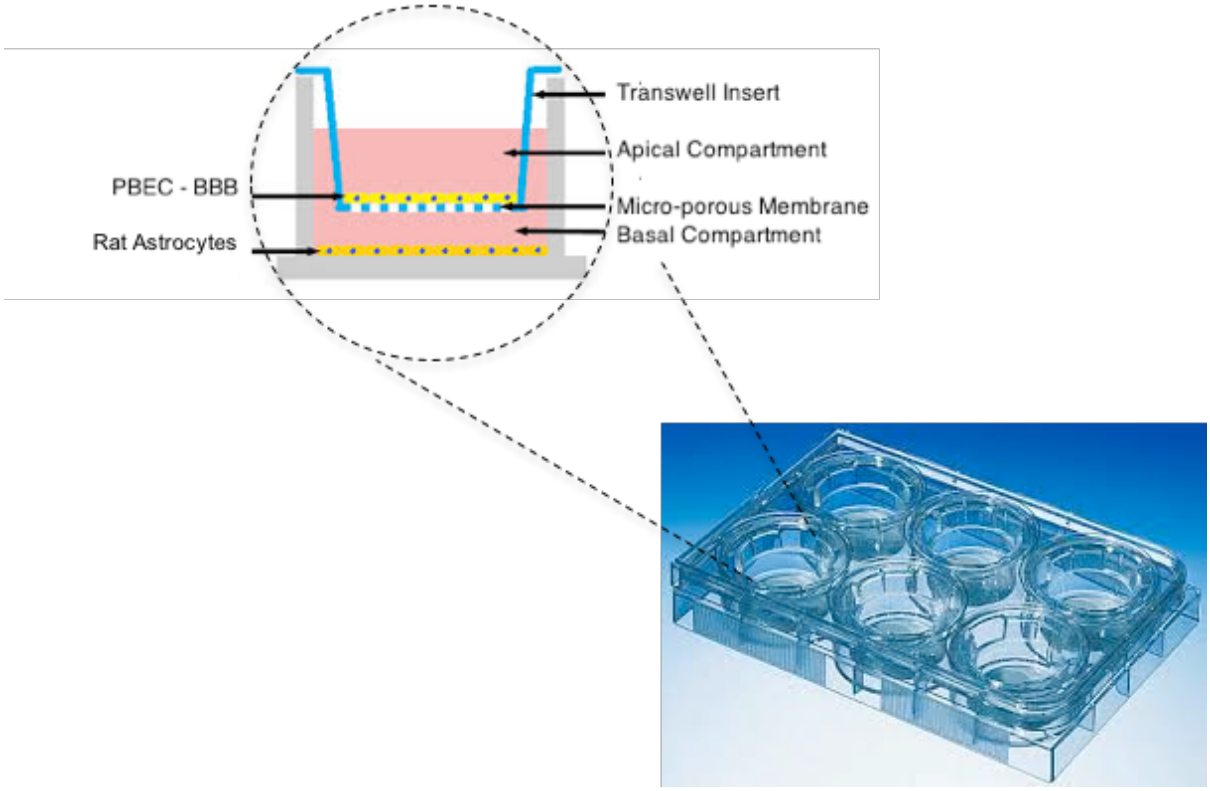

Figure 11: Schematic diagram of the *in vitro* non-contact co-culture of rat astrocytes with PBEC cells on Transwell® apparatus.

Cells were seeded onto 12-well Transwell®-inserts coated with lab-prepared rat tail collagen type I (300 µg/mL) and fibronectin (7.5 µg/mL), at a density of 1×10^5 cells/cm^2 in 0.5 mL medium. The Transwell®-inserts containing the PBECs were then carefully transferred onto a 12-well plate containing primary rat astrocytes, which had been refreshed with astrocyte culture medium 24 h prior (Section 2.6). The co-culture was then incubated at 37°C, 5 % CO_2, for 3 days (Figure 11).

Stimulation of Differentiation Factors in Co-culture

After 3 days of growth on the Transwell®-inserts, the culture medium was replaced with differentiation medium to induce characteristic BBB properties, especially tight junction

maturation [178-180]. Apical differentiation medium (0.5 mL/insert; DMEM with 10 % (v/v) BPDS, 100 U/mL penicillin, 100 µg/mL streptomycin, 2 mM glutamine, 125 µg/mL heparin, 250 µM pCPT-cAMP, 550 nM hydrocortisone, 17.5 µM RO-20-1724) was applied to the PBECs, and a serum-free basal differentiation medium (1.5 mL/well; DMEM with 100 U/mL penicillin, 100 µg/mL streptomycin, 125 µg/mL heparin, 250 µM pCPT-cAMP, 550 nM hydrocortisone, 17.5 µM RO-20-1724) was applied to the astrocytes. PBECs were used in experiments 48 h after this medium change (Appendix A).

2.5. Rat Astrocyte Cell Isolation

2.5.1. Materials

Rat pups (one litter, 0-2 days postnatal); Hank's Balanced Salt Solution without Ca^{2+} and Mg^{2+} (HBSS; H9394, Sigma®, UK); HEPES (H3375, Sigma®, UK); penicillin-streptomycin (P0781, Sigma®, UK); trypsin (T4549, Sigma®, UK); Dulbecco's Modified Eagle's Medium (DMEM; 31966, Gibco™, UK); Foetal Bovine Serum (FBS; F9665, Sigma®, UK); penicillin-streptomycin (P0781, Sigma®, UK); poly-L-lysine hydrobromide (P6282, Sigma®, UK); Nunc™ T-25 cell culture flasks with filter caps (Thermo Scientific™, UK); Vibrax SR/VXR orbital shaker (Camlab Ltd., UK); cytosine β-D-arabinofuranoside (C1768, Sigma®, UK); dimethyl sulfoxide (DMSO; D5879, Sigma®, UK); Mr. Frosty™ freezing container (Thermo Scientific™, UK); 1.8 mL Nunc™ Cryogenic Tubes (Thermo Scientific™, UK).

2.5.2. Method

Primary rat cortical astrocytes were isolated according to Rist *et al.* [181]. Animals (rat pups; 0–2 days old) were sacrificed by cervical dislocation and decapitated. The head was transferred into a sterile laminar flow hood and the skin incised longitudinally using a scalpel. The soft skull was then cut and the whole brain removed and placed into a Petri dish filled with cold dissection buffer (HBSS without $Ca^{2+}$and Mg^{2+}, with 10 mmol/L HEPES, 100 U/mL penicillin, 100 µg/mL streptomycin; *p*H 7.4) on ice.

The cerebellum, diencephalon and brain stem were then removed, followed by the tissue overlying the cortex and non-cortical structures. The cortex was then placed on a buffer–

soaked gauze and the meninges were gently peeled-off. Cortices were collected in cold dissection buffer (5 mL) and stored on ice. The process was repeated for all brains.
The pooled cortical matter was then finely chopped with a scalpel and digested at 37°C with trypsin (5 mL; 0.125 mg/mL in dissection buffer). After 30 minutes, trypsin was quenched by the addition of culture medium (10 mL; DMEM with 4500 mg/L glucose, GlutaMAX™ and pyruvate, 10 % (v/v) FBS, 100 U/mL penicillin, 100 µg/mL streptomycin). The suspension was centrifuged at 360 × *g* for 5 minutes, the supernatant aspirated, and the pellet re-suspended in culture medium (2 mL). After triturating with a fine–bore polished pipette and sedimentation, the cell-suspension was filtered through a sterile 73.5 µm tissue-sieve, counted with a haemocytometer, and seeded at a plating density of 25000 cells/cm^2 on coated (250 µg/mL poly-L-lysine) T-25 flasks. The cell cultures were incubated at 37°C, 5 % CO_2.

The culture medium was replaced 24 h after seeding and every 2–3 days thereafter. At sub-confluence (days 7-9 after plating), cell contaminants on top of the monolayer were separated from type 1 astrocytes by orbital-agitation at 37°C for 24 h. Detached cells, consisting mainly of oligodendrocytes, type 2 astrocytes and 0-2A progenitors, were aspirated and the culture medium replaced. Further purification of the cell cultures was achieved at confluence (day 14-16 after plating) by adding cytosine arabinoside (10 µM) to the culture medium for 5 days to kill contaminating dividing cells.
Cells were detached from the T-25 flasks with trypsin-EDTA solution (1 mL/T-25 flask; 2.5 % trypsin, 0.1 nM EDTA in PBS), incubated at 37°C, 5 % CO_2, for 5–7 minutes, and quenched with culture medium (5 mL). The cell-suspension was then centrifuged at 250 × *g*, 4°C, for 7 minutes, the supernatant aspirated, and cells re-suspended in freezing medium (10 % (v/v) DMSO in FBS) at a density of 4 × 10^6 cells/mL. Finally, the cells were aliquoted into cryovials (1 mL/vial), brought slowly to −80°C, and stored in liquid nitrogen.

2.6. Rat Astrocyte Cell Culture

2.6.1. Materials

Primary rat astrocytes (Section 2.5); Dulbecco's Modified Eagle's Medium (DMEM; 31966, Gibco™, UK); Foetal Bovine Serum (FBS; F9665, Sigma®, UK); penicillin-streptomycin (P0781, Sigma®, UK); poly-L-lysine hydrobromide (P6282, Sigma®, UK); Costar® 12-well plates (Corning® Inc., USA).

2.6.2. Method

Astrocytes were thawed and re-suspended in culture medium (17 mL/vial; DMEM with 4500 mg/L glucose, GlutaMAX™ and pyruvate, 10 % (v/v) FBS, 100 U/mL penicillin, 100 µg/mL streptomycin). Cells were seeded onto a pre-coated (250 µg/mL poly-L-lysine) 12-well plate (1.5 mL/well) and incubated at 37°C, 5 % CO_2.

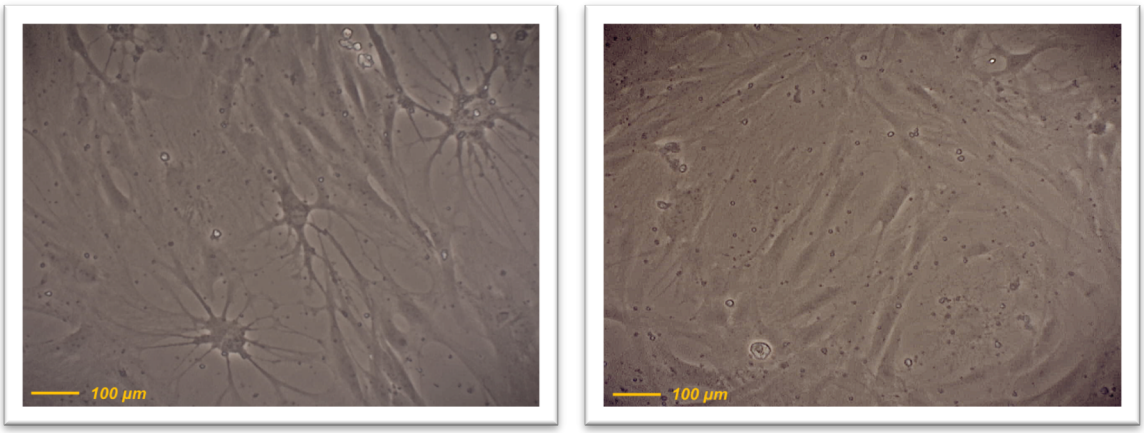

Figure 12: Primary rat astrocytes exhibiting D3 stellate morphology at 80 % confluence (left image), and quiescence at 100 % confluence (right image). Images were captured using a Dino-Lite AM4023X eyepiece camera with DinoXcope software.

Culture medium was replaced 6 h after seeding and every 3 days thereafter. The cell culture was maintained for a minimum of 14 days prior to co-culture with PBECs (Figure 12), 24 h before which the culture medium was refreshed (Appendix A).

2.7. Characterising the BBB Phenotype

2.7.1. Transendothelial Electrical Resistance (TEER)

Materials

EVOM™ voltohmmeter with STX100C electrodes (World Precision Instruments, UK).

Method

In combination with visual inspection under a light microscope, TEER measurements are the most reliable way of assessing confluency and tightness of the endothelial cell monolayer prior to experiments. TEER measurements are convenient, non-invasive, and give results in real-time.

TEER was determined using a voltohmmeter, where resistance is calculated in accordance to Ohm's law (Equation 1) [182] and is inversely proportional to ionic permeability of the *in vitro* BBB.

$$R = \frac{V}{I}$$

Equation 1: Ohm's law where R is resistance (ohms, Ω), V is voltage (volts) and I is current (amperes, Amps) [182].

TEERs were recorded across Transwell®-insert monolayers 24 h after changing to differentiation medium and a minimum of 3 h before assay. A guidance rig was manufactured in-house to ensure TEER apparatus were consistently positioned throughout the entire project.

The measured resistance of cells grown on Transwell®-inserts was corrected against the resistance across a 'blank' collagen/fibronectin-coated Transwell®-insert, and multiplied by surface area (1.12 cm^2 for a 12-well Transwell®-insert), to give TEER in $\Omega \cdot cm^2$ (Equation **2**) [183].

$$\mathbf{TEER}_{reported}\ (\Omega\ \mathrm{cm}^2) = (R_{total} - R_{blank}) \times SA_{insert}$$

Equation 2: TEER calculation where the reported TEER ($\Omega \cdot cm^2$) is equal to the difference between total resistance and resistance of a blank Transwell®-insert (Ω), multiplied by the surface area of the Transwell®-insert (cm^2) [183].

The higher the TEER, the lower the ionic permeability and, therefore, the greater the degree of characteristic tight-junction expression.

2.7.2. Paracellular Permeability

Materials

Synergy™ HT plate reader with KC4™ data analysis software (BioTek Instruments Ltd., UK); Lucifer Yellow dipotassium salt (L0144, Sigma®, UK); fluorescein isothiocyanate-dextran (FITC-40; FD40S, Sigma®, UK); Nunc™ MicroWell™ 96-well plates (Thermo Scientific™, UK).

Method

In addition to characterising BBB integrity with visualisation and quantitative TEER measurements, permeability markers were incorporated *in situ* to assess paracellular permeability during the assay procedure [164, 184]. This approach provided robust information about the functional parameters of the *in vitro* BBB, thereby serving as a reliable quality control for all assays.

The paracellular permeability marker Lucifer Yellow (~0.44 kDa; 10 μg/mL) or FITC-dextran (~40 kDa; 0.5 mg/mL) was added to the assay buffer of the 'donor' chamber in the Transwell® apparatus, and their paracellular permeability was analysed fluorometrically post-experiment; assay buffer was sampled (50 μL) apically and basally upon completion of the assay, transferred to a 96-well plate, and analysed on a fluorometer (Lucifer Yellow – excitation 400/30 nm, emission 528/20 nm, sensitivity 83; FITC-40 – excitation 485/20 nm, emission 528/20 nm, sensitivity 50).

Apparent permeability (P_{app}) of the paracellular markers was determined from the amount of compound transported per time (Section 2.8.2, Equation 3) [185]. P_{app} is proportional to the extent of paracellular transport exhibited, normalised for assay duration and surface area of the Transwell® filter; a low P_{app} is indicative of an integral BBB phenotype.

2.8. Apparent Permeability Assay

2.8.1. Materials

Hank's Balanced Salt Solution (HBSS; H8264, Sigma®, UK); IS89 multi-shelf shaker incubator (Wesbart Ltd., UK); Costar® 12-well plates (Corning® Inc., USA).

2.8.2. Method

The apparent permeability (P_{app}) of a compound is a well-documented and highly utilised method to investigate transport mechanisms across *in vitro* models of the BBB [167, 186, 187]. Both influx (blood-to-brain; apical -> basal) and efflux (brain-to-blood; basal -> apical) directions can be examined, separately (Figure 13).

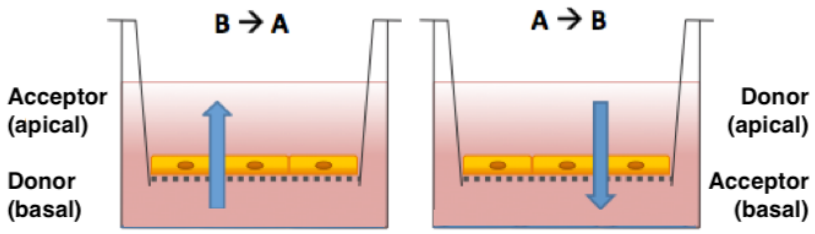

Figure 13: Schematic diagram of the apparent permeability assay for assessing apical-to-basal (blood-to-brain; **A -> B**) and basal-to-apical (brain-to-blood; **B -> A**) transport of molecules across the *in vitro* models of the BBB.

Immediately prior to assay, brain-endothelial cells on Transwell® filters were transferred to mono-culture in a new 12-well plate and washed with HBSS (× 2; 500 µL/insert, 1.5 mL/well) to remove any cell debris and residual differentiation medium. 'Donor' assay buffer containing the CoQ_{10} preparation was then applied to either the apical (500 µL) or basal (1.5 mL) chambers of the Transwell® apparatus, with an 'acceptor' buffer applied to the opposite chamber accordingly. The plates were subjected to gentle orbital-agitation (100 rpm; 37°C) as a means to replicate fluid dynamics *in vivo* and mitigate interference from the aqueous boundary layer, as indicted by *in silico* simulations of the model (Appendix B) [188, 189]. Upon completion of the assay, both chambers (apical and basal) were immediately sampled for subsequent analysis and/or storage at -80°C.

$$P_{app} = \left(\frac{dQ}{dt}\right) \times \left(\frac{1}{AC_0}\right)$$

Equation 3: Apparent permeability calculation where dQ/dt is the steady-state flux (rfu s^{-1} or µmol s^{-1}), A is the surface area of the filter (cm^2) and C_0 is the initial concentration of compound in the donor chamber (in rfu or µM) [185].

The apparent permeability coefficient (P_{app}, unit: cm s^{-1}) was determined from the amount of compound transported per time (Equation 3) [185].

2.9. Cell Viability Assay

2.9.1. Materials

3-[4,5-dimethylthiazol-2-yl]-2,5-diphenyl tetrazolium bromide (MTT; M5655, Sigma®, UK); Hank's Balanced Salt Solution (HBSS; H8264, Sigma®, UK); propan-2-ol (I9516, Sigma®, UK); Multiskan Ascent plate reader with Ascent software (MTX LabSystems, USA); Nunc™ MicroWell™ 96-well plates (Thermo Scientific™, UK).

2.9.2. Method

Cell viability was determined based upon the method described by Mosmann [190]. Cells were passaged onto 96-well plates, grown to confluence and washed with HBSS prior to the addition of 3-[4,5-dimethylthiazol-2-yl]-2,5-diphenyl tetrazolium bromide (MTT) (100 µL/well; 1 mg/mL MTT in DMEM without phenol red). Mitochondrial dehydrogenases of viable cells cleave the tetrazolium ring [191], producing purple MTT formazan crystals which are insoluble in aqueous solutions. After 4 h incubation at 37°C, 5 % CO_2, the medium was removed, and the formazan crystals dissolved in propan-2-ol (100 µL/well). The resulting purple solution was spectrophotometrically measured at 560 nm. Absorbance is proportional to cell viability, meaning the higher the absorbance the greater the number of viable cells present.

2.10. Inducing Coenzyme Q_{10} Deficiency

2.10.1. Materials

para-aminobenzoic acid (*p*ABA; A9878, Sigma®, UK).

2.10.2. Method

The use of *para*-aminobenzoic acid (*p*ABA) as a pharmacological reagent to induce CoQ_{10} deficiency was first described by Alam *et al.* [192], and has since been utilised by González-Aragón *et al.* [193] and Duberley *et al.* [194] for their studies in human myeloid leukemia HL-60 and human neuroblastoma SH-SY5Y cells respectively.

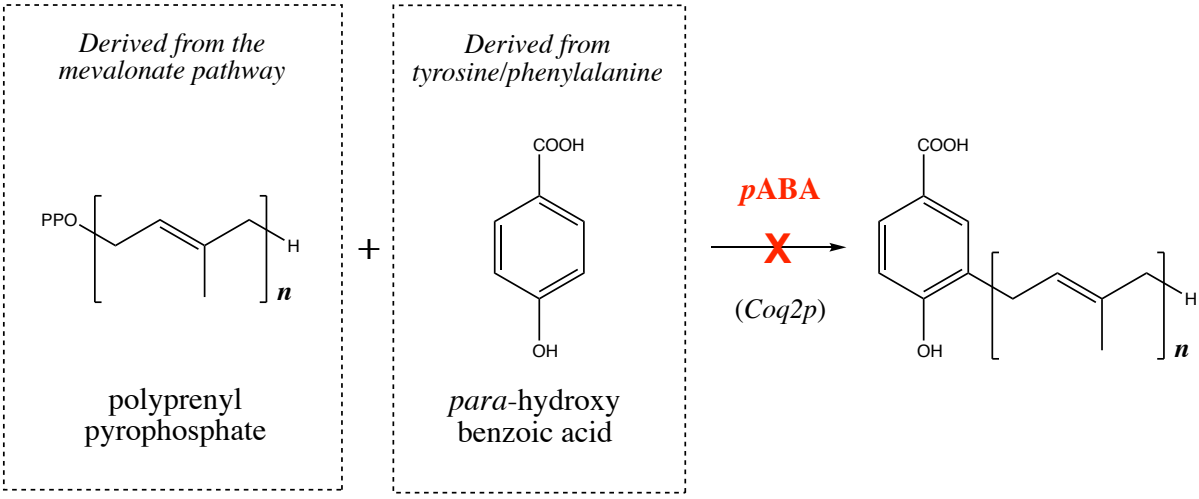

Figure 14: The inhibitory mechanism of action of *para*-aminobenzoic acid (*p*ABA) in CoQ_{10} biosynthesis. *p*ABA inhibits the CoQ_{10} biosynthetic step that is mediated by the Coq2p enzyme.

The mechanism of action is via the competitive inhibition of polyprenyl-4-hydroxybenzoate transferase (Coq2p), a key enzyme in the latter stages of the CoQ_{10} biosynthetic pathway (Figure 14).

Consistent with the aforementioned methods, 1 mmol/L *p*ABA was supplemented into culture medium over a 5-day time course for all cell types.

2.11. Confocal Microscopy

2.11.1. Materials

Nikon® Eclipse Ti-E inverted microscope with NIS-Elements Advanced Research imaging software (Nikon Instruments, Inc., USA); EPR3724 anti-LRP1 monoclonal antibody (ab92544, Abcam PLC, UK); goat anti-rabbit IgG (H+L) cross-adsorbed antibody, Cy5® (A10523, Life Technologies™, USA); clathrin heavy chain polyclonal antibody, Alexa Fluor® 555 conjugated (bs-2932R-A555, Bioss Antibodies™, Inc., USA); 4C3C2 anti-claudin-5 monoclonal antibody, Alexa Fluor® 488 (35-2500, Life Technologies™, USA); VECTASHIELD® antifade mounting medium with DAPI (H-1200, Vector Laboratories Ltd., UK); Dako REAL™ antibody diluent (Agilent Technologies, UK); Triton™ X-100 (T8787, Sigma®, UK); TWEEN® 20 (P9416, Sigma®, UK); Hank's Balanced Salt Solution (HBSS; H8264, Sigma®, UK); Dulbecco's Phosphate Buffered Saline (PBS; D8537, Sigma®, UK).

2.11.2. Methods

Fixing

Adherent cells grown on polyethylene Transwell®-inserts were immediately fixed, post-assay, for subsequent immunofluorescent analysis using confocal microscopy. The cells were washed with HBSS (× 2) prior to being treated with paraformaldehyde (0.4 mL apical, 1.2 mL basal; 4 % (w/v) in PBS) for 30 minutes at room temperature. The paraformaldehyde fixing solution was then removed and the cells washed with HBSS (× 2) before being stored at 4°C in glycerol solution (0.4 mL apical, 0.4 mL basal; 70 % (v/v) in PBS).

Staining

Cells were selectively stained for immunofluorescent imaging of the LDL transporter LRP-1, the tight junction protein claudin-5, the transcytic vesicular protein clathrin, and the nuclei. Prior to commencing the staining procedures, glycerol storage solution was

aspirated, the fixed cells were then washed with HBSS (× 3), permeabilised with Triton™ X-100 (0.1 % (v/v) in PBS) for 5 minutes, and subsequently washed again in HBSS (× 2).

The monoclonal primary antibody EPR3724 (anti-LRP1, rabbit IgG) was used for specific staining of LRP-1. Cells were treated with the antibody (200 μL; 1:49 (v/v) in DAKO antibody diluent) overnight in a humid box at 4°C. The primary antibody solution was then aspirated and the cells repeatedly washed with TWEEN® 20 (0.5 mL; 0.1 % (v/v) in PBS) for 10 minutes (× 3). Goat anti-rabbit IgG (H+L) cross-adsorbed secondary antibody, Cy5® conjugated (200 μL; 1:99 (v/v) in Dako antibody diluent), was then added for 3 h at 37°C for the detection of EPR3724 in the far red region. The secondary antibody solution was aspirated and the cells repeatedly washed with TWEEN® 20 (0.5 mL; 0.1 % (v/v) in PBS) for 10 minutes (× 3), and subsequently with HBSS before mounting.

The clathrin heavy-chain polyclonal antibody, Alexa Fluor® 555 conjugated (anti-clathrin, rabbit IgG), was used for the detection of clathrin in the red region. Cells were treated with the antibody (200 μL; 1:99 (v/v) in Dako antibody diluent) overnight in a humid box at 4°C. The antibody solution was then aspirated and the cells repeatedly washed with TWEEN® 20 (0.5 mL; 0.1 % (v/v) in PBS) for 10 minutes (× 3), and subsequently with HBSS before mounting.

The monoclonal antibody 4C3C2, Alexa Fluor® 488 conjugated (anti-claudin-5, mouse IgG1), was used for the detection of claudin-5 in the green region. Cells were treated with the antibody (200 μL; 1:79 (v/v) in Dako antibody diluent) overnight in a humid box at 4°C. The primary antibody solution was then aspirated and the cells repeatedly washed with TWEEN® 20 (0.5 mL; 0.1 % (v/v) in PBS) for 10 minutes (× 3), and subsequently with HBSS before mounting.

Once stained, the polyethylene filters were removed from the Transwell®-insert using a scalpel, and the cells mounted onto slides with VECTASHIELD® antifade mounting medium containing DAPI for the detection of the nuclei in the blue region. Slides were then sealed with nail varnish for later batch analysis.

Imaging

An A1 Nikon inverted confocal microscope was used to image the cells with a 40×/ objective lens. Laser wavelengths were set at (excitation/emission); DAPI blue 360/465 nm, Alexa Fluor® green 488/520 nm, Alexa Fluor® red 555/568 nm, Cy5® far-red 645/665 nm. The collected tif. files were analysed using image analysis software, ImageJ (National Institutes of Health).

2.12. Lipoprotein Fractionation

2.12.1. Materials

Calcium chloride (Merck Chemicals Ltd., UK); sodium chloride (S7653, Sigma®, UK); dextran sulfate (MWt. 2×10^6, Sigma®, UK); sodium dodecyl sulfate (436143, Sigma®, UK).

2.12.2. Method

Serum lipoproteins were fractionated in accordance to the method described by Ononogbu *et al.* [195]. The method is comprised of two parallel precipitation-centrifugation extractions, yielding a separation of the three major classes of lipoprotein; VLDL, LDL and HDL. Serum was sampled from an identical source for both stages of the fractionation process.

HDL Fractionation

Calcium chloride (50 µL; 22.2 % (w/v) in *dd*H_2O) and dextran sulfate (40 µL; 5 % (w/v) in *dd*H_2O) were added to an aliquot of serum-sample (1 mL), the contents mixed thoroughly, and the mixture set aside for 24 h, 4°C.

After 24 h, the mixture was centrifuged at 310 *g*, for 25 minutes, 4°C. The resulting supernatant was collected for analysis of CoQ_{10} content in the HDL fraction.

LDL/HDL Fractionation

Sodium dodecyl sulfate (75 µL; 10 % (w/v) in 0.15 M $NaCl_{(aq)}$) was added to an aliquot of serum-sample (1 mL), the contents mixed thoroughly, and the mixture set aside for 2 h, 37°C.
After 2 h, the mixture was centrifuged at 7800 *g*, for 10 minutes, 25°C. The resulting supernatant was collected for analysis of CoQ_{10} content in the LDL/HDL fraction.

2.13. Coenzyme Q_{10} Quantitation

2.13.1. High-Performance Liquid Chromatography

Materials

PU-980 intelligent HPLC pump (Jasco Inc., USA); AS-950 intelligent auto-sampler (Jasco Inc., USA); FP-920 intelligent UV detector (Jasco Inc., USA); HiQ sil™ 5 µm C18HS 4.6 × 150 mm column (KYA Technologies Corp., Japan); Jetstream II *Plus* column thermostat (Kromatek, UK); AZUR chromatography software (Kromatek, UK); Chromacol™ HPLC vials and caps (Thermo Scientific™, UK); 60 % (v/v) perchloric acid (HiPerSolv Chromanorm®, VWR International Ltd., UK); methanol (HiPerSolv Chromanorm®, VWR International Ltd., UK); ethanol (HiPerSolv Chromanorm®, VWR International Ltd., UK); *n*-hexane (HiPerSolv Chromanorm®, VWR International Ltd., UK); centrifugal vacuum concentrator 5301 (Eppendorf®, UK).

Method

The current 'gold-standard' method for CoQ_{10} quantitation in accredited clinical laboratories is based on a reversed-phase HPLC-UV technique described by Boitier *et al.* [196]. The lower limit of quantitation for this method is 10 nmol/L, with a limit of detection at 6 nmol/L, and linearity up to 200 nmol/L (Figure 16). The run-time (inject-to-inject) per sample is 25 minutes.

In an attempt to account for the loss of analyte during sample preparation a dipropoxy-CoQ_{10} internal standard (IS) was incorporated in a method first proposed by Duncan *et al*. [197]. IS (0.2 μmol/L) was added to each sample prior to extraction, samples then underwent a freeze-thaw process (× 3) to perturb the cellular membranes. CoQ_{10} was then extracted by the addition of hexane/ethanol (800 μL; 5:2, v/v). Samples were then vigorously mixed on a vortex for 1 minute, centrifuged at 18625 × *g* for 3 minutes, 20°C, and the top-layer of hexane collected. Hexane was evaporated to dryness using a centrifugal evaporator, the sample re-suspended in ethanol (300 μL) and passed through a 0.2 μm filter ahead of injection.

The mobile phase for the HPLC system was prepared by dissolving sodium perchlorate (7 g) in ethanol/methanol/60 % (v/v) perchloric acid (1 L; 700:300:1.2, v/v/v). An isocratic flow rate of 0.7 mL/min was maintained throughout.

A working standard (0.2 μM CoQ_{10} and 0.2 μM dipropoxy-CoQ_{10}) was injected for calibration. 50 μL of each sample was injected and separated on a C18 reversed-phase column, maintained at 25°C. CoQ_{10} was detected using an online UV detector at a wavelength of 275 nm (Figure 15).

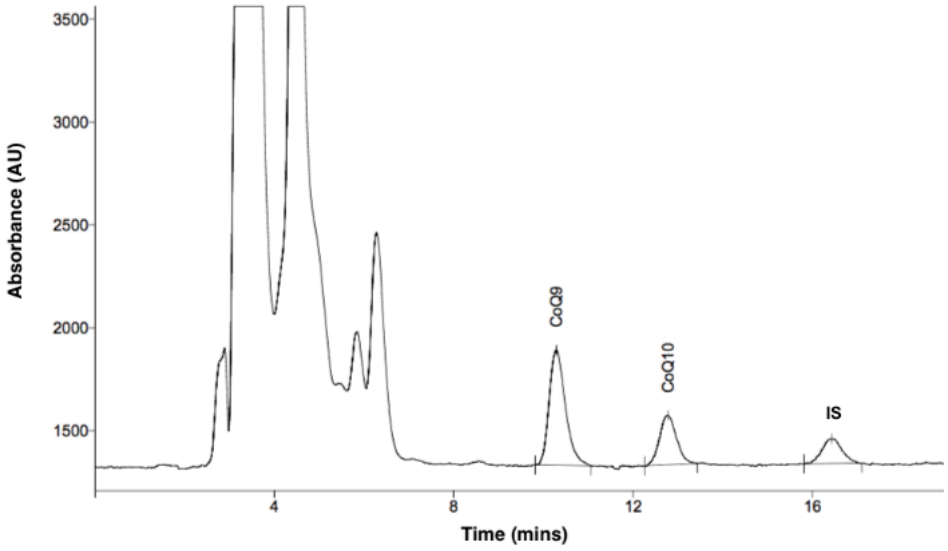

Figure 15: HPLC-UV chromatogram for CoQ_{10}, CoQ_9 and the in-house internal standard dipropoxy-CoQ_{10} (IS).

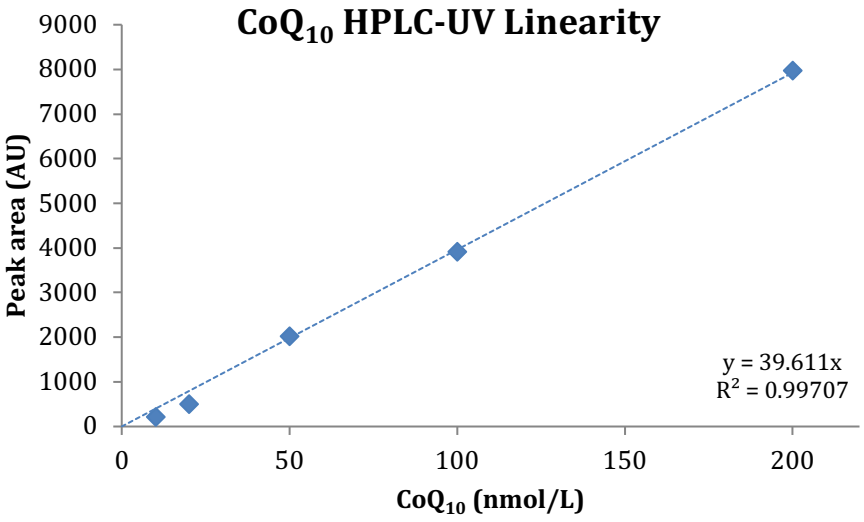

Figure 16: Serial dilution linearity of HPLC-UV CoQ_{10} peak area vs. CoQ_{10} concentration, reaching a lower limit of detection at 10 nmol/L.

CoQ_{10} was quantified using the following equation:

$$CoQ_{10}\ (\text{nmol/L}) = \left(\frac{\text{peak area}}{\text{IS peak area}}\right) \times \text{IS conc.}$$

Dilution factor:

$$\text{Final } CoQ_{10} \text{ conc.} = CoQ_{10} \text{ conc.} \times \left(\frac{\text{resuspension vol.}}{\text{extraction vol.}} \right)$$

For intracellular determination of CoQ_{10} the concentration was divided by total protein (mg/mL) and expressed as pmol/mg (nmol/g) of protein.

2.13.2. Tandem Mass Spectrometry

Materials

QTRAP® 6500 (ESI)-MS/MS system with Analyst® software v 1.6 (AB Sciex™, UK); 1200 Series LC system (Agilent Technologies, USA); HTS PAL® DLW-2 auto-sampler (CTC Analytics AG, Switzerland); ACE® UltraCore™ 2.5 µm SuperC18™ 30 × 2.1 mm column (Advanced Chromatography Technologies Ltd., UK); ACE® C18 2.1 mm guard-column and cartridges (Advanced Chromatography Technologies Ltd., UK); ACE® ColumnShield™ 0.5 µm pre-column filters (Advanced Chromatography Technologies Ltd., UK); Chromacol™ 300 µL fused-insert 9 mm screw-thread amber vials with auto-sampler caps (Thermo Scientific™, UK); 1-propanol (Chromasolv™, Honeywell™ Riedel-de Haën™, UK); methanol (M/4062, Fisher Chemical, UK); ethanol (AnalaR NORMAPUR®, VWR International Ltd., UK); hexane (HPLC Grade, Fisher Chemical, UK); 7.5 M ammonium acetate solution (A2706, Sigma®, UK); coenzyme Q_{10}–[$^2H_9$] (IsoSciences LLC, USA); coenzyme Q_{10} (C9538, Sigma®, UK); Uvikon XL spectrophotometer with LabPower software (Northstar Scientific Ltd., UK); sodium borohydride (ReagentPlus®, Sigma®, UK); CE100/CVP100 centrifugal vacuum evaporator (Genevac Ltd., UK).

Method

A novel CoQ_{10} LC-MS/MS method was established. The method is a modified version of that described by Itkonen *et al*. [198], in combination with the sample prep outlined in the HPLC-UV (Section 2.13.1). The lower limit of quantitation for this method is 0.25 nmol/L,

with a limit of detection 0.125 nmol/L, and linearity up to 500 nmol/L. The run-time (inject-to-inject) is 7 minutes per sample (Figure 17).

Calibrator Preparation

CoQ_{10}, and all other quinones in the homologous series, contain a 2,3-dimethoxy-5-methylbenzoquinone core which absorbs light in the UV region of the electromagnetic spectrum at 275 nm. In a method first described by Crane *et al.* [199], it is possible to spectrophotometrically analyse the decrease in absorbance in response to a reduction of the quinone core to 2,3-dimethyl-5-methylbenzoquinol using sodium borohydride ($NaBH_4$) and, therefore, quantify CoQ_{10} content of a pure calibrator standard.

$$c = \frac{\Delta A \; x \; l}{\varepsilon}$$

Equation 4: Beer-Lambert law where ΔA is the specific change in absorbance; ε = extinction coefficient; *l* = path length (1 cm); and *c* = moles [200].

Stock CoQ_{10} calibrator standard (1 mM) was diluted (1:99 (v/v) in ethanol) and aliquoted into analogous sample and reference quartz cuvettes (1 mL). $NaBH_4$ was added to the reference cuvette and the change in absorbance at 275 nm recorded after 5 minutes on a spectrophotometer. This process was repeated a further 3 times and an average taken. CoQ_{10} concentration was subsequently determined from the Beer-Lambert law (Equation 4) [200]. The molar coefficient of CoQ_{10} is 14.6×10^3 M^{-1} cm^{-1}.

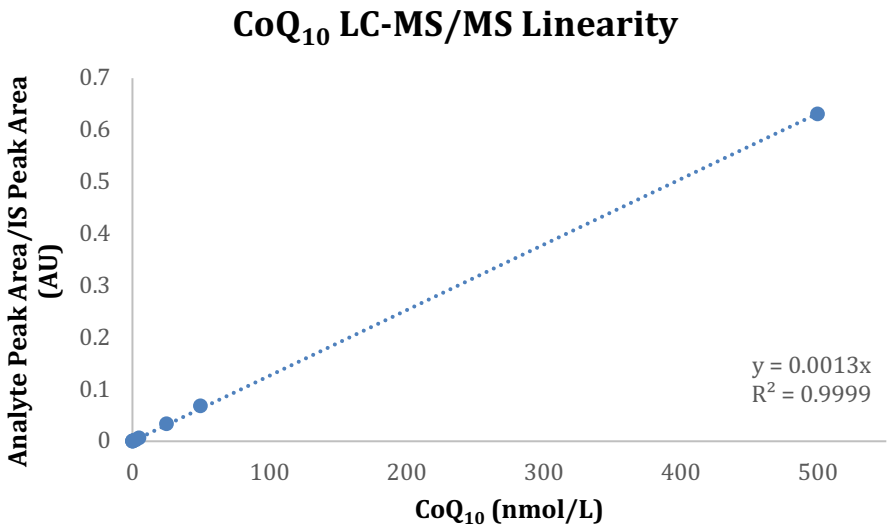

Figure 17: LC-MS/MS CoQ_{10} serial dilution linearity graph reaching a lower limit of detection at 0.125 nmol/L – calibration curves were derived using 1/x weighted linear least-squares regression, as calculated by the Analyst® software package. Calibration curves were accepted if $R^2 \geq 0.998$.

CoQ_{10} calibration curves were established by serial dilutions of a 1 mM stock solution as confirmed by spectrophotometric methods outlined above (200 µL; 0, 0.25, 0.5, 1.0, 2.5, 5.0, 25, 50, 500 nmol/L in ethanol). Stable isotope-labelled internal standard was added to each calibrator (CoQ_{10}–[$^2H_9$]; ~1 µmol/L), the calibrator standards were then vigorously mixed and evaporated to dryness on a centrifugal vacuum evaporator. Prior to analysis, calibrators were re-constituted in LC-MS/MS *'running solvent A'* (50 µL; 41:9 (v/v) methanol/1-propanol with 500 µmol/L ammonium acetate), vigorously mixed, and transferred into a suitable vial.

Fresh calibrators were made-up alongside every analytical batch. Calibrators were not extracted, as per sample preparation below, since there was no quantifiable difference in absolute values between 'extracted' versus 'non-extracted' calibrator standards.

Sample Preparation

Samples were prepared by the addition of stable isotope-labelled internal standard (CoQ_{10}–[$^2H_9$]; ~1 µmol/L) to each sample (200 µL), with a subsequent freeze-thaw process (× 3) to perturb cellular membranes. Extraction buffer was then added (800 uL/sample; 5:2 (v/v) hexane/ethanol) and the samples vigorously mixed on a vortex for

1 minute, centrifuged at 18625 × *g* for 3 minutes, and the top-layer of hexane collected. The hexane extract was evaporated to dryness using a centrifugal evaporator. Prior to analysis, calibrators were re-constituted in LC-MS/MS *'running solvent A'* (50 µL; 41:9 (v/v) methanol/1-propanol with 500 µmol/L ammonium acetate), vigorously mixed, and transferred into a suitable vial.

LC-MS/MS Acquisition Parameters

Chromatography was performed on a C18 reversed-phase column kept at 25°C with a gradient of running solvent A (41:9 (v/v) methanol/1-propanol with 500 µmol/L ammonium acetate) and running solvent B (1:1 (v/v) methanol/1-propanol with 500 µmol/L ammonium acetate). The gradient elution profile was maintained at 100 % A (0 – 0.2 min), ramped to 100 % B (0.21 – 1 min), maintained at 100 % B (1 – 3.5 min), and ramped back to 100 % A (3.51 – 3.6 min). Total run time was 6.5 minutes with a flow rate of 220 µL/min and inject volume of 10 µL.

The mass spectrometer was operated in positive ion mode with the ion source spray voltage at 5500 V, declustering potential at 50 V, temperature at 115°C, and collision energy at 27 V. The curtain gas was 48 L/min, gas 1 (nebuliser gas) 55 L/min, gas 2 (heater gas) 21 L/min, and collision gas on 'medium' setting. The mass spectrometer was programmed to follow the transitions of *m/z* 880.7 -> 197.1 (dwell time 200 ms) corresponding to the ammonium adduct of CoQ_{10}, and *m/z* 889.7 -> 206.1 (dwell time 200 ms) corresponding to the ammonium adduct of CoQ_{10}–[$^2H_9$].

Final CoQ_{10} concentrations (nmol/L) were calculated as a ratio of CoQ_{10}/CoQ_{10}–[$^2H_9$] peak areas, and quantified against the corresponding calibration curve (Figure 17), with dilution factors corrected for accordingly. For intracellular determination of CoQ_{10} the concentration was divided by total protein (mg/mL) and expressed as pmol/mg (nmol/g) of protein (Section 2.15).

2.14. Mitochondrial Respiratory Chain Enzyme (MRCE) Assays

2.14.1. Materials

Uvikon XL spectrophotometer with LabPower software (Northstar Scientific Ltd., UK); spectrophotometer cuvettes (C5416, Sigma®, UK); dipotassium hydrogen phosphate (K_2HPO_4; P5504, Sigma®, UK); potassium dihydrogen phosphate (KH_2PO_4; Sigma®, UK); Triton™ X-100 (T8787, Sigma®, UK); Trizma® base (T1503, Sigma®, UK); ethanol (AnalaR NORMAPUR®, VWR International Ltd., UK); Bovine Serum Albumin (BSA; A6003, Sigma®, UK); β-Nicotinamide Adenine Dinucleotide (β-NADH; N6785, Sigma®, UK); potassium cyanide (KCN; 60178, Sigma®, UK); magnesium chloride ($MgCl_2$; M2670, Sigma®, UK); coenzyme Q_1 (C9538, Sigma®, UK); rotenone (R8875, Sigma®, UK); ethylenediaminetetraacetic acid (EDTA; ED2P, Sigma®, UK); cytochrome *c* (C7752, Sigma®, UK); sodium succinate (S2378, Sigma®, UK); antimycin A (A8674, Sigma®, UK); sodium L-ascorbate (A7631, Sigma®, UK); PD-10 desalting column (GE Healthcare, UK); potassium ferricyanide (60299, Sigma®, UK); acetyl-coenzyme A (A2056, Sigma®, UK); 5,5'-dithio-bis(2-nitrobenzoic acid) (DNTB; D218200, Sigma®, UK); oxaloacetate (O4126, Sigma®, UK).

2.14.2. Methods

Complex I (NADH: ubiquinone reductase; EC 1.6.5.3)

Complex I activity was determined based on the method described by Reed *et al.* [201]. Electrons derived from the oxidation of NADH are transferred through complex I to exogenously added CoQ_1, which in turn is reduced to CoQ_1H_2. Complex I activity is subsequently measured as the rotenone-sensitive decrease in NADH at 340 nm.

Rotenone, a specific complex I inhibitor, is used to determine the background level of Complex I independent NADH oxidation. Rotenone acts on the matrix embedded long arm of the enzyme, arresting electron transfer from the Fe-S cluster to CoQ_1 [202].

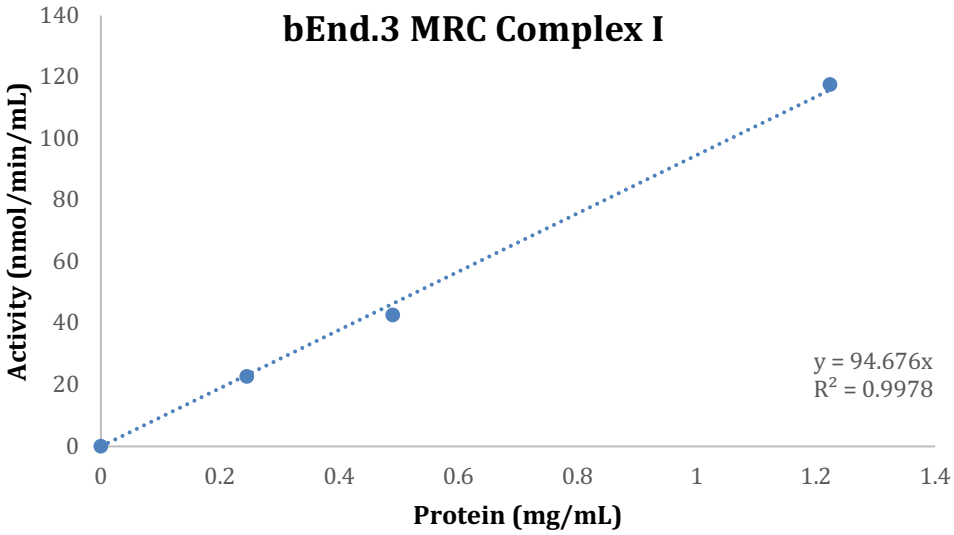

Figure 18: bEnd.3 MRC complex I activity linearity.

Sample (20 µL) was added to two analogous cuvettes (1 mL) containing BSA (2.5 mg/mL), β-NADH (0.15 mmol/L), and KCN (1 mmol/L) in a 20 mM potassium phosphate buffer (*p*H 7.2) with $MgCl_2$ (8 mmol/L). Duplicate cuvettes were then gently mixed by double inversion and placed into the corresponding reference and sample compartments of the spectrophotometer. The reaction was initiated by the addition of CoQ_1 (50 µmol/L) into the sample cuvette and monitored at an absorbance of 340 nm at 30 second intervals for 5 minutes, 30°C. Rotenone (20 µmol/L) was then added to each sample cuvette and the reaction monitored for a further 5 minutes to establish any background activity. Subtraction of the background absorbance from the initial absorbance yielded a specific rate of absorbance for Complex I.

Absorbance was converted to molar concentration using the Beer-Lambert law (Section 2.13.2, Equation 4) [200]. The extinction coefficient of NADH-CoQ_1 is 6.81×10^3 M^{-1} cm^{-1}. Results are expressed as nmol/min/mg of protein (Section 2.15) and/or as a ratio to citrate synthase activity (Figure 18).

Complex II-III (succinate dehydrogenase: cytochrome c reductase)

Complex II-III activity was determined based on the method described by Bhuvaneswaran *et al.* [203]. Complex II (succinate dehydrogenase; EC 1.3.5.1) catalyses the oxidation of succinate to fumarate and in the process reduces CoQ_{10} to $CoQ_{10}H_2$. Ubiquinol then acts as an electron carrier facilitating the reduction of cytochrome c catalysed by Complex III (ubiquinol-cytochrome c oxidoreductase; EC 1.10.2.2). Complex II-III activity is then selectively measured by the succinate-dependent Antimycin A sensitive reduction of cytochrome c at 550 nm.

Antimycin A, a complex III inhibitor that binds to the Q_i site of cytochrome c reductase, is added to determine the background level of complex II-III independent cytochrome *c* reduction.

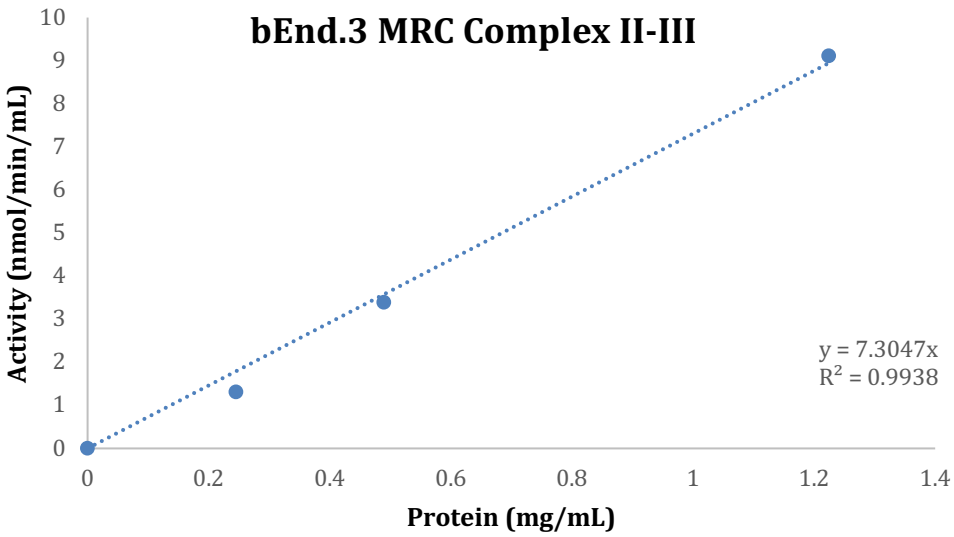

Figure 19: bEnd.3 MRC complex II-III activity linearity.

Sample (20 µL) was added to two analogous cuvettes (1 mL) containing EDTA (0.3 mmol/L), KCN (1 mmol/L), and cytochrome *c* (0.1 mmol/L) in a 100 mM potassium phosphate buffer (*p*H 7.4). Duplicate cuvettes were then gently mixed by double inversion and placed into the corresponding reference and sample compartments of the spectrophotometer. The reaction was initiated by the addition of succinate (20 mmol/L) in the sample cuvette. The reaction was measured at an absorbance of 550 nm at 30 second intervals for 5 minutes, 30°C. Antimycin A (10 µmol/L) was then added to each

sample cuvette and the measurement was continued for a further 5 minutes. Subtraction of the background absorbance from the initial absorbance yields a specific rate of absorbance for Complex II-III.

Absorbance was converted to molar concentration using the Beer-Lambert law (Section 2.13.2, Equation 4) [200]. The extinction coefficient of cytochrome *c* is 19.2 × 10^3 M^{-1} cm^{-1}. Results are expressed as nmol/min/mg of protein (Section 2.15) and/or as a ratio to citrate synthase activity (Figure 19).

Complex IV (cytochrome c oxidase; EC 1.9.3.1)

Complex IV was measured based on the method described by Tzagoloff *et al.* [204]. The assay measures the oxidation of cytochrome *c* catalysed by complex IV.

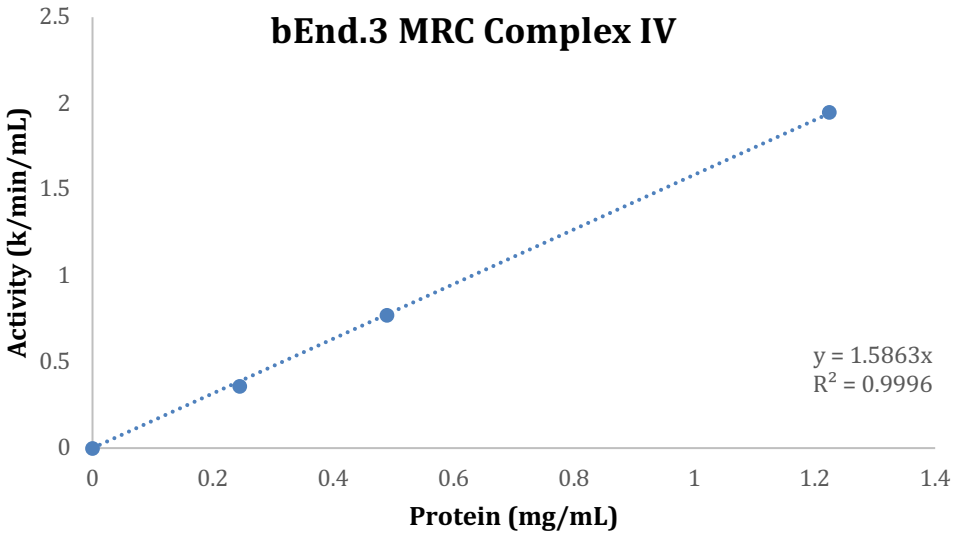

Figure 20: bEnd.3 MRC complex IV activity linearity.

Oxidized cytochrome c (0.8 M) is first reduced by the addition of a few crystals of ascorbic acid. The solution was then passed through a PD-10 desalting column, equilibrated with a 10 mM potassium phosphate buffer (*p*H 7.0), to remove the ascorbate. The concentration of the reduced cytochrome *c* was then determined against a reference sample; reduced cytochrome *c* was diluted (1:19 (v/v) in *dd*H_2O) and added to two analogous cuvettes (1 mL), the sample was blanked against the reference at 550 nm using

a spectrophotometer and ferricyanide (1 mmol/L) added to the reference cuvette, oxidising the cytochrome *c*. The absorbance was recorded after 1 minute and the concentration of reduced cytochrome *c* determined using Beer-Lambert law (Section 2.13.2, Equation 4) [200]. The extinction coefficient for reduced cytochrome *c* is 19.2×10^3 M^{-1} cm^{-1}.

Reduced Cytochrome c (50 µmol/L) was then added to analogous sample and reference cuvettes (1 mL) containing a 10 mM potassium phosphate buffer (*p*H 7.0). The sample was blanked against the reference at 550 nm using a spectrophotometer. Ferricyanide (1 mM) was added to the reference cuvette. The reaction was initiated by the addition of sample (20 µL) to the sample cuvette and the change in absorbance at 550 nm was recorded over 3 minutes, 30°C.

The reaction of complex IV with cytochrome c follows first-order kinetics as it is dependent on the concentration of cytochrome *c*. Activity is therefore expressed as a first order rate constant (k). k is calculated by plotting the natural log of absorbance against time and determining the gradient. Results are expressed as k/min/mg of protein (Section 2.15) and/or as a ratio to citrate synthase activity (Figure 20).

Citrate Synthase (EC 2.3.3.1)

Citrate synthase is an enzyme in the citric acid cycle which catalyses the condensation of oxaloacetate and acetyl-coenzyme A to form citric acid and coenzyme A. It is exclusively localised within the mitochondrial matrix and is widely accepted as a marker of mitochondrial enrichment or depletion [205].

The assay was performed based on methods described by Shepherd and Garland [206], and measures the production of 5-thio-2-nitrobenzoic acid (TNB) at 412 nm, via the reaction of coenzyme A with 5,5'-dithio-bis(2-nitrobenzoic acid) (DTNB).

Given that citrate synthase serves as a marker for intact mitochondria, corresponding MRCE values are often expressed as a ratio to citrate synthase.

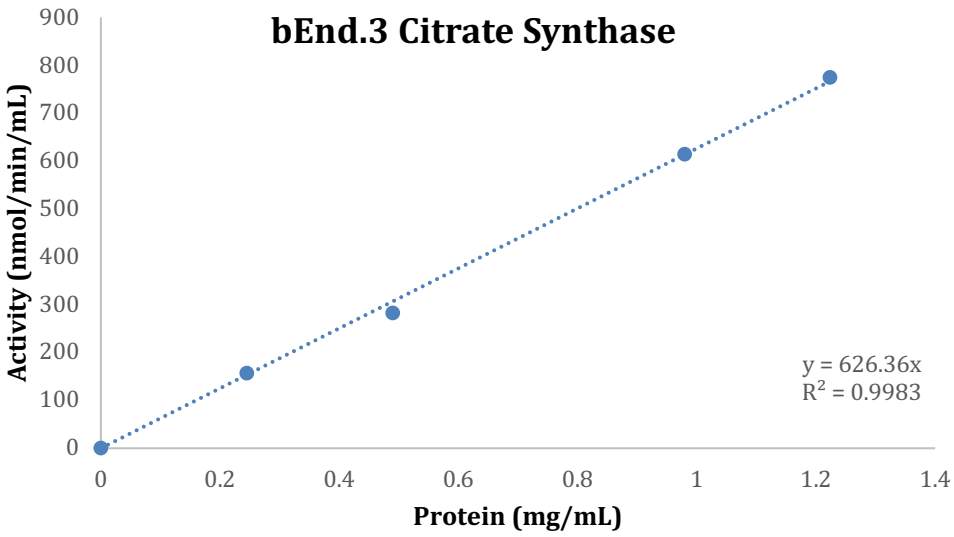

Figure 21: bEnd.3 citrate synthase linearity.

Sample (20 µL) was added to two analogous cuvettes containing acetyl-coenzyme A (0.1 mmol/L), DTNB (0.2 mmol/L) in a 100 mM tris buffer (*p*H 8.0) with triton X-100 (1 g/L). Duplicate cuvettes were then gently mixed by double inversion and placed into the corresponding reference and sample compartments of the spectrophotometer. The reaction was initiated by the addition of oxaloacetate (200 µmol/L) to the sample cuvette. The reaction was measured at 412 nm for 5 minutes at 30 second intervals, 30°C.

Absorbance was converted to molar concentration and calculated using the Beer-Lambert law (Section 2.13.2, Equation 4) [200]. The extinction coefficient of DTNB is 13.6 × 10^3 M^{-1} cm^{-1}. Results are expressed as nmol/min/mg of protein (Section 2.15).

2.15. Total Protein Determination

2.15.1. Materials

DC total protein assay Reagent A and Reagent B (Bio-Rad Laboratories Ltd., UK); Bovine Serum Albumin (BSA; A6003, Sigma®, UK); spectrophotometer cuvettes (C5416, Sigma®,

UK); Uvikon XL spectrophotometer with LabPower software (Northstar Scientific Ltd., UK).

2.15.2. Method

Total protein was determined by the Bio–Rad DC–protein assay. This assay is a modified method based on that of Lowry *et al.* [207] which monitors the reaction of protein with an alkaline copper tartrate solution and Folin reagent. There are two steps which lead to colour development; the reaction between protein and copper in an alkaline medium, and the subsequent reduction of Folin reagent by the copper-treated protein. Colour development is primarily due to the amino acids tyrosine and tryptophan, and to a lesser extent, cystine, cysteine, and histidine. Proteins effect a reduction of the Folin reagent by loss of 1, 2, or 3 oxygen atoms, thereby producing one or more of several possible reduced species which have a characteristic blue colour with maximum absorbance at 750 nm.

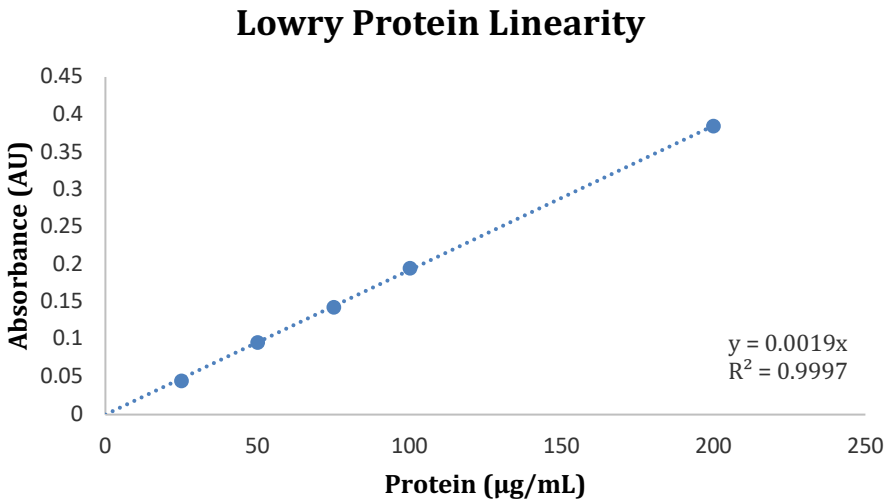

Figure 22: Lowry total protein determination – Bovine Serum Albumin (BSA) linearity.

The assay was performed as per the manufacturer's instructions. Briefly, all samples were diluted in *dd*H_2O, a 6–point standard curve was prepared with bovine serum albumin (BSA) solution (0, 25, 50, 75, 100, 200 µg/mL) (Figure 22). Reagent A (alkaline copper tartrate; 100 µL) and Reagent B (Folin-Ciocalteau phenol; 800 µL) were added to

the sample/standard solution (200 µL). Samples/standards were then vigorously mixed for 30 seconds, incubated for 25 minutes, 25^{o}C, in the dark, and subsequently measured at 750 nm on a spectrophotometer. Total protein was subsequently determined from linear regression of sample absorbance units against the BSA standard curve.

2.16. Statistical Analysis

All results are expressed as mean ± standard error of the mean (SEM). Individual comparisons of means were made using the two-sample Student's t-test and were carried out using Microsoft® Excel with AnalystSoft® StatPlus software. To reduce the incidence of type 1 error that is associated with performing multiple two-sample t-test's, one-way ANOVA was used for comparison of groups > 2, with Bonferroni post-hoc analysis. In all cases $p < 0.05$ was considered significant. Ratios were transformed prior to statistical analysis using the arcsine square-root transformation to minimise the negative skew of distribution produced when expressing proportions [208, 209].

3. Validation of Experimental and Analytical Procedures

3.1. Background

3.1.1. CoQ_{10} Analysis using Mass Spectrometry

The current 'gold-standard' analytical technique for CoQ_{10} determination in clinical laboratories is HPLC-UV. The method exploits the ability of the CoQ_{10} benzoquinone core to absorb UV light at 275 nm and is highly reliable. However, it is time consuming, with a run-time of *ca*. 20 minutes per sample, it has a quantitation limit of 10 nmol/L, and is susceptible to interference [197]. Consequently, alternative technologies are being explored to mitigate and overcome these limitations.

Although mass spectrometry (MS) has been around for many decades, the application of MS in routine clinical laboratories has increased significantly in recent years [210]. This is primarily due to the very high specificity, superior sensitivity, and simultaneous analysis of multiple analytes (> 100) that MS can offer. Furthermore, the coupling of tandem mass spectrometry with liquid chromatography (LC-MS/MS) has enabled the separation of isobaric compounds which once limited its application, and has been a key development in the rapid expansion of this technology [211-213].

In-line with the recent popularity of CoQ_{10} research, numerous LC-MS/MS methods for CoQ_{10} analysis have surfaced over the years, each offering superior sensitivity and speed compared to the HPLC-UV 'gold-standard', and they will most likely supersede the current methodology in clinical laboratories [198, 214-218].

A major incentive for this technological shift is an emerging clinical need for diagnosis and treatment monitoring in CSF, since there is a clear preponderance of ataxic and neurological presentation associated with CoQ_{10} deficiencies. Recent studies have tentatively indicted that the baseline concentrations of CoQ_{10} in CSF are < 9 nmol/L [214, 219, 220], a concentration that is undetectable by HPLC-UV. Additionally, the limited efficacy of CoQ_{10} treatment for neurological presentation suggests that there could be a poor

permeability of CoQ_{10} across the BBB, meaning HPLC-UV may also be insufficient for treatment monitoring. The other, more obvious, advantage of transitioning to LC-MS/MS is speed, since the high level of specificity afforded through selective reaction monitoring allows for a less intensive sample preparation and, in most cases, a reduced chromatographic separation. This enables quicker run-times and a more efficient diagnostic service – an essential criterion for successful implementation of innovation in the NHS [221].

Given the predicted poor permeability of CoQ_{10} at the BBB and the clear benefits of LC-MS/MS for low-level quantitation, a novel LC-MS/MS method to be used for *in vitro* BBB investigations and clinical diagnostics is proposed.

3.1.2. *In vitro* BBB Experimental Design

As introduced in Section 1.4, the BBB is a highly-specialised, low-permeability interface between the central nervous system and the circulating blood and is a primary component of the neurovascular unit which serves to maintain the finely balanced *interior milieu* of the brain parenchyma [142]. The specific structure and function of the BBB can make it difficult to replicate in an *in vitro* model. It is therefore important to establish a model that is as close to the *in vivo* environment as possible. With this in mind cell culture models, based on either primary or immortalised brain endothelial cell lines, have been developed in order to facilitate *in vitro* studies of molecular transport to the brain and endothelial cell pathophysiology [166, 167].

While no one model exactly mimics the *in vivo* BBB expression of enzymes, transporters, receptors, and structural proteins, it is the primary cell models which exhibit the best *in vivo* – *in vitro* correlation. Given that access to human primary brain material is very limited and restricted to biopsy or autopsy material from patients with established disease [222], researchers have resorted to isolations from healthy animals as a more feasible source of material for primary cultures. To date, the endothelial cells that have been characterised as providing *in vivo*-like functionality, tight barrier integrity, and low paracellular permeability are primary porcine [223], bovine [224], and rodent [166, 225, 226]. Due to the much lower yield of endothelial cells from rat brains (1–2 million cells per rat

brain), bovine and porcine brains (up to 200 million cells per brain) are the most popular choice for *in vitro* BBB models both in academia and industry [186].

The introduction of astrocytes in the growth stage of primary cultures has been shown to greatly improve functional parameters of the BBB [227], with astrocytic co-cultures of both bovine and porcine endothelial cells having been shown to produce a transendothelial resistance of up to 1600 $\Omega \cdot cm^2$ [167]. This is a result of crosstalk of secretion factors between the cell types that enhance maturation of the BBB to a level comparable with that *in vivo* [143]. Additionally, the primary cultures of the *in vitro* BBB have the lowest paracellular permeability and the most comprehensive expression and polarisation of characteristic BBB transporters. All these factors combined position them as the gold-standard for *in vitro* investigations into molecular transport at the BBB.

However, the use of primary cells is very expensive, time-consuming, technically demanding, and requires a high consumption of animals per isolation. Therefore, immortalised cell lines have been developed for BBB permeability studies and are commonly used as a platform for high-throughput and/or first-line investigations [228].

Immortalised cells of murine [229], rat [230], bovine [231], porcine [232], and human [233] have been established and, in addition to being considerably cheaper and far less technically demanding, these cell lines have the advantage of being usable over many passages with a higher reproducibility of results compared to primary cells. While the functional parameters of these immortalised cell lines are markedly inferior to the primary *in vitro* BBB models, with TEERs frequently as low as $\sim 50\ \Omega \cdot cm^2$, they are sufficient for large molecule investigations and are the best compromise between functionality and practicality [166, 167].

Based on the relative merit and limitations of the available *in vitro* models of the BBB, the investigation strategy adopted for this project was to perform initial studies on the commercially available mouse brain endothelial cell line, bEnd.3, with subsequent investigation of promising findings to be made on the primary porcine brain endothelial cell, PBEC, model in co-culture with primary rat astrocytes.

3.2. Materials and Methods

3.2.1. Materials

Coenzyme Q_{10} Plasma Control, Level I (0092, ChromSystems®, Germany); Bovine Plasma Derived Serum (BPDS; First Link Ltd., UK); Foetal Bovine Serum (FBS; F7524, Sigma®, UK); HEPES (H3375, Sigma®, UK); HEPES (H3375, Sigma®, UK); Hank's Balanced Salt Solution (HBSS; H8264, Sigma®, UK); Bovine Serum Albumin (BSA; A6003, Sigma®, UK); coenzyme Q_{10} (C9538, Sigma®, UK).

3.2.2. Methods

Coenzyme Q_{10} Quantitation

Unless otherwise stated, CoQ_{10} concentrations were determined using the LC-MS/MS method described in Section 2.13.2. Duplicate samples of ChromSystems® EQC Plasma, IQC 0 (HBSS with 50 % (v/v) BPDS, 0.5 % (w/v) BSA, 25 mmol/L HEPES), and IQC 10 (HBSS with 50 % (v/v) BPDS, 0.5 % (w/v) BSA, 25 mmol/L HEPES, 10 µmol/L CoQ_{10}) were run at the beginning and end of each batch to ensure a consistent intra-batch instrument performance.
Measurements made using the HPLC-UV technique were performed in accordance to Section 2.13.1.

Lipoprotein Fractionation

The CoQ_{10} content in the three major classes of serum lipoprotein was investigated by parallel isolation of the LDL/HDL and HDL fractions within an identical sample of cell culture serum, BPDS, as is outlined in Section 2.12.
In the case of treated-serum, exogenous CoQ_{10} (10 µmol/L) was incubated with BPDS for 45 minutes, 37°C, consistent with the protocol for the preparation of CoQ_{10} assay buffers.

VLDL CoQ_{10} content was calculated as the difference between the total CoQ_{10} in the sample and the CoQ_{10} content found in the LDL/HDL fraction, as determined by LC-MS/MS.

Cell Culture

bEnd.3 cells were cultured as outlined in Section 2.2 and passaged onto Transwell®-inserts for apparent permeability studies, into T-75 flasks for MRCE activity and total CoQ_{10} measurements, or onto 96-well plates for MTT cell viability analysis.
Primary PBECs were isolated and cultured as per Sections 2.3 and 2.4. Cells were passaged onto Transwell®-inserts for apparent permeability studies, into T-75 flasks for total CoQ_{10} measurements, or onto 96-well plates for MTT cell viability analysis.
Primary astrocytes were isolated and cultured in accordance to Sections 2.5 and 2.6, with co-culture coordinated as per Appendix A.

Cell Viability Assay

The effect of treatment conditions on cell viability were assessed against untreated controls using the MTT assay described in Section 2.9. Results are expressed as a relative percentage to untreated controls.

Assessing Barrier Integrity

TEERs were measured across cell mono-layers on Transwell®-inserts as described in Section 2.7.1. Apparent permeability (P_{app}) of *in situ* paracellular markers was evaluated following the experimental procedures outlined in Sections 2.7.2 and 2.8. Assay buffers were made up in HBSS at *p*H 7.4 (Table 6).

Table 6: Composition of assay buffers used in apparent permeability studies. Condition A is the acceptor buffer and conditions B and C are the donor buffers. The serum used in bEnd.3 investigations was FBS and for PBECs it was BPDS.

	BSA (*w/v*)	**HEPES (mmol/L)**	**Serum (*v/v*)**	**FITC-40 (mg/mL)**	**Lucifer Yellow (µg/mL)**
A	0.5 %	25	–	–	–
B	0.5 %	25	50 %	0.5	–
C	0.5 %	25	50 %	–	10

Inducing Coenzyme Q_{10} Deficiency

Cell cultures were pharmacologically induced with a CoQ_{10} deficiency by supplementing culture media with 1 mmol/L *para*-aminobenzoic acid (*p*ABA) for a duration of 5 days, in accordance to the method described in Section 2.10.

MRCE Activities and Cellular CoQ_{10} Determination

Cells were grown to confluence on T-75 flasks, harvested in accordance to their respective trypsination procedures, washed and subsequently collected in PBS (200 µL/confluent T-75 flask). MRCE activities were investigated as per Section 2.14 and total CoQ_{10} content determined by LC-MS/MS. MRCE activities and total CoQ_{10} content are expressed against protein, as determined by the Lowry method outlined in Section 2.15.

3.3. Results

3.3.1. LC-MS/MS Method Development

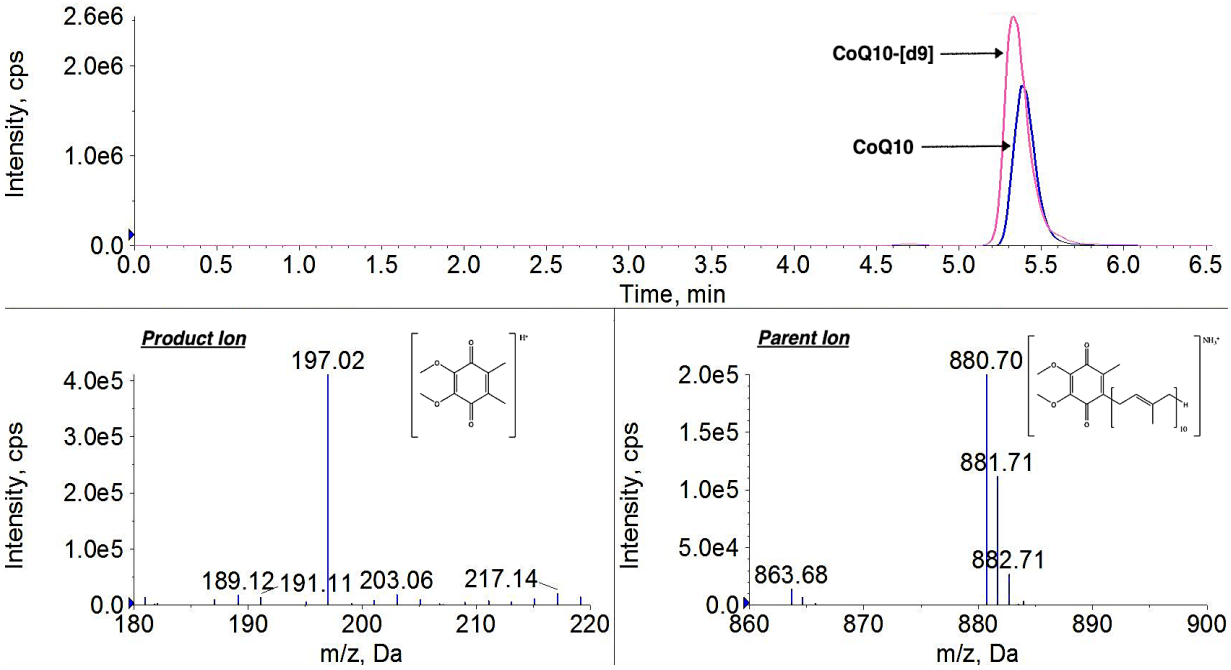

Figure 23: LC-MS/MS CoQ_{10} chromatogram of the top calibrator, 500 nmol/L CoQ_{10} (top chromatogram), with tuned MS scans of the CoQ_{10} product ion (bottom left mass spectrum) and the parent ammonium adduct ion (bottom right mass spectrum) in ESI+ mode.

The optimum combination of LC-MS/MS parameters to yield the highest signal response for CoQ_{10} was achieved by automatically ramping each parameter (ionisation voltages, temperature and interface gases) across a range and then manually fine-tuning. The specific Q1/Q3 transitions were determined by performing a product ion scan of the respective parent ion. The resulting chromatogram (Figure 23) shows very good sensitivity and chromatography for both the CoQ_{10} ammonium adduct (*m/z* 880.7 -> 197.1) and the stable-isotope labelled internal standard, CoQ_{10}-[$^2H_9$] ammonium adduct (*m/z* 889.7 -> 206.1), in selected-reaction monitoring mode.

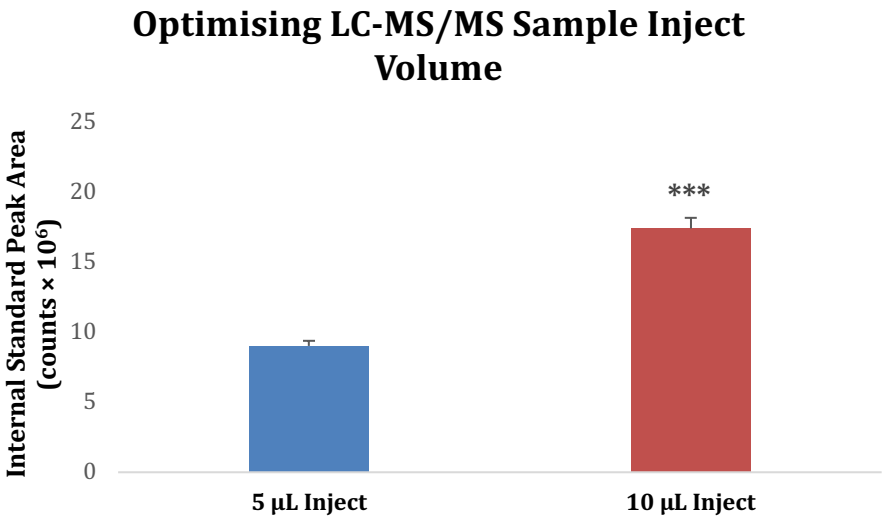

Figure 24: The effect of sample injection volume on analyte signal response in the CoQ_{10} LC-MS/MS method. For both conditions (n = 7). Error bars represent standard error of the mean (SEM).

In addition to optimal tuning of the physical LC-MS/MS parameters, sample injection volume was explored as a method for improving analyte signal response. Inject volume was shown to be directly proportional to signal response (Figure 24). However, it was important to impose an upper limit since excess sample can result in detrimental carry-over, detector saturation, and peak broadening due to column overload [234]. Thus, the lowest inject volume to give a sufficiently high analyte signal response was defined as 10 µL/sample. Extrapolating from this, the minimum re-constitution volume was calculated to be 50 µL/sample.

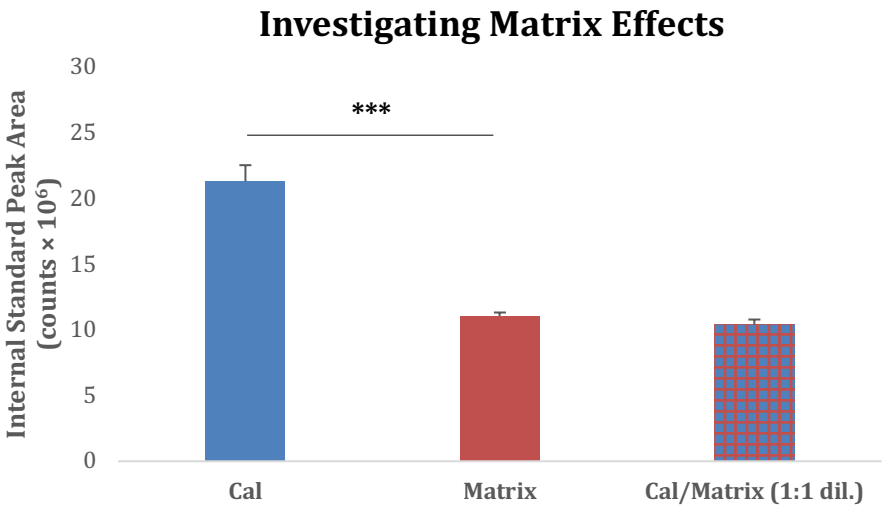

Figure 25: Assessment of ion suppression as a result of matrix effects in the CoQ_{10} LC-MS/MS method. For all conditions (n = 4). Error bars represent standard error of the mean (SEM).

It was noted that there was a significant 46 % ($p < 0.001$) relative decrease in internal standard (IS) response for matrix-extracted samples compared to corresponding un-extracted calibrator standards (Figure 25). To investigate if this was attributed to matrix effects or extraction efficiency, calibrator (0 nmol/L CoQ_{10} + IS) was diluted (1:1, v/v) with extracted native matrix (IQC '0' with no IS) and the response of the IS analysed. The resulting response for the IS in the diluted calibrator was roughly half (48.8 %) that of the undiluted control, meaning there were no notable matrix effects causing an ion suppression. Therefore, it was concluded that the significant decrease in internal standard signal was due to an inefficient extraction process, albeit the presence of the stable-isotope labelled internal standard mitigated the effect this has on absolute values for CoQ_{10} since they share identical extraction efficiencies.

3.3.2. LC-MS/MS Method Validation

Table 7: A comparison of performance parameters for the LC-MS/MS and HPLC-UV CoQ_{10} methods.

	LC-MS/MS	**HPLC-UV** [197]
LLOQ *(nmol/L)*	0.25	10
LLOD *(nmol/L)*	0.125	6
Linearity *(nmol/L)*	500	200
Run Time *(minutes)*	7	25

The lower limit of detection (LLOD) for the LC-MS/MS method was defined as a signal-to-noise ratio of 3 (n = 6). Linearity and lower limit of quantitation (LLOQ) were determined across a 10-point serial dilution (0 – 500 nmol/L) performed on 6 separate days with 6 separate preparations, and defined as the lowest concentration and range, respectively, that could be measured with an inaccuracy (percentage relative error) and imprecision (CV %) < 20 % (n = 6) – in accordance to the EMA and FDA Guidelines for bioanalytical method validation [235, 236].

The results (Table 7) show that the LC-MS/MS method surpasses the current gold-standard for CoQ_{10} determination, HPLC-UV, in every aspect of performance, with a much greater degree of sensitivity (40 × more sensitive) for low-level detection of CoQ_{10} at a markedly accelerated rate (3.5 × quicker).

Table 8: A summary of the validation metrics for the LC-MS/MS CoQ_{10} method.

	Intra-assay imprecision (CV %)	**Inter-assay imprecision (CV %)**	**Recovery (Ave. %)**
Baseline	3.6	7.2	-
Low Spike *(10 nmol/L)*	5.6	6.4	84
High Spike *(100 nmol/L)*	5.9	-	103
EQC Plasma	-	6.7	-

The precision of the LC-MS/MS method was assessed by evaluating the intra- and inter-assay coefficient of variation (CV), with acceptable CV values being defined as < 15 % [235-

[237]. The intra-assay precision was determined across replicates of 3 parallel samples of internal QC (IQC) material (n = 8; baseline, low spike, high spike). Inter-batch precision was calculated as the CV of average values for parallel samples of QC material over 7 separate days (n = 2; baseline, low spike, 'plasma' QC). The results (Table 8) indicate that the LC-MS/MS method has very good reproducibility at all levels.

Accuracy was investigated by examining the average recovery of known quantities of CoQ_{10} in replicates of spiked samples (n = 8; low spike (+ 10 nmol/L), high spike (+ 100 nmol/L)). A negligible inaccuracy (3 %) was observed for the high spike at 100 nmol/L. The relatively low, but consistent, recovery (84 %) for the low spiked CoQ_{10} sample at 10 nmol/L could be due to adsorption losses during sample preparation, but overall it can be said the method exhibits an acceptable degree of accuracy across the range.

Carryover between successive samples was assessed by analysing a blank sample immediately after the highest calibrator standard (ULOQ; 500 nmol/L) (n = 7). No quantifiable carryover was observed for the LC-MS/MS method.

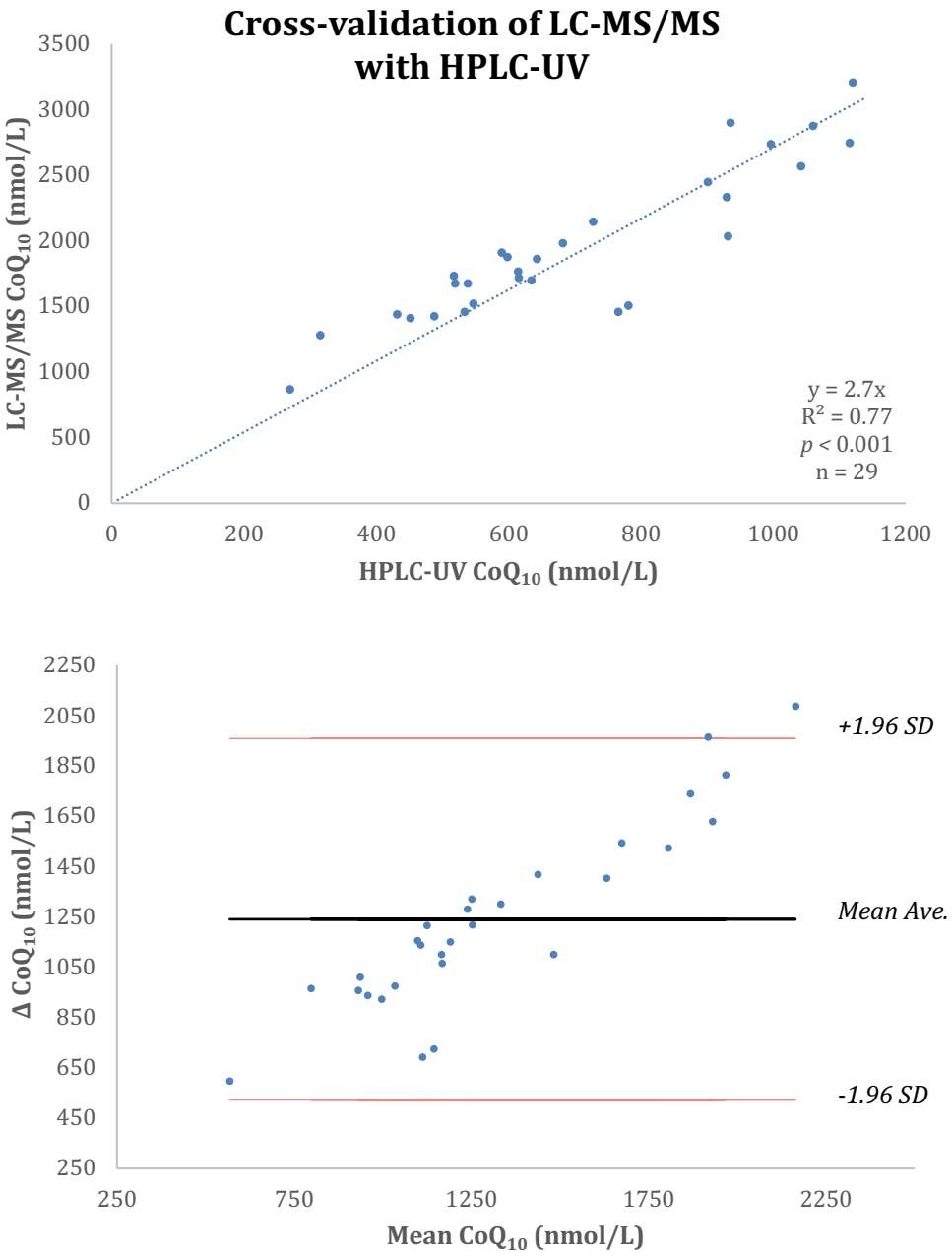

Figure 26: Cross-validation of the LC-MS/MS CoQ_{10} method against the gold-standard HPLC-UV CoQ_{10} method in human skeletal muscle samples. A significant ($p < 0.001$) correlation of results is shown (top graph), with a case of proportional error highlighted by a Bland-Altmann difference analysis (bottom graph). For both graphs (n = 29).

Cross-validation of the CoQ_{10} LC-MS/MS method against the gold-standard HPLC-UV was performed on human skeletal muscle samples provided by a collaborator at the University of Hull, UK. Identical samples were prepared in parallel in accordance to the respective extraction procedures and directly compared. Results indicate a significant

correlation between the two methods (R^2 = 0.77, p = 1.1 × 10^{-11}), confirming the LC-MS/MS as a viable method for CoQ_{10} analysis.

However, closer evaluation of the data (Figure 26) highlights a factor difference (× 2.7) between the absolute values of the two methods. This was confirmed as a case of proportional error by a Bland-Altman difference analysis [238, 239], suggesting the likely cause is a discrepancy in calibration and/or calculation.

Analysis of the LC-MS/MS CoQ_{10} calibrator stock solution by UV (Section 2.13.2) confirmed the concentration of the standard to be as stated (i.e. 1 mM). Assessment of the HPLC-UV CoQ_{10} calibrator stock solution on the LC-MS/MS system suggested the concentration to be half that of stated, confirming there is likely to be a calibration and/or calculation discrepancy contributing to the difference in absolute values.

3.3.3. Distribution of CoQ_{10} in Lipoprotein Fractions

Isolation of the main fractions of lipoprotein (VLDL, LDL and HDL) indicated that the majority of CoQ_{10} is incorporated within the LDL fraction (77.7 % of endogenous CoQ_{10}), and upon direct addition of exogenous CoQ_{10}, (i.e. not via a digestive process), it is the VLDL and LDL fractions which showed the greatest incorporation of CoQ_{10} (92.8 % of supplemented CoQ_{10}) (Figure 27). This suggests that transport of CoQ_{10} at the barrier will be mainly mediated by (V)LDL interactions.

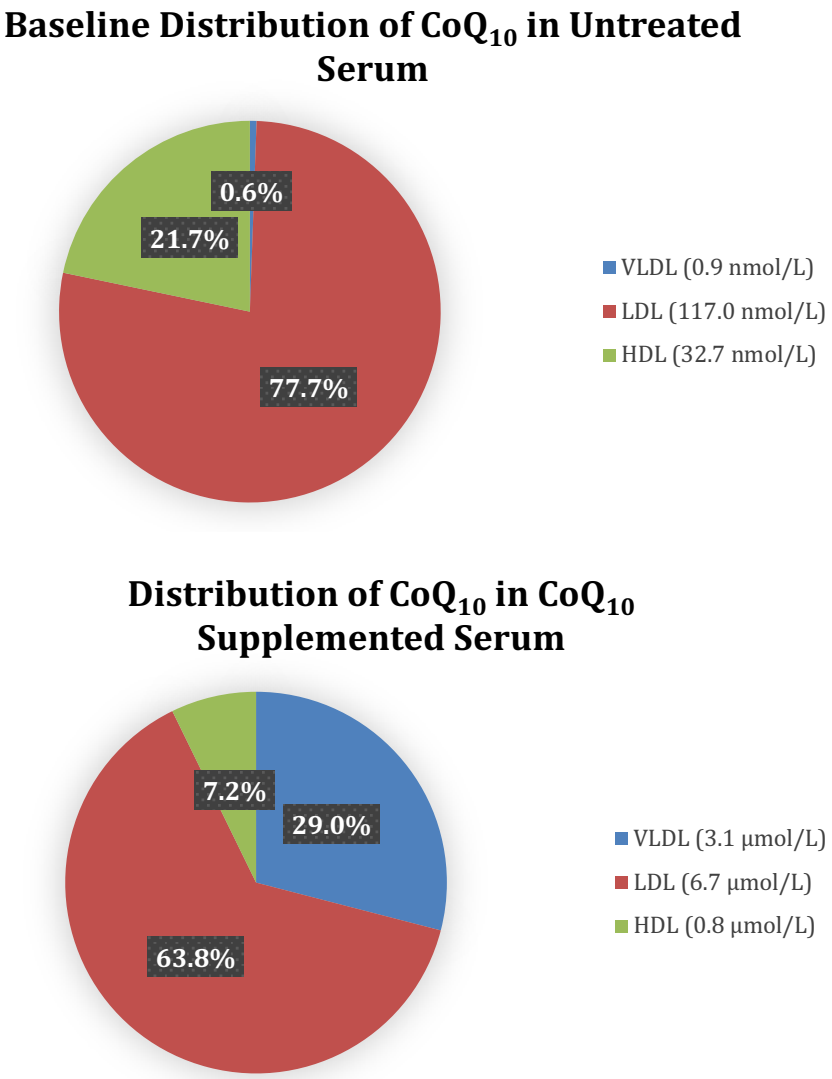

Figure 27: A graphical representation of the distribution of CoQ_{10} in the major lipoprotein fractions of untreated (top pie chart) and supplemented (10 µmol/L CoQ_{10}, 45 minutes, bottom pie chart) bovine plasma derived serum. For both untreated and supplemented conditions (n = 3). VLDL, very low-density lipoprotein; LDL, low-density lipoprotein; HDL, high-density lipoprotein.

3.3.4. Effect of CoQ_{10} Treatment on Cell Viability

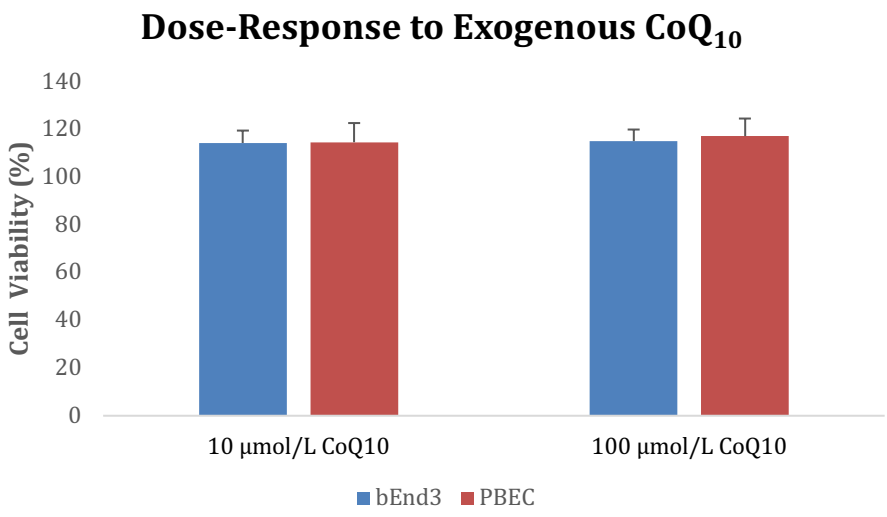

Figure 28: CoQ_{10} MTT cell viability assay in bEnd.3 cells and PBECs; cells were treated with CoQ_{10} for 60 minutes in '50 % Serum' assay buffer. For all conditions (n = 6). Error bars represent standard error of the mean (SEM).

An initial MTT assay to investigate mitochondrial dehydrogenase activity, a surrogate marker for cell proliferation and viability, as a function of CoQ_{10} concentration was performed on both bEnd.3 cells and PBECs (Figure 28).

Relative to untreated controls, there was no observable detrimental effect with increasing CoQ_{10}, indicating the both types of cell are compatible with exogenous CoQ_{10} up to a concentration of 100 µmol/L for 60 minutes.

3.3.5. Assessment of Barrier Integrity

The integrity of the BBB models was assessed using TEER and permeability of non-transported markers, Lucifer Yellow and FITC-40. A correlation was seen between these measures (Figure 30), where as expected, as TEER increased, paracellular permeability of markers decreased.

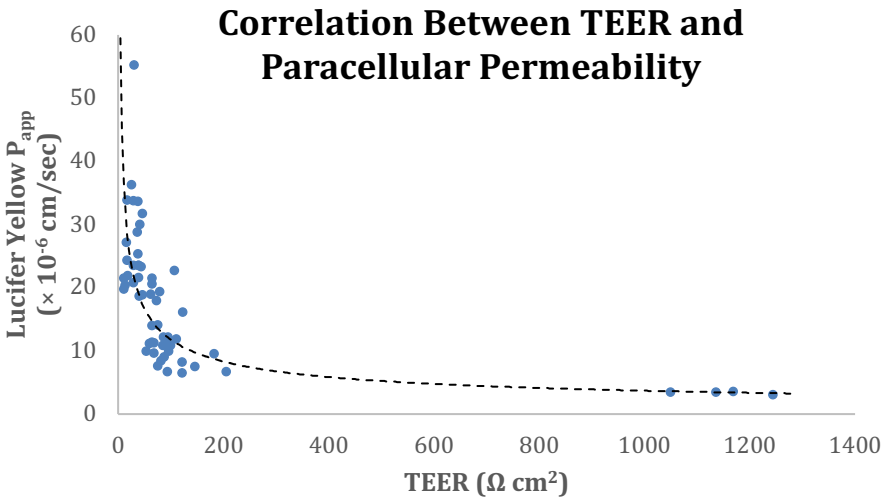

Figure 29: The correlation between TEER and Lucifer Yellow apparent permeability (P_{app}) in bEnd.3 and PBECs (n = 57).

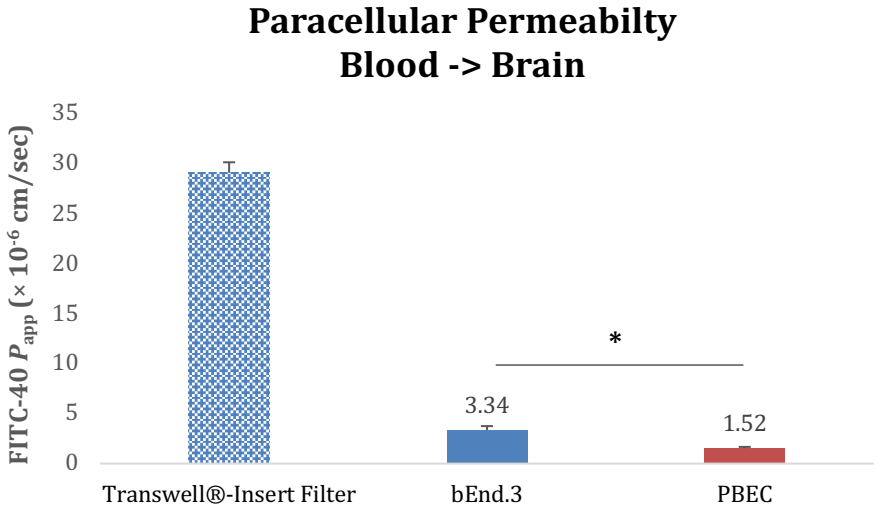

Figure 30: Comparison between the paracellular permeability (P_{app}) of the PBEC and bEnd.3-BBB models under 50 % (v/v) serum (control) assay conditions. Collagen/poly-L-lysine-coated Transwell®–insert filter (n = 6), bEnd.3 (n = 14), PBEC (n = 4). Error bars represent standard error of the mean (SEM).

Increasing TEER across cell monolayers is indicative of decreasing ion permeability as a direct result of tight-junction formation between adjacent cells. This is a functional characteristic of the brain endothelium that enables it to behave as a selective barrier. As expected, TEER correlated with the paracellular permeability of the *in situ* markers

(Figure 30), with Lucifer Yellow P_{app} (mean P_{app} = 14.58 × 10^{-6} cm/sec) following a sharp exponential decrease with increasing TEER, a trend reflective of excellent BBB integrity. Direct comparison of the two *in vitro* BBB models using the permeability marker FITC-40 (~40 kDa; 0.5 mg/mL), clearly illustrates that the PBEC-BBB (mean P_{app} = 1.52 × 10^{-6} cm/sec) exhibits significantly less paracellular permeability than the bEnd.3-BBB (mean P_{app} = 3.34 × 10^{-6} cm/sec) and, therefore, has a tighter BBB phenotype (Figure 30).

3.3.6. Pharmacologically Inducing CoQ_{10} Deficiency

The effect of a pharmacologically induced CoQ_{10} deficiency on bEnd.3 cell viability was determined against untreated controls using the MTT assay.

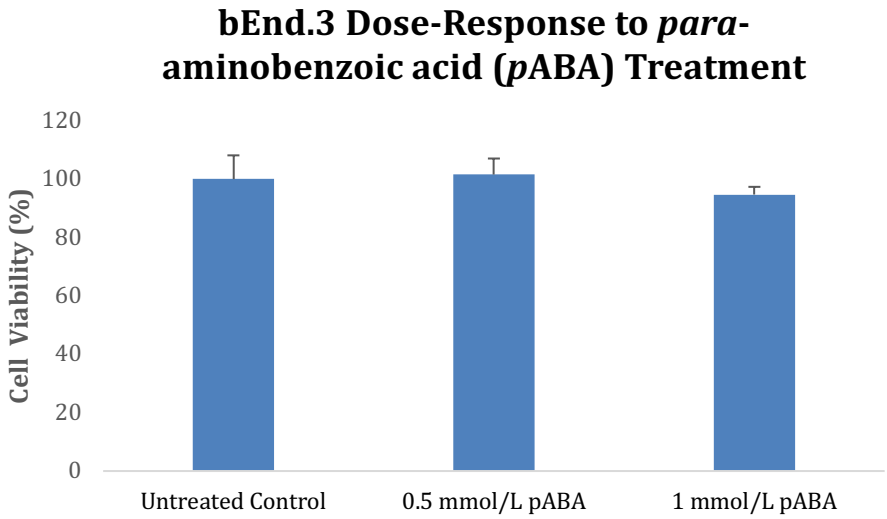

Figure 31: bEnd.3 *p*ABA MTT cell viability assay; cells were treated with *p*ABA for 5 days. For all conditions (n = 6). Error bars represent standard error of the mean (SEM).

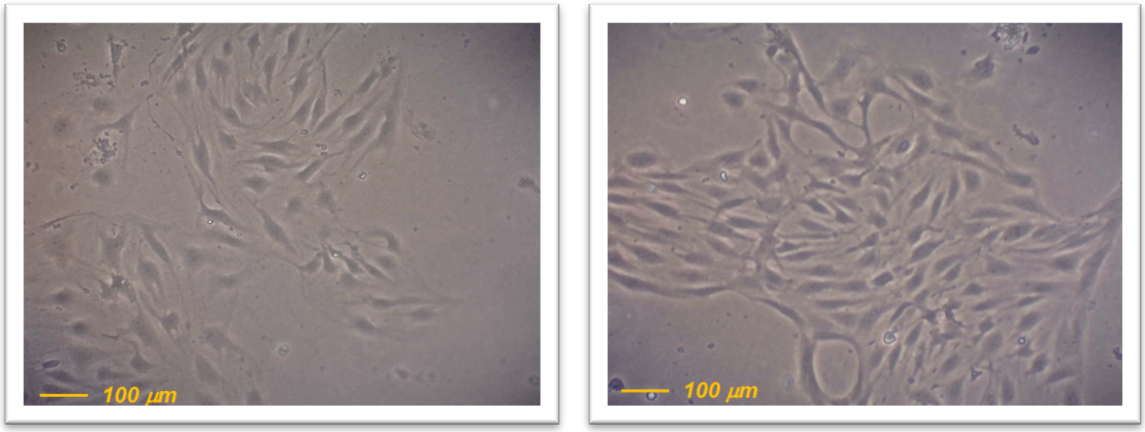

Figure 32: PBEC cells after 5 days growth; untreated PBECs (left image) and *p*ABA treated (1 mmol/L, 5 days) PBECs (right image). Images were captured using a Dino-Lite AM4023X eyepiece camera with DinoXcope software.

Results indicate that bEnd.3 cells are compatible with 1 mmol/L *p*ABA for up to 5 days (Figure 31), with no significant decrease in cell viability observed after said course of treatment.

Visual inspection (Figure 32) and comparison of total protein content in *p*ABA treated (1 mmol/L, 5 days) PBECs corroborate with the findings from the bEnd.3 MTT assay.

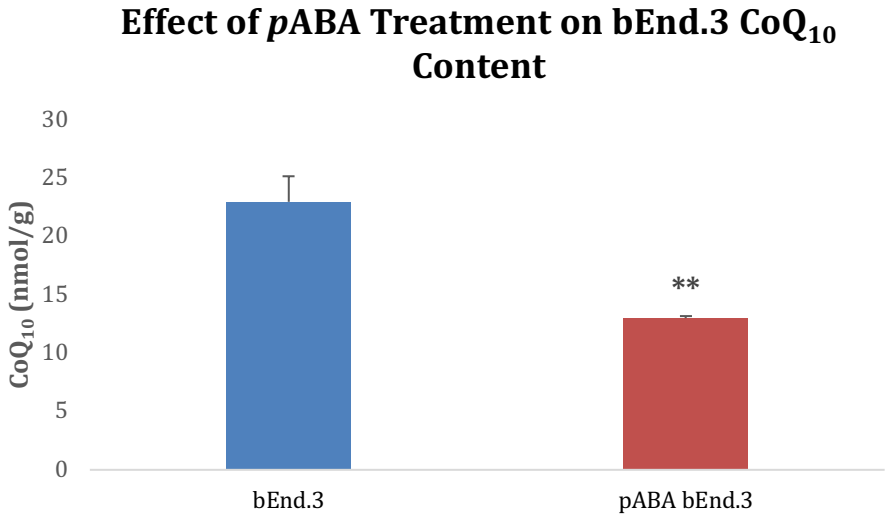

Figure 33: Effect of *p*ABA treatment (1 mmol/L, 5 days) on cellular CoQ_{10} content. bEnd.3 control (n = 4), *p*ABA bEnd.3 (n = 4). Error bars represent standard error of the mean (SEM).

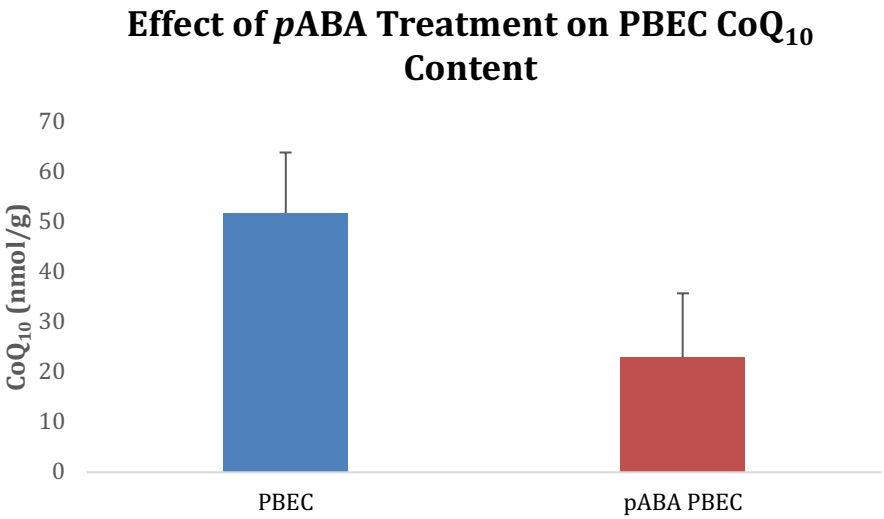

Figure 34: Effect of *p*ABA treatment (1 mmol/L, 5 days) on cellular CoQ_{10} content. PBEC control (n = 3), *p*ABA PBEC (n = 3). Error bars represent standard error of the mean (SEM).

Assessment of cellular CoQ_{10} content in response to *p*ABA treatment (1 mmol/L, 5 days) showed a significant 43.4 % ($p < 0.01$) depletion of CoQ_{10} relative to untreated controls in bEnd.3 cells (Figure 33), with PBEC cells exhibiting a comparable depletion of 55.6 % that is approaching significance ($p = 0.08$) (Figure 34). These results confirm that *p*ABA treatment (1 mmol/L, 5 days) induces a pronounced CoQ_{10} deficiency in both models of the *in vitro* BBB at a magnitude that is consistent with clinical presentation [240].

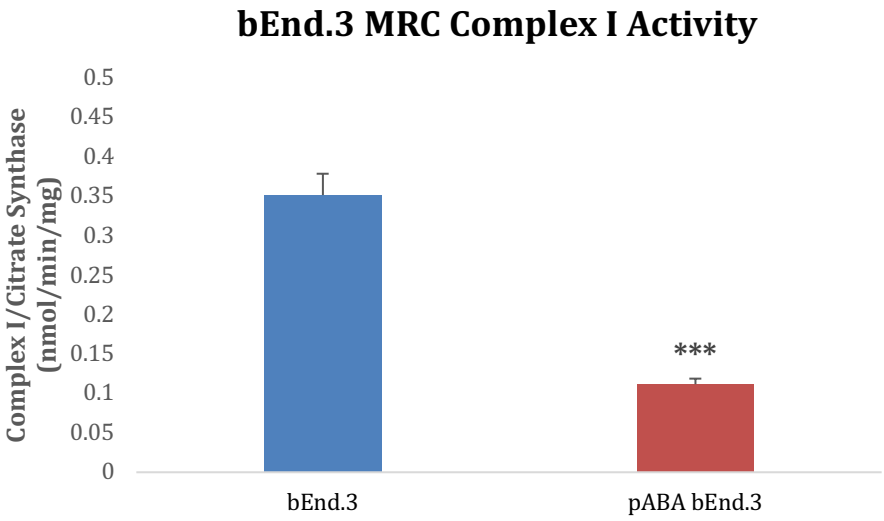

Figure 35: Effect of *p*ABA treatment (1 mmol/L, 5 days) on bEnd.3 MRC complex I activity. bEnd.3 control (n = 4), *p*ABA bEnd.3 (n = 4). Error bars represent standard error of the mean (SEM).

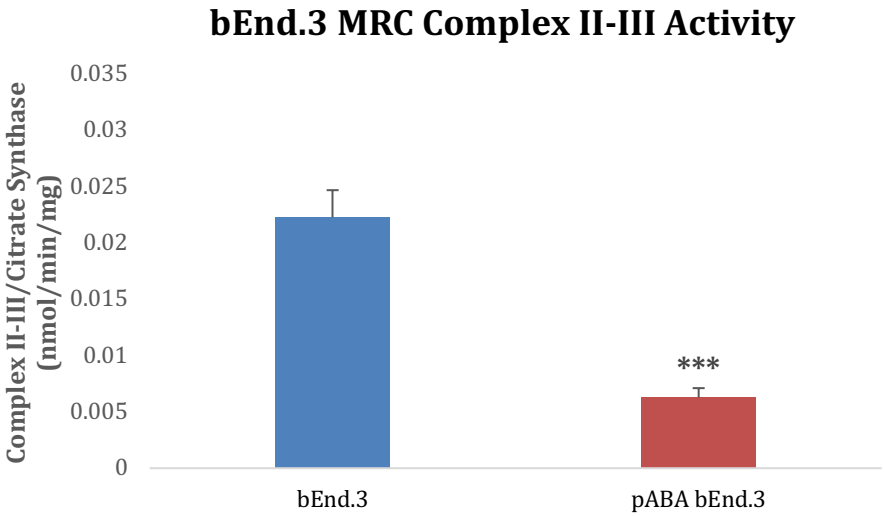

Figure 36: Effect of *p*ABA treatment (1 mmol/L, 5 days) on bEnd.3 MRC complex II-III activity. bEnd.3 control (n = 4), *p*ABA bEnd.3 (n = 4). Error bars represent standard error of the mean (SEM).

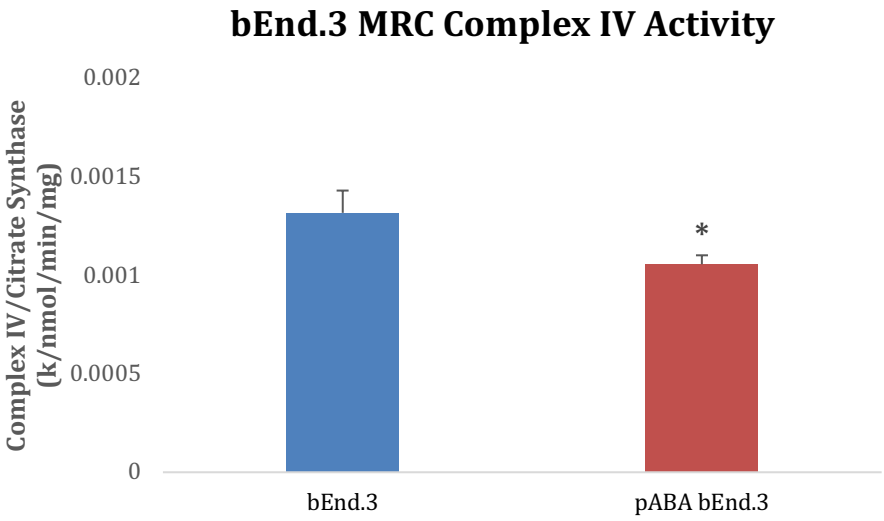

Figure 37: Effect of *p*ABA treatment (1 mmol/L, 5 days) on bEnd.3 MRC Complex IV activity. bEnd.3 control (n = 4), *p*ABA bEnd.3 (n = 4). Error bars represent standard error of the mean (SEM).

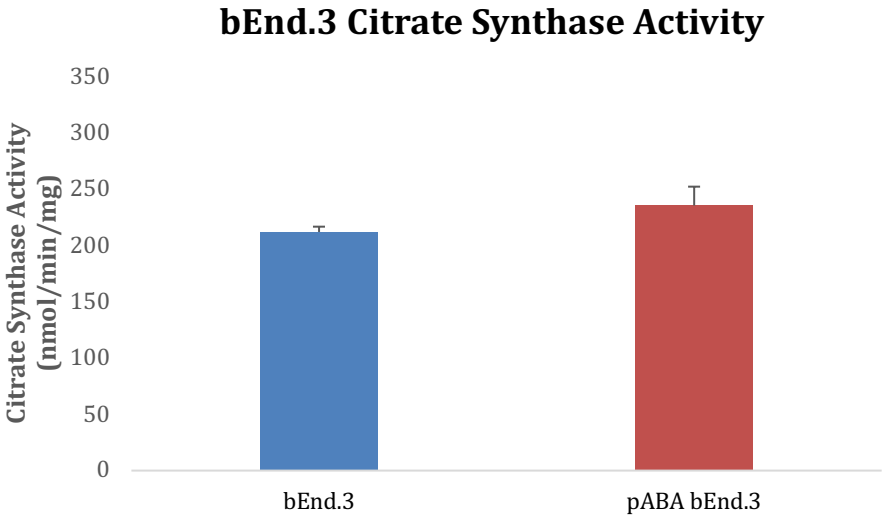

Figure 38: Effect of *p*ABA treatment (1 mmol/L, 5 days) on citrate synthase activity in bEnd.3 cells. bEnd.3 control (n = 4), *p*ABA bEnd.3 (n = 4). Error bars represent standard error of the mean (SEM).

Consistent with trends *in vivo* [240] and previous *in vitro* studies [194], a CoQ_{10} deficiency in the bEnd3 cells was associated with a significant decrease in MRC enzyme activity across all complexes, with MRC complexes I (Figure 35) and II-III (Figure 36) experiencing the greatest relative decline in activity (68 and 72 % decrease respectively, $p < 0.001$), and MRC complex IV (Figure 37) exhibiting a lesser effect (80.2 % of control, $p < 0.05$).

MRC complex activities were expressed as a ratio to citrate synthase, a mitochondrial marker enzyme, which enabled the effect of mitochondrial enrichment to be normalised across all samples, since there was a notable, but insignificant, mitochondrial enrichment (11.1 % increase) of bEnd.3 cells in response to *p*ABA treatment (Figure 38).

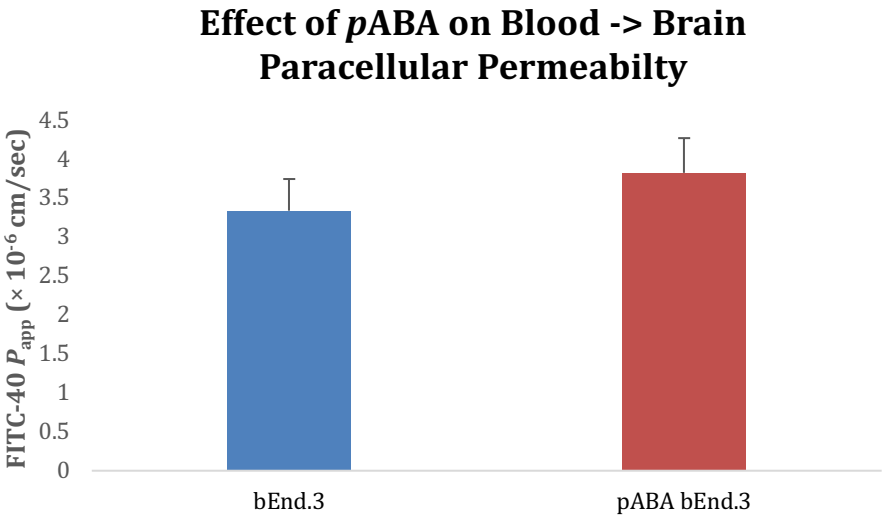

Figure 39: Effect of *p*ABA treatment (1 mmol/L, 5 days) on paracellular permeability in bEnd.3 cells. bEnd.3 control (n = 14), *p*ABA bEnd.3 (n = 12). Error bars represent standard error of the mean (SEM).

Although *p*ABA treatment showed a negligible effect on cell viability, it was unknown if this correlated to maturation of BBB characteristics. Evaluation of FITC-40 P_{app} data suggested there was no significant effect on paracellular permeability, in such that the CoQ_{10} deficient bEnd.3-BBB showed an insignificant 14.6 % increase in permeability (Figure 39). This suggests a potential, very marginal, decrease in tight-junction formation which may manifest with longer treatment.

3.3.7. Effect of CoQ_{10} Deficiency on Rat Astrocytes

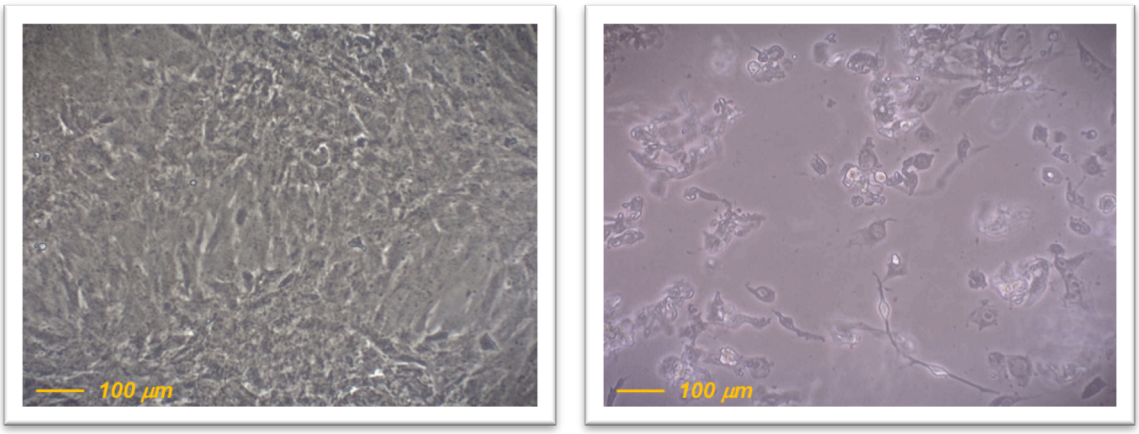

Figure 40: The effect of PBEC co-culture in *p*ABA treated (1 mmol/L, 5 days) primary rat astrocytes. Confluent co-cultured astrocytes displaying quiescence (left image) versus mono-cultured astrocytes displaying signs of cell death (right image). Images were captured using a Dino-Lite AM4023X eyepiece camera with DinoXcope software.

In an effort to maintain consistency, all astrocytes within a batch were supplemented the same across the full life-cycle of the culture protocol (Appendix A), regardless of whether or not they were in co-culture with PBECs. For *p*ABA-treated astrocytes, it was observed that cells in mono-culture (i.e. not in the presence of PBECs) began to detach and die, whereas astrocytes in co-culture with PBECs grew to confluence as expected (Figure 40). This provides qualitative evidence that suggests astrocytes share some bioenergetic cross-talk with neighbouring PBECs.

3.4. Discussion

Due to a predicted low permeability of CoQ_{10} across the BBB and a potential need for assessing CoQ_{10} in CSF samples as a diagnostic tool, a novel LC-MS/MS method was designed to circumvent the inherent limitations of current HPLC-UV methods.

Output from the validation procedure (Table 8) indicated that the LC-MS/MS method operates with very good reproducibility at all levels (intra- and inter-batch imprecision (CV %) consistently << 10 %), with good accuracy, no carry-over, and well within the acceptable clinical guidelines for a diagnostic assay [235-237].

When compared with the established 'gold-standard' HPLC-UV method, the newly developed and validated LC-MS/MS method surpassed the existing methodology in all aspects of performance (Table 7), particularly LLOQ (0.25 nmol/L compared with 10 nmol/L) and run-time (7 minutes compared with 25 minutes), an important improvement on HPLC-UV in the diagnosis of CoQ_{10} deficiencies.

Cross-validation of the analytical techniques, HPLC-UV and LC-MS/MS, showed a significant correlation ($R^2 = 0.77$, $p < 0.001$, n = 29) of results for CoQ_{10} in human skeletal muscle samples (Figure 26). However, while a small degree of inter-operator variability is to be expected, a proportional error (CoQ_{10} LC-MS/MS = 2.7 × CoQ_{10} HPLC-UV) between the absolute values of the two methods was apparent. In addition to probable calibration discrepancies, this could be partially attributed to the different internal standards; the HPCL-UV method utilises an in-house dipropoxy-derivative of CoQ_{10} for quantitation purposes, whereas the LC-MS/MS incorporates a commercially certified stable-isotope of CoQ_{10} (CoQ_{10}-[$^2H_9$]) (Figure 41).

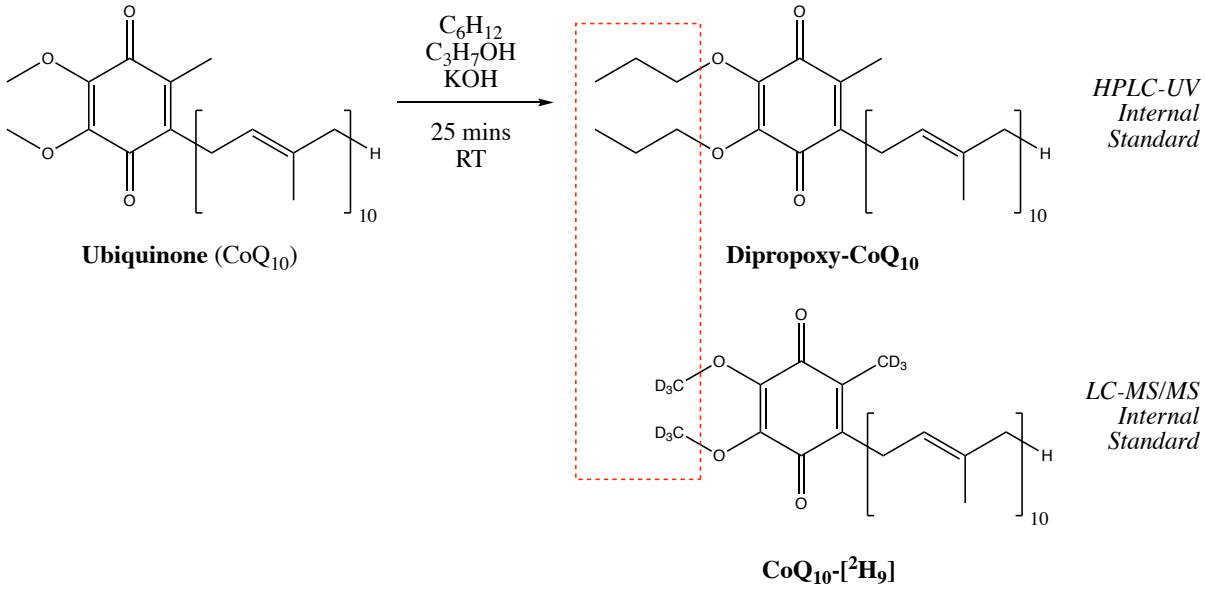

Figure 41: Skeletal structures of the HPLC-UV dipropoxy-CoQ_{10} internal standard, including the reaction scheme from CoQ_{10}, and the commercially certified LC-MS/MS stable-isotope labelled internal standard, CoQ_{10}-[$^2H_9$].

The increased alkoxy-chain length of the HPLC-UV internal standard will affect the physicochemical properties of the molecule relative to CoQ_{10}, especially its solubility. Indeed it has been shown that there is a marked decrease in polarisability with increasing alkoxy-chain length on substituted aromatic systems, as is consistent with the inductive effect of hydrocarbons and the mesomeric effect associated with extensive π-conjugation [241, 242]. HPLC confirms this disparity in polar properties with dipropoxy-CoQ_{10} displaying a delayed retention on the column relative to CoQ_{10} (Section 2.13.1, Figure 15). Hence, in a latent biphasic solution of ethanol and hexane, the basic principles of chemistry dictate that dipropoxy-CoQ_{10} is likely to have a greater extraction efficiency than CoQ_{10}, meaning the results from the HPLC-UV are likely to be an underestimation of the true value. The extent of which is unknown.

This highlights how vital it is to use an internal standard that will behave exactly the same as the analyte of interest, since there are several stages in the preparation and analytical process, each with an associated error. This is demonstrated in the inefficient extraction of CoQ_{10}-[$^2H_9$] (54 % of control) (Figure 25), in a process that is common to both analytical techniques, with an inefficiency that is unlikely to be equivalent for different compounds. Although, it should be noted that for clinical samples measured by HPLC-UV, the extraction process is repeated three times in recognition of this poor extraction efficiency, costing time and money.

Another possible consideration for the difference in absolute values between the analytical techniques is the much higher specificity of LC-MS/MS for both the analyte and the corresponding IS. This is known to, in some cases, have an effect when cross-validating different technologies [237].

That said, if the CoQ_{10} LC-MS/MS method were to be taken forward for use in clinical laboratories, new tissue-specific reference ranges would have to be established and a more extensive validation procedure would need to be performed. However, in the context of this project, absolute values of CoQ_{10} are far less critical since apparent permeability (P_{app}) is a relative measure of rate (Section 2.8, Equation 3), and the significant increase in sensitivity is highly advantageous. Therefore, the LC-MS/MS method was chosen as the primary method for CoQ_{10} determination.

To date, no studies have assessed CoQ_{10} permeability on *in vitro* models of the BBB, meaning our knowledge of the mechanisms governing uptake of the compound into the

brain is purely theoretical. Using a combination of the immortalised bEnd.3 cell line and the primary PBEC/astrocyte co-culture model, BBB permeability investigations under physiological and pathophysiological conditions were performed. Prior to performing these studies, it was imperative to first optimise and assess *in vitro* experimental procedures.

It is widely accepted that dietary, or supplementary, CoQ_{10} is absorbed at the small intestine and subsequently transported into systemic circulation by lipoproteins [12]. Of the major classes of lipoprotein, it is LDL which is reported to be the most prominent chaperone of CoQ_{10} [243-245]. As a means to replicate this in the *in vitro* models of the BBB, the donor assay buffer in apparent permeability investigations was comprised of 50 % (v/v) serum, more analogous to the proportion found in human blood when compared to the usual cell culture serum content of 10 % (v/v). Furthermore, to encourage association with the lipoproteins, the serum was pre-incubated (45 minutes, 37°C) with exogenous CoQ_{10} prior to being mixed with the remaining components of the assay buffer. Analysis of native serum and CoQ_{10} supplemented serum indicated a distribution of CoQ_{10} in the lipoprotein fractions that are in agreement with published data from *in vivo* studies (Figure 27) [243-245], thereby validating the pre-incubation process.

Further evaluation of these findings highlight a strong affinity of exogenous CoQ_{10} for the (V)LDL fractions (92.8 % of total CoQ_{10}), suggesting that the compound is, perhaps, associated to the lipid-membrane of the vesicle as opposed to being encapsulated within the vesicle. This would be consistent with the known *in vivo* cellular distribution and function of CoQ_{10} in preventing lipid-membrane peroxidation. Additionally, the results from this investigation support the common theory that uptake of CoQ_{10} at the barrier will be primarily mediated by (V)LDL interactions, of which apolipoprotein B (ApoB) is likely to dominate due to its abundance [246].

ApoB is known to be highly conserved between species (Figure 42), both in terms of the protein as a whole and the specific binding domain, meaning experimental procedures which span porcine, murine and bovine, as is the case with this project, are feasible [247].

(%)	***Human***	***Porcine***	***Murine***	***Bovine***
Human	-	70.3	69.7	68.0
Porcine	80.0	-	67.0	81.3
Murine	70.0	90.0	-	66.3
Bovine	70.0	90.0	80.0	-

```
                                                                3174
                                                                 |
  HumanAPOB_P04114   PLTIPEMRLPYTIIITTPPLKDFSLWEKTGLKEFLKTTKQSFDLSVKAQYKKNKHRHSITN
PigAPOB_A0A0F6TNY5   PLTIPEMTLPYTRLTVPQVKDISLWEKTGLKEFLKTTKQSFDLSVKAQYKKNKDKHSIPN
 BovineAPOB_E1BNR0   PLKIPEMTLPYTKLTTPQIKEISLWKKTGLKDFLKTTKQSFDLSVRAQYKKNKDKHSIPV
  MouseAPOB_E9Q414   PLTIPEINLPYTEFKTPLLKDFSIWEETGLKEFLKTTKQSFDLSVKAQYKKNSDKHSIVV

                                    3386
                                     |
  HumanAPOB_P04114   SSSSSVIDALQYKLEGTTRLTRKRGLKLATALSLSNKFVEGSHNSTVSLTTKNMEVSVAT
PigAPOB_A0A0F6TNY5   TFSSSVIDALQYKLEGTSSLMRKRGLKLATALSLSNKFMEGNHDSTISFTKKNVDASLTT
 BovineAPOB_E1BNR0   TSSSSVMDTLQYKLEGTSSLTRKRGLKLATALSLSNRFVEGNHDSTVSFTKKNVDASVTT
  MouseAPOB_E9Q414   SSSSFVTDALQYKLEGTSRLMRKRGLKLATAVSLTNKFVKGSHDSTISLTKKNMEASVRT
```

Figure 42: (Table - top) comparative homology of ApoB across four species. The comparisons are expressed as percentage homology between pairs of sequences. Left of the hyphen is the complete ApoB protein, right of hyphen is the binding region to the LDL receptor.
(Sequence - bottom) aligned nucleotide sequences of ApoB LDL receptor binding domain in four species. The numbering corresponds to the published human ApoB-100 sequence. Binding domains to LDL are highlighted in yellow and are highly conserved across the four species.
Sequences were aligned using UniProt and compared using BLAST.

Several reports have shown the rate for receptor-mediated endocytosis of lipoproteins to be very fast, with a half-life of less than 30 seconds [248-251]. As a means to isolate transcytic events and mitigate any interference from paracellular passive diffusion, it was important to minimise the timescale of permeability assays. With an upper limit of 2 h already imposed due to experimental procedures outside of optimal incubation conditions, a time-course of 1 h was chosen. This is in agreement with the protocols from other studies assessing similar transcytic mechanisms [252, 253].

In keeping with the excellent safety profile of CoQ_{10} *in vivo* [53], both bEnd.3 cells and PBECs were compatible with exogenous CoQ_{10} up to 100 μmol/L for a duration of 1 h (Figure 28). To date, the highest achievable CoQ_{10} plasma concentration observed after oral-supplementation *in vivo* is 10.7 μmol/L [52, 84], additionally, treatment with 10 μmol/L CoQ_{10} has been shown to restore MRC function in CoQ_{10} deficient human neuroblastoma

cells [88]. Therefore, 10 μmol/L CoQ_{10} was selected as the clinically relevant concentration for use in this study.

Viability of the *in vitro* BBB models was confirmed through combined and continuous monitoring of TEER and the *in situ* paracellular permeability markers Lucifer Yellow or FITC-40. These functional markers of barrier integrity are inversely proportional and served as a robust quality control for each batch of experiments (Figure 29). They also provide quantitative data relating to tight-junction formation/degradation in response to treatment conditions [254, 255].

It is good practise to incorporate a paracellular permeability marker that is of a similar size to the compound of interest. When associated to (V)LDL, CoQ_{10} is essentially a macromolecule meaning FITC-40 (~40 kDa) was the preferred marker for use throughout this project.

Due to a higher expression of the tight-junction proteins ZO-1, claudin-5 and occludin, the PBECs possess a more *in vivo* like BBB morphology compared to immortalised cell lines such as bEnd.3. This is reflected in a significantly lower paracellular permeability relative to the immortalised bEnd.3 cell line (FITC-40 P_{app}; PBEC = 1.52×10^{-6} cm/sec, bEnd.3 = 3.34×10^{-6} cm/sec, $p < 0.05$) (Figure 30). These data are in agreement with the literature and substantiate the proposed experimental strategy of subsequent testing of promising leads on the gold-standard PBEC model [167].

The pathophysiological, CoQ_{10} deficient, *in vitro* BBB model was established using the pharmacological reagent *para*-aminobenzoic acid (*p*ABA). Compared with alternative techniques for inducing CoQ_{10} deficiency, for example gene silencing [255-257], the use of *p*ABA, or other hydroxybenzoic acid derivates [258-260], is extremely cheap, very simple and highly reproducible.

Building on previous findings from Duberley *et al.* [194], both the bEnd.3 cells and PBECs exhibited a depletion of CoQ_{10} (bEnd.3 56.6 % of control, $p < 0.01$, and PBEC 44.4 % of control, p = ns) upon treatment with *p*ABA (1 mmol/L, 5 days). This was concomitant with a depletion of MRCE activity in bEnd.3 cells, in particular the CoQ_{10} dependent complex II-III (28.1 % of control, $p < 0.001$) (Figure 36) and complex I (31.8 % of control, $p < 0.001$) (Figure 35). However, the treatment did not correspond to a cytotoxic effect, as is consistent with previous studies [193, 194]. Interestingly, and in contrast to the work of

Duberley *et al.* [194], the activity of bEnd.3 MRC complex IV was the least effected (80.2 % of control, $p < 0.05$) (Figure 37), suggesting there is tissue-specific variation. Although, the overall deficiency profile is markedly similar to that seen in the fibroblasts of patients with a primary CoQ_{10} deficiency, making the *p*ABA-treated bEnd.3-BBB model an appropriate surrogate for pathophysiological investigations [240, 261, 262].

There was an emerging trend for small increases in citrate synthase activity (11.1 % increase, p = ns) and FITC-40 paracellular permeability (14.6 % increase, p = ns) in response to *p*ABA treatment in the bEnd.3 cells (Figure 38). This suggests a potential mitochondrial enrichment as a means to counteract a reduced OXPHOS capacity, albeit insignificant [263, 264]. Similarly, although insignificant, an increase in paracellular permeability suggests a minor breakdown of the bEnd.3-BBB in response to a compromised OXPHOS capacity. This trend has been observed in other *in vitro* barrier models, which noted an internalisation of the tight-junction protein, claudin [265]. However, the degree of breakdown exhibited is unlikely to have any notable effect on the paracellular transport of (V)LDL-CoQ_{10} due to its large size. Furthermore, the bEnd.3 cells on average expressed a very low TEER ($35.4 \pm 1.1\ \Omega \cdot cm^2$, result not shown) meaning the effect of TJ disruption by *p*ABA treatment is unlikely to cause any further paracellular transport than is already exhibited by the untreated, physiological, cells.

Unfortunately, the high cost of PBEC culture meant there were insufficient repeats for a full statistical validation of *p*ABA treatment. It should be noted, however, that the limited PBEC data gathered was consistent with the trends observed in the bEnd.3 cells and with published data [193, 194], confirming that *p*ABA treatment has most likely had the desired pathological effect in the PBECs.

In a somewhat serendipitous observation it was noted that *p*ABA treated astrocytes (1 mmol/L) began to die in the absence of co-culture with PBECs (Figure 40), giving strong support for the interactive neurovascular unit (NVU) [142].

It is well documented that astrocytes and neurons share an energetic interaction, in the so-called astrocyte-neuronal lactate shuttle, whereby astrocytes respond to neuronal activity by converting glucose into lactate that is subsequently taken up by neurons to satisfy their energy needs during activation [266-268]. However, very little is known about astrocyte-endothelial bioenergetic cross-talk aside from than the work published by Brix

et al. [269], who proposes a symbiotic relationship between the components of the NVU mediated by the neurometabolic marker nitric oxide, NO (Figure 43).

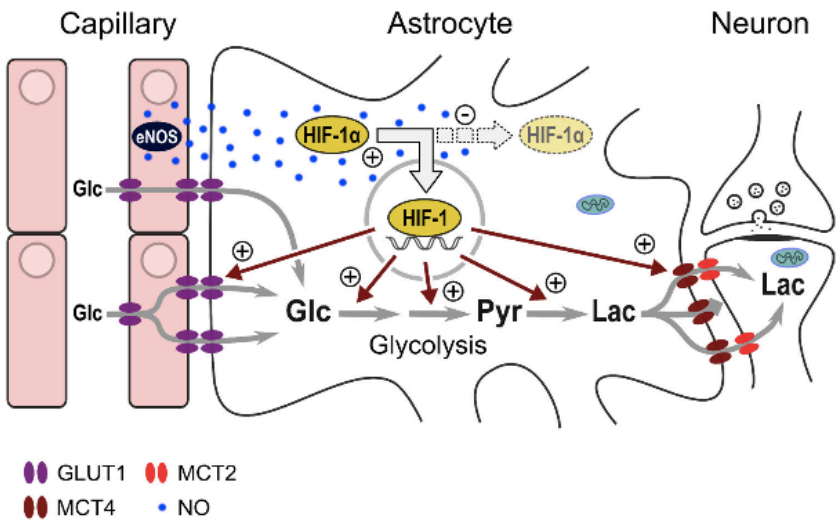

Figure 43: Proposed model of stimulated lactate production in astrocytes by nitric oxide (NO) released from endothelial cells. NO stabilises hypoxia-inducible factor 1α (HIF-1α) in astrocytes leading to an increased expression of key glycolytic enzymes and glucose/lactate transporters. Glucose uptake from arterial supply is increased in astrocytes via glucose transporter 1 (GLUT1), lactate production is increased through enhanced glycolysis and export of lactate from astrocytes involves monocarboxylate transporter 4 (MCT4) [269].

Based on the collective knowledge from previous studies in the group [194], whereby a neuronal cell line was not susceptible to cell-death post *p*ABA treatment, and results from this project which indicate that bEnd.3 cells (Figure 31) and PBECs (Figure 32) are also compatible with *p*ABA treatment, it would seem that astrocytes are the most affected cell type in the NVU to a CoQ_{10} deficiency. What role this has in the pathogenesis of the disease is unknown, nevertheless, these findings are a basis for further isolated investigation.

With confidence in the *in vitro* models of the BBB for the assessment of CoQ_{10} transport and with suitable analytical techniques established, focus moved to interrogating mechanisms of uptake and efflux of CoQ_{10} across the BBB under both physiological and pathophysiological conditions.

4. Coenzyme Q_{10} Transport at the Blood-Brain Barrier

4.1. Background

At present, our understanding of the mechanisms that govern CoQ_{10} uptake at the BBB are based upon the common physicochemical and biochemical properties that CoQ_{10} shares with vitamin E (α-toc), coupled with our knowledge of lipoprotein distribution [12, 270, 271]. While these predictions are logical in approach, they offer little proof or substantive evidence that can be built upon. Through gaining a more detailed understanding of the specific transport mechanisms that govern CoQ_{10} uptake at the BBB, it is hoped that CoQ_{10} therapies can be optimised for delivery into the brain parenchyma, thereby improving the efficacy of the treatment for neurological disorders.

Table 9: A comparative summary of the major lipoproteins and their physical parameters [246]. VLDL, very low-density lipoprotein; LDL, low-density lipoprotein; HDL, high-density lipoprotein.

Lipoprotein	Diameter (nm)	Density (g/mL)	Major Lipoprotein	Protein Content (~ %)
Chylomicrons	80–500	< 0.94	ApoB-48	2
VLDL	30–80	0.94–1.006	ApoB-100, ApoE	4–10
LDL	18–28	1.006–1.063	ApoB-100	25
HDL	5–12	1.063–1.21	ApoA-I/II	50

Lipoproteins serve to solubilise lipophilic compounds, such as CoQ_{10}, and transport them through the aqueous circulatory system. Specific apolipoproteins, present on the surface of the macromolecule, then facilitate the targeting of the lipoproteins to appropriate tissues by receptor-mediated endocytic processes. The main plasma lipoproteins include high-density lipoproteins (HDL, containing approximately 50 % protein of d = 1.063–1.21 g/mL), low-density lipoproteins (LDL, cholesteryl ester-enriched particles of d = 1.006–1.063 g/mL, approximately 25 % protein), very low-density lipoproteins (VLDL,

endogenous triacylglycerol-rich particles of *d* = 0.94–1.006 g/mL, approximately 4–10 % protein), and chylomicrons (dietary triacyglycerol-rich particles of *d* < 0.94 g/mL, approximately 2 % protein). They are classified according to their mass density in addition to association with specific apolipoproteins (Table 9) [246, 272-275].

Combined current knowledge of CoQ_{10} and α-toc ADME has led to the assumption that the low-density lipoprotein receptor (LDLR) superfamily and scavenger receptor class B type 1 (SR-B1) will most likely play a prominent role in the transcytosis of CoQ_{10} at the BBB and are therefore a focus of this project [12, 271, 276-278].

The LDLR superfamily includes several structurally homologous endocytic receptors; LDLR itself, apolipoprotein E receptor 2 (apoER2/LRP-8), very low-density lipoprotein receptor (VLDLR), multiple epidermal growth factor-like domains 7 (MEGF7/LRP-4), the LDLR-related protein 1 (LRP-1), glycoprotein 330 (gp330/megalin/LRP-2), and LRP-1B [131, 250, 279, 280]. Of the receptors in the superfamily, it is LRP-1 that has received the most interest and is best characterised on *in vitro* models of the BBB where it is reported to be a bidirectional transporter [167, 252, 281, 282]. Although, due to its proposed role in the clearance of amyloid-beta in Alzheimer's disease, it has been suggested there is an abluminal/basolateral distribution of LRP-1 leading to a net efflux from the brain [283-289].

LRP-1 is comprised of an extracellular 515 kDa α-chain that is non-covalently coupled to an 85 kDa transmembrane and cytoplasmic light β-chain domain. The α-chain contains four cysteine-rich ligand-binding domains (clusters I-IV), with domains II and IV being the major binding regions [290]. It has been suggested that the YXXL motif and distal di-leucine repeats of the cytoplasmic tail may be associated with the rapid endocytic rate of LRP-1 [248]. Recent work by Nyberg *et al.* [253] has offered insight into the transcytic mechanism by which LRP-1 operates, suggesting an initial ligand-binding and clustering, followed by a rapid dynamin-dependent tubular transcytosis on a scale of minutes [291]. This is in contrast to the classical vesicular theory that is isolated and mediated by caveolae or clathrin [292-294].

As the name implies, LRP-1 is best recognised for its role in the receptor-mediated transcytosis of (V)LDL, whereas SR-B1, an 82 kDa glycoprotein with two transmembrane domains separated by a large extracellular loop, is the main target for HDL transport [295-300]. Distributed in tissues throughout the body and expressed almost exclusively on the luminal/apical membrane of the brain endothelium [301], SR-B1 has been shown to be

pivotal in the transcytic influx and/or internalisation of HDL in a dynamin-dependent tubular mechanism that is markedly similar to LRP-1 [302].

While the aforementioned endocytic receptors are commonly associated with VLDL/LDL and HDL, ligand-binding to LRP-1 and SR-B1 is characterised by high affinity and broad specificity. As a consequence, these endocytic receptors recognise both lipoprotein and non-lipoprotein ligands and appear to participate in a wide variety of biological processes, making them prime candidates for drug delivery in general [125, 131, 303-306].

The receptor for advanced glycation end products (RAGE) is a 45 kDa pattern recognition multi-ligand surface receptor comprising three immunoglobulin domains, a single transmembrane region, and a short C-terminal cytoplasmic tail [307-310]. It is expressed in many cell types, including; brain endothelial cells, pericytes, astrocytes and microglia. The endocytic mechanism for RAGE is poorly understood, however some have suggested that it may follow a lipid-raft dependent pathway [311, 312]. In light of its proposed involvement with amyloid-β accumulation in Alzheimer's disease, in a process directly opposed to LRP-1 [284, 313], and in combination with its relative lack of specificity, RAGE has presented itself as a potential target for CoQ_{10} influx and will be explored further in this project [283, 284, 314-316].

P-glycoprotein (P-gp/ABCB1), a 170 kDa ATP-binding cassette (ABC) efflux-transporter, is distributed throughout the body in tissues with barrier function where it is responsible for mediating the cellular uptake and distribution of xenobiotics and toxic metabolites [317, 318]. It impedes the absorption, permeability, and retention of said compounds, extruding them out of the cell. Overexpressed on the luminal/apical membrane of the brain endothelium, P-gp is one of the most comprehensively characterised transport proteins of *in vitro* models of the BBB and is reported to be present in both bEnd.3 cells and PBECs [166, 167, 319-321]. There are hundreds of structurally diverse, although usually large (> 400 Da) and hydrophobic, substrates that bind to P-gp making it a highly proficient neuroprotective efflux-transporter [322, 323].

Findings from recent reports by Itagaki *et al.* [135, 324], using the Caco-2 intestinal epithelial-barrier model, have suggested that P-gp plays an interfering role in CoQ_{10} uptake such that inhibition of P-gp improves the permeability of the compound across the intestinal barrier. However, closer inspection of the experimental procedures indicate the use of

exogenous CoQ_{10} in its pure form as opposed to being associated with lipoprotein or in a digestive micelle, meaning the transport mechanisms described do not reflect the true *in vivo* environment. Furthermore, the Caco-2 intestinal barrier-model is a poor surrogate for BBB characteristics. Nevertheless, it is important to explore P-gp as a possible mode of CoQ_{10} efflux at the barrier, using a more robust and reliable model of the BBB.

4.2. Materials and Methods

4.2.1. Materials

Coenzyme Q_{10} Plasma Control, Level I (0092, ChromSystems®, Germany); Bovine Plasma Derived Serum (BPDS; First Link Ltd., UK); Foetal Bovine Serum (FBS; F7524, Sigma®, UK); HEPES (H3375, Sigma®, UK); HEPES (H3375, Sigma®, UK); Hank's Balanced Salt Solution (HBSS; H8264, Sigma®, UK); Bovine Serum Albumin (BSA; A6003, Sigma®, UK); coenzyme Q_{10} (C9538, Sigma®, UK); RAP (Enzo Life Sciences, Inc., UK); FPS-ZM1 (553030, Merck Chemicals Ltd., UK); (±)-verapamil hydrochloride (V4629, Sigma®, UK); BLT-1 (SML0059, Sigma®, UK).

4.2.2. Methods

Coenzyme Q_{10} Quantitation

Unless otherwise stated, CoQ_{10} concentrations were determined using the LC-MS/MS method described in Section 2.13.2. Duplicate samples of ChromSystems® EQC Plasma, IQC 0 (HBSS with 50 % (v/v) BPDS, 0.5 % (w/v) BSA, 25 mmol/L HEPES), and IQC 10 (HBSS with 50 % (v/v) BPDS, 0.5 % (w/v) BSA, 25 mmol/L HEPES, 10 µmol/L CoQ_{10}) were run at the beginning and end of each batch to ensure a consistent intra-batch instrument performance.

Cell Culture

bEnd.3 cells were cultured as outlined in Section 2.2 and passaged onto Transwell®-inserts for apparent permeability studies. Primary PBECs were isolated and cultured as per Sections 2.3 and 2.4, and passaged onto Transwell®-inserts for apparent permeability studies.
Primary astrocytes were isolated and cultured in accordance to Sections 2.5 and 2.6, with co-culture coordinated as per Appendix A.

Inducing Coenzyme Q_{10} Deficiency

Cell cultures were pharmacologically induced with a CoQ_{10} deficiency by supplementing culture media with 1 mmol/L *para*-aminobenzoic acid (*p*ABA) for a duration of 5 days, in accordance to the method described in Section 2.10.

Assessing Barrier Integrity

TEERs were measured across cell mono-layers on Transwell®-inserts as described in Section 2.7.1. Apparent permeability (P_{app}) of *in situ* paracellular marker FITC-40 was evaluated following the experimental procedures outlined in Sections 2.7.2 and 2.8.

Confocal Microscopy

Cell mono-layers grown on Transwell®-inserts were fixed, stained and imaged following the procedures outlined in Section 2.11.

Apparent Permeability

Apparent permeability (P_{app}) of CoQ_{10} was evaluated following the experimental procedures outlined in Section 2.8. Assay buffers were made up in HBSS at *p*H 7.4 (Table 10). CoQ_{10} was incubated with serum (45 minutes, 37^{o}C) prior to addition with the

remaining components of the assay buffer. Inhibitors were added in excess and pre-incubated with cells for 2 hours before assay [325-328].

Table 10: Composition of assay buffers used in apparent permeability studies. Condition A is the acceptor buffer and conditions B – F are donor buffers. B; CoQ_{10} control. C; LRP-1 inhibitor (RAP) [325]. D; RAGE inhibitor (FPS-ZM1) [326]. E; P-gp inhibitor (Verapamil) [327]. F; SR-B1 inhibitor (BLT-1) [328]. The serum used in bEnd.3 investigations was FBS, and for PBECs it was BPDS.

	BSA (*w/v*)	**HEPES (mmol/L)**	**Serum (*v/v*)**	**FITC-40 (mg/mL)**	**CoQ_{10} (µmol/L)**	**RAP (µmol/L)**	**FPS-ZM1 (µmol/L)**	**Verapamil (mmol/L)**	**BLT-1 (µmol/L)**
A	0.5 %	25	–	–	–	–	–	–	–
B	0.5 %	25	50 %	0.5	10	–	–	–	–
C	0.5 %	25	50 %	0.5	10	0.5	–	–	–
D	0.5 %	25	50 %	0.5	10	–	1.0	–	–
E	0.5 %	25	50 %	0.5	10	–	–	0.1	–
F	0.5 %	25	50 %	0.5	10	–	–	–	10

4.3. Results

4.3.1. Mechanisms of CoQ_{10} Uptake Across the bEnd.3 BBB

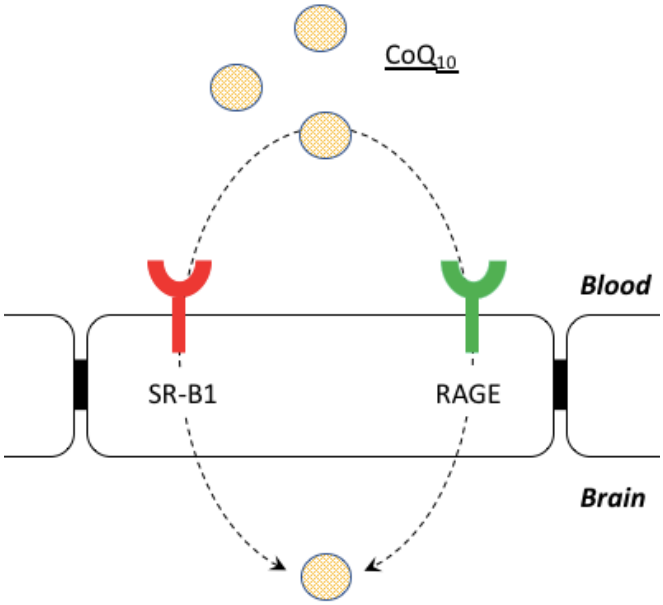

Figure 44: The proposed mechanisms for investigation in the receptor-mediated uptake of CoQ_{10} into the brain. Yellow spheres represent lipoprotein-associated CoQ_{10}.

Physiological Conditions

When assessed separately as influx (Figure 45) and efflux (Figure 46), isolated investigations into the receptor-mediated uptake of exogenous CoQ_{10} across the physiological bEnd.3 BBB (Figure 44) indicated no significant effect of transporter inhibition (RAGE inhibition; 1 µmol/L FPS-ZM1, and SR-B1 inhibition; 10 µmol/L BLT-1) on CoQ_{10} apparent permeability. Although, there was an insignificant trend to decrease blood-to-brain transport (RAGE inhibition; 23.1 % decrease, and SR-B1 inhibition; 30.8 % decrease) and increase brain-to-blood transport (RAGE inhibition; 20.0 % increase, and SR-B1 inhibition; 46.7 % increase) relative to controls.

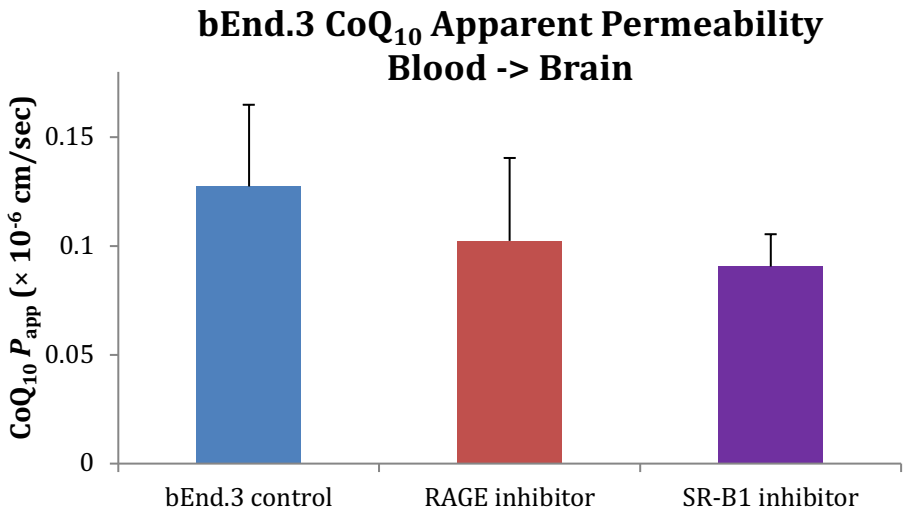

Figure 45: Effect of uptake inhibitors on CoQ_{10}, blood-to-brain, apparent permeability in the bEnd.3 BBB. bEnd.3 control (n = 12), RAGE inhibitor (FPS-ZM1; n = 4), SR-B1 inhibitor (BLT-1; n = 4). Error bars represent standard error of the mean (SEM).

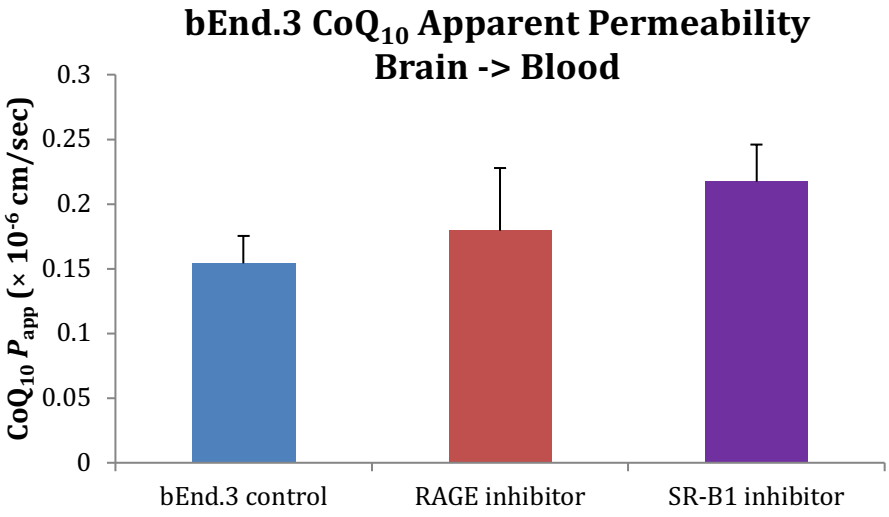

Figure 46: Effect of uptake inhibitors on CoQ_{10}, brain-to-blood, apparent permeability in the bEnd.3 BBB. bEnd.3 control (n = 9), RAGE inhibitor (FPS-ZM1; n = 5), SR-B1 inhibitor (BLT-1; n = 5). Error bars represent standard error of the mean (SEM).

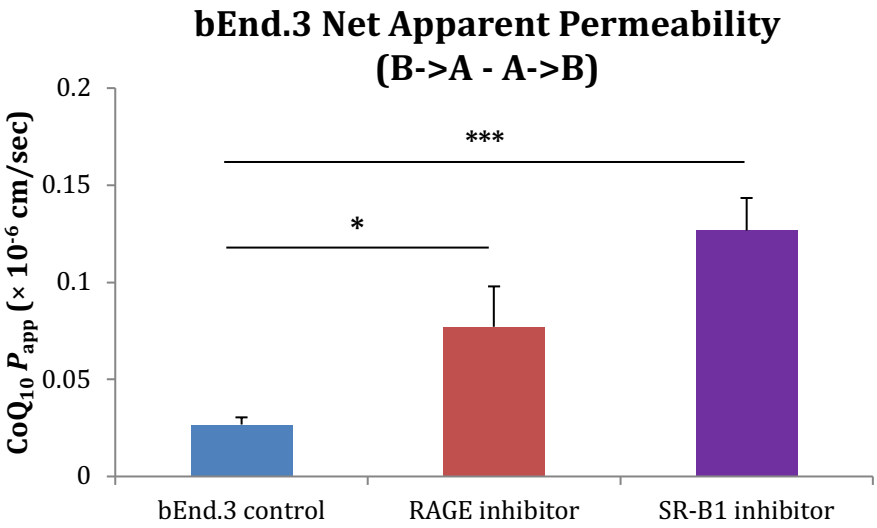

Figure 47: Net effect of uptake inhibitors on CoQ_{10} apparent permeability in the bEnd.3 BBB. bEnd.3 control (df = 19), RAGE inhibitor (FPS-ZM1; df = 7, $p < 0.05$), SR-B1 inhibitor (BLT-1; df = 7, $p < 0.001$). Error bars represent standard error of the mean (SEM).

Analysis of the combined difference between efflux and influx indicated a significant effect for both transport inhibitors (Figure 47). The inhibition of RAGE resulted in a significant ($p < 0.05$) 2-fold relative increase in net efflux of CoQ_{10} from brain-to-blood. The same was observed for the inhibition of SR-B1, which resulted in an even greater net efflux ($p < 0.001$) from brain-to-blood at the physiological bEnd.3 BBB. This implicates the involvement of both transporters in the receptor-mediated uptake of CoQ_{10} into the brain.

Pathophysiological Conditions

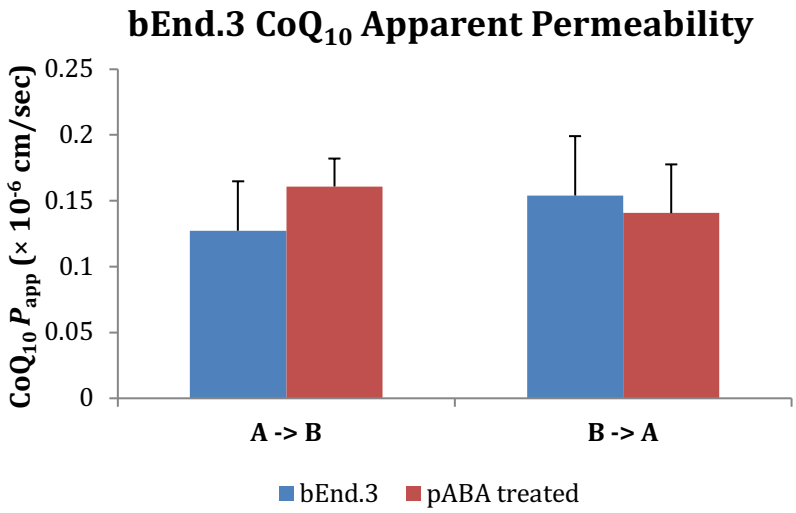

Figure 48: Effect of *p*ABA treatment (1 mmol/L, 5 days) on CoQ_{10} apparent permeability in the bEnd.3 BBB. bEnd.3 control; A->B (n = 12), B->A (n = 9). *p*ABA treated control; A->B (n = 9), B->A (n = 9). Error bars represent standard error of the mean (SEM).

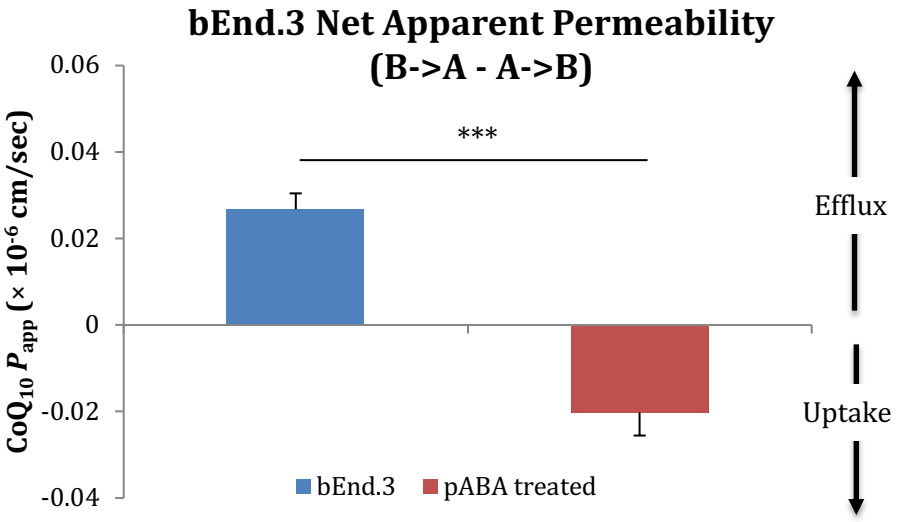

Figure 49: Net effect of *p*ABA treatment (1 mmol/L, 5 days) on CoQ_{10} apparent permeability in the bEnd.3 BBB. bEnd.3 control (df = 19), *p*ABA treated control (df = 16, $p < 0.001$). Error bars represent standard error of the mean (SEM).

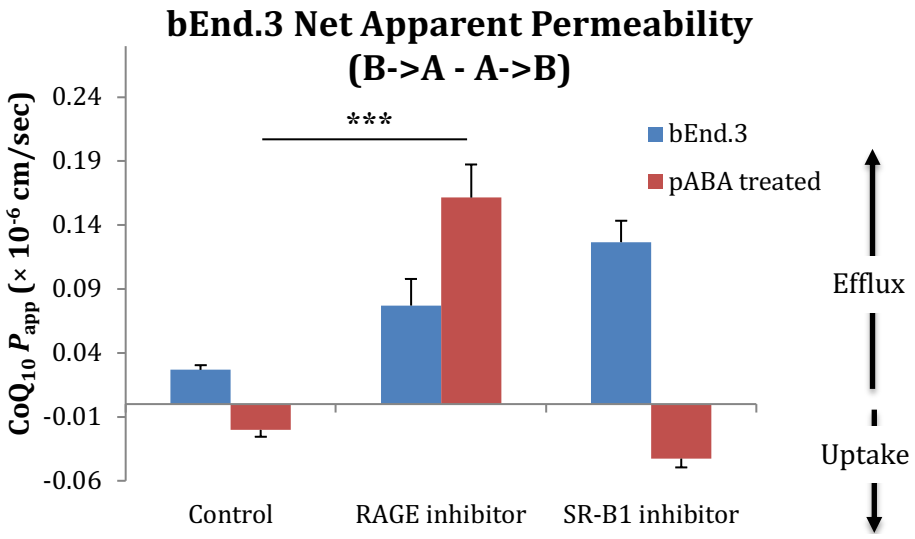

Figure 50: Net effect of *p*ABA treatment (1 mmol/L, 5 days) and uptake inhibitors on CoQ_{10} apparent permeability in the bEnd.3 BBB. Control; bEnd.3 (df = 19), *p*ABA treated (df = 16). RAGE inhibitor (FPS-ZM1); bEnd.3 (df = 7), *p*ABA treated (df = 9, $p < 0.001$). SR-B1 inhibitor (BLT-1); bEnd.3 (df = 7), *p*ABA treated (df = 8). Error bars represent standard error of the mean (SEM).

To further understand the pathophysiological consequence of a CoQ_{10} deficiency on the uptake of exogenous CoQ_{10} into the brain, a pharmacologically induced CoQ_{10} deficient bEnd.3 BBB model was established using *p*ABA (1 mmol/L, 5 days).

Again, when influx and efflux were assessed separately there was no statistically significant effect of *p*ABA treatment on the apparent permeability of CoQ_{10} (Figure 48). However, when expressed as a Net transport, results indicated that the CoQ_{10} deficient bEnd.3 BBB exhibited an overall net influx of CoQ_{10} from the blood to the brain (Figure 49). This effect was significant ($p < 0.001$) and opposed the observed net efflux of CoQ_{10} across the physiological bEnd.3 BBB model.

Assessment of the effect of a CoQ_{10} deficiency on the individual receptor-mediated transport mechanisms indicated a comparable effect on SR-B1 relative to controls, but an contrasting ($p < 0.001$) benign effect of *p*ABA treatment on RAGE (Figure 50). This suggests that uptake of CoQ_{10} across the BBB by RAGE is unaffected by a CoQ_{10} deficiency.

4.3.2. Mechanisms of CoQ_{10} Efflux Across the bEnd.3 BBB

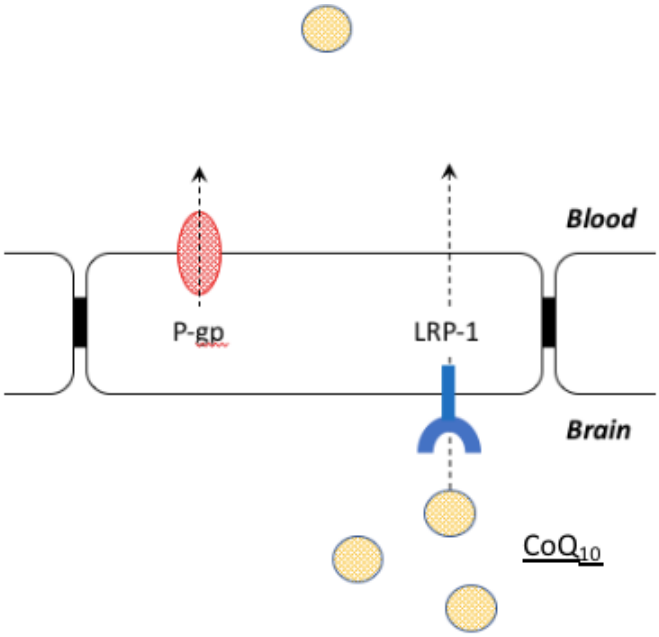

Figure 51: The proposed mechanisms for investigation in the receptor-mediated efflux of CoQ_{10} into the blood. Yellow spheres represent lipoprotein-associated CoQ_{10}.

Physiological Conditions

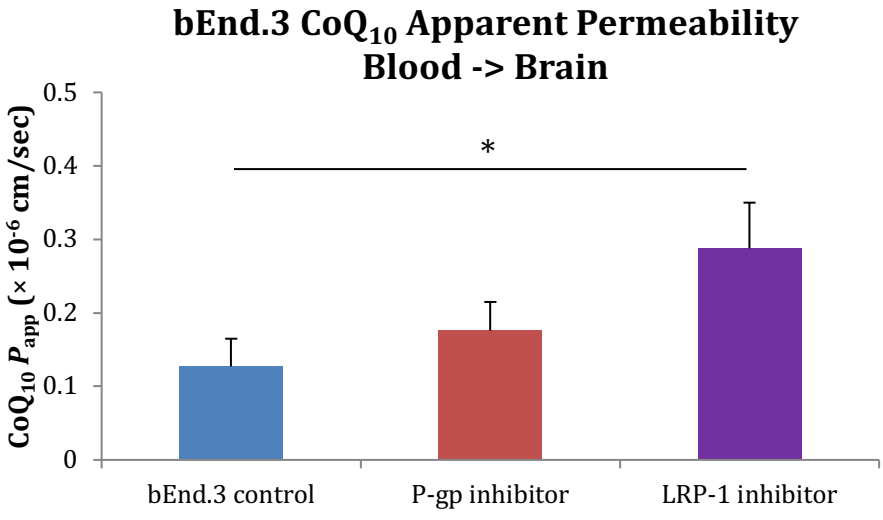

Figure 52: Effect of efflux inhibitors on CoQ_{10}, blood-to-brain, apparent permeability in the bEnd.3 BBB. bEnd.3 control (n = 12), P-gp inhibitor (Verapamil; n = 5), LRP-1 inhibitor (RAP; n = 5, $p < 0.05$). Error bars represent standard error of the mean (SEM).

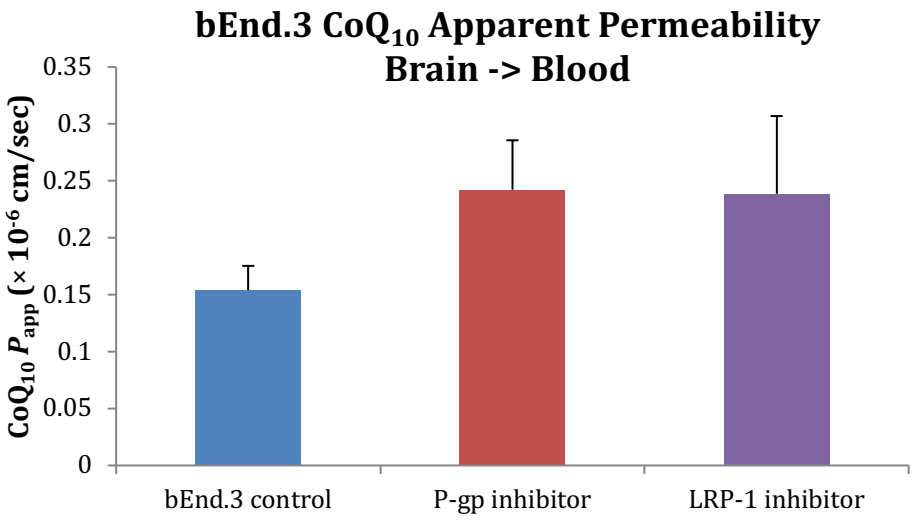

Figure 53: Effect of efflux inhibitors on CoQ_{10}, brain-to-blood, apparent permeability in the bEnd.3 BBB. bEnd.3 control (n = 9), P-gp inhibitor (Verapamil; n = 4), LRP-1 inhibitor (RAP; n = 4). Error bars represent standard error of the mean (SEM).

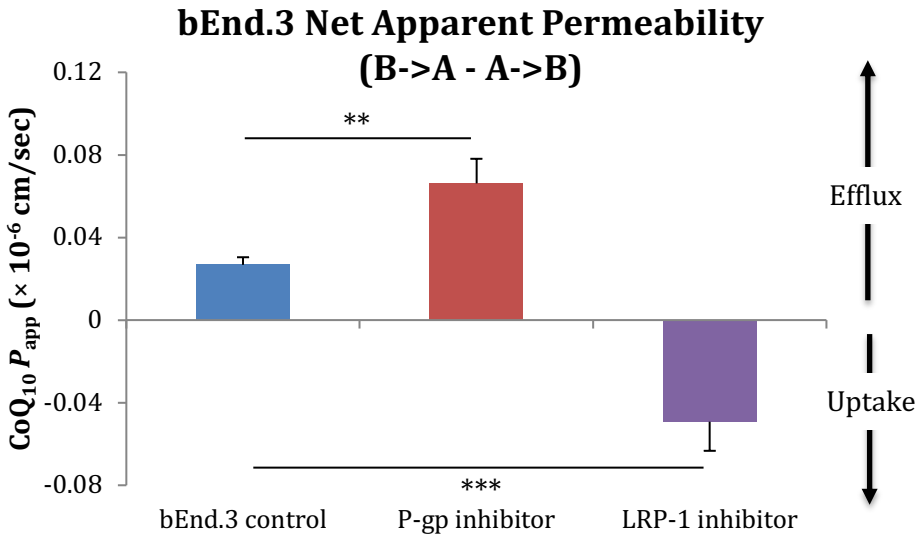

Figure 54: Net effect of efflux inhibitors on CoQ_{10} apparent permeability in the bEnd.3 BBB. bEnd.3 control (df = 19), P-gp inhibitor (Verapamil; df = 7, $p < 0.01$), LRP-1 inhibitor (RAP; df = 7, $p < 0.001$). Error bars represent standard error of the mean (SEM).

Using the same methods employed for the investigations into CoQ_{10} uptake, the mechanisms for transport-mediated efflux of CoQ_{10} at the physiological bEnd.3 BBB were examined (Figure 51).

There was a significant increase (126.8 % relative increase, $p < 0.05$) in blood-to-brain CoQ_{10} apparent permeability when the LRP-1 receptor was inhibited (0.5 μmol/L RAP)

relative to controls (Figure 52). This suggests an efflux mode of action for the LRP-1 receptor at the bEnd.3 BBB under physiological conditions. No significant effects were observed in the brain-to-blood CoQ_{10} apparent permeability when either the LRP-1 or P-gp receptors were inhibited (Figure 53).

Comparison of the net effect of transporter inhibition on CoQ_{10} apparent permeability confirmed a significant ($p < 0.001$) LRP-1 mediated efflux of CoQ_{10} from the brain to the blood at the bEnd.3 BBB. Somewhat unexpectedly, the effect of P-gp inhibition (0.1 mmol/L Verapamil) indicated a significant ($p < 0.01$) increase in net efflux of CoQ_{10}, suggesting an overall blood-to-brain, or uptake, mode of action for the P-gp receptor (Figure 54).

Pathophysiological Conditions

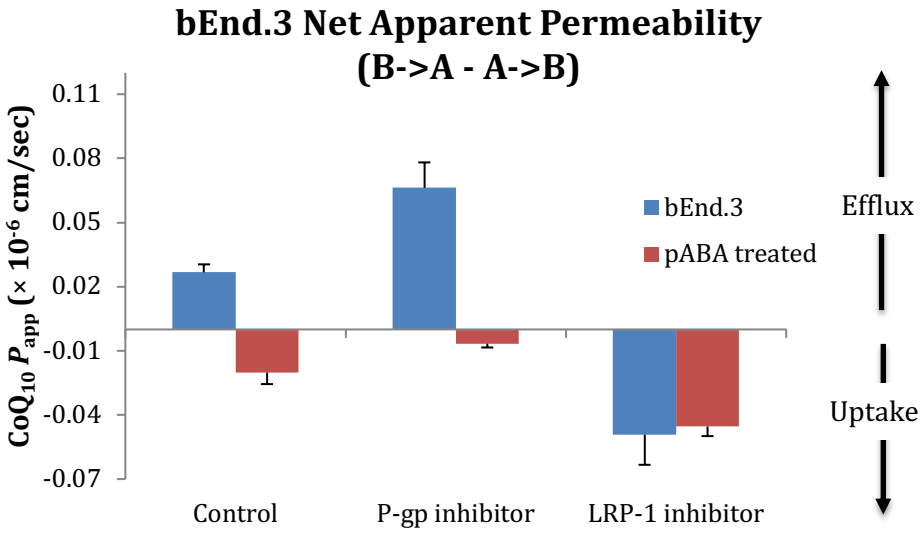

Figure 55: Net effect of *p*ABA treatment (1 mmol/L, 5 days) and efflux inhibitors on CoQ_{10} apparent permeability in the bEnd.3 BBB. Control; bEnd.3 (df = 19), *p*ABA treated (df = 16). P-gp inhibitor (Verapamil); bEnd.3 (df = 7), *p*ABA treated (df = 7). LRP-1 inhibitor (RAP); bEnd.3 (df = 7), *p*ABA treated (df = 7). Error bars represent standard error of the mean (SEM).

Under pathophysiological CoQ_{10} deficient conditions, inhibition of the P-gp receptor had no effect, suggesting that this efflux transporter was no longer active or polarised with *p*ABA treatment. However, akin to RAGE (Figure 50), results highlighted that a CoQ_{10} deficiency did not diminish efflux by LRP-1 at the bEnd.3 BBB (Figure 55).

4.3.3. Mechanisms of CoQ_{10} Transport at the PBEC BBB

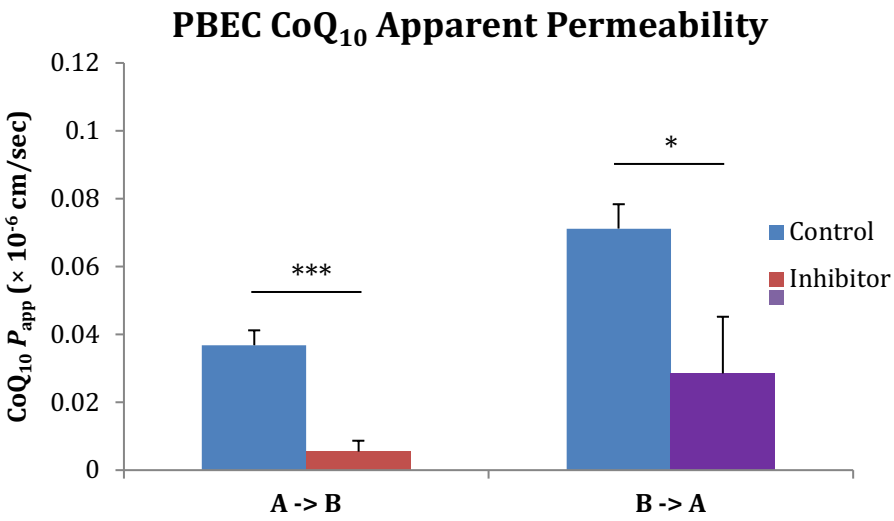

Figure 56: Effect of inhibitors on CoQ_{10} apparent permeability in the PBEC BBB.
A -> B; PBEC control (n = 3), RAGE inhibitor (FPS-ZM1; n = 4, $p < 0.001$). B -> A; PBEC control (n = 4), LRP-1 inhibitor (RAP; n = 4, $p < 0.05$). Error bars represent standard error of the mean (SEM).

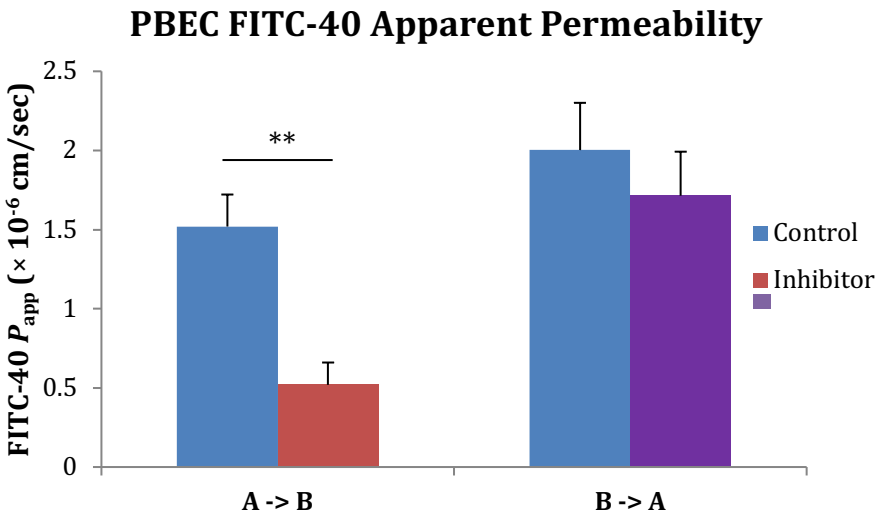

Figure 57: Effect of inhibitors on FITC-40 apparent permeability in the PBEC BBB.
A -> B; PBEC control (n = 3), RAGE inhibitor (FPS-ZM1; n = 4, $p < 0.01$). B -> A; PBEC control (n = 4), LRP-1 inhibitor (RAP; n = 4). Error bars represent standard error of the mean (SEM).

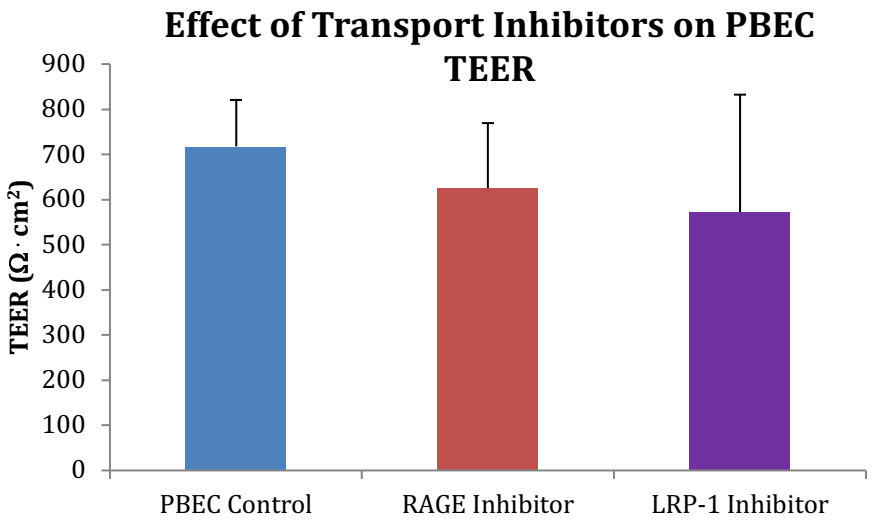

Figure 58: Effect of transport inhibitors on TEER in the PBEC BBB.
PBEC control (n = 7), RAGE inhibitor (FPS-ZM1; n = 4), LRP-1 inhibitor (RAP; n = 4). Error bars represent standard error of the mean (SEM).

Having explored some of the possible mechanisms for receptor-mediated uptake and efflux of exogenous CoQ_{10} across the bEnd.3 BBB, under physiological and pathophysiological conditions, the most promising candidates (RAGE and LRP-1) were taken forward for investigation in the gold-standard PBEC BBB model.

Assessment of the receptor-mediated uptake of CoQ_{10} by RAGE across the PBEC BBB indicted a significant decrease by 75 % ($p < 0.001$) in blood-to-brain CoQ_{10} apparent permeability when the transporter was inhibited (Figure 56). Similarly, inhibition of the LRP-1 receptor resulted in a significant decrease by 57 % ($p < 0.05$) in brain-to-blood CoQ_{10} apparent permeability (Figure 56), suggesting a receptor-mediated efflux role for LRP-1 at the physiological PBEC BBB. Both results corroborate with the findings from the physiological bEnd.3 BBB model (Sections 4.3.1 and 4.3.2).

Interestingly, the inhibition of RAGE corresponded to a significant decrease in FITC-40 apparent permeability (34.2 % of control, $p < 0.01$) which suggests a generalised reduction in baseline transcytosis (Figure 57). There was no effect on FITC-40 apparent permeability as a result of LRP-1 inhibition and neither of the transport inhibitors impacted PBEC TEER (Figure 58), meaning the observed effects were not subject to interference from paracellular events.

4.3.4. Effect of CoQ_{10} Deficiency on the PBEC BBB

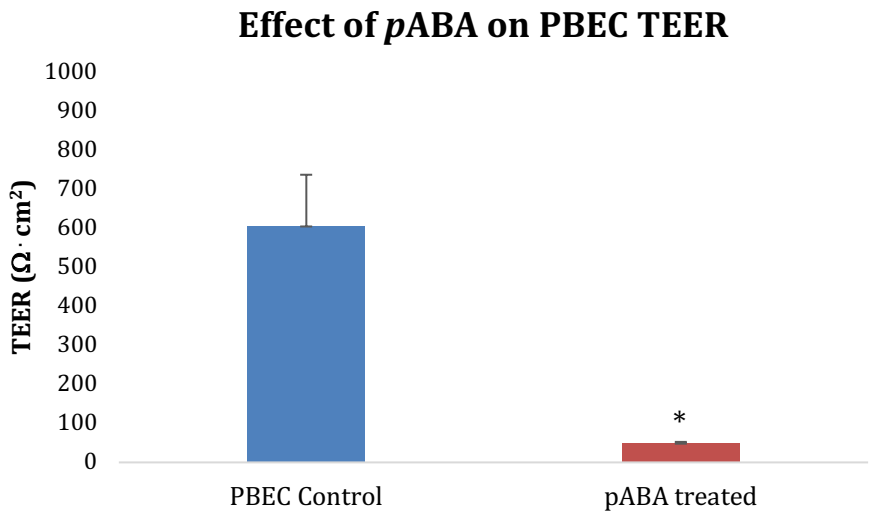

Figure 59: Effect of *p*ABA treatment (1 mmol/L, 5 days) on TEER in the PBEC BBB. PBEC control (n = 8), *p*ABA PBEC (n = 3, $p < 0.05$). Error bars represent standard error of the mean (SEM).

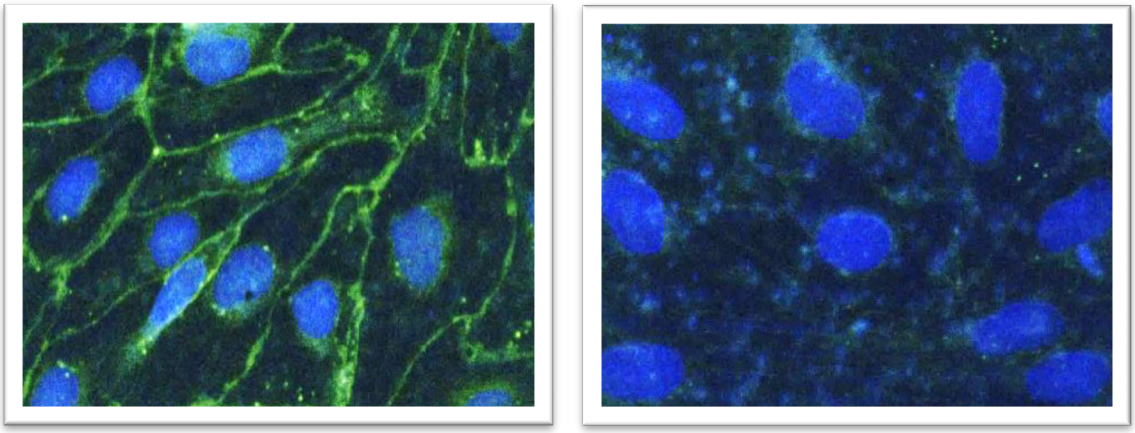

Figure 60: Immunofluorescent confocal images of the PBEC BBB. Left image; PBEC control. Right image; *p*ABA treated (1 mmol/L, 5 days) PBECs. Alexa Fluor® 488 (green) represents the tight-junction protein claudin-5. DAPI (blue) highlights the nuclei.

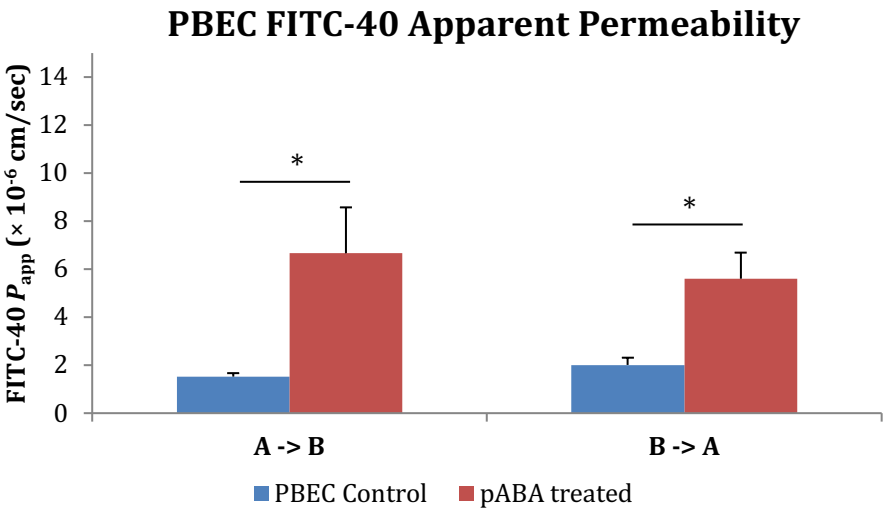

Figure 61: Effect of *p*ABA treatment (1 mmol/L, 5 days) on FITC-40 apparent permeability in the PBEC BBB. A -> B; PBEC control (n = 4), *p*ABA PBEC (n = 3, $p < 0.05$). B -> A; PBEC control (n = 4), *p*ABA PBEC (n = 3, $p < 0.05$). Error bars represent standard error of the mean (SEM).

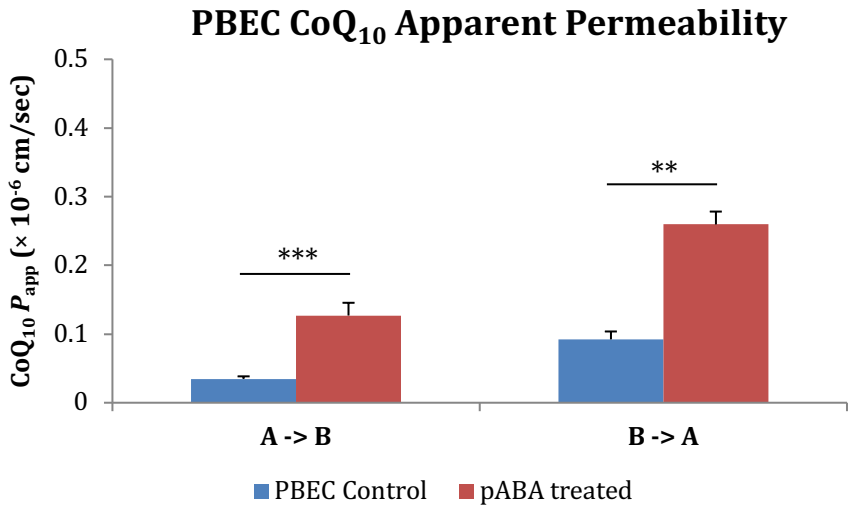

Figure 62: Effect of *p*ABA treatment (1 mmol/L, 5 days) on CoQ_{10} apparent permeability in the PBEC BBB. A -> B; PBEC control (n = 4), *p*ABA PBEC (n = 3, $p < 0.001$). B -> A; PBEC control (n = 3), *p*ABA PBEC (n = 3, $p < 0.01$). Error bars represent standard error of the mean (SEM).

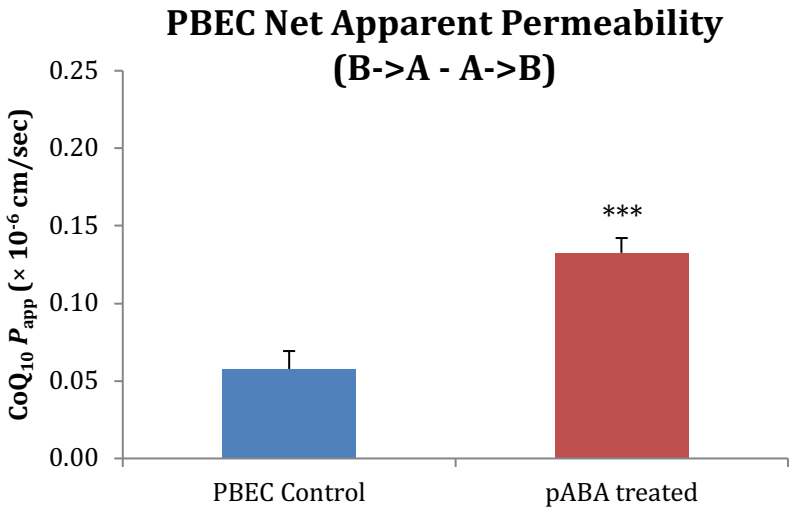

Figure 63: Net effect of *p*ABA treatment (1 mmol/L, 5 days) on CoQ_{10} apparent permeability in the PBEC BBB. PBEC control (df = 6), *p*ABA PBEC (df = 4, p < 0.001). Error bars represent standard error of the mean (SEM).

When a CoQ_{10} deficiency was induced in the PBEC BBB model, TEER was reduced significantly by 92 % ($p < 0.05$) (Figure 59) and FITC-40 apparent permeability was significantly increased in both directions (blood-to-brain; 338.2 % increase, $p < 0.05$ and brain-to-blood; 178.6 % increase, $p < 0.05$) (Figure 61). These results provide strong evidence for increased paracellular permeability in the PBEC BBB as a consequence of TJ breakdown due to a CoQ_{10} deficiency. This was confirmed by immunofluorescent confocal imaging, which clearly demonstrated a diminished cell surface expression of the TJ protein claudin-5 in the *p*ABA-treated PBEC BBB (Figure 60).

As would be expected from a degradation in BBB integrity, CoQ_{10} apparent permeability was significantly increased in both directions (blood-to-brain; 333.3 % increase, $p < 0.001$ and brain-to-blood; 188.9 % increase, $p < 0.01$) (Figure 62), with an overall significant increase in net efflux ($p < 0.001$) of CoQ_{10} from brain-to-blood (Figure 63).

4.4. Discussion

Under physiological conditions, findings from this study have indicated that there is a net efflux of exogenous CoQ_{10} from the brain to the blood in the bEnd.3 BBB model (0.03×10^{-6} cm/sec) (Sections 4.3.1 and 4.3.2). This profile was consistent with that observed in the physiological PBEC BBB (net CoQ_{10} efflux = 0.06×10^{-6} cm/sec) which is a more *in vivo*-like model, based on BBB characteristics (Section 4.3.3). Furthermore, through comparison of the PBEC CoQ_{10} P_{app} (0.04×10^{-6} cm/sec) with the PBEC FITC-40 P_{app} (1.52×10^{-6} cm/sec), CoQ_{10} does not appear to cross the BBB passively or paracellularly. This is the first time a receptor-mediated efflux mechanism has been implicated for CoQ_{10} at the BBB and it is certainly in agreement with the clinical ineffectiveness of CoQ_{10} therapy for the treatment of neurological disorders [329].

Another theory for the poor efficacy of CoQ_{10} therapy is the possible retention or metabolism of CoQ_{10} by the BBB, however, there was a full recovery of exogenous CoQ_{10} in every assay carried out (100.5 ± 0.8 %, n = 8 in PBEC and 100.5 %, n = 2 in *p*ABA PBEC, results not shown) and no accumulation of CoQ_{10} in the endothelial cells themselves, suggesting that the refractory nature is more likely dominated by unfavourable transcytic transport mechanisms. That's said, it was vitally important to understand these mechanisms in more detail and to further ascertain the pathophysiological consequences of a CoQ_{10} deficiency at the BBB.

The strategy adopted for investigating the precise mechanisms governing uptake and efflux of CoQ_{10} across the BBB was to perform initial studies on the commercially available immortalised bEnd.3 in vitro BBB model, primarily due to the ease of use and relatively high-throughput that could be achieved. Promising candidates from these studies were then taken forward to be assessed on the gold-standard primary PBEC BBB model to obtain results that better reflect *in vivo* conditions.

Based on the assumption of successful loading of exogenous CoQ_{10} into lipoproteins, as was indicated by the lipoprotein fractionation experiments (Section 3.3.3, Figure 27), it was possible to selectively investigate the uptake and efflux mechanisms operating at the *in vitro* BBB. Investigations into the receptor-mediated uptake of CoQ_{10} was achieved by the selective inhibition of RAGE and SR-B1, using an excess of the inhibitors FPS-ZM1 [330] and BLT-1 [331, 332] respectively. While verapamil [333-335], a commonly used first generation

inhibitor of P-gp, and RAP [281, 325], a potent inhibitor of LRP-1, were utilised to probe receptor-mediated efflux mechanisms.

The outcome from investigations in the physiological bEnd.3 BBB provided evidence for RAGE ($p < 0.05$) and SR-B1 ($p < 0.001$) mediated uptake, concomitant with an LRP-1 ($p < 0.001$) dependent efflux of CoQ_{10}. This combination of uptake and efflux is well documented for lipoproteins and is a prominent feature in the study of Alzheimer's disease for the clearance of amyloid-beta [283-287]. However, this is the first time these receptors have been confirmed as the route of transport for CoQ_{10} at the BBB. These results also validate lipoproteins as the primary carrier of exogenous CoQ_{10} and provide support for a robust experimental procedure.

Surprisingly, however, P-gp was shown to be operating as an influx receptor. This is in stark contrast to the findings of Itagaki *et al.* [135, 324] who illustrated a P-gp mediated efflux of CoQ_{10} at the intestinal epithelial-barrier, and against the numerous comprehensive studies that have characterised P-gp as a non-specific luminal efflux-transporter [166, 167, 319-321], meaning this result should be taken with caution. Reasoning behind this observed phenomena is as yet unknown, but could be due to the very poor TEER of the bEnd.3 BBB ($35.4 \pm 1.1\ \Omega \cdot cm^2$, n = 90), and therefore decreased polarisation of the endothelia, which could plausibly facilitate an atypical luminal/basolateral distribution of the receptor due to an increased motility throughout the lipid membrane. Nevertheless, there was a significant ($p < 0.01$) net effect of inhibition meaning the P-gp receptor is likely to be involved in the transport of the compound, whether that be in the uptake or efflux remains to be seen. If P-gp does emerge as an efflux receptor for CoQ_{10}, then perhaps a therapeutic strategy would be to administer exogenous CoQ_{10} in the evening as a means to reduce this effect, as has been proposed by Zhang *et al.* [336] who suggest that circadian rhythms regulate efflux at the BBB.

Having gained an understanding of the mechanisms governing uptake and efflux of CoQ_{10} at the physiological bEnd.3 BBB, a CoQ_{10} deficiency was pharmacologically induced using *p*ABA, yielding the first reported CoQ_{10} deficient *in vitro* model of the BBB.

Given that the TEER of the bEnd.3 BBB was already very low, the effect of *p*ABA treatment did not appear to perturb the TJs any further ($35.4 \pm 1.1\ \Omega \cdot cm^2$, n = 90 in bEnd.3 and $38.0 \pm 1.0\ \Omega \cdot cm^2$, n = 89 in *p*ABA treated bEnd.3, results not shown), although results are

generally deemed unreliable since there is a greater degree of instrumental error associated with the measurements of small TEER. Regardless, the model did enable investigations into the impact of a CoQ_{10} deficiency on the receptor-mediated transcytosis of exogenous CoQ_{10}.

Under pathophysiological conditions the observed net efflux of CoQ_{10} at the bEnd.3 BBB is reversed ($p < 0.001$). This suggests that the mechanisms governing CoQ_{10} efflux are either active processes or are more susceptible to a change in antioxidant capacity.

Further examination of the results indicates that RAGE and LRP-1 are unaffected by the induced CoQ_{10} deficiency, but both P-gp and SR-B1 showed a similar effect to controls suggesting a *p*ABA induced inactivity. This would imply that modes of uptake and efflux for CoQ_{10} are still present under pathophysiological conditions, albeit at a reduced capacity compared to normal controls.

To validate and strengthen the initial conclusions drawn from the bEnd.3 investigations, further analysis was performed on the gold-standard PBEC BBB model. However, due to the cost and complexity of the technique, only select mechanisms were investigated. Since there was no detrimental effect of pathology on the RAGE and LRP-1 receptors, these were taken forward as candidates for analysis on the PBEC BBB, albeit SR-B1 did exhibit a significant degree of net uptake in the physiological bEnd.3 BBB and should be considered in future experiments.

The results from the physiological PBEC BBB were in agreement with that of the bEnd.3 BBB model, such that RAGE was confirmed as an uptake receptor for CoQ_{10} ($p < 0.001$) and LRP-1 was confirmed as a mode of efflux for CoQ_{10} ($p < 0.05$) at the BBB (Section 4.3.3). While these findings are in themselves novel in nature, the data also provided some insight into the potential mechanism for RAGE uptake. Through closer inspection of the FITC-40 data it was noted that there was a significant decrease ($p < 0.001$) in FITC-40 P_{app} as a result of RAGE inhibition by FPS-ZM1, this observation suggests that RAGE operates via a large vesicular transcytic mechanism, since it is known that vicinal FITC-40 can be internalised during such processes [337, 338]. Following the same logic, it could be said that transcytosis via LRP-1 may proceed via an alternative mechanism, perhaps giving support to the recent findings of Nyberg *et al.* [253] who have suggested a 'tunnelling' process for LRP-1. However, there is debate over the inherent limitations of the

techniques used to support this theory, as the instruments were operating at the limit of temporal resolution which may have resulted in false positive motion artefacts.

As with the bEnd.3 model, the PBEC BBB was pharmacologically induced with a CoQ_{10} deficiency using *p*ABA, again, this is the first reported case for this pathophysiological BBB model. The most notable effect *p*ABA treatment had on the PBEC BBB was a significant ($p < 0.05$) decrease in TEER to a level comparable with that of the bEnd.3 BBB model. This implies that, perhaps, this is the maximum effect of a CoQ_{10} deficiency on the TJs, as *p*ABA failed to perturb TEER in the bEnd.3 model. Therefore, it could be said that the maintenance of the protein network responsible for this low level residual TJ formation, is ATP independent.

Further analysis using confocal microscopy suggested that an explanation for the observed TJ breakdown in the PBEC BBB may be due to an internalisation of the main TJ protein Claudin-5 from the cell surface to the cytosol. The findings from similar work by Duijghuijsen *et al.* [265], who noted a Claudin-7 internalisation after an induced ATP depletion in the Caco-2 intestinal epithelial-barrier model, are in agreement with this observation. These results, therefore, suggest that the expression and maintenance of a highly functional TJ network at the surface of the endothelia requires mitochondrial ATP or a finely balanced redox state.

As expected, the breakdown in TJ function corresponded to an increase in bidirectional paracellular and CoQ_{10} apparent permeability across the PBEC BBB. Interestingly, however, this did not correspond with a net uptake of exogenous CoQ_{10} from the blood to the brain, as was the case with the pathophysiological bEnd.3 BBB model, meaning the observed effect is likely due to the continued operation of efflux receptors and/or disproportional knockdown of uptake receptors. Either way, this does provide an explanation for the refractory nature of neurological symptoms associated with CoQ_{10} deficiencies with CoQ_{10} supplementation.

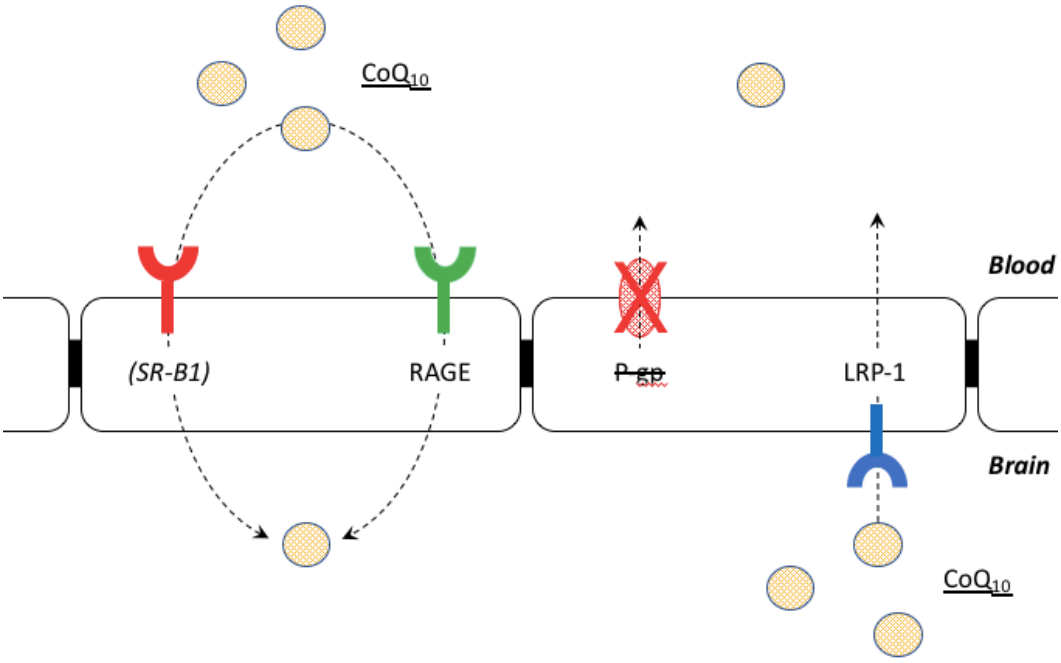

Figure 64: A summary of the findings from investigations into the mechanisms governing CoQ_{10} uptake and efflux at the BBB. The RAGE receptor was confirmed in both the bEnd.3 and PBEC BBB models as a mode of uptake, similarly the LRP-1 was confirmed as a mode of efflux. The SR-B1 receptor was implicated as a mode of uptake in the bEnd.3 model and the investigations into P-gp were inconclusive. Yellow spheres represent lipoprotein-associated CoQ_{10}.

Taken collectively, these results have demonstrated for first time a dynamic interplay of multiple transport receptors, with varying degrees of influence, for the uptake and efflux of CoQ_{10} across the BBB. While there is substantial evidence for the involvement of RAGE, LRP-1 and SR-B1 in the transport of CoQ_{10} across the BBB (Figure 64), these are not predicted to be a comprehensive representation of all the receptors involved in its transport. Results have shown that the mechanisms governing uptake/efflux are complex and it is likely there are many interactions occurring simultaneously, nevertheless, this study has narrowed down and isolated some key instigators, and also provided a solid foundation for further investigations.

From a clinical perspective, these findings have expanded our biochemical knowledge of CoQ_{10}, and imply that the uptake of exogenous CoQ_{10} into the brain could be improved by the administration an LRP-1 inhibitor, or by implementing interventions that stimulate a luminal overexpression of RAGE and SR-B1.

Recently, Wang *et al.* [284] provided evidence for the overexpression of LRP-1 and suppression of RAGE using peroxisome proliferator-activated receptor-γ (PPAR-γ) agonists in an effort to ameliorate diabetes-associated cognitive decline in rodents, based on this logic, perhaps a PPAR-γ antagonist would impart the opposite effect thereby increasing CoQ_{10} uptake into the brain [339-341]. However, due to the broad specificity of LRP-1, RAGE and SR-B1, and the important role they play in various other biological functions, there may be adverse side effects that outweigh the potential benefits of this approach. Nevertheless, it is a consideration for end-of-life care or in acute therapy to prevent irreversible damage, although further tests would need to be performed to understand the wider clinical implications of their inhibition/stimulation. A more risk averse alternative is to explore analogues of CoQ_{10} which may show improved brain uptake while imparting a comparable therapeutic effect.

5. Clinically Relevant Analogues of Coenzyme Q_{10}

5.1. Background

Mitochondrial disorders are among the most common inherited conditions that cause neurological impairment. Generally, once diagnosed, patients receive a 'mito-cocktail' treatment containing antioxidants and cofactors for the various constituents of the MRC [342-346]. The mito-cocktail is tailored to the patient and usually consists of antioxidants such as CoQ_{10}, α-toc, ascorbate, the flavoprotein precursor riboflavin, and creatine monohydrate to assist in ATP generation [347, 348]. With both α-toc and CoQ_{10} being amongst the most popular choices for treatment, particularly in ataxic patients [348-352].

As previously mentioned (Section 1.1.3), α-toc is structurally and biochemically similar to CoQ_{10}, both are potent lipid-soluble antioxidants, they share similar redox properties, and are thought to undergo analogous uptake and distribution processes [41]. However, due to the considerable similarities and subsequent competition, some have indicated that high doses of α-toc (1310 IU/kg) may impede CoQ_{10} uptake *in vivo*, resulting in lower plasma levels of the quinone. Conversely, in the same study, it was also suggested that low concentrations of α-toc (100 IU/kg) in conjugation with CoQ_{10} could improve overall uptake and distribution into tissue [353].

Since α-toc is a prominent component of the mito-cocktail, it is important to understand the effect this may have on the transport of CoQ_{10} into the brain, and indeed the peripheral tissue, in doing so the cocktail can be optimised to become a more efficacious treatment [354].

In addition to the nutraceutical approach of the mito-cocktail, numerous synthetic analogues of CoQ_{10} have been designed with an aim to improve bioavailability and enhance therapeutic potential. To date, the most promising synthetic small molecule candidates for the treatment of mitochondrial disorders include; idebenone, EPI-743, and MitoQ®. Each of these analogues share a common quinone core attached to different side-

chain moieties (Figure 65), suggesting all exhibit a similar redox function, albeit with a varied capacity to restore electron flux through the MRC enzymes.

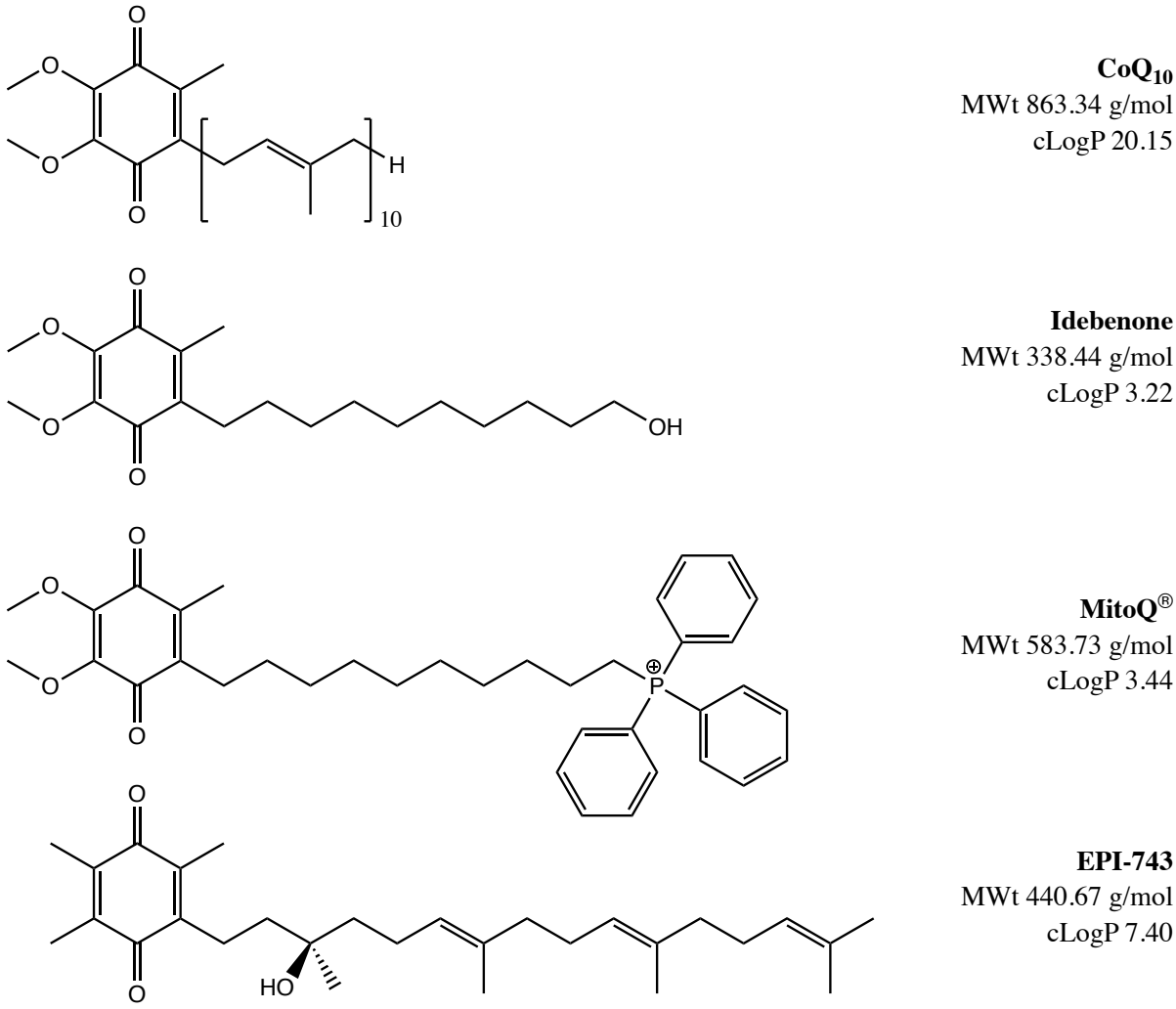

CoQ_{10}
MWt 863.34 g/mol
cLogP 20.15

Idebenone
MWt 338.44 g/mol
cLogP 3.22

MitoQ®
MWt 583.73 g/mol
cLogP 3.44

EPI-743
MWt 440.67 g/mol
cLogP 7.40

Figure 65: Skeletal structures and associated physicochemical properties of the main synthetic analogues of CoQ_{10}.

Initially developed by Takeda Pharmaceutical Company Ltd., Japan, for the treatment of Alzheimer's disease [355], idebenone is now a licensed drug (Raxone®/Catena®/ Sovrima®) that is clinically approved for the treatment of Leber's hereditary optic neuropathy [356, 357] and Duchenne muscular dystrophy [358], with a phase IIa randomised, double blind, placebo controlled, dose-finding study of idebenone in MELAS syndrome ongoing (trial ID: NCT01370447) [359]. Given that mitochondrial dysfunctions may play a key role in progressive axonal loss in Multiple Sclerosis (MS), a phase II trial of idebenone efficacy in Primary Progressive MS is currently underway (trial ID: NCT01854359) [360]. Additionally,

idebenone has demonstrated some efficacy in the treatment of Friedreich's ataxia, where studies have shown; improved cardiac measures [361, 362]; a correlation between serum idebenone levels and International Cooperative Ataxia Rating Scale (ICARS) scores; as well as a stabilisation of neurological progression in paediatric patients [363, 364].

The mechanism of action for idebenone is thought to restore both mitochondrial membrane potential ($\Delta\psi_m$) and cellular antioxidant status: Bypassing complex I, idebenone is reduced by the cytosolic flavoprotein DT-diaphorase (NQO1 or NAD(P)H: quinone oxidoreductase), feeding electrons directly into complex III of the MRC to restore $\Delta\psi_m$ and subsequent ATP production [365-367]. The redox-active quinone core affords a potent antioxidant function to the molecule, as is the case with all the aforementioned synthetic analogues of CoQ_{10} [368].

However, while idebenone has proven to be an effective treatment for some mitochondrial disorders, there are several reports of idebenone inhibiting complex I activity and promoting superoxide production *in vitro* [369-374], with some even demonstrating a cytotoxic effect at high-doses (> 25 μM) [375]. King *et al.* [376] provided a detailed investigation into this phenomenon and concluded that idebenone has a high affinity for the quinone-binding site within complex I, resulting in a strong association and slow dissociation. Consequently, it acts as a competitive substrate that impairs endogenous CoQ_{10} function without substituting for its electron transfer function to complex III. Furthermore, idebenone is shown to bind to a second hydrophilic site within complex I where it is reduced by flavin mononucleotide to form an unstable semiquinone that generates superoxide.

Interestingly, King *et al*. [376] also suggested decylubiquinone to be the most appropriate substrate for complex I in systems that lack endogenous CoQ_{10}. Indeed this is supported by the work of Fash *et al.* [50] who investigated the effect of alkyl side chain modification on 2,3-dimethoxy-5-methylbenzoquinones, showing decylubiquinone to be more effective than idebenone in restoring MRC function, antioxidant capacity, and $\Delta\psi_m$. However, very limited *in vivo* investigations have focussed on decylubiquinone as a therapeutic candidate for the treatment of mitochondrial disorders [377].

MitoQ® was designed on the turn of the century by M. P. Murphy and R. A. J. Smith, and synthesised by G. Kelso, at the University of Otago, New Zealand [378]. It has a similar chemical structure to idebenone, and is a variant of decylubiquinone, with the addition

of a triphenylphosphonium (TPP) cation moiety on the terminal carbon of the alkyl side chain.

The Nernst equation indicates that the uptake of singly charged cations increases 10-fold for every 61.5 mV of membrane potential at 37°C [379], meaning there is a 100 – 1000-fold accumulation of MitoQ® into the mitochondrial matrix in response to the $\Delta\psi_m$ (-150 to -180 mV, negative inside) and the delocalised positive charge of the TPP moiety [380-382]. Uptake into cells is also driven by the cellular plasma membrane potential (-30 to -60 mV, negative inside). Hence, MitoQ® is a selective mitochondria-targeted antioxidant [383].

Once within the mitochondria, MitoQ® is primarily adsorbed to the matrix surface of the inner membrane where it is continually recycled to the quinol form by complex II, meaning it behaves as a potent antioxidant against lipid peroxidation [384]. However, MitoQ® is unable to restore MRC function in mitochondria lacking CoQ_{10} since the reduced quinol form of MitoQ® is not oxidised by complex III and therefore cannot act as an electron carrier [385, 386].

Some pre-clinical studies have demonstrated great promise for MitoQ® in the treatment of Alzheimer's [387, 388] and Parkinson's [389] disease. However, when trialled on 128 newly diagnosed untreated patients with Parkinson's disease, there was no difference between MitoQ® and placebo on any measure of Parkinson's disease progression [390]. This is thought to be due to irreversible neuronal damage by the time parkinsonism becomes clinically evident, meaning MitoQ®, and other analogues, could still have a neuroprotective effect if administered prior to symptomatic presentation [390]. Other explanations for the observed difference between pre-clinical models and clinical investigations include a possible drug-drug interaction between MitoQ® and 1-methyl-4-phenylpyridinium (MPP+), an active metabolite of the neurotoxin 1-methyl-4-phenyl-1,2,3,6-tetrahydropyridine (MPTP) which is commonly used to induce Parkinson's disease [391-393], and/or insufficient brain penetration of MitoQ® in human [394].

While there was no notable therapeutic efficacy, this study did provide important safety data for the long-term administration of MitoQ® in humans, demonstrating MitoQ® can be safely administered as a daily oral tablet to patients for a year. This is particularly pertinent when considering the recent findings that indicate MitoQ® could ameliorate the mitochondrial impairment and subsequent progression of spinocerebellar ataxia type I [395].

The most recent small molecule synthetic quinone to show therapeutic potential is EPI-743. Initially designed to modulate the biochemistry of aging [396], at the start of the decade, EPI-743 was rapidly repurposed for the treatment of inherited mitochondrial disease [397]. Unlike idebenone and MitoQ®, the chemical structure of EPI-743 is not based upon decylubquinone, but is derived from the hydrolysis of α-toc. Nevertheless, it does share some basic commonalities with the other synthetic analogues of CoQ_{10}, namely a quinone core and a relatively short carbon side chain.

Perhaps in an effort to mimic the translocation of CoQ_{10} *in vivo*, and to reduce the inhibitory effects exhibited by idebenone on the MRC, the side chain of EPI-743 contains repeating isoprenoid units. When tested on human fibroblast assays modelling the effects of mitochondrial disease, the resulting compound was approximated to be 1000 to 10000-fold more potent than CoQ_{10} or idebenone in protecting cells from oxidative stress [396, 397].

Although its precise mechanism of cellular action has yet to be fully elucidated, EPI-743 treatment has been shown to replenish the level of the antioxidant, reduced glutathione (GSH), possibly resulting from its ability to facilitate the transfer of electrons between NOQ1 and GSH reductase [82]. In addition to its ability to restore cellular GSH status, the beneficial effects of EPI-743 in the treatment of mitochondrial disease may result from its possible interaction with the transcription factor, nuclear factor E2-related factor 2 (Nrf2), which regulates both the expression of antioxidant proteins and cellular energy metabolism [398].

Double blind, placebo-controlled, randomised clinical trials of EPI-743 are currently in progress for Leigh syndrome, Kearns-Sayre syndrome, Friedreich's ataxia, Rett syndrome, and Parkinson's disease, with the US FDA having also granted approval to use EPI-743 to treat patients with genetically confirmed MRC disease who are considered to be within 90 days of end-of-life care [399].

Given the small size of all the synthetic quinone analogues in relation to CoQ_{10}, and the associated decrease in relative lipophilicity, each of the synthetic molecules are either reported or purported to cross the BBB [396, 400-403]. However, no studies have directly compared this in relation to exogenous CoQ_{10}.

It is of particular importance to compare the relative uptake of idebenone into the brain, since it is the only clinically approved and commercially certified analogue of CoQ_{10} that can be used in the treatment of neurological disorders associated with mitochondrial dysfunction.

5.2. Materials and Methods

5.2.1. Materials

Coenzyme Q_{10} Plasma Control, Level I (0092, ChromSystems®, Germany); Bovine Plasma Derived Serum (BPDS; First Link Ltd., UK); Foetal Bovine Serum (FBS; F7524, Sigma®, UK); HEPES (H3375, Sigma®, UK); HEPES (H3375, Sigma®, UK); Hank's Balanced Salt Solution (HBSS; H8264, Sigma®, UK); Bovine Serum Albumin (BSA; A6003, Sigma®, UK); coenzyme Q_{10} (C9538, Sigma®, UK); (+)-α-tocopherol (vitamin E; T3634, Sigma®, UK); trolox (238813, Sigma®, UK).

QTRAP® 6500 (ESI)-MS/MS system with Analyst® software v 1.6 (AB Sciex™, UK); 1200 Series LC system (Agilent Technologies, USA); HTS PAL® DLW-2 auto-sampler (CTC Analytics AG, Switzerland); ACE® UltraCore™ 2.5 µm SuperC18™ 30 × 2.1 mm column (Advanced Chromatography Technologies Ltd., UK); ACE® C18 2.1 mm guard-column and cartridges (Advanced Chromatography Technologies Ltd., UK); ACE® ColumnShield™ 0.5 µm pre-column filters (Advanced Chromatography Technologies Ltd., UK); CE100/CVP100 centrifugal vacuum evaporator (Genevac Ltd., UK); 96-Deepwell Plates (Porvair Science Ltd., UK); idebenone (I5659, Sigma®, UK); idebenone–[$^{13}CD_3$] (Qmx Laboratories Ltd., UK); acetonitrile (RH1015, Rathburn Chemicals Ltd., UK); formic acid (5.33002, Sigma®, UK).

5.2.2. Methods

Coenzyme Q_{10} Quantitation

Unless otherwise stated, CoQ_{10} concentrations were determined using the LC-MS/MS method described in Section 2.13.2. Duplicate samples of ChromSystems® EQC Plasma, IQC 0 (HBSS with 50 % (v/v) BPDS, 0.5 % (w/v) BSA, 25 mmol/L HEPES), and IQC 10 (HBSS with 50 % (v/v) BPDS, 0.5 % (w/v) BSA, 25 mmol/L HEPES, 10 µmol/L CoQ_{10}) were run at the beginning and end of each batch to ensure a consistent intra-batch instrument performance.

Idebenone Quantitation

A novel idebenone LC-MS/MS method was established. The method is a modified version of that described by Bodmer *et al*. [404]. The lower limit of quantitation for this method is 1 nmol/L, with a limit of detection 0.5 nmol/L, and linearity up to 500 nmol/L (Figure 66). The run-time (inject-to-inject) is 4 minutes per sample.

Idebenone calibration curves were established by serial dilutions of a 1 mM stock solution (200 µL; 0, 0.5, 1.0, 2.5, 5.0, 25, 50, 500 nmol/L in ethanol). Stable isotope-labelled internal standard was added to each calibrator (idebenone–[$^{13}CD_3$]; ~100 nmol/L), the calibrator standards were then vigorously mixed and evaporated to dryness on a centrifugal vacuum evaporator. Prior to analysis, calibrators were re-constituted in LC-MS/MS running solvent mixture (100 µL; 3:1 (v/v) *dd*H_2O/acetonitrile with 0.05 % (v/v) formic acid), vigorously mixed, and transferred into a 96-deepwell plate. Fresh calibrators were made-up alongside every analytical batch.

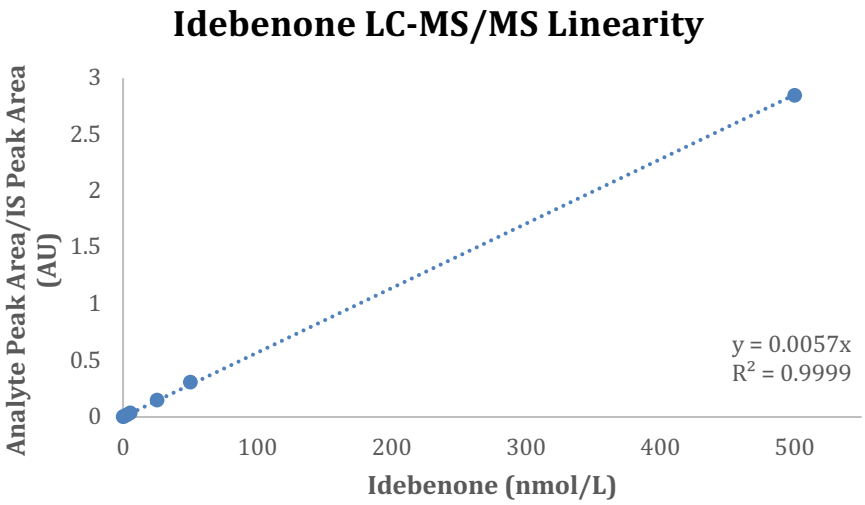

Figure 66: LC-MS/MS idebenone serial dilution linearity graph reaching a lower limit of detection at 0.5 nmol/L – calibration curves were derived using 1/x weighted linear least-squares regression, as calculated by the Analyst® software package. Calibration curves were accepted if $R^2 \geq 0.998$.

Samples were prepared by the addition of stable isotope-labelled internal standard (idebenone–[$^{13}CD_3$]; ~100 nmol/L) to each sample (200 µL). Idebenone was then extracted and protein precipitated by the addition of ethanol (600 µL); the samples were vigorously mixed on a vortex for 1 minute, centrifuged at 18625 × *g* for 3 minutes, and the supernatant collected. The ethanol extract was evaporated to dryness using a centrifugal evaporator. Prior to analysis, calibrators were re-constituted in LC-MS/MS running solvent mixture (100 µL; 3:1 (v/v) *dd*H_2O/acetonitrile with 0.05 % (v/v) formic acid), vigorously mixed, and transferred into a 96-deepwell plate.

Chromatography was performed on a C18 reversed-phase column kept at 25°C with a gradient of running solvent A (*dd*H_2O with 0.05 % (v/v) formic acid) and running solvent B (acetonitrile with 0.05 % (v/v) formic acid). The gradient elution profile was maintained at 75 % A (0 – 0.2 min), ramped to 100 % B (0.21 – 1 min), maintained at 100 % B (1 – 2 min), and ramped back to 75 % A (2.01 – 2.1 min). Total run time was 3.5 minutes with a flow rate of 220 µL/min and inject volume of 10 µL.

The mass spectrometer was operated in positive ion mode with the ion source spray voltage at 5500 V, declustering potential at 100 V, temperature at 115°C, and collision energy at 25 V. The curtain gas was 48 L/min, gas 1 (nebuliser gas) 55 L/min, gas 2

(heater gas) 21 L/min, and collision gas on 'medium' setting. The mass spectrometer was programmed to follow the transitions of *m/z* 339.2 -> 197.1 (dwell time 100 ms) corresponding to idebenone, and *m/z* 343.2 -> 201.1 (dwell time 100 ms) corresponding to idebenone–[$^{13}CD_3$].

Final idebenone concentrations (nmol/L) were calculated as a ratio of idebenone/ idebenone–[$^{13}CD_3$] peak areas, and quantified against the corresponding calibration curve (Figure 66), with dilution factors corrected for accordingly.

Cell Culture

bEnd.3 cells were cultured as outlined in Section 2.2 and passaged onto Transwell®-inserts for apparent permeability studies. Primary PBECs were isolated and cultured as per Sections 2.3 and 2.4, and passaged onto Transwell®-inserts for apparent permeability studies.
Primary astrocytes were isolated and cultured in accordance to Sections 2.5 and 2.6, with co-culture coordinated as per Appendix A.

Inducing Coenzyme Q_{10} Deficiency

Cell cultures were pharmacologically induced with a CoQ_{10} deficiency by supplementing culture media with 1 mmol/L *para*-aminobenzoic acid (*p*ABA) for a duration of 5 days, in accordance to the method described in Section 2.10.

Assessing Barrier Integrity

TEERs were measured across cell mono-layers on Transwell®-inserts as described in Section 2.7.1. Apparent permeability (P_{app}) of *in situ* paracellular marker FITC-40 was evaluated following the experimental procedures outlined in Sections 2.7.2 and 2.8.

Apparent Permeability

Table 11: Composition of assay buffers used in apparent permeability studies. Condition A is the acceptor buffer and conditions B–E are donor buffers. The serum used in bEnd.3 investigations was FBS and for PBECs it was BPDS.

	BSA (*w/v*)	**HEPES (mmol/L)**	**Serum (*v/v*)**	**FITC-40 (mg/mL)**	**CoQ_{10} (µmol/L)**	**α-toc [405, 406] (µmol/L)**	**Trolox (µmol/L)**	**Idebenone (µmol/L)**
A	0.5 %	25	–	–	–	–	–	–
B	0.5 %	25	50 %	0.5	10	–	–	–
C	0.5 %	25	50 %	0.5	10	50	–	–
D	0.5 %	25	50 %	0.5	10	–	50	–
E	0.5 %	25	50 %	0.5	-	–	–	10

Apparent permeability (P_{app}) of CoQ_{10} and the synthetic analogue idebenone was evaluated following the experimental procedures outlined in Section 2.8. Assay buffers were made up in HBSS at *p*H 7.4 (Table 11). CoQ_{10} was incubated with serum (45 minutes, 37°C) prior to addition with the remaining components of the assay buffer.

5.3. Results

5.3.1. Effects of Vitamin E on CoQ_{10} BBB Transport

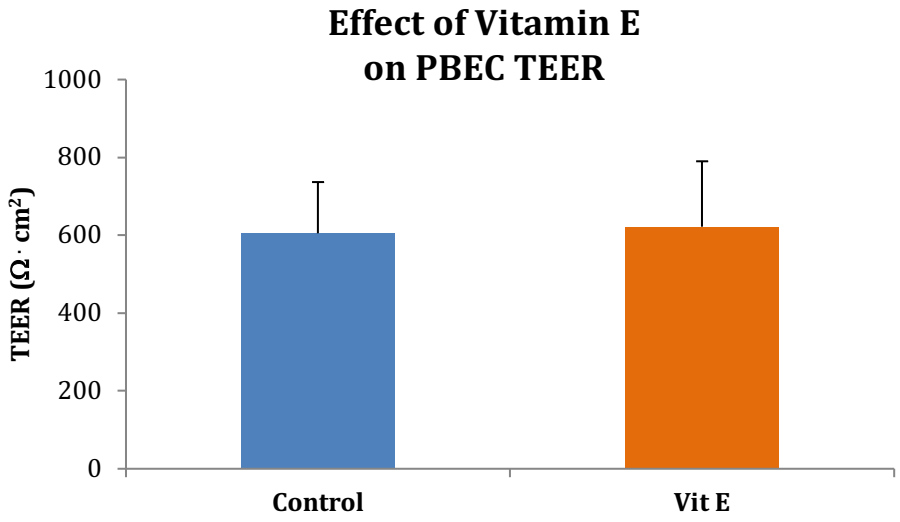

Figure 67: Effect of co-administered vitamin E (50 µmol/L) on TEER in the PBEC BBB. PBEC control (n = 8), vitamin E treated PBEC (n = 8). Error bars represent standard error of the mean (SEM).

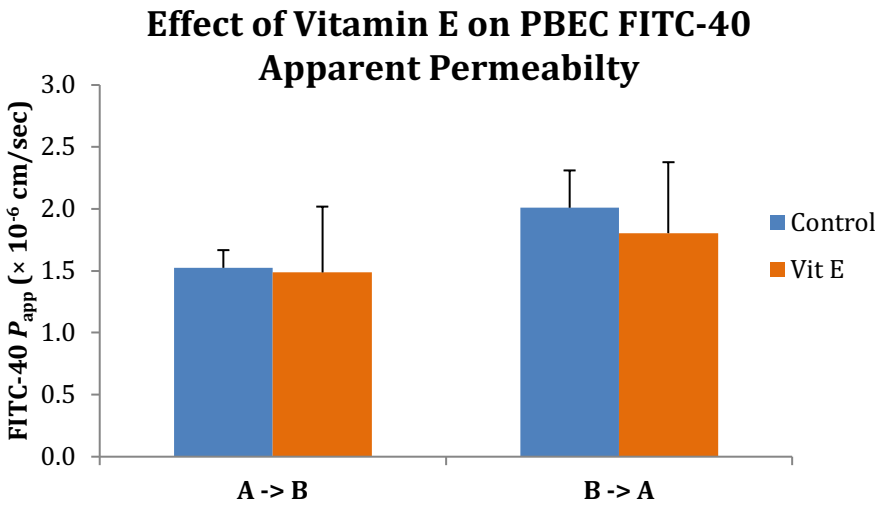

Figure 68: Effect of co-administered vitamin E (50 µmol/L) on FITC-40 apparent permeability in the PBEC BBB. A -> B; PBEC control (n = 4), vitamin E treated PBEC (n = 4). B -> A; PBEC control (n = 4), vitamin E treated PBEC (n = 4). Error bars represent standard error of the mean (SEM).

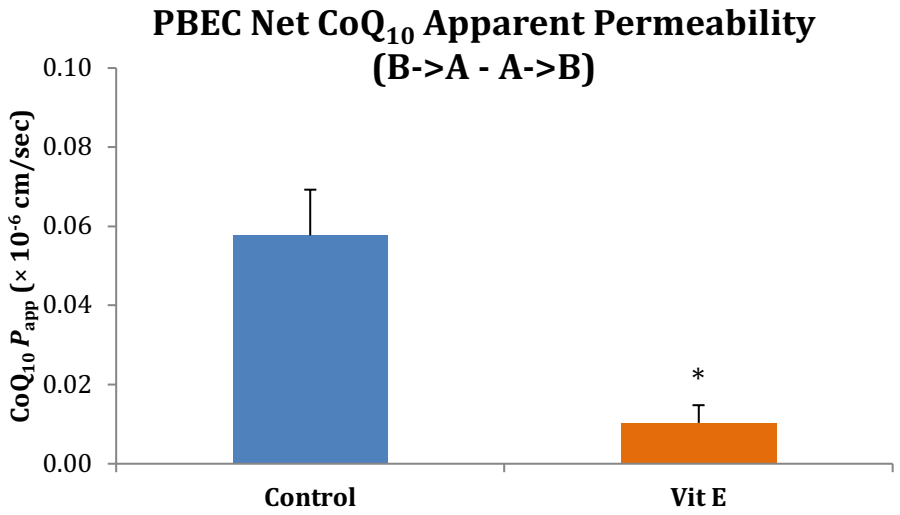

Figure 69: Net effect of co-administered vitamin E (50 µmol/L) on CoQ_{10} apparent permeability in the PBEC BBB. PBEC control (df = 6), vitamin E treated PBEC (df = 6, $p < 0.05$). Error bars represent standard error of the mean (SEM).

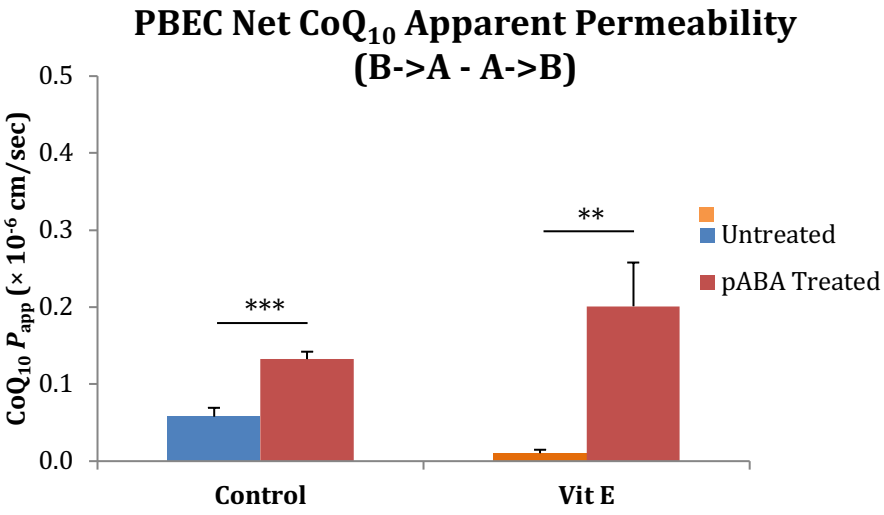

Figure 70: Net effect of co-administered vitamin E (50 µmol/L) on CoQ_{10} apparent permeability in the PBEC BBB. PBEC control (df = 6), vitamin E treated PBEC (df = 6). *p*ABA PBEC control (df = 4), *p*ABA vitamin E treated PBEC (df = 6). Error bars represent standard error of the mean (SEM).

The potent antioxidant and 'mito-cocktail' component vitamin E was assessed alongside CoQ_{10} to monitor its effect on CoQ_{10} apparent permeability across the PBEC BBB.

As expected, vitamin E had no effect on PBEC TEER (Figure 67) and subsequent FITC-40 P_{app} (Figure 68), suggesting BBB integrity was maintained. Of notable clinical importance, however, was a significant decrease (to 16.7 % of control, $p < 0.05$) in net brain-to-blood CoQ_{10} apparent permeability when co-administered with vitamin E in the physiological PBEC BBB model (Figure 69). To see if this trend was sustained under pathophysiological conditions, *p*ABA (1 mmol/L, 5 days) was used to pharmacologically induce a CoQ_{10} deficiency in the PBEC BBB. Results indicate that a CoQ_{10} deficiency in the PBEC BBB causes a reversal of the vitamin E effect to an absolute magnitude of net CoQ_{10} permeability that is consistent with *p*ABA-treated controls (Figure 70).

5.3.2. LC-MS/MS Method Development

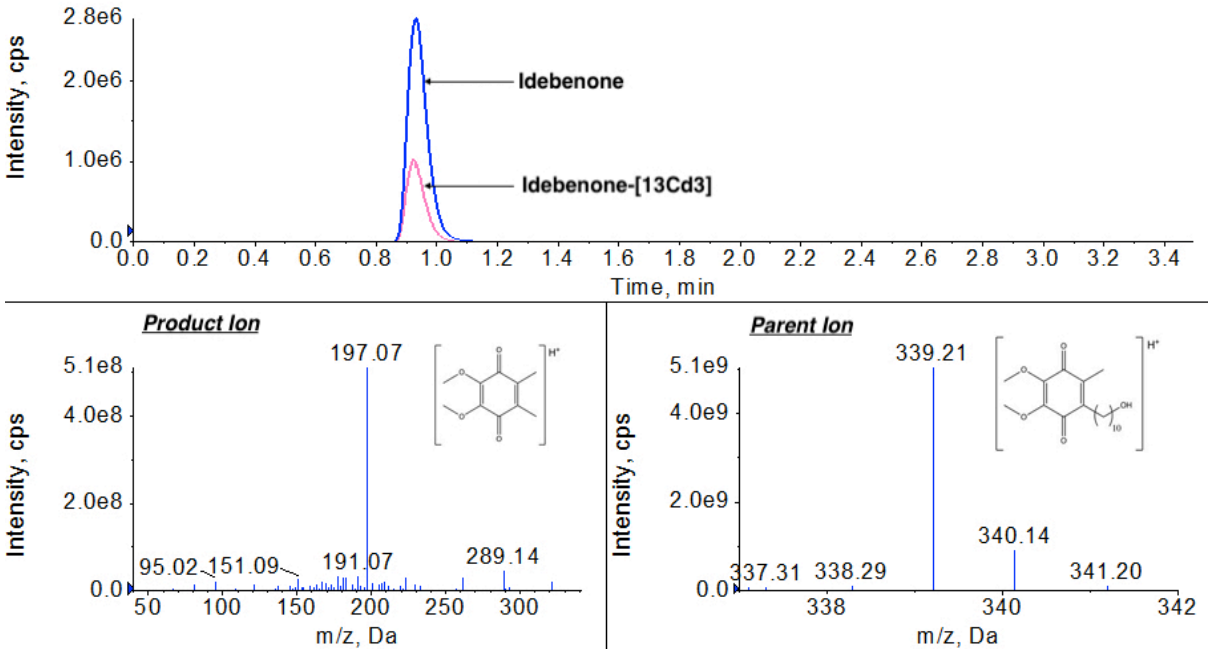

Figure 71: LC-MS/MS idebenone chromatogram of the top calibrator, 500 nmol/L idebenone (top chromatogram), with tuned MS scans of the idebenone product ion (bottom left mass spectrum) and the parent ion (bottom right mass spectrum) in ESI+ mode.

The optimum combination of LC-MS/MS parameters to yield the highest signal response for idebenone was achieved by automatically ramping each parameter (ionisation voltages, temperature and interface gases) across a range and then manually fine-tuning.

The specific Q1/Q3 transitions were determined by performing a product ion scan of the respective parent ion. The resulting chromatogram (Figure 71) shows very good sensitivity and chromatography for both idebenone (*m/z* 339.2 -> 197.1) and the stable-isotope labelled internal standard, idebenone–[$^{13}CD_3$] (*m/z* 343.2 -> 201.1), in selected-reaction monitoring mode.

Table 12: A summary of performance parameters for the LC-MS/MS idebenone method.

Performance Parameters	Idebenone LC-MS/MS
LLOQ *(nmol/L)*	1.0
LLOD *(nmol/L)*	0.5
Linearity *(nmol/L)*	500
Run Time *(minutes)*	4
Intra-assay Imprecision *(CV %)*	3.0
Recovery *(Ave. %)*	105

The lower limit of detection (LLOD) for the LC-MS/MS method was defined as a signal-to-noise ratio of 3 (n = 3). Linearity and lower limit of quantitation (LLOQ) were determined across an 8-point serial dilution (0 – 500 nmol/L) performed on 3 separate sample preparations, and defined as the lowest concentration and range, respectively, that could be measured with an inaccuracy (percentage relative error) and imprecision (CV %) < 20 % (n = 3), as is consistent with the criteria set for the CoQ_{10} method (Section 3.3.2).

The precision of the LC-MS/MS method was assessed by evaluating the intra-assay coefficient of variation (CV), with acceptable CV values being defined as < 15 % [235-237]. The intra-assay precision was determined across replicates of 2 parallel samples of internal QC (IQC) material (n = 10; baseline and medium-spike). The results (Table 12) indicate that the LC-MS/MS method has very good reproducibility within batch.

Accuracy was investigated by examining the average recovery of known quantities of idebenone in replicates of spiked sample (n = 10; medium-spike (+ 250 nmol/L)). A negligible inaccuracy (5 %) was observed, but overall it can be said the method exhibits an acceptable degree of accuracy for use in this study.

Carryover between successive samples was assessed by analysing a blank sample immediately after the highest calibrator standard (ULOQ; 500 nmol/L) (n = 3). No quantifiable carryover was observed for the LC-MS/MS method.

5.3.3. Mechanisms of Idebenone BBB Transport

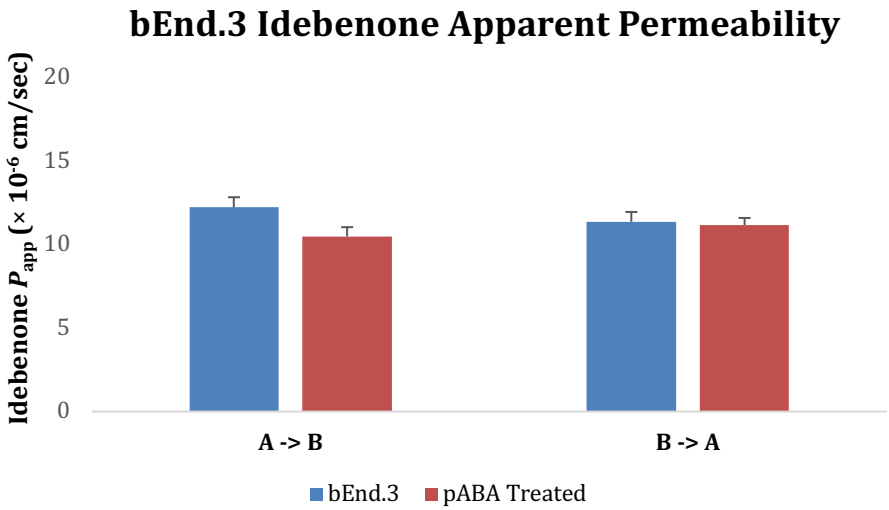

Figure 72: Idebenone apparent permeability in the bEnd.3 BBB.
A -> B; bEnd.3 control (n = 6), *p*ABA bEnd.3 (n = 6). B -> A; bEnd.3 control (n = 6), *p*ABA bEnd.3 (n = 5). Error bars represent standard error of the mean (SEM).

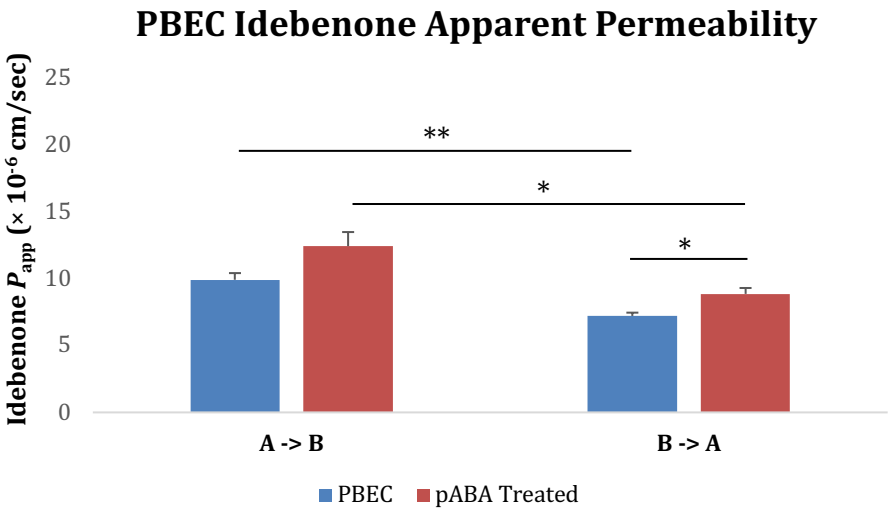

Figure 73: Idebenone apparent permeability in the PBEC BBB.
A -> B; PBEC control (n = 4), *p*ABA PBEC (n = 4). B -> A; PBEC control (n = 4), *p*ABA PBEC (n = 4). Error bars represent standard error of the mean (SEM).

Assessment of idebenone (10 μmol/L) apparent permeability across the bEnd.3 BBB indicated no significant differences between blood-to-brain and brain-to-blood transport (Figure 72). More notably, the value for P_{app} was considerably higher than that observed in any of the CoQ_{10} studies, at a level akin to passive transport. Further examination of these results showed no difference between physiological and pathophysiological conditions, further strengthening the passive theory since the mode of transport is, therefore, likely governed by concentration gradients with limited interference from the physical and transport barriers of the endothelia.

Interestingly, when the idebenone permeability assays were translated onto the gold-standard PBEC BBB, the results were in contrast to that observed in the bEnd.3 BBB. The PBEC results, instead, suggest there is a difference between blood-to-brain and brain-to-blood transport of idebenone for both the physiological ($p < 0.01$) and pathophysiological ($p < 0.05$) BBB models (Figure 73), such that the BBB is serving to impede the transport of the compound in favour of a net influx from the blood to the brain.

5.4. Discussion

Alongside CoQ_{10}, vitamin E (tocopherol) is a key component of the mito-cocktail, a therapeutic mixture of potent antioxidants and cofactors administered for the treatment of mitochondrial disorders. Due to the well documented similarities in ADME that tocopherol shares with CoQ_{10}, namely an association with circulatory lipoprotein, in addition to similar proposed uptake mechanisms that are mediated by the SR-B1 receptor [282, 296, 407], it is important to understand the implications of co-administration of tocopherol on CoQ_{10} BBB transport.

There are four forms of tocopherol found in nature. They are categorised based on the degree of methylation in the hydrocarbon side-chain and each of these four, in turn, has eight stereoisomers. The mammalian body predominantly recognises *RRR*-α-tocopherol (α-toc), a highly lipid-soluble compound, with approximately 90 % of tocopherol in brain and other tissue displaying this isomeric form [278, 408, 409]. For this reason, *RRR*-α-toc was the chosen isoform for investigations in this study.

Disruption of the BBB endothelial TJs in response to an increased oxidative incident is extensively documented [410-414], similarly, it is known that TJ disruption can be prevented in the presence of antioxidants [415]. Therefore, and perhaps unsurprising, there was no observed effect of α-toc co-administration on the PBEC BBB integrity relative to controls (TEER control = $605 \pm 131\ \Omega \cdot cm^2$, TEER α-toc = $622 \pm 168\ \Omega \cdot cm^2$). These findings were further strengthened by an unaffected FITC-40 apparent permeability for α-toc relative to controls (A->B FITC-40 P_{app}; control = 1.52×10^{-6} cm/sec, α-toc = 1.49×10^{-6} cm/sec. B->A FITC-40 P_{app}; control = 2.01×10^{-6} cm/sec, α-toc = 1.80×10^{-6} cm/sec), meaning paracellular events across the PBEC BBB were analogous with or without the addition of α-toc.

With a proven and integral PBEC BBB model, the effect of α-toc co-administration on CoQ_{10} apparent permeability was interrogated. Of considerable interest was a significant effect of α-toc co-administration on net CoQ_{10} apparent permeability such that net efflux from the brain was reduced to 16.7 % of controls ($p < 0.05$) (Figure 69). These results are

in agreement with the findings of Ibrahim *et al.* [353] who assessed the effect of α-toc co-administration on CoQ_{10} uptake in rat tissue, noting an increased uptake of CoQ_{10} when co-administered with low dose α-toc. However, at high dose α-toc Ibrahim *et al.* [353] noted a detrimental effect on CoQ_{10} tissue uptake, giving rise to the theory that α-toc may compete for uptake into circulatory lipoproteins thereby reducing the maximal load of CoQ_{10} in the carrier [64, 353]. Nevertheless, the likely cause of the observed effect in this study is due to the potent antioxidant properties associated with α-toc. Indeed this was confirmed by assessing the effect of Trolox, a water-soluble synthetic analogue of α-toc [416, 417], on CoQ_{10} apparent permeability across the bEnd.3 BBB (Appendix C).

The exact reasoning for why an increased antioxidant capacity would have a desirable effect on CoQ_{10} apparent permeability, in favour of a reduced efflux from the brain, is unknown. However, it is possible that the co-administered α-toc further prevents peroxidation of the lipoprotein carriers, and/or offers increased stability to the BBB transport receptors, in particular RAGE [418], although, further work would need to be performed in order to prove these hypotheses.

To investigate whether the promising results obtained from the physiological PBEC BBB were maintained under pathophysiological conditions, the PBEC BBB was pharmacological induced with a CoQ_{10} deficiency and the α-toc co-administration apparent permeability experiments repeated.

Unfortunately, and in contrast to the observations made under physiological conditions, the co-administration of α-toc with CoQ_{10} did not reduce the net efflux of CoQ_{10} at the pathophysiological PBEC BBB (Figure 70). Instead, the results suggest that the presence of a CoQ_{10} deficiency supresses the beneficial effects of low dose α-toc co-administration, such that efflux of CoQ_{10} from the brain is amplified ($p < 0.01$) to levels akin to controls.

While this finding questions the notion of α-toc co-administration being a beneficial therapeutic strategy for the improved delivery of CoQ_{10} into the brain of patients with a CoQ_{10} deficiency, it does offer deeper insight into the mechanisms governing CoQ_{10} transport at the BBB. Taken collectively, these results highlight that the BBB transporters responsible for CoQ_{10} uptake are highly sensitive to an oxidative insult and hence may be the first to falter during the onset of a deficiency, additionally they indicate that the efflux transporters are more robust to a mitochondrial dysfunction.

Presently, there are no recommended clinical guidelines for the administration of the mito-cocktail, with the composition varying greatly depending on the physician, meaning the effect is varied and somewhat disputed. This study has successfully highlighted the interdependency that individual components of the mito-cocktail may have with respect to tissue uptake.

Although, the observed effects from this investigation were proven beneficial under physiological conditions, the converse could also be true for other components of the mito-cocktail [64]. Therefore, future studies should investigate a range of permutations and concentrations to establish the most efficacious composition that is tailored to the clinical presentation.

As has been clearly demonstrated, the co-administration of natural antioxidants may serve to improve the uptake of CoQ_{10} into tissue, however, an alternative and increasingly popular approach is to harness the potential of small synthetic analogues in place of CoQ_{10}.

With a recent surge in popularity due to promising effects in the treatment of neurological disorders such as Leber's hereditary optic neuropathy [356, 357] and Duchenne muscular dystrophy [361, 362], idebenone is the only clinically approved synthetic analogue of CoQ_{10}. However, there is a distinct paucity of information pertaining to its uptake into the brain, in particular the mechanisms by which it may or may not cross the BBB.

Small synthetic analogues such as idebenone have the potential benefit of circumventing mediated transport processes, since their size enables passive diffusion across a concentration gradient. Indeed pharmacokinetic data for idebenone has already hinted at different ADME to CoQ_{10} [419, 420], additionally, physicochemical analysis suggests this may hold true for BBB transport (< 400-500 Da and < 8 H-bonds) [127], although no one has directly assessed this.

Investigations in the bEnd.3 BBB highlighted no significant differences between blood-to-brain and brain-to-blood transport of idebenone, with a P_{app} that is markedly greater than that observed for CoQ_{10} (idebenone $P_{app} = 12.2 \times 10^{-6}$ cm/sec, CoQ_{10} $P_{app} = 0.13 \times 10^{-6}$ cm/sec), strongly suggesting a passive mechanism of transport for idebenone across the BBB (Figure 72). Moreover, there was no difference between idebenone apparent

permeability under physiological and pathophysiological conditions, implying that the transport mechanism is ATP independent and unimpeded by BBB function.

These findings, which implicate a passive mechanism of transport, are in agreement with the wider pharmacokinetic properties of idebenone *in vivo*. Outcomes from a recent phase I clinical trial, assessing the safety and tolerability of idebenone in the treatment of Freidrich's ataxia, indicate that the time taken to reach maximum plasma concentration following oral supplementation is 2.1 hours [420]. The mean terminal half-life of total idebenone was 10.8 hours and absorption characteristics were linear with increasing dose [419, 420]. This is in contrast to transport-mediated CoQ_{10} which takes approximately 6 hours to reach maximum plasma concentration following oral supplementation, with a secondary peak at 24 hours, a half-life of approximately 36 hours, and non-linear absorption characteristics [12, 56, 57]. Therefore, it is highly possible that a passive BBB transport mechanism for idebenone exists and there is less association with lipoprotein or similar bio-carriers.

The average TEER measured in the bEnd.3 BBB across the full scope of this project was very low (35.4 $\Omega \cdot cm^2$) in comparison to the PBEC BBB (605.17 $\Omega \cdot cm^2$). For studies that focus on receptor-mediated transport of large molecules, a low TEER is not a limitation of the model, however, for small molecule investigations a low TEER has the potential to skew results due to paracellular leak. Therefore, idebenone apparent permeability studies were repeated on the PBEC BBB model.

Results from investigations in the PBEC BBB shared some similarities with the bEnd.3, in so far as the magnitude of the idebenone P_{app} was comparably high (bEnd.3 idebenone P_{app} = 12.2 × 10^{-6} cm/sec, PBEC idebenone P_{app} = 9.9 × 10^{-6} cm/sec), confirming a prominent passive mechanism of transport across the BBB, however, there were also some important differences. Of note, was a significant difference between blood-to-brain and brain-to-blood permeability, this was maintained under both physiological ($p < 0.01$) and pathophysiological ($p < 0.05$) conditions (Figure 73). This suggests that there may be mediated transport processes in play, albeit in favour of a net influx from blood-to-brain. Idebenone is not hyper-lipophilic, with a cLogP of 3.22 compared to 20.15 for CoQ_{10} (Figure 65) [50, 421], nevertheless, it is still hydrophobic and may have some association with lipoprotein, or other serum proteins, albeit with a considerably lower affinity than CoQ_{10}. Although the reasoning behind the observed significant differences in blood-to-brain and

brain-to-blood permeability is as of yet unknown, these physicochemical properties of idebenone may contribute to a minor degree of mediated transport.

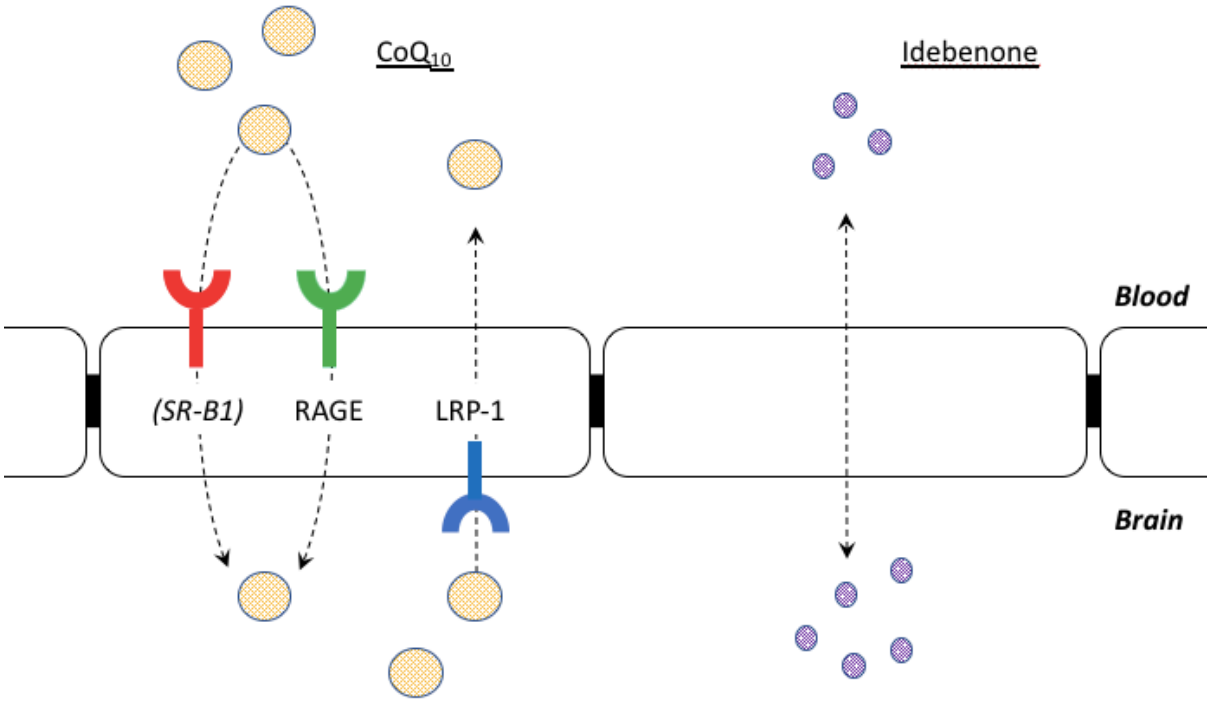

Figure 74: An overall comparative summary of the mechanisms of transport for CoQ_{10} and idebenone across the BBB, as established from findings in this study. CoQ_{10} BBB transport is mediated by specific uptake (RAGE and SR-B1) and efflux (LRP-1) transporters of the BBB and is dependent upon lipoprotein interactions, whereas idebenone appears to passively diffuse bidirectionally across the BBB. Yellow spheres represent lipoprotein-associated CoQ_{10} and purple spheres represent idebenone.

For most of the assays, the bEnd.3 and PBEC BBB results correlated with one another and provided strong evidence for a passive mechanism of transport for idebenone across the BBB (Figure 74). This makes idebenone a very promising synthetic compound for successful brain delivery and is certainly advantageous over its native parent compound, CoQ_{10}. The disadvantage of passive transport is unselective distribution and quick clearance. This should be noted when considering the best regime for therapeutic administration.

There was a full recovery of exogenous idebenone throughout this study (96.2 ± 0.8 %, n = 10 in PBEC and 94.8 % ± 1.5 %, n = 8 in *p*ABA PBEC, results not shown) suggesting no retention of idebenone by the endothelial cells in the *in vitro* models of the BBB.

While it is important to first compare the relative uptake of individual synthetic analogues, particularly with regards to penetration of the BBB for neurological disorders, several studies have shown that the provision of individual antioxidants as supplements are either ineffective, or can be deleterious to health. This is because every antioxidant can, under certain circumstances, also behave as a pro-oxidant [422, 423]. As such, antioxidants are best administered redox coupled to other vicinal antioxidants, hence, future studies should focus on finding the optimum combination of the most effective candidates, and a standardised therapy recommended.

Throughout this study, mass spectrometry was utilised as the choice method of analysis. Given the considerable difference in lipophilicity idebenone has compared to CoQ_{10} (Figure 65), and with knowledge of the inefficiency associated with the latent biphasic extraction (Section 3.3.1, Figure 25), it was decided a single phase extraction using ethanol would be more appropriate. The resulting new method displayed very good performance metrics (Table 12) and, although it is not fully validated to a clinical standard, it does show great promise and could be further developed for implementation in a clinical laboratory.

6. The Neurological Implications of Statin Therapy

6.1. Background

Discovered in 1976 and their clinical significance realised in 1987, statins, 3-hydroxy-3-methylglutaryl-coenzyme A (HMG-CoA) reductase inhibitors, remain the most widely prescribed drug for the treatment of hypercholesterolaemia and are undoubtedly one of the most influential advancements in therapeutic cardiovascular medicine [36, 424, 425]. The popularity of statin treatment by clinicians is due to their excellent efficacy and safety profiles. Although usually well tolerated by the majority of patients, there is a notable incidence of adverse effects, with a recent international survey suggesting a nonadherence rate of 11-29 % of which 72 % were related to myopathic symptoms, ranging from benign myalgias to potentially fatal rhabdomyolysis [426, 427]. Additionally, it has been suggested there may be a correlation between the prevalence of adverse effects and increased dosage, as well as age [428-430]. As such, it is recommended to prescribe the lowest statin dose that will achieve the desired therapeutic effect [431, 432].

The pathogenesis of the adverse myopathic effects associated with statin therapy has yet to be fully elucidated. However, lactic acidosis and elevated lactate: pyruvate ratios have been reported in patients following statin therapy, indicating evidence of MRC impairment [37, 38].

Statins competitively inhibit HMG-CoA reductase, the rate-limiting enzyme common to both cholesterol and CoQ_{10} biosynthesis (Figure 75). Based on the essential electron carrier role CoQ_{10} plays in the MRC and the association of MRC dysfunction with statin therapy, a number of studies have assessed the effect of statin therapy upon endogenous CoQ_{10} status [40].

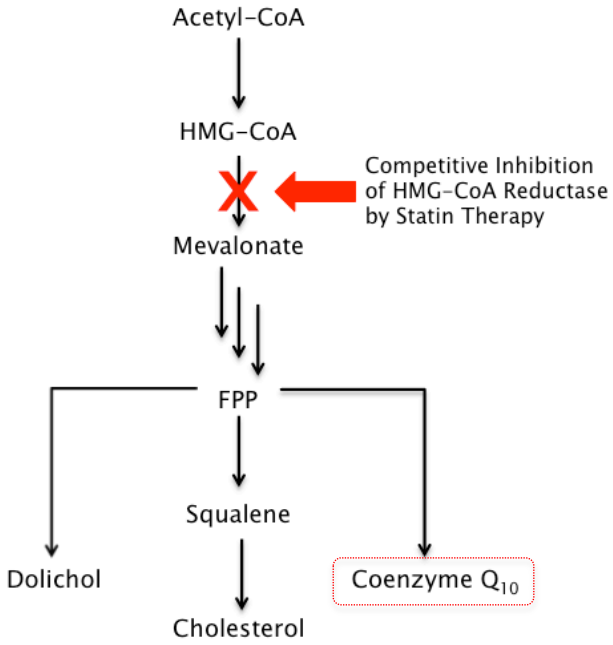

Figure 75: The mevalonate synthetic pathway, common in the biosynthesis of cholesterol, coenzyme Q_{10} and dolichol. Statins competitively inhibit the reduction of HMG-CoA to mevalonate, the rate determining step of the pathway. FFP, farnesyl pyrophosphate; HMG-CoA, 3-hydroxy-3-methyl-glutaryl-coA.

When the effect of statin treatment is determined upon circulatory CoQ_{10} levels, a number of studies have reported evidence of deficit in plasma CoQ_{10} status [40]. However, since statins target the liver causing a decrease in hepatic synthesis of LDL, the decrease in plasma CoQ_{10} status associated with this pharmacotherapy may simply reflect the lowering of the level of circulatory LDL by the drug therapy [40]. Few studies have assessed the effect on statin therapy upon tissue/cellular CoQ_{10} levels and, of the limited number that have, some have reported evidence of a deficit in CoQ_{10} status in association with this pharmacotherapy [433-436].

A decrease in CoQ_{10} status (an approximate 34 % decrease from baseline levels) has been reported in skeletal muscle of 48 hypercholesterolemia patients following simvastatin treatment (80 mg/day) for 8 weeks. A study that assessed the effect of rosuvastatin therapy upon blood mononuclear cell (MNC) CoQ_{10} status in children with familial hypercholesterolemia reported a 32 % decrease in MNC CoQ_{10} status following 29 weeks of therapy [437]. Interestingly, MNC ATP synthesis was not affected by the 34 % decrease in cellular CoQ_{10} status [437]. While there is possibility that an up-regulation in glycolysis may have accounted for the unimpaired MNC ATP synthesis following statin therapy, an

insufficient deficit in CoQ_{10} status to perturb MRC function could be an alternative explanation.

In contrast, a study by Duberley *et al.* [194] reported that a 24 % decrease in neuroblastoma cell CoQ_{10} status was sufficient to perturb oxidative phosphorylation as indicated by the decrease in cellular ATP status commensurate with a loss of mitochondrial membrane potential. Therefore, the degree to which cellular CoQ_{10} status has to be decreased before MRC function becomes compromised may be cell/tissue specific and further studies are required to investigate this threshold phenomena.

In addition to the primary deleterious effects on CoQ_{10} biosynthesis, statins inhibit the synthesis of several selenoproteins, including thioreductase redoxin 1, which play a key role in the redox cycle of CoQ_{10}, thereby perturbing its antioxidant function [438, 439].

It has been suggested that patients presenting with myopathies following statin therapy are likely to have contributing subclinical mitochondrial disorders and/or be exasperated by exercise [440-443]. In particular, patients with inherited mitochondrial disorders such as mitochondrial myopathy, encephalopathy, lactic acidosis and stroke-like episodes (MELAS syndrome), myoadenylate deaminase (MADA) deficiency, and variations of the COQ genes appear to have higher susceptibility for statin-associated myopathy [444].

Following these trends, polymorphisms in the COQ2 gene, which encodes for the CoQ_{10} biosynthetic enzyme, 4-hydroxy-benzoate polyprenyl transferase, has been suggested as a predictive marker of possible muscular side effects in patients treated with statins [445].

Mitochondrial disorders have a prevalence of more than 1 in 5000 [343], which is relatively rare, however, the widespread popularity of statins globally means this corresponds to a considerable incidence in susceptible subjects. Recognising this, an international panel of 35 mitochondrial medicine specialists, through the Mitochondrial Medicine Society, USA, released clinical care guidelines stating statins should be avoided in patients with mitochondrial disease when possible and, if given, they should be used with caution [343]. Indeed, this was preceded by Health Canada who imposed a CoQ_{10} depletion warning on all statin drugs. Similarly, an expert group on statin-associated muscle symptoms (SAMS) justified prescribing CoQ_{10} with statins for patients with coexisting cardiomyopathies [446]. Furthermore, Backes *et al*. [447] recommend starting CoQ_{10} supplementation 2 weeks

before introducing statins as a means to offset a statin-induced reduction in CoQ_{10} serum concentrations and allow for improved tolerability.
Perhaps anticipating an inevitable shift, and with full appreciation for the benefits of co-administration of CoQ_{10} with statins, Merck & Co., Inc. filed a US patent for simvastatin-CoQ_{10} combination products in 1989 [448]. These patents have since expired having never been exercised, highlighting the fact that co-administration is not yet common practise, albeit the evidence is building.

Adverse side-effects are not always myopathic and isolated to the periphery. Recently, Teive *et al.* [449] reported four cases of acquired cerebellar ataxia due to statin use, a neurological condition commonly associated with a CoQ_{10} deficiency [66, 68, 69]. Patients had a mean age of 67.5 years, were prescribed with either atorvastatin or simvastatin, and presented with gait ataxia. After statin withdrawal, and treatment with CoQ_{10} (300 mg/day) in three cases, all had progressive improvement of gait ataxia. When re-challenged with statins, there was a recurrence of the progressive gait ataxia, which improved again after statin withdrawal. These findings corroborate observations from J.E. Berner [450] who reported two cases of ataxia and bipolar disorder as a result of statin therapy, patients in these cases had a mean age of 58 years and were prescribed atorvastatin and simvastatin respectively.
Numerous cases of impaired cognitive function as a consequence of taking statins have emerged over the years, with many patients reporting of memory loss, forgetfulness, or confusion as a common side-effect [451]. Some have even suggested a direct correlation between statin use and progression of Parkinson's disease in susceptible subjects [452-454]. However, data from several large epidemiological studies have not reliably demonstrated a robust association between incident cognitive impairment and statin use, leading to the suggestion that the cause of cognitive impairment may be a result of combined therapies alongside statins [455-458].

Prescriptions of statins are expected to increase in response to an ageing population and as a result of cardiovascular disease (CVD) campaigns such as the World Health Organisation's Global Hearts initiative. Given that the rate of CoQ_{10} *de novo* biosynthesis is inversely proportional to age [13], and with the emerging evidence for a tissue-specific threshold effect on MRC function [459], it could be logical to conclude that there will be an

increased prevalence of CoQ_{10} dependent statin-induced mitochondrial disorders [460]. When coupled with the recently reported cases of statin-associated ataxias and impaired cognitive function, it is vital we channel efforts into understanding the potential neuropathological implications of statin therapy, starting with the brain's gatekeeper, the blood-brain barrier.

6.2. Materials and Methods

6.2.1. Materials

Coenzyme Q_{10} Plasma Control, Level I (0092, ChromSystems®, Germany); Bovine Plasma Derived Serum (BPDS; First Link Ltd., UK); HEPES (H3375, Sigma®, UK); HEPES (H3375, Sigma®, UK); Hank's Balanced Salt Solution (HBSS; H8264, Sigma®, UK); Bovine Serum Albumin (BSA; A6003, Sigma®, UK); coenzyme Q_{10} (C9538, Sigma®, UK); simvastatin (S6196, Sigma®, UK).

Male Wistar Rats (Charles River Laboratories Ltd., UK), Teklad global 18 % protein rodent chow (Envigo, UK), simvastatin and CoQ_{10} supplemented rodent diet (PharmaNord, Denmark), isoflurane (Abbott Laboratories Ltd., UK), 0.96 mm PVC tubing catheter (Biocorp Ltd., Australia).

PU-1580 intelligent HPLC pump (Jasco Inc., USA); AS-2055 *Plus* intelligent auto-sampler (Jasco Inc., USA); HiQ sil™ 5 µm C18HS 4.6 × 150 mm column (KYA Technologies Corp., Japan); Jetstream II *Plus* column thermostat (Kromatek, UK); Coulochem® II electrochemical detector (ESA Biosciences Inc., USA); 5010 analytical cell (ESA Biosciences Inc., USA); AZUR chromatography software (Kromatek, UK); Chromacol™ HPLC vials and caps (Thermo Scientific™, UK); centrifugal vacuum concentrator 5301 (Eppendorf®, UK); orthophosphoric acid (04102, Sigma®, UK).

6.2.2. Methods

Coenzyme Q_{10} Quantitation

Unless otherwise stated, CoQ_{10} concentrations were determined using the LC-MS/MS method described in Section 2.13.2. Duplicate samples of ChromSystems® EQC Plasma, IQC 0 (HBSS with 50 % (v/v) BPDS, 0.5 % (w/v) BSA, 25 mmol/L HEPES), and IQC 10 (HBSS with 50 % (v/v) BPDS, 0.5 % (w/v) BSA, 25 mmol/L HEPES, 10 µmol/L CoQ_{10}) were run at the beginning and end of each batch to ensure a consistent intra-batch instrument performance.

The HPLC-UV technique was used for the analysis of rat cerebral CoQ_9 and CoQ_{10} in accordance to Section 2.13.1.

Cell Culture

bEnd.3 cells were cultured as outlined in Section 2.2 and passaged onto Transwell®-inserts for apparent permeability studies. Primary PBECs were isolated and cultured as per Sections 2.3 and 2.4, and passaged onto Transwell®-inserts for apparent permeability studies.

Primary astrocytes were isolated and cultured in accordance to Sections 2.5 and 2.6, with co-culture coordinated as per Appendix A. Cells were treated with simvastatin (0.1 µmol/L in culture medium) for a duration of 72 h prior to assay [461-464].

Inducing Coenzyme Q_{10} Deficiency

Cell cultures were pharmacologically induced with a CoQ_{10} deficiency by supplementing culture media with 1 mmol/L *para*-aminobenzoic acid (*p*ABA) for a duration of 5 days, in accordance to the method described in Section 2.10.

Assessing Barrier Integrity

TEERs were measured across cell mono-layers on Transwell®-inserts as described in Section 2.7.1. Apparent permeability (P_{app}) of *in situ* paracellular marker FITC-40 was evaluated following the experimental procedures outlined in Sections 2.7.2 and 2.8.

Apparent Permeability

Apparent permeability (P_{app}) of CoQ_{10} was evaluated following the experimental procedures outlined in Section 2.8. Assay buffers were made up in HBSS at *p*H 7.4 (Table 13). CoQ_{10} was incubated with serum (45 minutes, 37°C) prior to addition with the remaining components of the assay buffer.

Table 13: Composition of assay buffers used in apparent permeability studies. Condition A is the acceptor buffer and conditions B is the donor buffer. The serum used in bEnd.3 investigations was FBS and for PBECs it was BPDS.

	BSA (*w/v*)	**HEPES (mmol/L)**	**Serum (*v/v*)**	**FITC-40 (mg/mL)**	**CoQ_{10} (µmol/L)**
A	0.5 %	25	–	–	–
B	0.5 %	25	50 %	0.5	10

In Vivo Studies

Male Wistar rats averaging 317.6 g body weight were used for the *in vivo* study, performed by Dr Alex Dyson in the UK according to local ethics committee (University College London, UK) and UK Home Office guidelines under the Animals (Scientific Procedures) Act 1986. Animals were certified pathogen-free, and housed in cages of 4 on a 12 h light/dark cycle, with food and water *ad libitum* prior to experimentation. Standard cages and bedding were used. Additional tissue paper was provided for comfort, and cardboard tubes for cage enrichment.

Prior to randomisation, animals were separated into cages of 2 or 3 giving a total of n = 5 per treatment group. Four treatment groups were studied (Table 14).

Table 14: A summary of the treatment groups for the *in vivo* investigation of simvastatin and CoQ_{10} effects in rat brain. For each treatment group (n = 5).

Group 1	Group 2	Group 3	Group 4
Food with placebo vehicle	Simvastatin treated (1000 mg/kg food)	CoQ_{10} treated (400 mg/kg food)	CoQ_{10} + Simvastatin treated (400 + 1000 mg/kg food)

On the first day of experimentation, animals were weighed and assigned a randomization number. Standard rodent chow was replaced with *ad libitum* chow supplemented as above. Food provided was weighed at the start, and additional food weighed such that the total food consumed by weight per cage could be calculated for the entire study period (1 week). At experiment end, animals were re-weighed and then subjected to a surgical procedure for the removal of blood. Animals were anaesthetised by 5 % isoflurane in room air (reduced to 2 % post-induction) and placed on a heated mat to maintain rectal temperature at 37°C. Inhaled isoflurane was used as it allows better cardiorespiratory stability over other agents in spontaneously-breathing animals. Animals were then sacrificed by cervical dislocation, and a bilateral craniotomy performed. The whole brain was removed and snap frozen in liquid nitrogen. This too was transferred to cryogenic vials and frozen (-80^{o}C) until later batch analysis.

MRCE Activities

Rat cerebral MRCE activities were investigated as per Section 2.14 and expressed against protein, as determined by the Lowry method outlined in Section 2.15.

Reduced Glutathione Quantitation

Glutathione is the most abundant intracellular thiol. It plays a key role in cellular free radical defence. Dysfunction of the MRC is associated with a redox imbalance and abnormally low levels of reduced glutathione have been reported in patients with primary genetic mitochondrial disorders, as well as in conditions associated with secondary mitochondrial impairment [465, 466]. These trends make reduced glutathione a suitable biomarker for mitochondrial dysfunction.

Reduced glutathione (GSH) was measured using reversed-phase HPLC with coulometric electrochemical detection in accordance to the method described by Riederer *et al.* [467]. The mobile phase was orthophosphoric acid (15 mM) with a flow rate of 0.5 mL/min and run-time of 30 minutes.

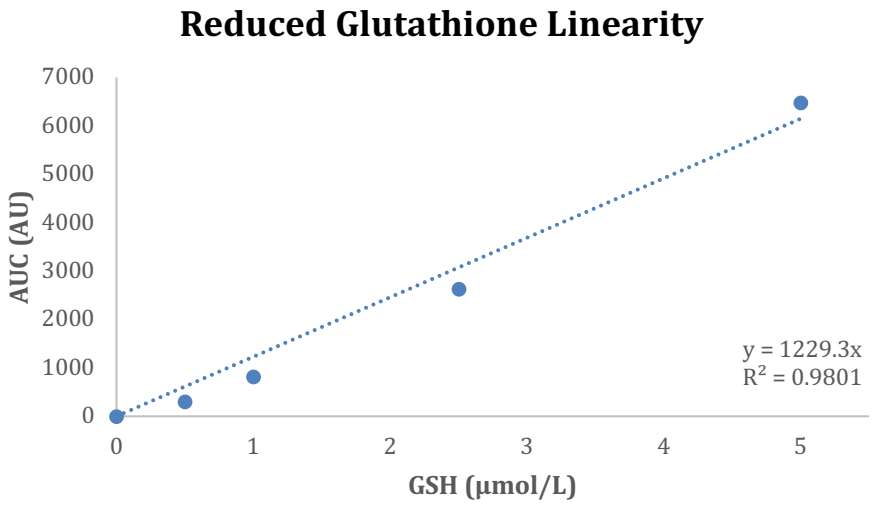

Figure 76: Limits of linearity for the reduced glutathione (GSH) assay.

Samples underwent a freeze-thaw process (× 3) to perturb the cellular membranes and were subsequently extracted in orthophosphoric acid (15 mM), centrifuged at 18625 × *g* for 5 minutes, 5°C, and the supernatant collected for analysis. 50 µL of each sample was injected and separated on a C18 reversed phase column maintained at 25˚C. The screening electrode (E1) was set to 50 mV to oxidise analytes of low oxidation potential. The optimum potential for the detector electrode (E2) was determined to be 750 mV. Samples were quantified against an external standard of GSH (5 µmol/L) diluted in

orthophosphoric acid (15 mM). A calibration curve confirmed linearity between 0.5 – 5 µmol/L GSH (Figure 76).

GSH was quantified using the following equation:

$$\text{GSH (µmol/L)} = \left(\frac{\text{sample peak area}}{\text{external standard peak area}}\right) \times \text{external standard conc.}$$

For intracellular determination of GSH, values were divided by total protein (mg/mL) and expressed as nmol/mg of protein (Section 2.15).

6.3. Results

6.3.1. Effect of Statins on Physiological BBB

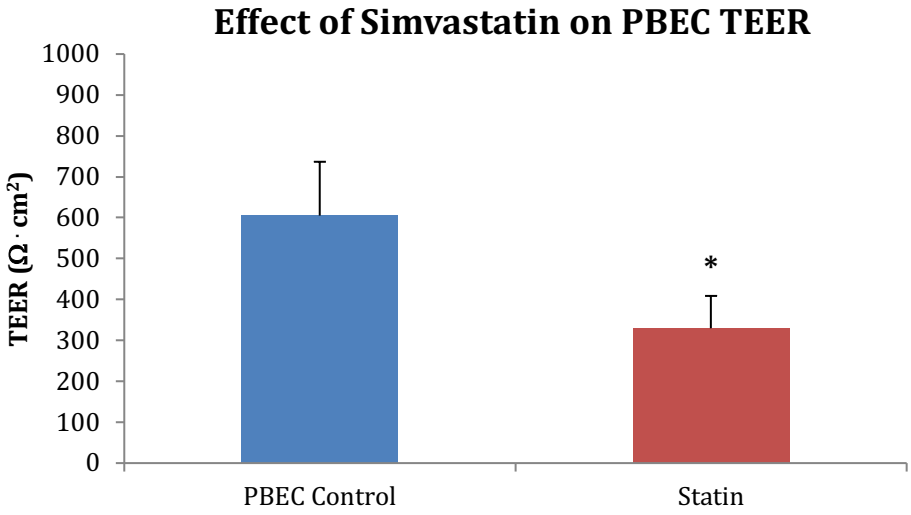

Figure 77: Effect of simvastatin treatment (0.1 µmol/L, 3 days) on TEER in the PBEC BBB. PBEC control (n = 4), PBEC statin-treated (n = 6, $p < 0.05$). Error bars represent standard error of the mean (SEM).

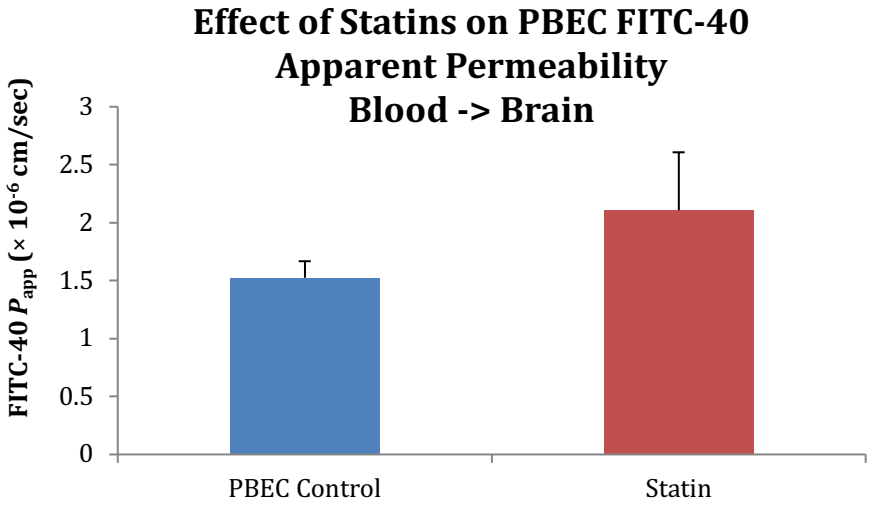

Figure 78: Effect of simvastatin treatment (0.1 µmol/L, 3 days) on FITC-40 apparent permeability at the PBEC BBB. PBEC control (n = 4), PBEC statin-treated (n = 6). Error bars represent standard error of the mean (SEM).

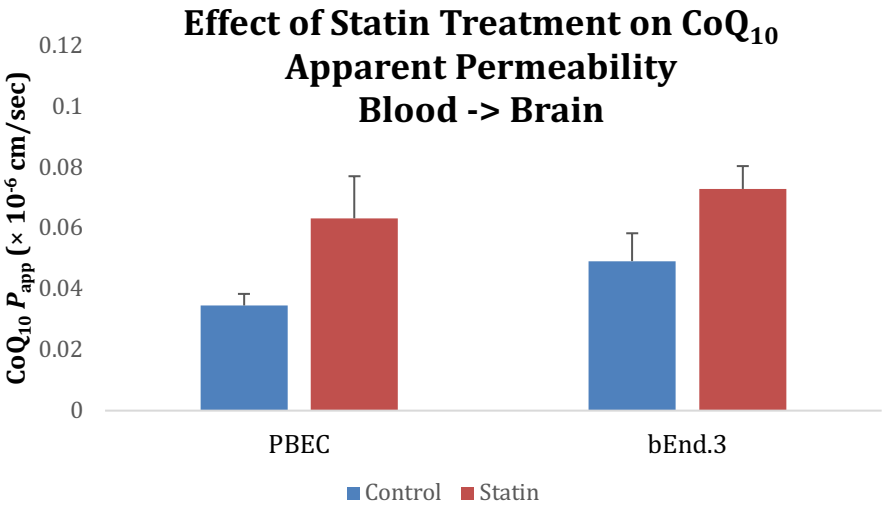

Figure 79: Effect of simvastatin treatment (0.1 µmol/L, 3 days) on CoQ_{10} apparent permeability at the PBEC and bEnd.3 BBB. PBEC control (n = 4), PBEC statin-treated (n = 6), bEnd.3 control (n = 7), bEnd.3 statin-treated (n = 6). Error bars represent standard error of the mean (SEM).

Isolated investigations into the effect of statin therapy (simvastatin, 0.1 µmol/L, 3 days) on *in vitro* models of the BBB under physiological conditions indicated a significant decrease in TEER of 45 % of control ($p < 0.05$) subsequent to statin therapy (Figure 77).

This correlated with a notable, albeit insignificant, (38.8 %) increase in FITC-40 apparent permeability through the PBEC BBB from blood-to-brain (Figure 78).

Perhaps expectedly, given the detrimental effect of statins on the aforementioned functional parameters of the BBB, a consistent yet insignificant increasing trend in blood-to-brain CoQ_{10} apparent permeability was observed in both models of the BBB after statin therapy (49 % increase in bEnd.3 BBB and 80 % increase in the PBEC BBB) (Figure 79).

6.3.2. Effect of Statins on the Pathophysiological BBB

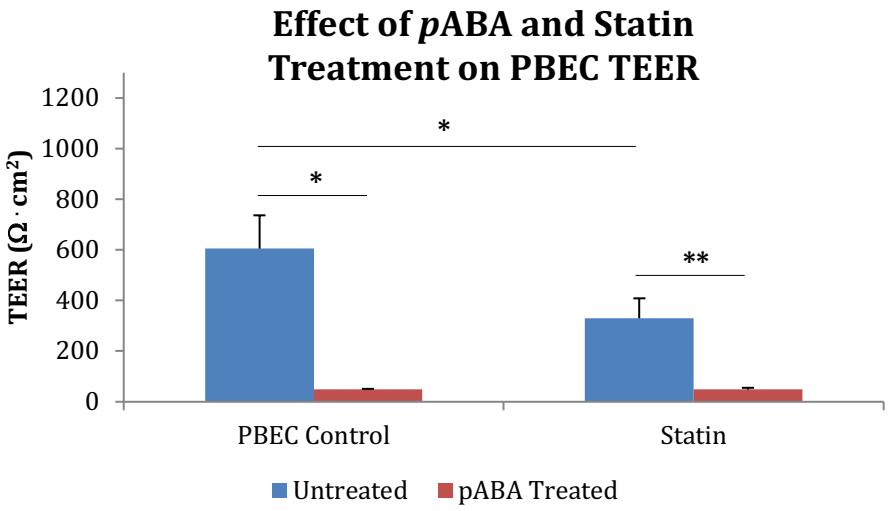

Figure 80: Effect of simvastatin (0.1 µmol/L, 3 days) and pABA (1 mmol/L, 5 days) treatment on TEER in the PBEC BBB. PBEC control (n = 4), *p*ABA PBEC control (n = 3, $p < 0.05$), PBEC statin-treated (n = 6), *p*ABA PBEC statin-treated (n = 5, $p < 0.01$). Error bars represent standard error of the mean (SEM).

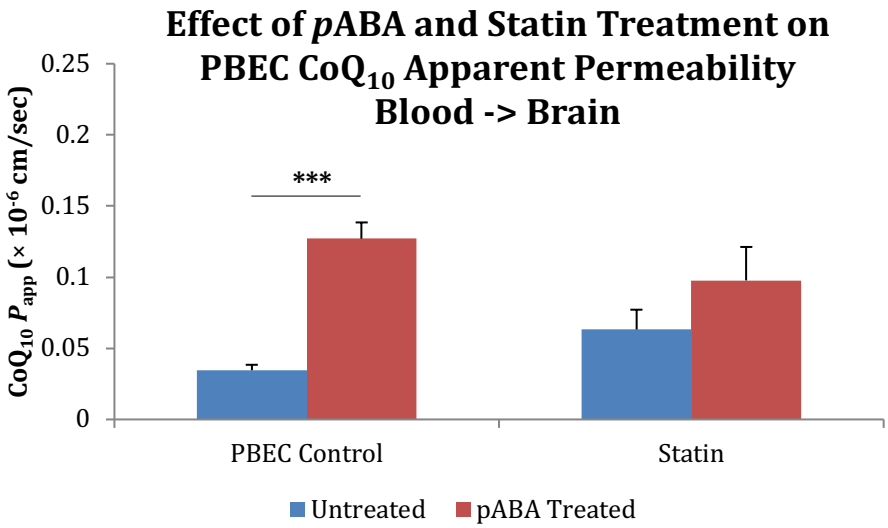

Figure 81: Effect of simvastatin (0.1 µmol/L, 3 days) and pABA (1 mmol/L, 5 days) treatment on CoQ_{10} apparent permeability in the PBEC BBB. PBEC control (n = 4), *p*ABA PBEC control (n = 3), PBEC statin-treated (n = 6), *p*ABA PBEC statin-treated (n = 5). Error bars represent standard error of the mean (SEM).

The pathophysiological CoQ_{10} deficient PBEC BBB model was established using *p*ABA (1 mmol/L, 5 days). Comparison of the resulting TEER in response to a pharmacologically induced CoQ_{10} deficiency indicated no difference between statin-treated and untreated control conditions, although *p*ABA consistently caused a significant decrease in TEER relative to physiological models of the BBB (8.1 % of physiological BBB in PBEC control, $p < 0.05$; 14.6 % of physiological BBB in statin-treated PBECs, $p < 0.01$) (Figure 80).
The significant decrease in TEER due to the induced CoQ_{10} deficiency correlated with an insignificant increase in CoQ_{10} apparent permeability for statin treated PBECs to a level analogous to that observed in PBEC controls (Figure 81), suggesting this may be the upper limit of CoQ_{10} apparent permeability across the endothelial cells.

6.3.3. Investigations *in vivo*

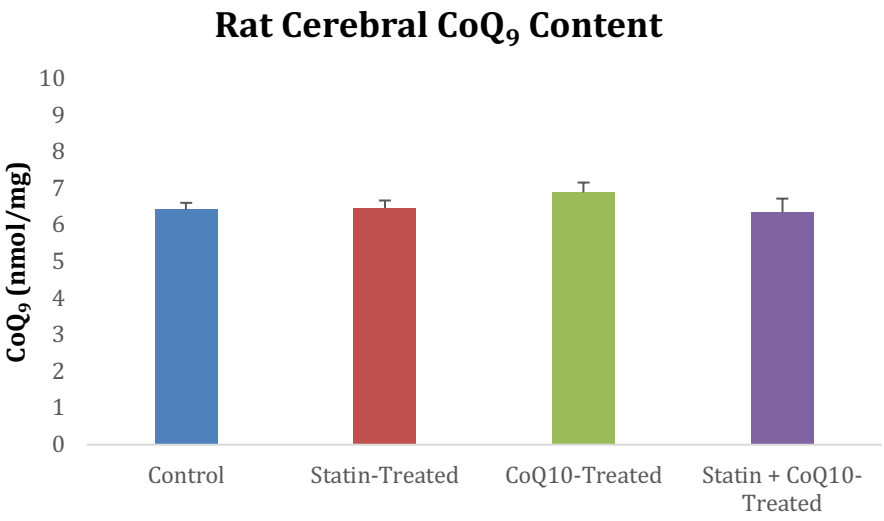

Figure 82: The effect of oral simvastatin (1 g/kg food) and CoQ_{10} (400 mg/kg food) treatment (7 days) on cerebral CoQ_9 content in rat. For both conditions (n = 5). Error bars represent standard error of the mean (SEM).

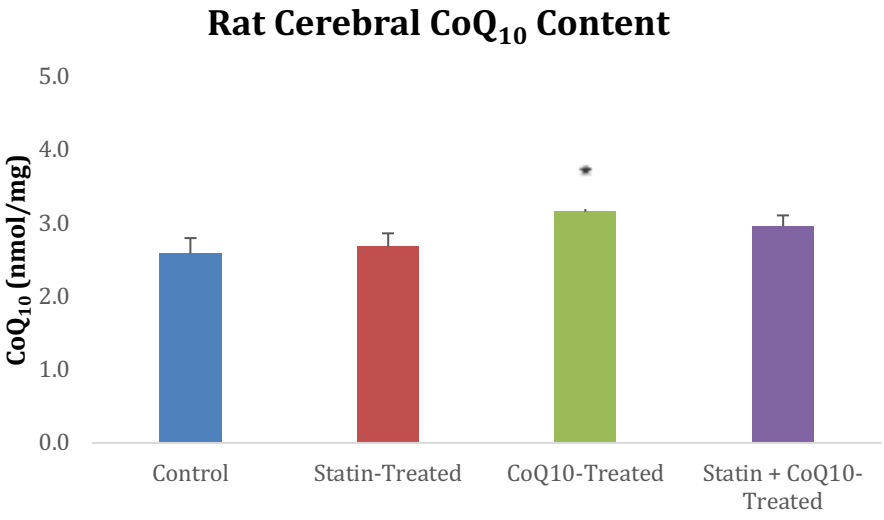

Figure 83: The effect of oral simvastatin (1 g/kg food) and CoQ_{10} (400 mg/kg food) treatment (7 days) on cerebral CoQ_{10} content in rat. For both conditions (n = 5). Control vs. CoQ_{10}-treated rats ($p < 0.05$). Error bars represent standard error of the mean (SEM).

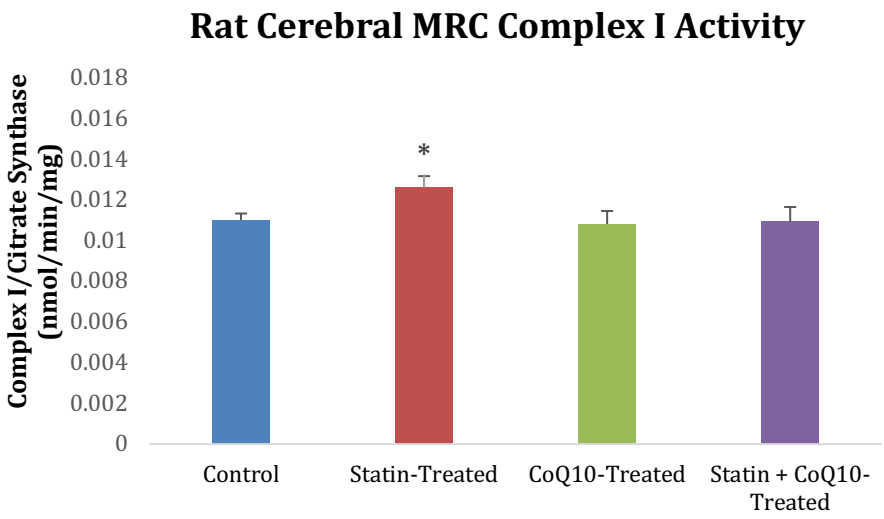

Figure 84: The effect of oral simvastatin (1 g/kg food) and CoQ_{10} (400 mg/kg food) treatment (7 days) on cerebral MRC complex I activity in rat. For all conditions (n = 5). Control vs. statin-treated rats ($p < 0.05$). Error bars represent standard error of the mean (SEM).

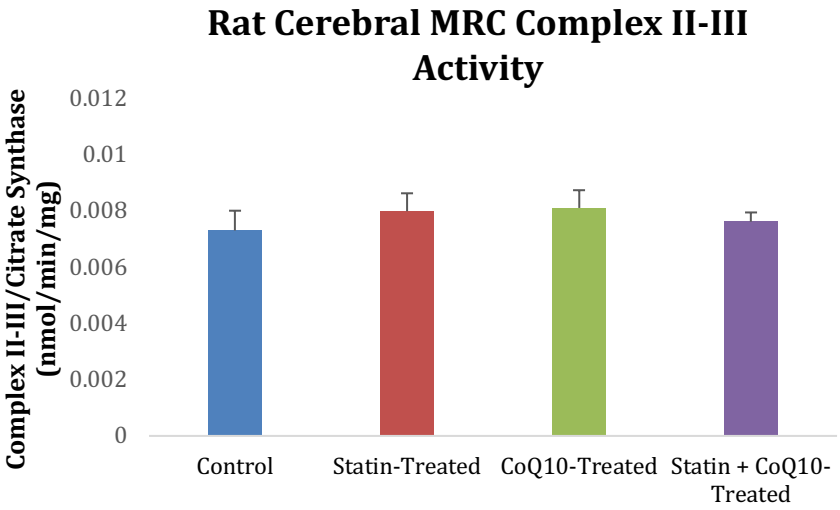

Figure 85: The effect of oral simvastatin (1 g/kg food) and CoQ_{10} (400 mg/kg food) treatment (7 days) on cerebral MRC complex II-III activity in rat. For all conditions (n = 5). Error bars represent standard error of the mean (SEM).

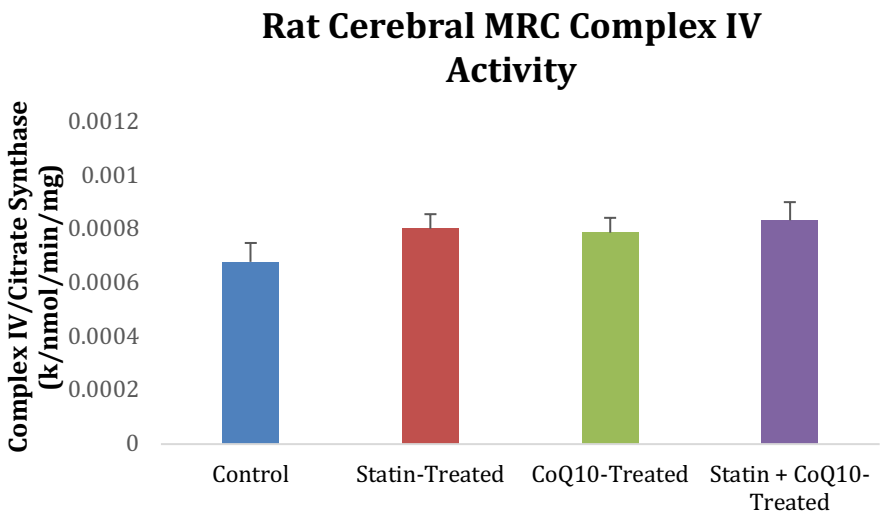

Figure 86: The effect of oral simvastatin (1 g/kg food) and CoQ_{10} (400 mg/kg food) treatment (7 days) on cerebral MRC complex IV activity in rat. For all conditions (n = 5). Error bars represent standard error of the mean (SEM).

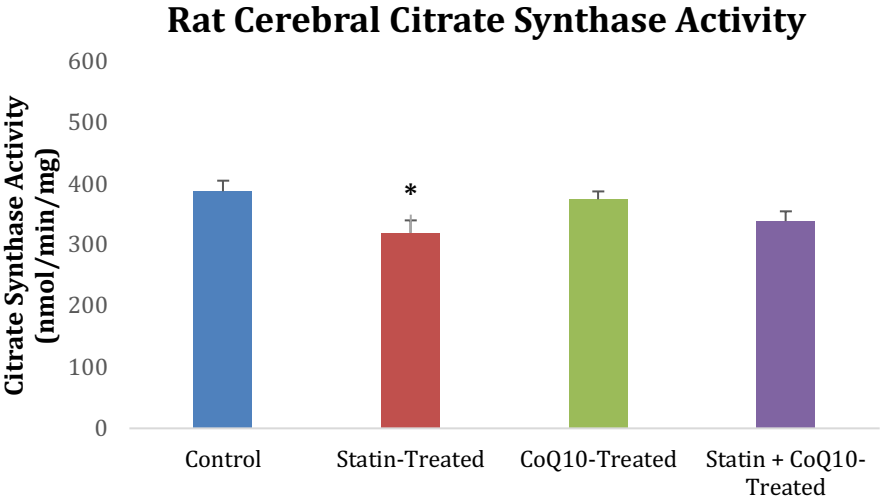

Figure 87: The effect of oral simvastatin (1 g/kg food) and CoQ_{10} (400 mg/kg food) treatment (7 days) on cerebral citrate synthase activity in rat. For all conditions (n = 5). Control vs. statin-treated rats ($p < 0.05$). Error bars represent standard error of the mean (SEM).

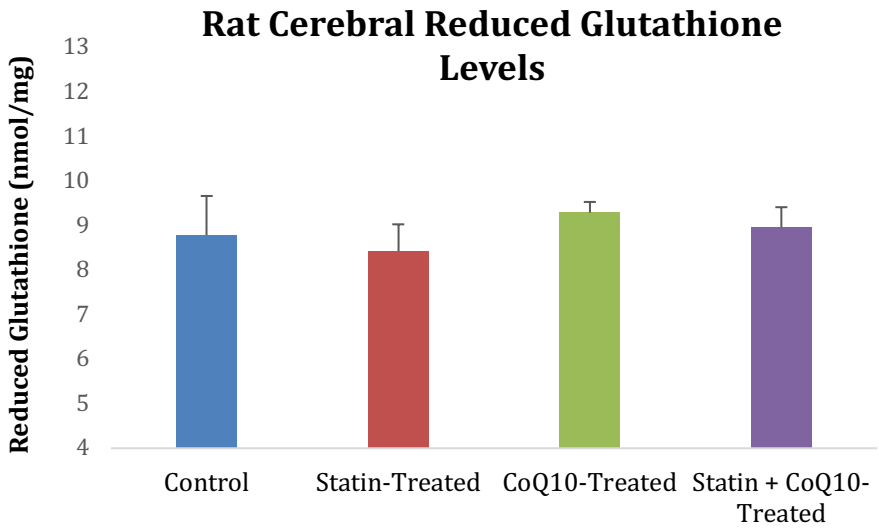

Figure 88: The effect of oral simvastatin (1 g/kg food) and CoQ_{10} (400 mg/kg food) treatment (7 days) on cerebral reduced glutathione levels in rat. For all conditions (n = 5). Error bars represent standard error of the mean (SEM).

To assess the effect of statin therapy *in vivo*, and to investigate the potential benefits of CoQ_{10} as a co-therapy, rats were subjected to a combination of treatment conditions over a period of 7 days (Table 14). Results indicate that exogenous CoQ_{10}, administered orally, may be capable of permeating the rat BBB and entering the brain parenchyma ($p < 0.05$) (Figure 83). Statins showed no effect on cerebral CoQ_9 (Figure 82) or CoQ_{10} (Figure 83) content.

The only observable effect of treatment conditions on cerebral MRCEs was in complex I of statin-treated rats, whereby a 14.5 % ($p < 0.05$) relative increase in activity was recorded (Figure 84). This corresponded to a 17.5 % ($p < 0.05$) relative decrease in citrate synthase activity (Figure 87). There was no effect across all treatment conditions on MRC complex II-III (Figure 85) or complex IV (Figure 86).

Surprisingly, there was no evidence of a deficit in reduced glutathione levels in any of the treatment conditions (Figure 88).

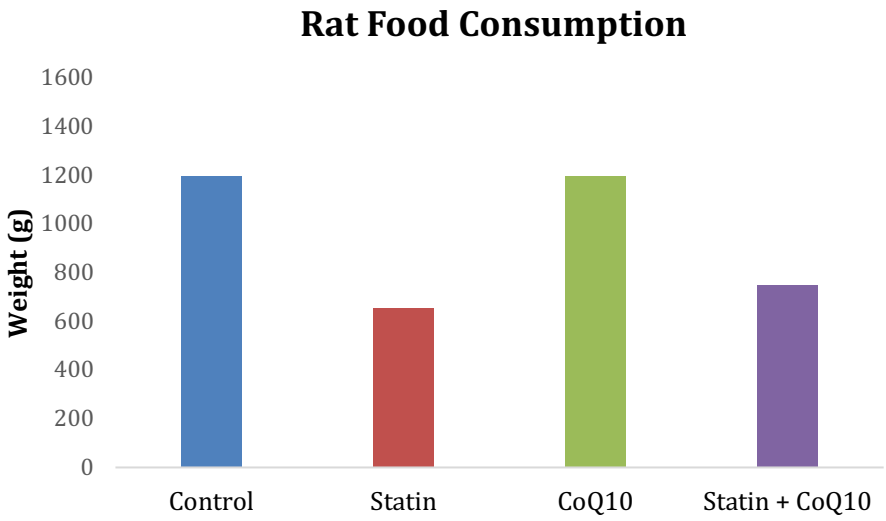

Figure 89: Food consumption by rats across the duration of the treatment period (7 days). For all conditions (n = 5). Values represent the cumulative consumption of food by 5 rats, per treatment condition.

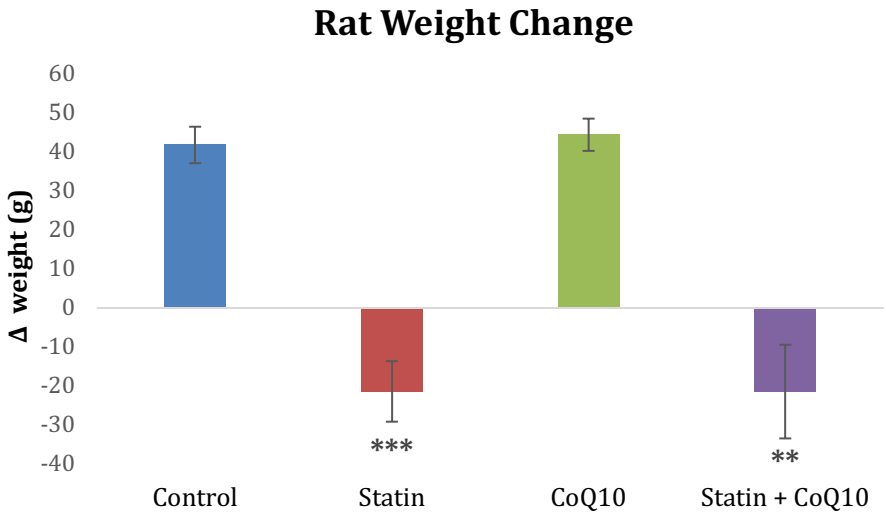

Figure 90: Weight change by rats across the duration of the treatment period (7 days). For all conditions (n = 5). Control vs. statin-treated ($p < 0.001$), control vs. statin plus CoQ_{10}-treated ($p < 0.01$). Error bars represent standard error of the mean (SEM).

During the time course of this study, a considerable decrease in rat weight was observed for those animals subjected to simvastatin treatment. Analysis of food consumption (Figure 89) and weight change (Figure 90) indicated that rats under the statin regime experienced a significant ($p < 0.001$) weight loss of, on average, 21.4 grams. This

correlated with a 45.2 % decrease in food consumption relative to control conditions. Similarly, rats under the statin plus CoQ_{10} regime experienced a significant ($p < 0.01$) weight loss at an average of 21.5 grams, which correlated to a 37.4 % decrease in food consumption relative to control conditions.

6.4. Discussion

Simvastatin (Zocor®) and Atorvastatin (Lipitor®) are the most commonly prescribed statins in the UK, both are lipophilic and both are linked to the reported cases of statin-associated neurological impairment [449, 450, 468]. Due to its lipophilicity, some have suggested that simvastatin has the potential capacity for BBB penetration [469-471], however, no studies have isolated the direct effect of statin treatment on the BBB in conjunction with a CoQ_{10} deficiency and/or with CoQ_{10} therapy.

Using the bEnd.3 and PBEC *in vitro* BBB models, it was possible to assess the effect of simvastatin (0.1 μmol/L, 3 days [461, 462]) treatment on the physical parameters of the BBB under physiological conditions (Section 6.3.1). Evaluation of the TEER in response to statin treatment indicated a significant 45.5 % decrease ($p < 0.05$) suggesting a breakdown in BBB integrity (Figure 77). This correlated with a consistent trend of increasing FITC-40 (Figure 78) and CoQ_{10} (Figure 79) blood-to-brain apparent permeability.

The combination of a significantly decreased TEER and trend for increased FITC-40 P_{app}, confirms a breakdown in BBB integrity and subsequent increase in barrier permeability following statin treatment. This infers that statins have an impact on the BBB that could, potentially, disrupt the finely balanced *interior milieu* of the brain parenchyma. This would be detrimental to normal brain homeostasis, particularly given the BBBs major role in limiting brain entry of plasma excitotoxins calcium, and glutamate, and could plausibly be a contributing factor to the pathogenesis of adverse neurological side-effects associated with statin therapy [472].

These findings are in contrast to Yang *et al.* [473] and Wu *et al.* [474] who have suggested an acute neuroprotective role for statins by reducing BBB permeability after intracerebral

haemorrhage and traumatic brain injury respectively. However, the observed effect in both cases was relative to a diseased baseline, following a traumatic incident, and the reduction in BBB permeability may be reflective of the anti-inflammatory action of statins as opposed to an evaluation of their isolated effect on BBB permeability under physiological conditions [475-477]. Another study by Ifergan *et al.* [478], investigating lesion formation in Multiple Sclerosis, noted a reduced leukocyte migration to the brain parenchyma after simvastatin or lovastatin treatment. Authors noted biochemical consequences independent of structural TJ proteins as the cause of the observed effect, however, their method did not provide any measurement of TJ functionality as is demonstrated by TEER, rather they focussed on overall TJ protein expression. It could be the case that the TJ proteins were not operational at the peripheral inter-membrane region and were instead internalised to be more cytosolic, as was the case with *p*ABA-treated endothelia in this project (Section 4.3.4, Figure 60). Nevertheless, it does support the notion that statins can impart perturbations of biochemical process at the BBB.

While it would be logical to surmise that the consistently increasing trend of CoQ_{10} P_{app} in response to statin treatment is due to a leaky barrier, an alternative, or parallel, explanation may be stimulation of transport mechanisms; statins have been shown to induce an upregulation of LDLR and downregulation of P-gp and RAGE [479-481]. Both RAGE and LDL-related transporters have previously been shown, within this project (Chapter 4) to be the route of transport for CoQ_{10} across the BBB. Given the reduced BBB integrity in response to statin treatment, there is likely to be a greater degree of membrane-protein motility, meaning the distribution of the transporters may be atypical. This atypical luminal/basolateral distribution of over/under-expressed transporters could, in turn, contribute to the observed trend for CoQ_{10} P_{app}. However, the precise reason for the increasing trend in CoQ_{10} P_{app} as a response to statin therapy will probably be a combination of both BBB leak and perturbed transport dynamics, although, further work needs to be performed to confirm this.

Since the reported cases of statin-associated neurological impairment have shown to improve after cession of statin therapy and/or with CoQ_{10} supplementation [449, 450], it could be suggested that the BBB effects are reversible. Again, further studies would need to be performed to support this notion as, evidently, the 1 hour time-course of CoQ_{10} supplementation in the confines of this study was insufficient to cause a full reparation of the BBB following statin therapy.

With knowledge of the effects that statins have on the physiological BBB, it was important to further understand how this translated to the pathophysiological CoQ_{10} deficient BBB. Using *p*ABA (1 mmol/L, 5 days) to pharmacologically induce a CoQ_{10} deficiency, the *in vitro* PBEC BBB was treated with simvastatin (0.1 µmol/L, 3 days) and CoQ_{10} permeability was assessed alongside functional parameters of the BBB (Section 6.3.2).

Of note, were significant decreases in TEER as a result of *p*ABA treatment (Figure 80). This effect was consistent in both the untreated and statin treated PBEC BBB. The significantly decreased TEER in the pathophysiological BBB corresponded with an insignificant trend for increased blood-to-brain CoQ_{10} P_{app} in the statin treated PBECs (66.7 % increase) (Figure 81). As previously mentioned, this is likely indicative of a 'leaky' barrier in conjunction with atypical transporter distribution. Given that the absolute magnitude of the resulting TEER and CoQ_{10} P_{app} for the untreated versus statin treated PBECs was comparable, it may be that the dominant factor was the pharmacologically induced CoQ_{10} deficiency and the observed trends are likely the upper limit of this effect. Extrapolating these findings, statins imparted a mild, yet significant, transient effect on the functionality of the BBB which could contribute to the reported neurological side-effects. This provides support for a CoQ_{10} co-therapy, with prolonged pre-administration to increase baseline status of the quinone prior to commencing statin therapy, since an established or sub-clinical mitochondrial dysfunction, as indicated by the pharmacologically induced CoQ_{10} deficiency in this study, has been shown to exacerbate the effects on the BBB, potentially leading to harmful neurological sequalae. Furthermore, given the correlation of increased age with the administration of statins, it would be feasible to expect naturally diminished levels of endogenous CoQ_{10} in addition to a progressively compromised BBB [482-485], therefore increasing the risk of incidence by way of a compound effect.

While this is the first time that statins have been shown to have a direct detrimental effect on the BBB, statins have previously been shown to induce endothelial dysfunction in the patients with pre-disposed or established mitochondrial dysfunction [486], further strengthening the conclusions drawn from these *in vitro* studies.

The PBEC BBB is considered the gold-standard *in vitro* model of the BBB, providing the best *in vitro* – *in vivo* correlation [166], however, it does not provide any quantifiable

information on the clinical consequence of a compromised BBB on the brain parenchyma. For this it is imperative to perform investigations *in vivo* (Section 6.3.3).

There is ongoing debate regarding the delivery of exogenous CoQ_{10} to the brain parenchyma since CoQ_{10} therapy can be ineffective for the treatment of neurological disorders in human. Some previous studies have reported CoQ_{10} uptake into animal brain following supplementation [48, 83, 487], including this study (22.1 % increase, $p < 0.05$) (Figure 83). However, it must be noted that while these results indicate an overall increase of cerebral CoQ_{10}, there are notable caveats that should be considered, including, whether the rat BBB is leakier or possesses different transporters to human. Additionally, the microvasculature was still present in the dissected brain samples, meaning the CoQ_{10} measured may not be a true representation of pure brain tissue, but could be reflective of contamination with residual plasma. These limitations should also be considered when critiquing other work reported by the scientific community.

Interestingly, and unexpectedly, there was no observed effect of simvastatin on the cerebral levels of CoQ_9 (Figure 82), the prominent ubiquinone in rat, and CoQ_{10} (Figure 83). This is surprising as the emerging consensus would dictate a depletion of CoQ levels in response to a perturbation of the mevalonate pathway by the HMG-CoA reductase inhibitor [37, 38, 40]. Indeed this is an underlying premise for the clinical manifestation of statin-associated myopathies [433-436]. However, while the results presented here suggest statins have reached the brain parenchyma, because of the effect on the MRC (Figure 84), it is unknown to what extent. This means we are unable to ascertain what concentration of statin is required to cause a deleterious effect on cerebral CoQ biosynthesis, if at all. Further studies should focus on determining this by direct measurement and comparison of plasma and brain simvastatin levels [464].

It has been estimated that 1–3 % of the electrons that flow through the MRC are released as free radicals, primarily at complexes I and III. More recent estimates place this value at about 0.15 % under basal physiological conditions, however, the production of free radicals is known to increase with the inhibition of the MRC complexes I/III [488-490]. Results from this study indicate an increase in MRC complex I activity (14.5 % increase, $p < 0.05$) following simvastatin treatment (Figure 84). This suggests that the simvastatin treatment did not exert enough of a deficit on CoQ_{10} levels to hinder the flux of electrons through the MRC, but did induce hypersensitivity to an oxidative incident, which is

reflected by an increased complex I activity as a compensatory mechanism for upholding the mitochondrial membrane potential [436, 491-493]. This correlated with a decrease in citrate synthase activity (17.5 % decrease, $p < 0.05$) indicating a relative depletion of mitochondria (Figure 87). The sequence and inter-relation of the observed events is unknown, but previous reports have cited mitochondrial calcium signalling as a likely contributor to statin-associated myopathies, be it dependent or independent of CoQ_{10}, and is certainly an avenue for further exploration [494-500].

Although various effects have been observed as an apparent consequence of simvastatin treatment *in vivo*, a consideration that shouldn't be overlooked is the weight change of the rats during the course of the treatment period (Figure 90). Either the smell of the statin-chow or appetite suppression caused a significant decrease in the weight of rats who were subjected to simvastatin treatment (Figure 89). Appetite loss has previously been reported in conjunction with sleep disturbances for patients undergoing lovastatin therapy [501], however, the majority of weight loss side-effects are more commonly a result of conjunctive dieting and exercise as is prescribed for hypercholesterolaemic patients. This means the weight loss may well be a reflection of a repulsive smell associated with the statin-chow.
Whatever the reason for the weight loss, it does have an implication for the reliability of the observed effects, since it is unknown if the effect on the MRC enzymes described here are an exclusive consequence of simvastatin treatment or a bioenergetic adaptation in response to a loss of appetite/starvation [502-504]. Indeed it has recently been shown that calorie restriction modifies ubiquinone and COQ transcript levels in mouse tissues [505], potentially having an effect on the overall stability of the respirasome. That said, any future *in vivo* investigations involving high-dose statins should adhere to administration by gavage or intravenous injection to ensure a reliable treatment regime.

Although the validity of the *in vivo* investigations may be disputed, the effect of statin treatment on the *in vitro* PBEC BBB is isolated and reliable. As previously mentioned, it is unclear as to how these effects will manifest clinically and what role they may/may not play in the neurological adverse effects associated with statin therapy, but there is no disputing the detrimental effect on the functional parameters of the BBB.

It is common protocol to provide extensive evidence as to why a drug should be used for the treatment of a particular disease. This is often due the compound being a synthetic analogue with unknown *in vivo* interactions. However, in the case of co-administration of CoQ_{10} with statins, we are dealing with an endogenous compound that is fundamental to bioenergetics, has a direct association with statins, and has an exemplary safety profile. As such, it would be more logical to ask; '*why shouldn't we use CoQ_{10} in conjunction with statins?*', a question to which there are very few answers and is probably best directed at health economists.

Opposition to CoQ_{10} and statin co-administration may be due to studies which have proven inconclusive, however these studies have been small-scale in relation to the magnitude of statin use globally and therefore may not reflect a true demographic. Or perhaps the main prohibiting factor is cost, in which case commercial entitles should respond accordingly and realise the enormous market they have been gifted. Either way, there is mounting evidence, including findings from this study, which supports the use of CoQ_{10} as a preventative measure to alleviate the adverse effects of statins, thereby improving adherence and further strengthening statin use as a highly effective therapy against one of the biggest pandemics facing the planet, CVD.

7. Conclusions and Future Direction

Through developing *in vitro* BBB models compatible with investigating CoQ_{10} transport, this study has provided the first insights into the mechanisms by which CoQ_{10} crosses the BBB. Furthermore, a method for pharmacologically inducing a CoQ_{10} deficiency in bEnd.3 cells and PBECs has been proposed. This will enable further comparative assessments of the pathophysiological effects of a deficit in CoQ_{10} status on BBB transport and mitochondrial function.

The mechanisms that have emerged as the modes of efflux and influx of CoQ_{10} across the *in vitro* BBB within this study, namely LRP-1 mediated efflux, and RAGE and SR-B1 mediated influx, are not thought to be an exhaustive representation of all the processes in action (Chapter 4, Figure 64). Rather, they represent some of the most prominent mechanisms operating and provide evidence for lipoprotein-dependent transport of CoQ_{10} across the BBB.

Through providing this evidence we have better defined the possible routes for CoQ_{10} transport across the BBB, thereby extending our understanding of the biochemical function of CoQ_{10} *in vivo*, and affording future researchers a more focussed scope of investigation. Of particular interest would be to isolate the precise mode of transcytosis, whether that be via large vesicular transport, tunnelling, or endocytic intracellular repackaging. This could be achieved by fluorescently labelling CoQ_{10} and visualising the event [506].

In addition to the novel mechanistic insight, this study has provided the first models of a CoQ_{10} deficient *in vitro* BBB. The effect of this pathology detrimentally impacted the physical parameters of the BBB by reducing TEER, increasing paracellular permeability, and altering CoQ_{10} transport parameters (Section 4.3.4). The precise cause of these effects are unknown, but both ATP depletion and a decreased redox capacity are likely mechanisms [265, 418].

This theory was strengthened by investigations into the 'mito-cocktail', specifically the effect of vitamin E co-administration on CoQ_{10} BBB permeability (Section 5.3.1), where results highlighted that the transporters responsible for CoQ_{10} uptake are sensitive to changes in antioxidant capacity and hence may be the first to falter during the onset of a CoQ_{10} deficiency. Additionally, the results indicated that the efflux receptors are more robust to a mitochondrial dysfunction. Perhaps the key message to take from this is that, if antioxidant capacity could be preserved during a CoQ_{10} deficiency, through the administration of excess antioxidant, there is potential for improved uptake during pathophysiological conditions. However, the antioxidant of choice should not compete with CoQ_{10} for circulatory lipoprotein. That said, future studies should focus on understanding this in more detail and discovering the optimal co-therapies.
Additionally, it would be interesting to see if the physical defects expressed by the pathophysiological BBB, induced by a CoQ_{10} deficiency, could be reversed through long-term treatment with exogenous CoQ_{10}.

Since primary CoQ_{10} deficiencies are inherited and present from the beginning of brain development *in utero*, an alternative, and equally important line of investigation, would be to assess the effect of a CoQ_{10} deficiency on the maturation of the BBB. The culture of human induced pluripotent stem cells (hiPSCs) in combination with *p*ABA could offer insight into the effect of a CoQ_{10} deficiency on the glial switch which, in turn, would have implications for BBB maturation [507]. This would enable us to better understand the condition *in utero* and its clinical manifestation in neonates.

Regardless of the mechanistic processes operating, the delivery of exogenous CoQ_{10} to the brain is limited by receptor-mediated efflux and, ultimately, determined by low-density lipoprotein BBB transport (Section 3.3.3). The transport of circulatory lipoprotein into the brain is already known to be low, with CSF concentrations of most plasma-derived proteins at < 1 % of the corresponding plasma concentrations [508].
An approach to circumvent these inherent limitations include the loading of CoQ_{10} into alternative circulatory carriers. For example, the selective loading of CoQ_{10} into HDL, an SR-B1 ligand, which is known to be a prevalent lipoprotein found in the CNS, could potentially reduce efflux at the BBB. Similarly, loading into synthetic nanoparticles could facilitate a 'Trojan-horse' style of delivery to the brain. However, the synthetic approach

is burdened by more stringent pharmaceutical testing relative to the use of endogenous lipoprotein, hence, a comparative study of LDL versus HDL could be a simple and effective next-line of investigation.

An increasingly popular method for the treatment of neurological disorders associated with mitochondrial dysfunction is through utilising small synthetic analogues of CoQ_{10}. Currently, the only clinically approved synthetic analogue of CoQ_{10} is idebenone, which shares the antioxidant properties of CoQ_{10} and is able to restore electron flux through the MRC, albeit to a lesser extent than CoQ_{10} itself [365-367].

Due to its small size, many have purported passive diffusion as the mechanism of uptake for idebenone across the BBB and into the brain parenchyma [400-402], however, no research has so far studied the specific transport mechanisms. This study has provided the first insight into the capacity for idebenone to cross the BBB, at relatively high levels, in both the PBEC and bEnd.3 BBB models (Section 5.3.3).

These results therefore suggest that idebenone may be a more effective treatment for neurological disorders than CoQ_{10}. However, much like CoQ_{10}, the therapy should be optimised since the bioavailability of oral idebenone is known to be around 1 % and, due to its lack of association with circulatory lipoproteins, its clearance is considerably more rapid than CoQ_{10}. Furthermore, *in vitro* studies have previously demonstrated a potential toxic effect for idebenone due to competitive binding with complex I of the MRC [376].

Given the similarities between idebenone and CoQ_{10} as antioxidants, and with knowledge of the beneficial effects of co-administration with vitamin E, as proven in this study, idebenone therapies may also benefit from combined administration with other potent antioxidants. This avenue should therefore be explored further.

While there is a clear, and logical, rationale for performing BBB investigations in the commercially available *in vitro* immortalised cell lines, the differences observed in the bEnd.3 and PBEC BBB models within this study demonstrate why it is important to use a model that has the best *in vivo – in vitro* correlation, and to not directly compare or contrast data from different models.

It should also be noted that, although the astrocyte-PBEC co-culture BBB is currently the gold-standard for the *in vitro* analysis of permeability, there is a thriving field of research focussed on developing these models further, with great promise being shown for a

human BBB derived from human pluri- and multipotent stem cells [509, 510]. These models are still in the very early stages of development and currently require an even greater demand on resource, skill and time than the PBEC BBB model. Nevertheless, they have the potential to supersede the primary animal cell BBB models for routine use and their progress should, therefore, be monitored closely.

In summary, this study has provided the first substantive evidence for bi-directional transport mechanisms which limit CoQ_{10} transfer across the BBB, it has identified a rapid mechanism for idebenone transport, and it has shown that CoQ_{10} efflux at the BBB can be reduced in the presence of other potent antioxidants.
All of this information is invaluable if we are to optimise CoQ_{10} therapies, however, it has not provided any information on how CoQ_{10} is released from lipoprotein carriers, or how CoQ_{10} and idebenone are taken up by cells in the brain parenchyma. Even though co-culture with glia during the P_{app} assay could help shed some light on this, the most appropriate strategy going forward would be to translate any promising *in vitro* findings onto a robust *in vivo* model.

There is considerable and increasing theoretical knowledge surrounding CoQ_{10}, and it could be said that the main issue now faced is overcoming rather than necessarily understanding, therefore, future studies should transition to pragmatic investigation. With regards to overcoming the BBB, a multi-faceted approach of an increased circulatory CoQ_{10} concentration, in conjunction with optimised co-therapies, and perhaps the inhibition of known BBB efflux transporters [284] is a highly promising tactic for the improved delivery of CoQ_{10} to the brain. Realistically, the best chance of achieving this is through high-dose intravenous administration of CoQ_{10}, and investigations into this could be ground-breaking, leading to an efficacious therapy for acute presentation, or for neonates of parents with known deficiencies – either primary or secondary. Given the irreversible neurological implications of a CoQ_{10} deficiency, establishing a more effective therapy really could be life-changing.

The other, highly pertinent, focus of this research was to better understand the neurological implications of statin therapy (Chapter 6), in particular the effects at the BBB.

Statins inhibit a key enzyme, HMG-CoA reductase, in the biosynthetic pathway of CoQ_{10} (Section 5.1, Figure 75), and this deleterious effect is implicated as the cause of muscular and neurological adverse side-effects. In a first of its kind study, *in vitro* models of the BBB were treated with simvastatin and the impact of this treatment directly assessed using TEER measurements and apparent permeability markers (Section 6.3.1).
The outcome of this study indicated that simvastatin treatment induces a breakdown of the BBB integrity. This could plausibly disrupt the finely balanced *interior milieu* of the brain parenchyma and may be a contributing factor to the pathogenesis of adverse neurological side-effects associated with statin therapy. The precise series of events leading to the BBB leak is unclear, with dysregulation of the *de novo* biosynthesis of CoQ_{10} and/or a reduced antioxidant capacity being viable explanations. However, an emerging theory implicating a calcium-induced mitochondrial permeability transition, which would fit with the observed trends, warrants further investigation [494-500].
To test whether the findings from these *in vitro* investigations are consistent *in vivo*, an option is to analyse peripheral markers of BBB breakdown in statin patients presenting with either neurological and/or muscular side-effects [511, 512]. It would also be of interest to observe the effects of co-administered exogenous CoQ_{10} with the statin treatment on the PBEC BBB model to deduce whether the BBB derangement is CoQ_{10} dependent and could therefore be prevented, perhaps utilising this platform to investigate the potential protective effects of CoQ_{10} pre-treatment, additionally.

It is known that endogenous CoQ_{10} levels decrease with age [13]. Considering that statins are most prominently prescribed to the elderly, and taking into account the deleterious effect statins can have on the *de novo* biosynthesis of CoQ_{10}, it is logical to surmise that there is an increased risk of developing CoQ_{10} dependent statin-induced adverse side-effects with increasing age. This would be consistent with the emerging consensus that there may be a CoQ_{10} threshold, below which triggers the pathogenesis of mitochondrial dysfunction associated with a CoQ_{10} deficiency. Theoretically, this could be exacerbated by statin therapy, causing previously sub-clinical subjects to present within the clinical reference range.
The benefit of pharmacologically inducing a CoQ_{10} deficiency using *p*ABA is the ability to titrate the level of CoQ_{10} depletion, thereby enabling the investigation of a threshold between CoQ_{10} status and mitochondrial (dys)function. Hence, future studies should

explore the legitimacy of the proposed phenomenon by probing the effect of iterative CoQ_{10} depletion on the MRC enzyme activities, TEER, and P_{app} in BBB models. This can then be correlated with statin effects to find the critical concentration that will induce a symptomatic effect.

Further studies could determine the neurological risk in the general population by assessing cerebral CoQ_{10} levels in the elderly versus young healthy controls to gauge depletion in relation to CoQ_{10} deficient references, and therefore the susceptibility to statin therapy with age. Of interest would be noting any regional CoQ_{10} differences in the brain, as this will give some indication of the resulting neurological presentation. However, this would be a significant and expensive study, which may suffer from having a lack of brain sample material from young healthy controls. However, the highly sensitive LC-MS/MS method developed within this study (Section 3.3.2) may circumvent this issue should the CSF emerge as a reliable conduit for assessing neurological CoQ_{10} status.

While this study raises questions about statin therapy, it is important to remember statins are one of the most effective interventions in cardiovascular medicine, and this study aims to address some flaws by proposing solutions. Ultimately the intention is to increase adherence to statins and reduce CVD even further.

To counteract the potentially deleterious effect of statins on CoQ_{10} biosynthesis, alongside CoQ_{10} co-therapy, many have proposed pre-administration of CoQ_{10}. Interestingly, while the observed beneficial effect of vitamin E on reducing CoQ_{10} efflux at the BBB only occurred under physiological conditions, this is nonetheless significant as it could aid in improving brain CoQ_{10} uptake during pre-treatment. Each of these strategies should be tested on a robust *in vivo* model.

Another option would be to administer soluble precursors of the CoQ_{10} biosynthetic pathway, as HMG-CoA reductase inhibitors act relatively far upstream, there is lots of scope for this approach [260].

Overall, this project has spanned analytical chemistry, clinical biochemistry, cell biology, neuroscience and, to an extent, medicine. This exemplifies the importance and wide-reaching impact CoQ_{10} has and could have. Although a seemingly insignificant simple molecule it is key to maintaining the powerhouse of the cell, the mitochondria.

Considerable progress has been made in the context of this project, yet it has also opened the door for various avenues of further research, and it is likely that the clinical significance of the compound will only increase with time.

References

1. Lovern, J. A.; Morton, R. A.; Ireland, J., The distribution of vitamins A and A(2). II. *Biochem J* **1939,** *33* (3), 325-9.

2. Festenstein, G. N.; Heaton, F. W.; Lowe, J. S.; Morton, R. A., A constituent of the unsaponifiable portion of animal tissue lipids (lambda max. 272 m mu). *Biochem J* **1955,** *59* (4), 558-66.

3. Crane, F. L.; Hatefi, Y.; Lester, R. L.; Widmer, C., Isolation of a quinone from beef heart mitochondria. *Biochim Biophys Acta* **1957,** *25* (1), 220-1.

4. Wolf, D. E.; Hoffman, C. H.; Trenner, N. R.; Arison, B. H.; Shunk, C. H.; Linn, B. O.; McPherson, J. F.; Folkers, K., Coenzyme Q. I. Structure Studies on the Coenzyme Q Group. *JACS* **1958,** *80* (17), 4752-4752.

5. Ernster, L.; Lee, I. Y.; Norling, B.; Persson, B., Studies with ubiquinone-depleted submitochondrial particles. Essentiality of ubiquinone for the interaction of succinate dehydrogenase, NADH dehydrogenase, and cytochrome b. *Eur J Biochem* **1969,** *9* (3), 299-310.

6. Mitchell, P. D. The Nobel Prize in Chemistry 1978.

7. Mitchell, P., Chemiosmotic coupling in oxidative and photosynthetic phosphorylation. *Biol Rev Camb Philos Soc* **1966,** *41* (3), 445-502.

8. Mitchell, P., Coupling of phosphorylation to electron and hydrogen transfer by a chemi-osmotic type of mechanism. *Nature* **1961,** *191*, 144-8.

9. Mitchell, P., The protonmotive Q cycle: a general formulation. *FEBS Lett* **1975,** *59* (2), 137-9.

10. Nomenclature, I.-I. C. o. B., Nomenclature of Quinones with Isoprenoid Side-Chains. Recommendations, 19731. *Eur J Biochem* **1975,** *53* (1), 15-18.

11. Acosta, M. J.; Vazquez Fonseca, L.; Desbats, M. A.; Cerqua, C.; Zordan, R.; Trevisson, E.; Salviati, L., Coenzyme Q biosynthesis in health and disease. *Biochim Biophys Acta* **2016,** *1857* (8), 1079-1085.

12. Bhagavan, H. N.; Chopra, R. K., Coenzyme Q10: absorption, tissue uptake, metabolism and pharmacokinetics. *Free Radic Res* **2006,** *40* (5), 445-53.

13. Kalen, A.; Appelkvist, E. L.; Dallner, G., Age-related changes in the lipid compositions of rat and human tissues. *Lipids* **1989,** *24* (7), 579-84.

14. Ernster, L.; Dallner, G., Biochemical, physiological and medical aspects of ubiquinone function. *Biochim Biophys Acta* **1995,** *1271* (1), 195-204.

15. Crane, F. L., Biochemical functions of coenzyme Q10. *J Am Coll Nutr* **2001,** *20* (6), 591-8.

16. Sazanov, L. A., A giant molecular proton pump: structure and mechanism of respiratory complex I. *Nat Rev Mol Cell Biol* **2015,** *16* (6), 375-88.

17. Lapuente-Brun, E.; Moreno-Loshuertos, R.; Acin-Perez, R.; Latorre-Pellicer, A.; Colas, C.; Balsa, E.; Perales-Clemente, E.; Quiros, P. M.; Calvo, E.; Rodriguez-Hernandez, M. A.; Navas, P.; Cruz, R.; Carracedo, A.; Lopez-Otin, C.; Perez-Martos, A.; Fernandez-Silva, P.; Fernandez-Vizarra, E.; Enriquez, J. A., Supercomplex assembly determines electron flux in the mitochondrial electron transport chain. *Science* **2013,** *340* (6140), 1567-70.

18. Acin-Perez, R.; Fernandez-Silva, P.; Peleato, M. L.; Perez-Martos, A.; Enriquez, J. A., Respiratory active mitochondrial supercomplexes. *Mol Cell* **2008,** *32* (4), 529-39.

19. Guaras, A.; Perales-Clemente, E.; Calvo, E.; Acin-Perez, R.; Loureiro-Lopez, M.; Pujol, C.; Martinez-Carrascoso, I.; Nunez, E.; Garcia-Marques, F.; Rodriguez-Hernandez, M. A.; Cortes, A.; Diaz, F.; Perez-Martos, A.; Moraes, C. T.; Fernandez-Silva, P.; Trifunovic, A.; Navas, P.; Vazquez, J.; Enriquez, J. A., The CoQH2/CoQ Ratio Serves as a Sensor of Respiratory Chain Efficiency. *Cell Rep* **2016,** *15* (1), 197-209.

20. Crane, F. L.; Dilley, R. A., Determination of Coenzyme Q (Ubiquinone). 11 ed.; Glick, D., Ed. John Wiley & Sons, Inc.: Hoboken, NJ, USA, 1963; pp 279-306.

21. Vos, M.; Esposito, G.; Edirisinghe, J. N.; Vilain, S.; Haddad, D. M.; Slabbaert, J. R.; Van Meensel, S.; Schaap, O.; De Strooper, B.; Meganathan, R.; Morais, V. A.; Verstreken, P., Vitamin K2 is a mitochondrial electron carrier that rescues pink1 deficiency. *Science* **2012,** *336* (6086), 1306-10.

22. Hildebrandt, T. M.; Grieshaber, M. K., Three enzymatic activities catalyze the oxidation of sulfide to thiosulfate in mammalian and invertebrate mitochondria. *FEBS J* **2008,** *275* (13), 3352-61.

23. Cervellati, R.; Greco, E., In vitro Antioxidant Activity of Ubiquinone and Ubiquinol, Compared to Vitamin E. *Helvetica Chimica Acta* **2016,** *99* (1), 41-45.

24. Crane, F. L.; Navas, P., The diversity of coenzyme Q function. *Mol Aspects Med* **1997,** *18 Suppl*, S1-6.

25. Turunen, M.; Olsson, J.; Dallner, G., Metabolism and function of coenzyme Q. *Biochim Biophys Acta* **2004,** *1660* (1-2), 171-99.

26. Echtay, K. S.; Winkler, E.; Klingenberg, M., Coenzyme Q is an obligatory cofactor for uncoupling protein function. *Nature* **2000,** *408* (6812), 609-13.

27. Bentinger, M.; Tekle, M.; Dallner, G., Coenzyme Q--biosynthesis and functions. *Biochem Biophys Res Commun* **2010,** *396* (1), 74-9.

28. Pierrel, F.; Hamelin, O.; Douki, T.; Kieffer-Jaquinod, S.; Muhlenhoff, U.; Ozeir, M.; Lill, R.; Fontecave, M., Involvement of mitochondrial ferredoxin and para-aminobenzoic acid in yeast coenzyme Q biosynthesis. *Chem Biol* **2010,** *17* (5), 449-59.

29. Marbois, B.; Xie, L. X.; Choi, S.; Hirano, K.; Hyman, K.; Clarke, C. F., para-Aminobenzoic acid is a precursor in coenzyme Q6 biosynthesis in Saccharomyces cerevisiae. *J Biol Chem* **2010,** *285* (36), 27827-38.

30. Kawamukai, M., Biosynthesis of coenzyme Q in eukaryotes. *Biosci Biotechnol Biochem* **2016,** *80* (1), 23-33.

31. Alcazar-Fabra, M.; Navas, P.; Brea-Calvo, G., Coenzyme Q biosynthesis and its role in the respiratory chain structure. *Biochim Biophys Acta* **2016,** *1857* (8), 1073-1078.

32. Wang, Y.; Hekimi, S., Molecular genetics of ubiquinone biosynthesis in animals. *Crit Rev Biochem Mol Biol* **2013,** *48* (1), 69-88.

33. Marbois, B.; Gin, P.; Faull, K. F.; Poon, W. W.; Lee, P. T.; Strahan, J.; Shepherd, J. N.; Clarke, C. F., Coq3 and Coq4 define a polypeptide complex in yeast mitochondria for the biosynthesis of coenzyme Q. *J Biol Chem* **2005,** *280* (21), 20231-8.

34. Ashraf, S.; Gee, H. Y.; Woerner, S.; Xie, L. X.; Vega-Warner, V.; Lovric, S.; Fang, H.; Song, X.; Cattran, D. C.; Avila-Casado, C.; Paterson, A. D.; Nitschke, P.; Bole-Feysot, C.; Cochat, P.; Esteve-Rudd, J.; Haberberger, B.; Allen, S. J.; Zhou, W.; Airik, R.; Otto, E. A.; Barua, M.; Al-Hamed, M. H.; Kari, J. A.; Evans, J.; Bierzynska, A.; Saleem, M. A.; Bockenhauer, D.; Kleta, R.; El Desoky, S.; Hacihamdioglu, D. O.; Gok, F.; Washburn, J.; Wiggins, R. C.; Choi, M.; Lifton, R. P.; Levy, S.; Han, Z.; Salviati, L.; Prokisch, H.; Williams, D. S.; Pollak, M.; Clarke, C. F.; Pei, Y.; Antignac, C.; Hildebrandt, F., ADCK4 mutations promote steroid-resistant nephrotic syndrome through CoQ10 biosynthesis disruption. *J Clin Invest* **2013,** *123* (12), 5179-89.

35. Salviati, L.; Trevisson, E.; Doimo, M.; Navas, P., *Primary Coenzyme Q10 Deficiency*. Seattle, 2017.

36. Grundy, S. M., HMG-CoA reductase inhibitors for treatment of hypercholesterolemia. *N Engl J Med* **1988,** *319* (1), 24-33.

37. Goli, A. K.; Goli, S. A.; Byrd, R. P., Jr.; Roy, T. M., Simvastatin-induced lactic acidosis: a rare adverse reaction? *Clin Pharmacol Ther* **2002,** *72* (4), 461-4.

38. De Pinieux, G.; Chariot, P.; Ammi-Said, M.; Louarn, F.; Lejonc, J. L.; Astier, A.; Jacotot, B.; Gherardi, R., Lipid-lowering drugs and mitochondrial function: effects of HMG-CoA reductase inhibitors on serum ubiquinone and blood lactate/pyruvate ratio. *Br J Clin Pharmacol* **1996,** *42* (3), 333-7.

39. Hargreaves, I. P.; Al Shahrani, M.; Wainwright, L.; Heales, S. J., Drug-Induced Mitochondrial Toxicity. *Drug Saf* **2016,** *39* (7), 661-74.

40. Hargreaves, I. P.; Duncan, A. J.; Heales, S. J.; Land, J. M., The effect of HMG-CoA reductase inhibitors on coenzyme Q10: possible biochemical/clinical implications. *Drug Saf* **2005,** *28* (8), 659-76.

41. Katayama, K.; Fujita, T., Studies on Lymphatic Absorption of 1', 2'-(3H)-Coenzyme Q10 in Rats. *Chem Pharm Bull* **1972,** *20* (12), 2585-2592.

42. Bhagavan, H. N.; Chopra, R. K.; Craft, N. E.; Chitchumroonchokchai, C.; Failla, M. L., Assessment of coenzyme Q10 absorption using an in vitro digestion-Caco-2 cell model. *Int J Pharm* **2007,** *333* (1-2), 112-7.

43. Aberg, F.; Appelkvist, E. L.; Dallner, G.; Ernster, L., Distribution and redox state of ubiquinones in rat and human tissues. *Arch Biochem Biophys* **1992,** *295* (2), 230-4.

44. Miles, M. V.; Horn, P. S.; Morrison, J. A.; Tang, P. H.; DeGrauw, T.; Pesce, A. J., Plasma coenzyme Q10 reference intervals, but not redox status, are affected by gender and race in self-reported healthy adults. *Clinica Chimica Acta* **2003,** *332* (1-2), 123-132.

45. Naini, A.; Lewis, V. J.; Hirano, M.; DiMauro, S., Primary coenzyme Q10 deficiency and the brain. *Biofactors* **2003,** *18* (1-4), 145-52.

46. Schottlaender, L. V.; Bettencourt, C.; Kiely, A. P.; Chalasani, A.; Neergheen, V.; Holton, J. L.; Hargreaves, I.; Houlden, H., Coenzyme Q10 Levels Are Decreased in the Cerebellum of Multiple-System Atrophy Patients. *PLoS One* **2016,** *11* (2).

47. Garrido-Maraver, J.; Cordero, M. D.; Oropesa-Avila, M.; Fernandez Vega, A.; de la Mata, M.; Delgado Pavon, A.; de Miguel, M.; Perez Calero, C.; Villanueva Paz, M.; Cotan, D.; Sanchez-Alcazar, J. A., Coenzyme q10 therapy. *Mol Syndromol* **2014,** *5* (3-4), 187-97.

48. Bentinger, M.; Dallner, G.; Chojnacki, T.; Swiezewska, E., Distribution and breakdown of labeled coenzyme Q10 in rat. *Free Radic Biol Med* **2003,** *34* (5), 563-75.

49. Cheng, T.; Zhao, Y.; Li, X.; Lin, F.; Xu, Y.; Zhang, X.; Li, Y.; Wang, R.; Lai, L., Computation of octanol-water partition coefficients by guiding an additive model with knowledge. *J Chem Inf Model* **2007,** *47* (6), 2140-8.

50. Fash, D. M.; Khdour, O. M.; Sahdeo, S. J.; Goldschmidt, R.; Jaruvangsanti, J.; Dey, S.; Arce, P. M.; Collin, V. C.; Cortopassi, G. A.; Hecht, S. M., Effects of alkyl side chain modification of coenzyme Q10 on mitochondrial respiratory chain function and cytoprotection. *Bioorg Med Chem* **2013,** *21* (8), 2346-2354.

51. Zhang, Y.; Aberg, F.; Appelkvist, E. L.; Dallner, G.; Ernster, L., Uptake of dietary coenzyme Q supplement is limited in rats. *J Nutr* **1995,** *125* (3), 446-53.

52. Bhagavan, H. N.; Chopra, R. K., Plasma coenzyme Q10 response to oral ingestion of coenzyme Q10 formulations. *Mitochondrion* **2007,** *7 Suppl*, S78-88.

53. Hathcock, J. N.; Shao, A., Risk assessment for coenzyme Q10 (Ubiquinone). *Regul Toxicol Pharmacol* **2006,** *45* (3), 282-8.

54. Ochiai, A.; Itagaki, S.; Kurokawa, T.; Kobayashi, M.; Hirano, T.; Iseki, K., Improvement in intestinal coenzyme q10 absorption by food intake. *Yakugaku Zasshi* **2007,** *127* (8), 1251-4.

55. Zaki, N. M., Strategies for oral delivery and mitochondrial targeting of CoQ10. *Drug Deliv* **2016,** *23* (6), 1868-81.

56. Shults, C. W.; Flint Beal, M.; Song, D.; Fontaine, D., Pilot trial of high dosages of coenzyme Q10 in patients with Parkinson's disease. *Exp Neurol* **2004,** *188* (2), 491-4.

57. Miles, M. V.; Horn, P.; Miles, L.; Tang, P.; Steele, P.; Degrauw, T., Bioequivalence of coenzyme Q 10 from over-the-counter supplements. *Nutrition Research* **2002,** *22*, 919-929.

58. Weis, M.; Mortensen, S. A.; Rassing, M. R.; Moller-Sonnergaard, J.; Poulsen, G.; Rasmussen, S. N., Bioavailability of four oral coenzyme Q10 formulations in healthy volunteers. *Mol Aspects Med* **1994,** *15 Suppl*, s273-80.

59. Parikh, S.; Saneto, R.; Falk, M. J.; Anselm, I.; Cohen, B. H.; Haas, R., A Modern Approach to the Treatment of Mitochondrial Disease. *Curr Treat Options Neurol* **2009,** *11*, 414-430.

60. Maroz, A.; Anderson, R. F.; Smith, R. A.; Murphy, M. P., Reactivity of ubiquinone and ubiquinol with superoxide and the hydroperoxyl radical: implications for in vivo antioxidant activity. *Free Radic Biol Med* **2009,** *46* (1), 105-9.

61. Langsjoen, P. H.; Langsjoen, A. M., Supplemental ubiquinol in patients with advanced congestive heart failure. *Biofactors* **2008,** *32* (1-4), 119-28.

62. Mitsui, J.; Koguchi, K.; Momose, T.; Takahashi, M.; Matsukawa, T.; Yasuda, T.; Tokushige, S. I.; Ishiura, H.; Goto, J.; Nakazaki, S.; Kondo, T.; Ito, H.; Yamamoto, Y.; Tsuji, S., Three-Year Follow-Up of High-Dose Ubiquinol Supplementation in a Case of Familial Multiple System Atrophy with Compound Heterozygous COQ2 Mutations. *Cerebellum* **2017,** *16* (3), 664-672.

63. Hosoe, K.; Kitano, M.; Kishida, H.; Kubo, H.; Fujii, K.; Kitahara, M., Study on safety and bioavailability of ubiquinol (Kaneka QH™) after single and 4-week multiple oral administration to healthy volunteers. *Regul Toxicol Pharmacol* **2007,** *47* (1), 19-28.

64. López-Lluch, G.; del Pozo-Cruz, J.; Sánchez-Cuesta, A.; Cortés-Rodríguez, A. B.; Navas, P., Bioavailability of coenzyme Q10 supplements depends on carrier lipids and solubilization. *Nutrition* **2018,** *(in press)*.

65. Yubero, D.; Montero, R.; Artuch, R.; Land, J. M.; Heales, S. J. R.; Hargreaves, I. P., Biochemical Diagnosis of Coenzyme Q10 Deficiency. *Molecular Syndromology* **2014,** *5* (3-4), 147-155.

66. Quinzii, C. M.; Hirano, M.; Naini, A., Cerebellar Ataxia and CoQ10 Deficiency. *J Neurol Disord Stroke* **2013,** *1* (1), 1004-.

67. Desbats, M. A.; Lunardi, G.; Doimo, M.; Trevisson, E.; Salviati, L., Genetic bases and clinical manifestations of coenzyme Q10 (CoQ 10) deficiency. *J Inherit Metab Dis* **2015,** *38* (1), 145-56.

68. Lamperti, C.; Naini, A.; Hirano, M.; De Vivo, D. C.; Bertini, E.; Servidei, S.; Valeriani, M.; Lynch, D.; Banwell, B.; Berg, M.; Dubrovsky, T.; Chiriboga, C.; Angelini, C.; Pegoraro, E.; DiMauro, S., Cerebellar ataxia and coenzyme Q10 deficiency. *Neurology* **2003,** *60* (7), 1206-8.

69. Musumeci, O.; Naini, A.; Slonim, A. E.; Skavin, N.; Hadjigeorgiou, G. L.; Krawiecki, N.; Weissman, B. M.; Tsao, C. Y.; Mendell, J. R.; Shanske, S.; De Vivo, D. C.; Hirano, M.; DiMauro, S., Familial cerebellar ataxia with muscle coenzyme Q10 deficiency. *Neurology* **2001,** *56* (7), 849-55.

70. Neergheen, V.; Hargreaves, I. P., Secondary Coenzyme Q10 Deficiency: Causes and Consequence. In *Coenzyme Q10: Uses, Health Effects and Role in Disease*, Grigoryeva, S., Ed. Nova Science Publishers, Inc.: New York, 2018.

71. Potgieter, M.; Pretorius, E.; Pepper, M. S., Primary and secondary coenzyme Q10 deficiency: the role of therapeutic supplementation. *Nutr Rev* **2013,** *71* (3), 180-8.

72. Malicdan, M. C. V.; Vilboux, T.; Ben-Zeev, B.; Guo, J.; Eliyahu, A.; Pode-Shakked, B.; Dori, A.; Kakani, S.; Chandrasekharappa, S. C.; Ferreira, C. R.; Shelestovich, N.; Marek-Yagel, D.; Pri-Chen, H.; Blatt, I.; Niederhuber, J. E.; He, L.; Toro, C.; Taylor, R. W.; Deeken, J.; Yardeni, T.; Wallace, D. C.; Gahl, W. A.; Anikster, Y., A novel inborn error of the coenzyme Q10 biosynthesis pathway: cerebellar ataxia and static encephalomyopathy due to COQ5 C-methyltransferase deficiency. *Hum Mutat* **2018,** *39* (1), 69-79.

73. Sacconi, S.; Trevisson, E.; Salviati, L.; Ayme, S.; Rigal, O.; Redondo, A. G.; Mancuso, M.; Siciliano, G.; Tonin, P.; Angelini, C.; Aure, K.; Lombes, A.; Desnuelle, C., Coenzyme Q10 is frequently reduced in muscle of patients with mitochondrial myopathy. *Neuromuscul Disord* **2010,** *20* (1), 44-8.

74. Montero, R.; Grazina, M.; Lopez-Gallardo, E.; Montoya, J.; Briones, P.; Navarro-Sastre, A.; Land, J. M.; Hargreaves, I. P.; Artuch, R., Coenzyme Q10 deficiency in mitochondrial DNA depletion syndromes. *Mitochondrion* **2013,** *13* (4), 337-41.

75. Quinzii, C. M.; Kattah, A. G.; Naini, A.; Akman, H. O.; Mootha, V. K.; DiMauro, S.; Hirano, M., Coenzyme Q deficiency and cerebellar ataxia associated with an aprataxin mutation. *Neurology* **2005,** *64* (3), 539-41.

76. Gempel, K.; Topaloglu, H.; Talim, B.; Schneiderat, P.; Schoser, B. G.; Hans, V. H.; Palmafy, B.; Kale, G.; Tokatli, A.; Quinzii, C.; Hirano, M.; Naini, A.; DiMauro, S.; Prokisch, H.; Lochmuller, H.; Horvath, R., The myopathic form of coenzyme Q10 deficiency is caused by mutations in the electron-transferring-flavoprotein dehydrogenase (ETFDH) gene. *Brain* **2007,** *130* (Pt 8), 2037-44.

77. Aeby, A.; Sznajer, Y.; Cave, H.; Rebuffat, E.; Van Coster, R.; Rigal, O.; Van Bogaert, P., Cardiofaciocutaneous (CFC) syndrome associated with muscular coenzyme Q10 deficiency. *J Inherit Metab Dis* **2007,** *30* (5), 827.

78. Yang, X.; Zhang, Y.; Xu, H.; Luo, X.; Yu, J.; Liu, J.; Chang, R. C., Neuroprotection of Coenzyme Q10 in Neurodegenerative Diseases. *Curr Top Med Chem* **2016,** *16* (8), 858-66.

79. Overvad, K.; Diamant, B.; Holm, L.; Holmer, G.; Mortensen, S. A.; Stender, S., Coenzyme Q10 in health and disease. *Eur J Clin Nutr* **1999,** *53* (10), 764-70.

80. Maladkar, M.; Patil, S.; Sood, S., Coenzyme Q10: The Cardiac Bio-energizer in Cardiovascular Diseases. *JOCCT* **2016,** *1* (2).

81. Trevisson, E.; DiMauro, S.; Navas, P.; Salviati, L., Coenzyme Q deficiency in muscle. *Curr Opin Neurol* **2011,** *24* (5), 449-56.

82. Neergheen, V.; Chalasani, A.; Wainwright, L.; Yubero, D.; Montero, R.; Artuch, R.; Hargreaves, I., Coenzyme Q10 in the Treatment of Mitochondrial Disease. *JIEMS* **2017,** *5*, 1-8.

83. Kwong, L. K.; Kamzalov, S.; Rebrin, I.; Bayne, A.-C. V.; Jana, C. K.; Morris, P.; Forster, M. J.; Sohal, R. S., Effects of coenzyme Q10 administration on its tissue concentrations, mitochondrial oxidant generation, and oxidative stress in the rat. *Free Radic Biol Med* **2002,** *33* (5), 627-638.

84. Mancini, A.; Festa, R.; Raimondo, S.; Pontecorvi, A.; Littarru, G. P., Hormonal influence on coenzyme Q(10) levels in blood plasma. *Int J Mol Sci* **2011,** *12* (12), 9216-25.

85. Molyneux, S. L.; Young, J. M.; Florkowski, C. M.; Lever, M.; George, P. M., Coenzyme Q10: is there a clinical role and a case for measurement? *Clin Biochem Rev* **2008,** *29* (2), 71-82.

86. Shults, C. W.; Oakes, D.; Kieburtz, K.; Beal, M. F.; Haas, R.; Plumb, S.; Juncos, J. L.; Nutt, J.; Shoulson, I.; Carter, J.; Kompoliti, K.; Perlmutter, J. S.; Reich, S.; Stern, M.; Watts, R. L.; Kurlan, R.; Molho, E.; Harrison, M.; Lew, M.; Parkinson Study, G., Effects of coenzyme Q10 in early Parkinson disease: evidence of slowing of the functional decline. *Arch Neurol* **2002,** *59* (10), 1541-50.

87. Belardinelli, R.; Mucaj, A.; Lacalaprice, F.; Solenghi, M.; Seddaiu, G.; Principi, F.; Tiano, L.; Littarru, G. P., Coenzyme Q10 and exercise training in chronic heart failure. *Eur Heart J* **2006,** *27* (22), 2675-81.

88. Duberley, K. E.; Heales, S. J.; Abramov, A. Y.; Chalasani, A.; Land, J. M.; Rahman, S.; Hargreaves, I. P., Effect of Coenzyme Q10 supplementation on mitochondrial electron transport chain activity and mitochondrial oxidative stress in Coenzyme Q10 deficient human neuronal cells. *Int J Biochem Cell Biol* **2014,** *50* (0), 60-3.

89. Desbats, M. A.; Vetro, A.; Limongelli, I.; Lunardi, G.; Casarin, A.; Doimo, M.; Spinazzi, M.; Angelini, C.; Cenacchi, G.; Burlina, A.; Rodriguez Hernandez, M. A.; Chiandetti, L.; Clementi, M.; Trevisson, E.; Navas, P.; Zuffardi, O.; Salviati, L., Primary coenzyme Q10 deficiency presenting as fatal neonatal multiorgan failure. *Eur J Hum Genet* **2015,** *23* (9), 1254-8.

90. Rotig, A.; Mollet, J.; Rio, M.; Munnich, A., Infantile and pediatric quinone deficiency diseases. *Mitochondrion* **2007,** *7 Suppl*, S112-21.

91. Garcia-Corzo, L.; Luna-Sanchez, M.; Doerrier, C.; Ortiz, F.; Escames, G.; Acuna-Castroviejo, D.; Lopez, L. C., Ubiquinol-10 ameliorates mitochondrial encephalopathy associated with CoQ deficiency. *Biochim Biophys Acta* **2014,** *1842* (7), 893-901.

92. Hawkins, B. T.; Davis, T. P., The blood-brain barrier/neurovascular unit in health and disease. *Pharmacol Rev* **2005,** *57* (2), 173-85.

93. Fenstermacher, J.; Gross, P.; Sposito, N.; Acuff, V.; Pettersen, S.; Gruber, K., Structural and Functional Variations in Capillary Systems within the Brain. *Ann N Y Acad Sci* **1988,** *529* (1 Fourth Colloq), 21-30.

94. Sedlakova, R.; Shivers, R. R.; Del Maestro, R. F., Ultrastructure of the blood-brain barrier in the rabbit. *J Submicrosc Cytol Pathol* **1999,** *31* (1), 149-61.

95. Oldendorf, W. H.; Cornford, M. E.; Brown, W. J., The large apparent work capability of the blood-brain barrier: a study of the mitochondrial content of capillary endothelial cells in brain and other tissues of the rat. *Ann Neurol* **1977,** *1* (5), 409-17.

96. Redzic, Z., Molecular biology of the blood-brain and the blood-cerebrospinal fluid barriers: similarities and differences. *Fluids Barriers CNS* **2011,** *8* (1), 3.

97. Cipolla, M. J., Barriers of the CNS. In *The Cerebral Circulation*, Morgan & Claypool Life Sciences: San Rafael (CA), 2009.

98. Kandel, E. R.; Schwartz, J. H.; Jessell, T. M., *Principles of Neural Science*. Fourth Edition ed.; McGraw-Hill, Health Professions Division: New York, 2000.

99. Hladky, S. B.; Barrand, M. A., Mechanisms of fluid movement into, through and out of the brain: evaluation of the evidence. *Fluids Barriers CNS* **2014,** *11* (1), 26.

100. Abbott, N. J., Blood-brain barrier structure and function and the challenges for CNS drug delivery. *J Inherit Metab Dis* **2013,** *36* (3), 437-49.

101. Abbott, N. J.; Patabendige, A. A. K.; Dolman, D. E. M.; Yusof, S. R.; Begley, D. J., Structure and function of the blood–brain barrier. *Neurobiol Dis* **2010,** *37* (1), 13-25.

102. Palmer, A. M., The blood-brain barrier. *Neurobiol Dis* **2010,** *37* (1), 1-2.

103. Begley, D. J.; Brightman, M. W., Structural and functional aspects of the blood-brain barrier. Birkhäuser Basel: Basel, 2003; pp 39-78.

104. Duvernoy, H. M.; Risold, P. Y., The circumventricular organs: an atlas of comparative anatomy and vascularization. *Brain Res Rev* **2007,** *56* (1), 119-47.

105. Ueno, M., Molecular anatomy of the brain endothelial barrier: an overview of the distributional features. *Curr Med Chem* **2007,** *14* (11), 1199-206.

106. Holmes, F. L., Origins of the concept of milieu interieur. In *Claude Bernard and Experimental Medicine*, Grande, F.; Visscher, M. B., Eds. Schenkman: Cambndge (MA), 1967; pp 179-191.

107. Abbott, N. J.; Ronnback, L.; Hansson, E., Astrocyte-endothelial interactions at the blood-brain barrier. *Nat Rev Neurosci* **2006,** *7* (1), 41-53.

108. Abbott, N. J.; Pizzo, M. E.; Preston, J. E.; Janigro, D.; Thorne, R. G., The role of brain barriers in fluid movement in the CNS: is there a 'glymphatic' system? *Acta Neuropathol* **2018,** *135* (3), 387-407.

109. Sweeney, M. D.; Ayyadurai, S.; Zlokovic, B. V., Pericytes of the neurovascular unit: key functions and signaling pathways. *Nat Neurosci* **2016,** *19* (6), 771-83.

110. Olesen, S. P.; Crone, C., Electrical resistance of muscle capillary endothelium. *Biophys J* **1983,** *42* (1), 31-41.

111. Butt, A. M.; Jones, H. C.; Abbott, N. J., Electrical resistance across the blood-brain barrier in anaesthetized rats: a developmental study. *J Physiol* **1990,** *429*, 47-62.

112. Kniesel, U.; Wolburg, H., Tight junctions of the blood-brain barrier. *Cell Mol Neurobiol* **2000,** *20* (1), 57-76.

113. Zhao, Z.; Nelson, A. R.; Betsholtz, C.; Zlokovic, B. V., Establishment and Dysfunction of the Blood-Brain Barrier. *Cell* **2015,** *163* (5), 1064-1078.

114. Luissint, A. C.; Artus, C.; Glacial, F.; Ganeshamoorthy, K.; Couraud, P. O., Tight junctions at the blood brain barrier: physiological architecture and disease-associated dysregulation. *Fluids Barriers CNS* **2012,** *9* (1), 23.

115. Furuse, M.; Sasaki, H.; Tsukita, S., Manner of interaction of heterogeneous claudin species within and between tight junction strands. *J Cell Biol* **1999,** *147* (4), 891-903.

116. Citi, S.; Sabanay, H.; Jakes, R.; Geiger, B.; Kendrick-Jones, J., Cingulin, a new peripheral component of tight junctions. *Nature* **1988,** *333* (6170), 272-6.

117. Furuse, M.; Hirase, T.; Itoh, M.; Nagafuchi, A.; Yonemura, S.; Tsukita, S., Occludin: a novel integral membrane protein localizing at tight junctions. *J Cell Biol* **1993,** *123* (6 Pt 2), 1777-88.

118. Mitic, L. L.; Van Itallie, C. M.; Anderson, J. M., Molecular physiology and pathophysiology of tight junctions I. Tight junction structure and function: lessons from mutant animals and proteins. *Am J Physiol Gastrointest Liver Physiol* **2000,** *279* (2), G250-4.

119. Ebnet, K.; Schulz, C. U.; Meyer Zu Brickwedde, M. K.; Pendl, G. G.; Vestweber, D., Junctional adhesion molecule interacts with the PDZ domain-containing proteins AF-6 and ZO-1. *J Biol Chem* **2000,** *275* (36), 27979-88.

120. Garrido-Urbani, S.; Bradfield, P. F.; Imhof, B. A., Tight junction dynamics: the role of junctional adhesion molecules (JAMs). *Cell Tissue Res* **2014,** *355* (3), 701-15.

121. Aurrand-Lions, M.; Johnson-Leger, C.; Wong, C.; Du Pasquier, L.; Imhof, B. A., Heterogeneity of endothelial junctions is reflected by differential expression and specific subcellular localization of the three JAM family members. *Blood* **2001,** *98* (13), 3699-707.

122. Huber, J. D.; Egleton, R. D.; Davis, T. P., Molecular physiology and pathophysiology of tight junctions in the blood-brain barrier. *Trends Neurosci* **2001,** *24* (12), 719-25.

123. Lampugnani, M. G.; Corada, M.; Caveda, L.; Breviario, F.; Ayalon, O.; Geiger, B.; Dejana, E., The molecular organization of endothelial cell to cell junctions: differential association of plakoglobin, beta-catenin, and alpha-catenin with vascular endothelial cadherin (VE-cadherin). *J Cell Biol* **1995,** *129* (1), 203-17.

124. Matter, K.; Balda, M. S., Signalling to and from tight junctions. *Nat Rev Mol Cell Biol* **2003,** *4* (3), 225-36.

125. Pardridge, W. M., Drug transport across the blood-brain barrier. *J Cereb Blood Flow Metab* **2012,** *32* (11), 1959-72.

126. Dorovini-Zis, K.; Nag, S., *Morphological and Functional Properties of the Blood-Brain Barrier*. CRC Press: 2015; Vol. Volume One; Morphology, Biology and Immune Function.

127. Oller-Salvia, B.; Sanchez-Navarro, M.; Giralt, E.; Teixido, M., Blood-brain barrier shuttle peptides: an emerging paradigm for brain delivery. *Chem Soc Rev* **2016,** *45* (17), 4690-707.

128. Zlokovic, B. V., The blood-brain barrier in health and chronic neurodegenerative disorders. *Neuron* **2008,** *57* (2), 178-201.

129. Tosi, G.; Fano, R. A.; Bondioli, L.; Badiali, L.; Benassi, R.; Rivasi, F.; Ruozi, B.; Forni, F.; Vandelli, M. A., Investigation on mechanisms of glycopeptide nanoparticles for drug delivery across the blood-brain barrier. *Nanomedicine (Lond)* **2011,** *6* (3), 423-36.

130. Davoust, N.; Vuaillat, C.; Androdias, G.; Nataf, S., From bone marrow to microglia: barriers and avenues. *Trends Immunol* **2008,** *29* (5), 227-34.

131. Krieger, M.; Herz, J., Structures and functions of multiligand lipoprotein receptors: macrophage scavenger receptors and LDL receptor-related protein (LRP). *Annu Rev Biochem* **1994,** *63* (1), 601-37.

132. Gabathuler, R., Approaches to transport therapeutic drugs across the blood-brain barrier to treat brain diseases. *Neurobiol Dis* **2010,** *37* (1), 48-57.

133. Auderset, L.; Cullen, C. L.; Young, K. M., Low Density Lipoprotein-Receptor Related Protein 1 Is Differentially Expressed by Neuronal and Glial Populations in the Developing and Mature Mouse Central Nervous System. *PLoS One* **2016,** *11* (6).

134. Wang, D.; El-Amouri, S. S.; Dai, M.; Kuan, C. Y.; Hui, D. Y.; Brady, R. O.; Pan, D., Engineering a lysosomal enzyme with a derivative of receptor-binding domain of apoE enables delivery across the blood-brain barrier. *PNAS* **2013,** *110* (8), 2999-3004.

135. Itagaki, S.; Ochiai, A.; Kobayashi, M.; Sugawara, M.; Hirano, T.; Iseki, K., Interaction of coenzyme Q10 with the intestinal drug transporter P-glycoprotein. *J Agric Food Chem* **2008,** *56* (16), 6923-7.

136. Ghosh, C.; Puvenna, V.; Gonzalez-Martinez, J.; Janigro, D.; Marchi, N., Blood-brain barrier P450 enzymes and multidrug transporters in drug resistance: a synergistic role in neurological diseases. *Curr Drug Metab* **2011,** *12* (8), 742-9.

137. Shawahna, R.; Uchida, Y.; Decleves, X.; Ohtsuki, S.; Yousif, S.; Dauchy, S.; Jacob, A.; Chassoux, F.; Daumas-Duport, C.; Couraud, P. O.; Terasaki, T.; Scherrmann, J. M., Transcriptomic and quantitative proteomic analysis of transporters and drug metabolizing enzymes in freshly isolated human brain microvessels. *Mol Pharm* **2011,** *8* (4), 1332-41.

138. Ghersi-Egea, J. F.; Minn, A.; Siest, G., A new aspect of the protective functions of the blood-brain barrier: activities of four drug-metabolizing enzymes in isolated rat brain microvessels. *Life Sci* **1988,** *42* (24), 2515-23.

139. Minn, A.; Ghersi-Egea, J. F.; Perrin, R.; Leininger, B.; Siest, G., Drug metabolizing enzymes in the brain and cerebral microvessels. *Brain Res Brain Res Rev* **1991,** *16* (1), 65-82.

140. Agundez, J. A.; Jimenez-Jimenez, F. J.; Alonso-Navarro, H.; Garcia-Martin, E., Drug and xenobiotic biotransformation in the blood-brain barrier: a neglected issue. *Front Cell Neurosci* **2014,** *8* (335), 335.

141. Kapitulnik, J., Drug transport and metabolism in the blood-brain barrier. *Front Pharmacol* **2011,** *2* (37), 37.

142. Iadecola, C., The Neurovascular Unit Coming of Age: A Journey through Neurovascular Coupling in Health and Disease. *Neuron* **2017,** *96* (1), 17-42.

143. Freese, C.; Hanada, S.; Fallier-Becker, P.; Kirkpatrick, C. J.; Unger, R. E., Identification of neuronal and angiogenic growth factors in an in vitro blood-brain barrier model system: Relevance in barrier integrity and tight junction formation and complexity. *Microvasc Res* **2017,** *111*, 1-11.

144. Janzer, R. C.; Raff, M. C., Astrocytes induce blood-brain barrier properties in endothelial cells. *Nature* **1987,** *325* (6101), 253-7.

145. Armulik, A.; Genove, G.; Mae, M.; Nisancioglu, M. H.; Wallgard, E.; Niaudet, C.; He, L.; Norlin, J.; Lindblom, P.; Strittmatter, K.; Johansson, B. R.; Betsholtz, C., Pericytes regulate the blood-brain barrier. *Nature* **2010,** *468* (7323), 557-61.

146. O'Donnell, M. E., *The Neurovascular Unit*. CRC Press: 2015; Vol. Volume One; Morphology, Biology and Immune Function.

147. Neuwelt, E. A.; Bauer, B.; Fahlke, C.; Fricker, G.; Iadecola, C.; Janigro, D.; Leybaert, L.; Molnar, Z.; O'Donnell, M. E.; Povlishock, J. T.; Saunders, N. R.; Sharp, F.; Stanimirovic, D.; Watts, R. J.; Drewes, L. R., Engaging neuroscience to advance translational research in brain barrier biology. *Nat Rev Neurosci* **2011,** *12* (3), 169-82.

148. Daneman, R., The blood-brain barrier in health and disease. *Ann Neurol* **2012,** *72* (5), 648-72.

149. Persidsky, Y.; Ramirez, S. H.; Haorah, J.; Kanmogne, G. D., Blood-brain barrier: structural components and function under physiologic and pathologic conditions. *J Neuroimmune Pharmacol* **2006,** *1* (3), 223-36.

150. Shroff, S.; Jain, R.; Najjar, S.; Alotaibi, F. M.; Zagzag, D., *The Blood-Brain-Barrier in Brain Tumors*. CRC Press: 2015; Vol. Volume Two: Pathophysiology and Pathology.

151. Minagar, A.; Alexander, J. S., Blood-brain barrier disruption in multiple sclerosis. *Mult Scler* **2003,** *9* (6), 540-9.

152. Correale, J.; Villa, A., The blood-brain-barrier in multiple sclerosis: functional roles and therapeutic targeting. *Autoimmunity* **2007,** *40* (2), 148-60.

153. Brylev, L. V.; Zakharova, M. N.; Zavalishin, I. A.; Gulyaeva, N. V., Disruption of blood-brain barrier in amyotrophic lateral sclerosis: an update. *Neurochem J* **2012,** *6* (1), 64-70.

154. Bowman, G. L.; Quinn, J. F., Alzheimer's disease and the Blood-Brain Barrier: Past, Present and Future. *J Aging Health* **2008,** *4* (1), 47-55.

155. Sweeney, M. D.; Sagare, A. P.; Zlokovic, B. V., Blood-brain barrier breakdown in Alzheimer disease and other neurodegenerative disorders. *Nat Rev Neurol* **2018,** *14* (3), 133-150.

156. Lee, H.; Pienaar, I. S., Disruption of the blood-brain barrier in Parkinson's disease: curse or route to a cure? *Front Biosci (Landmark Ed)* **2014,** *19*, 272-80.

157. Oby, E.; Janigro, D., The blood-brain barrier and epilepsy. *Epilepsia* **2006,** *47* (11), 1761-74.

158. Marchi, N.; Granata, T.; Ghosh, C.; Janigro, D., Blood-brain barrier dysfunction and epilepsy: pathophysiologic role and therapeutic approaches. *Epilepsia* **2012,** *53* (11), 1877-86.

159. Merkel, S. F.; Ramirez, S. H.; Persidsky, Y., *Blood Brain Barrier (BBB) Dysfunction in HIV Infection*. 2015; Vol. Volume Two: Pathophysiology and Pathology.

160. Begley, D. J.; Pontikis, C. C.; Scarpa, M., Lysosomal storage diseases and the blood-brain barrier. *Curr Pharm Des* **2008,** *14* (16), 1566-80.

161. Haley, M. J.; Lawrence, C. B., The blood-brain barrier after stroke: Structural studies and the role of transcytotic vesicles. *J Cereb Blood Flow Metab* **2017,** *37* (2), 456-470.

162. Rodriguez, J. I.; Kern, J. K., Evidence of microglial activation in autism and its possible role in brain underconnectivity. *Neuron Glia Biol* **2011,** *7* (2-4), 205-13.

163. Varatharaj, A.; Galea, I., The blood-brain barrier in systemic inflammation. *Brain Behav Immun* **2017,** *60*, 1-12.

164. Saunders, N. R.; Dziegielewska, K. M.; Mollgard, K.; Habgood, M. D., Markers for blood-brain barrier integrity: how appropriate is Evans blue in the twenty-first century and what are the alternatives? *Front Neurosci* **2015,** *9*, 385.

165. Abbott, N. J., Prediction of blood-brain barrier permeation in drug discovery from in vivo, in vitro and in silico models. *Drug Discov Today Technol* **2004,** *1* (4), 407-16.

166. Avdeef, A.; Deli, M. A.; Neuhaus, W., In Vitro Assays for Assessing BBB Permeability. In *Blood-Brain Barrier in Drug Discovery*, John Wiley & Sons, Inc: Hoboken, NJ, 2015; pp 188-237.

167. Helms, H. C.; Abbott, N. J.; Burek, M.; Cecchelli, R.; Couraud, P. O.; Deli, M. A.; Forster, C.; Galla, H. J.; Romero, I. A.; Shusta, E. V.; Stebbins, M. J.; Vandenhaute, E.; Weksler, B.; Brodin, B., In vitro models of the blood-brain barrier: An overview of commonly used brain endothelial cell culture models and guidelines for their use. *J Cereb Blood Flow Metab* **2016,** *36* (5), 862-90.

168. Michalopoulos, G.; Pitot, H. C., Primary culture of parenchymal liver cells on collagen membranes. Morphological and biochemical observations. *Exp Cell Res* **1975,** *94* (1), 70-8.

169. Chlapowski, F. J.; Haynes, L., The growth and differentiation of transitional epithelium in vitro. *J Cell Biol* **1979,** *83* (3), 605-14.

170. Karasek, M. A.; Charlton, M. E., Growth of postembryonic skin epithelial cells on collagen gels. *J Invest Dermatol* **1971,** *56* (3), 205-10.

171. Tilling, T.; Korte, D.; Hoheisel, D.; Galla, H. J., Basement Membrane Proteins Influence Brain Capillary Endothelial Barrier Function In Vitro. *J Neurochem* **2002,** *71* (3), 1151-1157.

172. Strom, S. C.; Michalopoulos, G., Collagen as a substrate for cell growth and differentiation. *Methods Enzymol* **1982,** *82 Pt A*, 544-55.

173. Ichaso, N.; Dilworth, S. M., Cell transformation by the middle T-antigen of polyoma virus. *Oncogene* **2001,** *20* (54), 7908-16.

174. Williams, R. L.; Courtneidge, S. A.; Wagner, E. F., Embryonic lethalities and endothelial tumors in chimeric mice expressing polyoma virus middle T oncogene. *Cell* **1988,** *52* (1), 121-31.

175. Brown, R. C.; Morris, A. P.; O'Neil, R. G., Tight junction protein expression and barrier properties of immortalized mouse brain microvessel endothelial cells. *Brain Res* **2007,** *1130* (1), 17-30.

176. Patabendige, A.; Skinner, R. A.; Morgan, L.; Abbott, N. J., A detailed method for preparation of a functional and flexible blood-brain barrier model using porcine brain endothelial cells. *Brain Res* **2013,** *1521* (0), 16-30.

177. Perriere, N.; Demeuse, P.; Garcia, E.; Regina, A.; Debray, M.; Andreux, J. P.; Couvreur, P.; Scherrmann, J. M.; Temsamani, J.; Couraud, P. O.; Deli, M. A.; Roux, F.,

Puromycin-based purification of rat brain capillary endothelial cell cultures. Effect on the expression of blood-brain barrier-specific properties. *J Neurochem* **2005,** *93* (2), 279-89.

178. Hoheisel, D.; Nitz, T.; Franke, H.; Wegener, J.; Hakvoort, A.; Tilling, T.; Galla, H. J., Hydrocortisone reinforces the blood-brain properties in a serum free cell culture system. *Biochem Biophys Res Commun* **1998,** *247* (2), 312-5.

179. Rubin, L. L.; Hall, D. E.; Porter, S.; Barbu, K.; Cannon, C.; Horner, H. C.; Janatpour, M.; Liaw, C. W.; Manning, K.; Morales, J.; et al., A cell culture model of the blood-brain barrier. *J Cell Biol* **1991,** *115* (6), 1725-35.

180. Forster, C., Tight junctions and the modulation of barrier function in disease. *Histochem Cell Biol* **2008,** *130* (1), 55-70.

181. Rist, R. J.; Romero, I. A.; Chan, M. W.; Couraud, P. O.; Roux, F.; Abbott, N. J., F-actin cytoskeleton and sucrose permeability of immortalised rat brain microvascular endothelial cell monolayers: effects of cyclic AMP and astrocytic factors. *Brain Res* **1997,** *768* (1-2), 10-8.

182. Ohm, G. S., Vorläufige Anzeige des Gesetzes, nach welchem Metalle die Contaktelektricität leiten - Ohm - 1825 - Annalen der Physik - Wiley Online Library. *Ann Phys* **1825,** *80* (5), 79-88.

183. Srinivasan, B.; Kolli, A. R.; Esch, M. B.; Abaci, H. E.; Shuler, M. L.; Hickman, J. J., TEER measurement techniques for in vitro barrier model systems. *J Lab Autom* **2015,** *20* (2), 107-26.

184. Yusof, S. R.; Avdeef, A.; Abbott, N. J., In vitro porcine blood-brain barrier model for permeability studies: pCEL-X software pKa(FLUX) method for aqueous boundary layer correction and detailed data analysis. *Eur J Pharm Sci* **2014,** *65* (0), 98-111.

185. Palumbo, P.; Picchini, U.; Beck, B.; van Gelder, J.; Delbar, N.; DeGaetano, A., A general approach to the apparent permeability index. *J Pharmacokinet Pharmacodyn* **2008,** *35* (2), 235-48.

186. Reichel, A.; Begley, D. J.; Abbott, N. J., An Overview of In Vitro Techniques for Blood-Brain Barrier Studies. Humana Press: New Jersey, 2003; pp 307-324.

187. Bickel, U., How to measure drug transport across the blood-brain barrier. *NeuroRx* **2005,** *2* (1), 15-26.

188. Karlsson, J.; Artursson, P., A method for the determination of cellular permeability coefficients and aqueous boundary layer thickness in monolayers of intestinal epithelial (Caco-2) cells grown in permeable filter chambers. *Int J Pharm* **1991,** *71* (1-2), 55-64.

189. Patlak, C. S.; Paulson, O. B., The role of unstirred layers for water exchange across the blood-brain barrier. *Microvasc Res* **1981,** *21* (1), 117-27.

190. Mosmann, T., Rapid colorimetric assay for cellular growth and survival: application to proliferation and cytotoxicity assays. *J Immunol Methods* **1983,** *65* (1-2), 55-63.

191. Slater, T. F.; Sawyer, B.; Straeuli, U., Studies on Succinate-Tetrazolium Reductase Systems. Iii. Points of Coupling of Four Different Tetrazolium Salts. *Biochim Biophys Acta* **1963,** *77*, 383-93.

192. Alam, S. S.; Nambidiri, A. M.; Rudney, H.; Nambudiri, A. M., 4-Hydroxybenzoate: polyprenyl transferase and the prenylation of 4-aminobenzoate in mammalian tissues. *Arch Biochem Biophys* **1975,** *171* (1), 183-90.

193. Gonzalez-Aragon, D.; Buron, M. I.; Lopez-Lluch, G.; Herman, M. D.; Gomez-Diaz, C.; Navas, P.; Villalba, J. M., Coenzyme Q and the regulation of intracellular steady-state levels of superoxide in HL-60 cells. *Biofactors* **2005,** *25* (1-4), 31-41.

194. Duberley, K. E.; Abramov, A. Y.; Chalasani, A.; Heales, S. J.; Rahman, S.; Hargreaves, I. P., Human neuronal coenzyme Q10 deficiency results in global loss of mitochondrial respiratory chain activity, increased mitochondrial oxidative stress and reversal of ATP synthase activity: implications for pathogenesis and treatment. *J Inherit Metab Dis* **2013,** *36* (1), 63-73.

195. Ononogbu, I. C.; Lewis, B., Lipoprotein fractionation by a precipitation method. a simple quantitative procedure. *Clinica Chimica Acta* **1976,** *71* (3), 397-402.

196. Boitier, E.; Degoul, F.; Desguerre, I.; Charpentier, C.; Francois, D.; Ponsot, G.; Diry, M.; Rustin, P.; Marsac, C., A case of mitochondrial encephalomyopathy associated with a muscle coenzyme Q10 deficiency. *J Neurol Sci* **1998,** *156* (1), 41-6.

197. Duncan, A. J.; Heales, S. J.; Mills, K.; Eaton, S.; Land, J. M.; Hargreaves, I. P., Determination of coenzyme Q10 status in blood mononuclear cells, skeletal muscle, and plasma by HPLC with di-propoxy-coenzyme Q10 as an internal standard. *Clin Chem* **2005,** *51* (12), 2380-2.

198. Itkonen, O.; Suomalainen, A.; Turpeinen, U., Mitochondrial coenzyme Q10 determination by isotope-dilution liquid chromatography-tandem mass spectrometry. *Clin Chem* **2013,** *59* (8), 1260-7.

199. Crane, F. L.; Lester, R. L.; Widmer, C.; Hatefi, Y., Studies on the electron transport system. XVIII. Isolation of coenzyme Q (Q275) from beef heart and beef heart mitochondria. *Biochim Biophys Acta* **1959,** *32* (1), 73-9.

200. Swinehart, D. F., The Beer-Lambert Law. *J Chem Educ* **1962,** *39* (7), 333-333.

201. Reed, J. S.; Ragan, C. I., The effect of rate limitation by cytochrome c on the redox state of the ubiquinone pool in reconstituted NADH: cytochrome c reductase. *Biochem J* **1987,** *247* (3), 657-62.

202. Friedrich, T.; Heek, P.; Leif, H.; Ohnishi, T.; Forche, E.; Kunze, B.; Jansen, R.; Trowitzsch-Kienast, W.; Hofle, G.; Reichenbach, H.; Weiss, H., Two binding sites of inhibitors in NADH:ubiquinone oxidoreductase (complex I). Relationship of one site with the ubiquinone-binding site of bacterial glucose:ubiquinone oxidoreductase. *Eur J Biochem* **1994,** *219* (1-2), 691-698.

203. Bhuvaneswaran, C.; King, T. E., Succinate-dehydrogenating activity and cytochromes of hepatic microsomes. *Biochim Biophys Acta* **1967,** *132* (2), 282-9.

204. Wharton, D. C.; Tzagoloff, A., Cytochrome oxidase from beef heart mitochondria. *Methods Enzymol* **1967,** *10*, 245-250.

205. Bowling, A. C.; Mutisya, E. M.; Walker, L. C.; Price, D. L.; Cork, L. C.; Beal, M. F., Age-dependent impairment of mitochondrial function in primate brain. *J Neurochem* **1993,** *60* (5), 1964-7.

206. Shepherd, D.; Garland, P. B., [2] Citrate synthase from rat liver: [EC 4.1.3.7 Citrate oxaloacetage-lyase (CoA-acetylating)]. *Methods Enzymol* **1969,** *13*, 11-16.

207. Lowry, O. H.; Rosebrough, N. J.; Farr, A. L.; Randall, R. J., Protein measurement with the Folin phenol reagent. *J Biol Chem* **1951,** *193* (1), 265-75.

208. McDonald, J. H., *Handbook of Biological Statistics*. Third ed.; Sparky House Publishing: Baltimore, Maryland, USA, 2014.

209. Sakal, R. R.; Rohlf, F. J., *Biometry: The Principles and Practice of Statistics in Biological Research*. Fourth ed.; WH Freman and Company: New York, 1995.

210. Urban, P. L., Quantitative mass spectrometry: an overview. *Philos Trans A Math Phys Eng Sci* **2016,** *374* (2079).

211. Garg, U.; Zhang, Y. V., Mass Spectrometry in Clinical Laboratory: Applications in Therapeutic Drug Monitoring and Toxicology. Humana Press, New York, NY: 2016; pp 1-10.

212. Leung, K. S.; Fong, B. M., LC-MS/MS in the routine clinical laboratory: has its time come? *Anal Bioanal Chem* **2014,** *406* (9-10), 2289-301.

213. Seger, C., Usage and limitations of liquid chromatography-tandem mass spectrometry (LC-MS/MS) in clinical routine laboratories. *Wien Med Wochenschr* **2012,** *162* (21-22), 499-504.

214. Duberley, K. E. C.; Hargreaves, I. P.; Chaiwatanasirikul, K. A.; Heales, S. J. R.; Land, J. M.; Rahman, S.; Mills, K.; Eaton, S., Coenzyme Q10 quantification in muscle, fibroblasts and cerebrospinal fluid by liquid chromatography/tandem mass spectrometry using a novel deuterated internal standard. *Rapid Commun Mass Spectrom* **2013,** *27* (9), 924-930.

215. Tang, Z.; Li, S.; Guan, X.; Schmitt-Kopplin, P.; Lin, S.; Cai, Z., Rapid assessment of the coenzyme Q 10 redox state using ultrahigh performance liquid chromatography tandem mass spectrometry. *Analyst* **2014,** *139* (21), 5600-5604.

216. Mathieu, R. E., Jr.; Riley, C. P., Quantitation of Ubiquinone (Coenzyme Q(1)(0)) in Serum/Plasma Using Liquid Chromatography Electrospray Tandem Mass Spectrometry (ESI-LC-MS/MS). *Methods Mol Biol* **2016,** *1378*, 61-9.

217. Teshima, K.; Kondo, T., Analytical method for ubiquinone-9 and ubiquinone-10 in rat tissues by liquid chromatography/turbo ion spray tandem mass spectrometry with 1-alkylamine as an additive to the mobile phase. *Anal Biochem* **2005,** *338* (1), 12-9.

218. Arias, A.; Garcia-Villoria, J.; Rojo, A.; Bujan, N.; Briones, P.; Ribes, A., Analysis of coenzyme Q(10) in lymphocytes by HPLC-MS/MS. *J Chromatogr B Analyt Technol Biomed Life Sci* **2012,** *908*, 23-6.

219. Isobe, C.; Abe, T.; Terayama, Y., Levels of reduced and oxidized coenzyme Q-10 and 8-hydroxy-2'-deoxyguanosine in the cerebrospinal fluid of patients with living Parkinson's disease demonstrate that mitochondrial oxidative damage and/or oxidative DNA damage contributes to the neurodegenerative process. *Neurosci Lett* **2010,** *469* (1), 159-63.

220. Artuch, R.; Aracil, A.; Mas, A.; Monros, E.; Vilaseca, M. A.; Pineda, M., Cerebrospinal fluid concentrations of idebenone in Friedreich ataxia patients. *Neuropediatrics* **2004,** *35* (2), 95-8.

221. Stevens, S. *Next Steps on the NHS Five Year Forward View*; NHS England: 2017.

222. Bernas, M. J.; Cardoso, F. L.; Daley, S. K.; Weinand, M. E.; Campos, A. R.; Ferreira, A. J.; Hoying, J. B.; Witte, M. H.; Brites, D.; Persidsky, Y.; Ramirez, S. H.; Brito, M. A., Establishment of primary cultures of human brain microvascular endothelial cells to provide an in vitro cellular model of the blood-brain barrier. *Nat Protoc* **2010,** *5* (7), 1265-72.

223. Nielsen, S. S. E.; Siupka, P.; Georgian, A.; Preston, J. E.; Toth, A. E.; Yusof, S. R.; Abbott, N. J.; Nielsen, M. S., Improved Method for the Establishment of an In Vitro Blood-Brain Barrier Model Based on Porcine Brain Endothelial Cells. *J Vis Exp* **2017,** (127).

224. Miller, D. W.; Audus, K. L.; Borchardt, R. T., Application of cultured endothelial cells of the brain microvasculature in the study of the blood-brain barrier. *J Tissue Cult Methods* **1992,** *14* (4), 217-224.

225. Shayan, G.; Choi, Y. S.; Shusta, E. V.; Shuler, M. L.; Lee, K. H., Murine in vitro model of the blood-brain barrier for evaluating drug transport. *Eur J Pharm Sci* **2011,** *42* (1-2), 148-55.

226. Sipos, I.; Domotor, E.; Abbott, N. J.; Adam-Vizi, V., The pharmacology of nucleotide receptors on primary rat brain endothelial cells grown on a biological extracellular matrix: effects on intracellular calcium concentration. *Br J Pharmacol* **2000,** *131* (6), 1195-203.

227. Gaillard, P. J.; Voorwinden, L. H.; Nielsen, J. L.; Ivanov, A.; Atsumi, R.; Engman, H.; Ringbom, C.; de Boer, A. G.; Breimer, D. D., Establishment and functional characterization of an in vitro model of the blood-brain barrier, comprising a co-culture of brain capillary endothelial cells and astrocytes. *Eur J Pharm Sci* **2001,** *12* (3), 215-22.

228. Qosa, H.; Mohamed, L. A.; Al Rihani, S. B.; Batarseh, Y. S.; Duong, Q. V.; Keller, J. N.; Kaddoumi, A., High-Throughput Screening for Identification of Blood-Brain Barrier

Integrity Enhancers: A Drug Repurposing Opportunity to Rectify Vascular Amyloid Toxicity. *J Alzheimers Dis* **2016,** *53* (4), 1499-516.

229. Omidi, Y.; Campbell, L.; Barar, J.; Connell, D.; Akhtar, S.; Gumbleton, M., Evaluation of the immortalised mouse brain capillary endothelial cell line, b.End3, as an in vitro blood-brain barrier model for drug uptake and transport studies. *Brain Research* **2003,** *990* (1-2), 95-112.

230. Roux, F.; Couraud, P. O., Rat brain endothelial cell lines for the study of blood-brain barrier permeability and transport functions. *Cell Mol Neurobiol* **2005,** *25* (1), 41-58.

231. Sobue, K.; Yamamoto, N.; Yoneda, K.; Hodgson, M. E.; Yamashiro, K.; Tsuruoka, N.; Tsuda, T.; Katsuya, H.; Miura, Y.; Asai, K.; Kato, T., Induction of blood-brain barrier properties in immortalized bovine brain endothelial cells by astrocytic factors. *Neurosci Res* **1999,** *35* (2), 155-64.

232. Teifel, M.; Friedl, P., Establishment of the permanent microvascular endothelial cell line PBMEC/C1-2 from porcine brains. *Exp Cell Res* **1996,** *228* (1), 50-7.

233. Eigenmann, D. E.; Xue, G.; Kim, K. S.; Moses, A. V.; Hamburger, M.; Oufir, M., Comparative study of four immortalized human brain capillary endothelial cell lines, hCMEC/D3, hBMEC, TY10, and BB19, and optimization of culture conditions, for an in vitro blood-brain barrier model for drug permeability studies. *Fluids Barriers CNS* **2013,** *10* (1), 33.

234. Dolan, J. W., How Much Can I Inject? Part I: Injecting in Mobile Phase. *LCGC North America* **2014,** *32* (10), 780-785.

235. U.S. Department of Health and Human Services, F. D. A., Bioanalytical Method Validation. In *Guidance for Industry*, 2018.

236. Committee for Medicinal Products for Human Use, E. M. A., Guideline on Bioanalytical Method Validation. 2012.

237. Leaver, N., *A practical guide to implementing clinical mass spectrometry systems*. ILM Publications: 2011; p 84-84.

238. Altman, D. G.; Bland, J. M., Measurement in Medicine: The Analysis of Method Comparison Studies. *The Statistician* **1983,** *32* (3), 307-307.

239. Giavarina, D., Understanding Bland Altman analysis. *Biochem Med (Zagreb)* **2015,** *25* (2), 141-51.

240. Yubero, D.; Montero, R.; Artuch, R.; Land, J. M.; Heales, S. J.; Hargreaves, I. P., Biochemical diagnosis of coenzyme q10 deficiency. *Mol Syndromol* **2014,** *5* (3-4), 147-55.

241. Roushdy, M., Effect of substituents and alkoxy chain length on the phase behaviour and optical properties of 4-substituted-phenyl 4-alkoxybenzoates. *Liquid Crystals* **2004,** *31* (3), 371-375.

242. Nonella, M., A Generalized Resonance Model for Substituted 1,4-Benzoquinones. *J Phys Chem A* **1999,** *103* (35), 7069-7075.

243. Tomasetti, M.; Alleva, R.; Solenghi, M. D.; Littarru, G. P., Distribution of antioxidants among blood components and lipoproteins: Significance of lipids/CoQ10ratio as a possible marker of increased risk for atherosclerosis. *BioFactors* **1999,** *9* (2-4), 231-240.

244. Sunesen, V. H.; Weber, C.; Hùlmer, G., Lipophilic antioxidants and polyunsaturated fatty acids in lipoprotein classes: distribution and interaction. *Eur J Clin Nutr* **2001,** *55*, 115-123.

245. Karlsson, J.; Diamant, B.; Theorell, H.; Folkers, K., Ubiquinone and alpha-tocopherol in plasma; means of translocation or depot. *Clin Investig* **1993,** *71* (8 Suppl), S84-91.

246. Ordovas, J. M., Lipoproteins. In *Encyclopedia of Food Sciences and Nutrition*, Second ed.; Caballero, B.; Trugo, L.; Finglas, P. M., Eds. Elsevier: 2003; pp 3543-3552.

247. Law, A.; Scott, J., A cross-species comparison of the apolipoprotein B domain that binds to the LDL receptor. *J Lipid Res* **1990,** *31* (6), 1109-20.

248. Li, Y.; Lu, W.; Marzolo, M. P.; Bu, G., Differential functions of members of the low density lipoprotein receptor family suggested by their distinct endocytosis rates. *J Biol Chem* **2001,** *276* (21), 18000-6.

249. Emonard, H.; Theret, L.; Bennasroune, A. H.; Dedieu, S., Regulation of LRP-1 expression: make the point. *Pathol Biol (Paris)* **2014,** *62* (2), 84-90.

250. Lillis, A. P.; Van Duyn, L. B.; Murphy-Ullrich, J. E.; Strickland, D. K., LDL receptor-related protein 1: unique tissue-specific functions revealed by selective gene knockout studies. *Physiol Rev* **2008,** *88* (3), 887-918.

251. Li, Y.; Marzolo, M. P.; van Kerkhof, P.; Strous, G. J.; Bu, G., The YXXL motif, but not the two NPXY motifs, serves as the dominant endocytosis signal for low density lipoprotein receptor-related protein. *J Biol Chem* **2000,** *275* (22), 17187-94.

252. Tian, X.; Nyberg, S.; P, S. S.; Madsen, J.; Daneshpour, N.; Armes, S. P.; Berwick, J.; Azzouz, M.; Shaw, P.; Abbott, N. J.; Battaglia, G., LRP-1-mediated intracellular antibody delivery to the Central Nervous System. *Sci Rep* **2015,** *5* (1), 11990.

253. Nyberg, S.; Tian, X.; Poma, A.; Battaglia, G., LRP1 targeting and clustering mediate fast transcytosis in brain endothelial cells. *(in press)* **2018**.

254. Stamatovic, S. M.; Keep, R. F.; Andjelkovic, A. V., Brain endothelial cell-cell junctions: how to "open" the blood brain barrier. *Curr Neuropharmacol* **2008,** *6* (3), 179-92.

255. Kashiba, M.; Terashima, M.; Sagawa, T.; Yoshimura, S.; Yamamoto, Y., Prosaposin knockdown in Caco-2 cells decreases cellular levels of coenzyme Q10 and ATP, and results in the loss of tight junction barriers. *J Clin Biochem Nutr* **2017,** *60* (2), 81-85.

256. Ziosi, M.; Di Meo, I.; Kleiner, G.; Gao, X. H.; Barca, E.; Sanchez-Quintero, M. J.; Tadesse, S.; Jiang, H.; Qiao, C.; Rodenburg, R. J.; Scalais, E.; Schuelke, M.; Willard, B.; Hatzoglou, M.; Tiranti, V.; Quinzii, C. M., Coenzyme Q deficiency causes impairment of the sulfide oxidation pathway. *EMBO Mol Med* **2017,** *9* (1), 96-111.

257. Cullen, J. K.; Abdul Murad, N.; Yeo, A.; McKenzie, M.; Ward, M.; Chong, K. L.; Schieber, N. L.; Parton, R. G.; Lim, Y. C.; Wolvetang, E.; Maghzal, G. J.; Stocker, R.; Lavin, M. F., AarF Domain Containing Kinase 3 (ADCK3) Mutant Cells Display Signs of Oxidative Stress, Defects in Mitochondrial Homeostasis and Lysosomal Accumulation. *PLoS One* **2016,** *11* (2).

258. Quinzii, C. M.; Tadesse, S.; Naini, A.; Hirano, M., Effects of inhibiting CoQ10 biosynthesis with 4-nitrobenzoate in human fibroblasts. *PLoS One* **2012,** *7* (2).

259. Forsman, U.; Sjoberg, M.; Turunen, M.; Sindelar, P. J., 4-Nitrobenzoate inhibits coenzyme Q biosynthesis in mammalian cell cultures. *Nat Chem Biol* **2010,** *6* (7), 515-7.

260. Pierrel, F., Impact of Chemical Analogs of 4-Hydroxybenzoic Acid on Coenzyme Q Biosynthesis: From Inhibition to Bypass of Coenzyme Q Deficiency. *Front Physiol* **2017,** *8*, 436.

261. Lagier-Tourenne, C.; Tazir, M.; Lopez, L. C.; Quinzii, C. M.; Assoum, M.; Drouot, N.; Busso, C.; Makri, S.; Ali-Pacha, L.; Benhassine, T.; Anheim, M.; Lynch, D. R.; Thibault, C.; Plewniak, F.; Bianchetti, L.; Tranchant, C.; Poch, O.; DiMauro, S.; Mandel, J. L.; Barros, M. H.; Hirano, M.; Koenig, M., ADCK3, an ancestral kinase, is mutated in a form of recessive ataxia associated with coenzyme Q10 deficiency. *Am J Hum Genet* **2008,** *82* (3), 661-72.

262. Brea-Calvo, G.; Haack, T. B.; Karall, D.; Ohtake, A.; Invernizzi, F.; Carrozzo, R.; Kremer, L.; Dusi, S.; Fauth, C.; Scholl-Burgi, S.; Graf, E.; Ahting, U.; Resta, N.; Laforgia, N.; Verrigni, D.; Okazaki, Y.; Kohda, M.; Martinelli, D.; Freisinger, P.; Strom, T. M.; Meitinger, T.; Lamperti, C.; Lacson, A.; Navas, P.; Mayr, J. A.; Bertini, E.; Murayama, K.; Zeviani, M.; Prokisch, H.; Ghezzi, D., COQ4 mutations cause a broad spectrum of mitochondrial disorders associated with CoQ10 deficiency. *Am J Hum Genet* **2015,** *96* (2), 309-17.

263. Tronstad, K. J.; Nooteboom, M.; Nilsson, L. I.; Nikolaisen, J.; Sokolewicz, M.; Grefte, S.; Pettersen, I. K.; Dyrstad, S.; Hoel, F.; Willems, P. H.; Koopman, W. J., Regulation and quantification of cellular mitochondrial morphology and content. *Curr Pharm Des* **2014,** *20* (35), 5634-52.

264. Mishra, P.; Chan, D. C., Metabolic regulation of mitochondrial dynamics. *J Cell Biol* **2016,** *212* (4), 379-87.

265. Duijghuijsen, L. M. J.; Grefte, S.; de Boer, V. C. J.; Zeper, L.; van Dartel, D. A. M.; van der Stelt, I.; Bekkenkamp-Grovenstein, M.; van Norren, K.; Wichers, H. J.; Keijer, J., Mitochondrial ATP Depletion Disrupts Caco-2 Monolayer Integrity and Internalizes Claudin 7. *Front Physiol* **2017,** *8*, 794.

266. Magistretti, P. J.; Allaman, I., A cellular perspective on brain energy metabolism and functional imaging. *Neuron* **2015,** *86* (4), 883-901.

267. Pellerin, L.; Magistretti, P. J., Glutamate uptake into astrocytes stimulates aerobic glycolysis: a mechanism coupling neuronal activity to glucose utilization. *PNAS* **1994,** *91* (22), 10625-9.

268. Brown, A. M.; Ransom, B. R., Astrocyte glycogen and brain energy metabolism. *Glia* **2007,** *55* (12), 1263-71.

269. Brix, B.; Mesters, J. R.; Pellerin, L.; Johren, O., Endothelial cell-derived nitric oxide enhances aerobic glycolysis in astrocytes via HIF-1alpha-mediated target gene activation. *J Neurosci* **2012,** *32* (28), 9727-35.

270. Kayden, H. J.; Traber, M. G., Absorption, lipoprotein transport, and regulation of plasma concentrations of vitamin E in humans. *J Lipid Res* **1993,** *34* (3), 343-58.

271. Rigotti, A., Absorption, transport, and tissue delivery of vitamin E. *Mol Aspects Med* **2007,** *28* (5-6), 423-36.

272. Dasgupta, A.; Wahed, A., Lipid Metabolism and Disorders. In *Clinical Chemistry, Immunology and Laboratory Quality Control*, Elsevier: 2014; pp 85-105.

273. German, J. B.; Smilowitz, J. T.; Zivkovic, A. M., Lipoproteins: When size really matters. *Curr Opin Colloid Interface Sci* **2006,** *11* (2-3), 171-183.

274. von Zychlinski, A.; Williams, M.; McCormick, S.; Kleffmann, T., Absolute quantification of apolipoproteins and associated proteins on human plasma lipoproteins. *J Proteomics* **2014,** *106*, 181-90.

275. Vezina, C. A.; Milne, R. W.; Weech, P. K.; Marcel, Y. L., Apolipoprotein distribution in human lipoproteins separated by polyacrylamide gradient gel electrophoresis. *J Lipid Res* **1988,** *29* (5), 573-85.

276. Miles, M. V., The uptake and distribution of coenzyme Q (10). *Mitochondrion* **2007,** *7*, S72-S77.

277. Takada, T.; Suzuki, H., Molecular mechanisms of membrane transport of vitamin E. *Mol Nutr Food Res* **2010,** *54* (5), 616-22.

278. Traber, M. G.; Arai, H., Molecular mechanisms of vitamin E transport. *Annu Rev Nutr* **1999,** *19*, 343-55.

279. Goldstein, J. L.; Ho, Y. K.; Basu, S. K.; Brown, M. S., Binding site on macrophages that mediates uptake and degradation of acetylated low density lipoprotein, producing massive cholesterol deposition. *PNAS* **1979,** *76* (1), 333-7.

280. Anderson, R. G.; Brown, M. S.; Goldstein, J. L., Role of the coated endocytic vesicle in the uptake of receptor-bound low density lipoprotein in human fibroblasts. *Cell* **1977,** *10* (3), 351-64.

281. Taylor, D. R.; Hooper, N. M., The low-density lipoprotein receptor-related protein 1 (LRP1) mediates the endocytosis of the cellular prion protein. *Biochem J* **2007,** *402* (1), 17-23.

282. Goti, D.; Hammer, A.; Galla, H. J.; Malle, E.; Sattler, W., Uptake of Lipoprotein-Associated α-Tocopherol by Primary Porcine Brain Capillary Endothelial Cells. *J Neurochem* **2002,** *74* (4), 1374-1383.

283. Donahue, J. E.; Flaherty, S. L.; Johanson, C. E.; Duncan, J. A., 3rd; Silverberg, G. D.; Miller, M. C.; Tavares, R.; Yang, W.; Wu, Q.; Sabo, E.; Hovanesian, V.; Stopa, E. G., RAGE, LRP-1, and amyloid-beta protein in Alzheimer's disease. *Acta Neuropathol* **2006,** *112* (4), 405-15.

284. Wang, H.; Chen, F.; Zhong, K. L.; Tang, S. S.; Hu, M.; Long, Y.; Miao, M. X.; Liao, J. M.; Sun, H. B.; Hong, H., PPARgamma agonists regulate bidirectional transport of amyloid-beta across the blood-brain barrier and hippocampus plasticity in db/db mice. *Br J Pharmacol* **2016,** *173* (2), 372-85.

285. Qosa, H.; Abuasal, B. S.; Romero, I. A.; Weksler, B.; Couraud, P. O.; Keller, J. N.; Kaddoumi, A., Differences in amyloid-beta clearance across mouse and human blood-brain barrier models: kinetic analysis and mechanistic modeling. *Neuropharmacology* **2014,** *79*, 668-78.

286. Storck, S. E.; Meister, S.; Nahrath, J.; Meissner, J. N.; Schubert, N.; Di Spiezio, A.; Baches, S.; Vandenbroucke, R. E.; Bouter, Y.; Prikulis, I.; Korth, C.; Weggen, S.; Heimann, A.; Schwaninger, M.; Bayer, T. A.; Pietrzik, C. U., Endothelial LRP1 transports amyloid-beta(1-42) across the blood-brain barrier. *J Clin Invest* **2016,** *126* (1), 123-36.

287. Zlokovic, B. V.; Deane, R.; Sagare, A. P.; Bell, R. D.; Winkler, E. A., Low-density lipoprotein receptor-related protein-1: a serial clearance homeostatic mechanism controlling Alzheimer's amyloid beta-peptide elimination from the brain. *J Neurochem* **2010,** *115* (5), 1077-89.

288. Sagare, A. P.; Bell, R. D.; Zlokovic, B. V., Neurovascular dysfunction and faulty amyloid beta-peptide clearance in Alzheimer disease. *Cold Spring Harb Perspect Med* **2012,** *2* (10).

289. Zerbinatti, C. V.; Bu, G., LRP and Alzheimer's disease. *Rev Neurosci* **2005,** *16* (2), 123-35.

290. Meijer, A. B.; Rohlena, J.; van der Zwaan, C.; van Zonneveld, A. J.; Boertjes, R. C.; Lenting, P. J.; Mertens, K., Functional duplication of ligand-binding domains within low-density lipoprotein receptor-related protein for interaction with receptor associated protein, alpha2-macroglobulin, factor IXa and factor VIII. *Biochim Biophys Acta* **2007,** *1774* (6), 714-22.

291. Bomsel, M.; Parton, R.; Kuznetsov, S. A.; Schroer, T. A.; Gruenberg, J., Microtubule- and motor-dependent fusion in vitro between apical and basolateral endocytic vesicles from MDCK cells. *Cell* **1990,** *62* (4), 719-31.

292. Preston, J. E.; Abbott, N. J.; Begley, D. J., Transcytosis of macromolecules at the blood-brain barrier. *Adv Pharmacol* **2014,** *71*, 147-63.

293. Goldstein, J. L.; Anderson, R. G.; Brown, M. S., Coated pits, coated vesicles, and receptor-mediated endocytosis. *Nature* **1979,** *279* (5715), 679-85.

294. Lajoie, P.; Nabi, I. R., Lipid Rafts, Caveolae, and Their Endocytosis. 2010; Vol. 282, pp 135-163.

295. Reboul, E.; Klein, A.; Bietrix, F.; Gleize, B.; Malezet-Desmoulins, C.; Schneider, M.; Margotat, A.; Lagrost, L.; Collet, X.; Borel, P., Scavenger receptor class B type I (SR-BI) is involved in vitamin E transport across the enterocyte. *J Biol Chem* **2006,** *281* (8), 4739-45.

296. Goti, D.; Hrzenjak, A.; Levak-Frank, S.; Frank, S.; van der Westhuyzen, D. R.; Malle, E.; Sattler, W., Scavenger receptor class B, type I is expressed in porcine brain capillary endothelial cells and contributes to selective uptake of HDL-associated vitamin E. *J Neurochem* **2001,** *76* (2), 498-508.

297. Acton, S.; Rigotti, A.; Landschulz, K. T.; Xu, S.; Hobbs, H. H.; Krieger, M., Identification of scavenger receptor SR-BI as a high density lipoprotein receptor. *Science* **1996,** *271* (5248), 518-20.

298. Murao, K.; Terpstra, V.; Green, S. R.; Kondratenko, N.; Steinberg, D.; Quehenberger, O., Characterization of CLA-1, a Human Homologue of Rodent Scavenger Receptor BI, as a Receptor for High Density Lipoprotein and Apoptotic Thymocytes. *J Biol Chem* **1997,** *272* (28), 17551-17557.

299. Neculai, D.; Schwake, M.; Ravichandran, M.; Zunke, F.; Collins, R. F.; Peters, J.; Neculai, M.; Plumb, J.; Loppnau, P.; Pizarro, J. C.; Seitova, A.; Trimble, W. S.; Saftig, P.; Grinstein, S.; Dhe-Paganon, S., Structure of LIMP-2 provides functional insights with implications for SR-BI and CD36. *Nature* **2013,** *504* (7478), 172-6.

300. Valacchi, G.; Sticozzi, C.; Lim, Y.; Pecorelli, A., Scavenger receptor class B type I: a multifunctional receptor. *Ann N Y Acad Sci* **2011,** *1229* (1), E1-7.

301. Balazs, Z.; Panzenboeck, U.; Hammer, A.; Sovic, A.; Quehenberger, O.; Malle, E.; Sattler, W., Uptake and transport of high-density lipoprotein (HDL) and HDL-associated alpha-tocopherol by an in vitro blood-brain barrier model. *J Neurochem* **2004,** *89* (4), 939-50.

302. Fung, K. Y.; Wang, C.; Nyegaard, S.; Heit, B.; Fairn, G. D.; Lee, W. L., SR-BI Mediated Transcytosis of HDL in Brain Microvascular Endothelial Cells Is Independent of Caveolin, Clathrin, and PDZK1. *Front Physiol* **2017,** *8*, 841.

303. PrabhuDas, M. R.; Baldwin, C. L.; Bollyky, P. L.; Bowdish, D. M. E.; Drickamer, K.; Febbraio, M.; Herz, J.; Kobzik, L.; Krieger, M.; Loike, J.; McVicker, B.; Means, T. K.; Moestrup, S. K.; Post, S. R.; Sawamura, T.; Silverstein, S.; Speth, R. C.; Telfer, J. C.; Thiele, G. M.; Wang, X. Y.; Wright, S. D.; El Khoury, J., A Consensus Definitive Classification of Scavenger Receptors and Their Roles in Health and Disease. *J Immunol* **2017,** *198* (10), 3775-3789.

304. Gonias, S. L.; Campana, W. M., LDL receptor-related protein-1: a regulator of inflammation in atherosclerosis, cancer, and injury to the nervous system. *Am J Pathol* **2014,** *184* (1), 18-27.

305. Mooberry, L. K.; Sabnis, N. A.; Panchoo, M.; Nagarajan, B.; Lacko, A. G., Targeting the SR-B1 Receptor as a Gateway for Cancer Therapy and Imaging. *Front Pharmacol* **2016,** *7*, 466.

306. Wagner, S.; Zensi, A.; Wien, S. L.; Tschickardt, S. E.; Maier, W.; Vogel, T.; Worek, F.; Pietrzik, C. U.; Kreuter, J.; von Briesen, H., Uptake mechanism of ApoE-modified nanoparticles on brain capillary endothelial cells as a blood-brain barrier model. *PLoS One* **2012,** *7* (3).

307. Fritz, G., RAGE: a single receptor fits multiple ligands. *Trends Biochem Sci* **2011,** *36* (12), 625-32.

308. Schmidt, A. M.; Vianna, M.; Gerlach, M.; Brett, J.; Ryan, J.; Kao, J.; Esposito, C.; Hegarty, H.; Hurley, W.; Clauss, M., Isolation and characterization of two binding proteins for advanced glycosylation end products from bovine lung which are present on the endothelial cell surface. *J Biol Chem* **1992,** *267* (21), 14987-97.

309. Park, H.; Adsit, F. G.; Boyington, J. C., The 1.5 A crystal structure of human receptor for advanced glycation endproducts (RAGE) ectodomains reveals unique features determining ligand binding. *J Biol Chem* **2010,** *285* (52), 40762-70.

310. Li, J.; Schmidt, A. M., Characterization and functional analysis of the promoter of RAGE, the receptor for advanced glycation end products. *J Biol Chem* **1997,** *272* (26), 16498-506.

311. Lai, A. Y.; McLaurin, J., Mechanisms of amyloid-Beta Peptide uptake by neurons: the role of lipid rafts and lipid raft-associated proteins. *Int J Alzheimers Dis* **2010,** *2011*, 548380.

312. Lin, H. J.; Hsu, F. Y.; Chen, W. W.; Lee, C. H.; Lin, Y. J.; Chen, Y. Y.; Chen, C. J.; Huang, M. Z.; Kao, M. C.; Chen, Y. A.; Lai, H. C.; Lai, C. H., Helicobacter pylori Activates HMGB1 Expression and Recruits RAGE into Lipid Rafts to Promote Inflammation in Gastric Epithelial Cells. *Front Immunol* **2016,** *7*, 341.

313. Deane, R.; Wu, Z.; Zlokovic, B. V., RAGE (yin) versus LRP (yang) balance regulates alzheimer amyloid beta-peptide clearance through transport across the blood-brain barrier. *Stroke* **2004,** *35* (11 Suppl 1), 2628-31.

314. Deane, R.; Du Yan, S.; Submamaryan, R. K.; LaRue, B.; Jovanovic, S.; Hogg, E.; Welch, D.; Manness, L.; Lin, C.; Yu, J.; Zhu, H.; Ghiso, J.; Frangione, B.; Stern, A.; Schmidt, A. M.; Armstrong, D. L.; Arnold, B.; Liliensiek, B.; Nawroth, P.; Hofman, F.; Kindy, M.; Stern, D.; Zlokovic, B., RAGE mediates amyloid-beta peptide transport across the blood-brain barrier and accumulation in brain. *Nat Med* **2003,** *9* (7), 907-13.

315. Yan, S. D.; Chen, X.; Fu, J.; Chen, M.; Zhu, H.; Roher, A.; Slattery, T.; Zhao, L.; Nagashima, M.; Morser, J.; Migheli, A.; Nawroth, P.; Stern, D.; Schmidt, A. M., RAGE and amyloid-beta peptide neurotoxicity in Alzheimer's disease. *Nature* **1996,** *382* (6593), 685-91.

316. Deane, R. J., Is RAGE still a therapeutic target for Alzheimer's disease? *Future Med Chem* **2012,** *4* (7), 915-25.

317. Ambudkar, S. V.; Kimchi-Sarfaty, C.; Sauna, Z. E.; Gottesman, M. M., P-glycoprotein: from genomics to mechanism. *Oncogene* **2003,** *22* (47), 7468-85.

318. Jin, M. S.; Oldham, M. L.; Zhang, Q.; Chen, J., Crystal structure of the multidrug transporter P-glycoprotein from Caenorhabditis elegans. *Nature* **2012,** *490* (7421), 566-9.

319. Park, R.; Kook, S. Y.; Park, J. C.; Mook-Jung, I., Abeta 1-42 reduces P-glycoprotein in the blood-brain barrier through RAGE-NF-kappaB signaling. *Cell Death Dis* **2014,** *5* (6), e1299.

320. Patabendige, A.; Skinner, R. A.; Abbott, N. J., Establishment of a simplified in vitro porcine blood-brain barrier model with high transendothelial electrical resistance. *Brain Res* **2013,** *1521* (0), 1-15.

321. Kubo, Y.; Ohtsuki, S.; Uchida, Y.; Terasaki, T., Quantitative Determination of Luminal and Abluminal Membrane Distributions of Transporters in Porcine Brain Capillaries by Plasma Membrane Fractionation and Quantitative Targeted Proteomics. *J Pharm Sci* **2015,** *104* (9), 3060-8.

322. Schinkel, A. H., P-Glycoprotein, a gatekeeper in the blood-brain barrier. *Adv Drug Deliv Rev* **1999,** *36* (2-3), 179-194.

323. Sharom, F. J., The P-glycoprotein multidrug transporter. *Essays Biochem* **2011,** *50* (1), 161-78.

324. Itagaki, S.; Ochiai, A.; Kobayashi, M.; Sugawara, M.; Hirano, T.; Iseki, K., Grapefruit juice enhance the uptake of coenzyme Q10 in the human intestinal cell-line Caco-2. *Food Chem* **2010,** *120* (2), 552-555.

325. Ulery, P. G.; Beers, J.; Mikhailenko, I.; Tanzi, R. E.; Rebeck, G. W.; Hyman, B. T.; Strickland, D. K., Modulation of beta-amyloid precursor protein processing by the low density lipoprotein receptor-related protein (LRP). Evidence that LRP contributes to the pathogenesis of Alzheimer's disease. *J Biol Chem* **2000,** *275* (10), 7410-5.

326. May, J. M.; Jayagopal, A.; Qu, Z. C.; Parker, W. H., Ascorbic acid prevents high glucose-induced apoptosis in human brain pericytes. *Biochem Biophys Res Commun* **2014,** *452* (1), 112-7.

327. Jones, C. R.; Pasanisi, F.; Elliott, H. L.; Reid, J. L., Effects of verapamil and nisoldipine on human platelets: in vivo and in vitro studies. *Br J Clin Pharmacol* **1985,** *20* (3), 191-6.

328. Gonzalez-Pecchi, V.; Valdes, S.; Pons, V.; Honorato, P.; Martinez, L. O.; Lamperti, L.; Aguayo, C.; Radojkovic, C., Apolipoprotein A-I enhances proliferation of human endothelial progenitor cells and promotes angiogenesis through the cell surface ATP synthase. *Microvasc Res* **2015,** *98*, 9-15.

329. Mitochondrial disorders in children: Co-enzyme Q10. NICE, Ed. National Institute for Health and Care Excellence: 2017.

330. Deane, R.; Singh, I.; Sagare, A. P.; Bell, R. D.; Ross, N. T.; LaRue, B.; Love, R.; Perry, S.; Paquette, N.; Deane, R. J.; Thiyagarajan, M.; Zarcone, T.; Fritz, G.; Friedman, A. E.; Miller, B. L.; Zlokovic, B. V., A multimodal RAGE-specific inhibitor reduces amyloid beta-mediated brain disorder in a mouse model of Alzheimer disease. *J Clin Invest* **2012,** *122* (4), 1377-92.

331. Nieland, T. J.; Penman, M.; Dori, L.; Krieger, M.; Kirchhausen, T., Discovery of chemical inhibitors of the selective transfer of lipids mediated by the HDL receptor SR-BI. *PNAS* **2002,** *99* (24), 15422-7.

332. Dockendorff, C.; Faloon, P. W.; Yu, M.; Youngsaye, W.; Penman, M.; Nieland, T. J.; Nag, P. P.; Lewis, T. A.; Pu, J.; Bennion, M.; Negri, J.; Paterson, C.; Lam, G.; Dandapani, S.; Perez, J. R.; Munoz, B.; Palmer, M. A.; Schreiber, S. L.; Krieger, M., Indolinyl-Thiazole Based Inhibitors of Scavenger Receptor-BI (SR-BI)-Mediated Lipid Transport. *ACS Med Chem Lett* **2015,** *6* (4), 375-380.

333. Bansal, T.; Mishra, G.; Jaggi, M.; Khar, R. K.; Talegaonkar, S., Effect of P-glycoprotein inhibitor, verapamil, on oral bioavailability and pharmacokinetics of irinotecan in rats. *Eur J Pharm Sci* **2009,** *36* (4-5), 580-90.

334. Amin, M. L., P-glycoprotein Inhibition for Optimal Drug Delivery. *Drug Target Insights* **2013,** *7*, 27-34.

335. Matsson, P.; Pedersen, J. M.; Norinder, U.; Bergstrom, C. A.; Artursson, P., Identification of novel specific and general inhibitors of the three major human ATP-binding cassette transporters P-gp, BCRP and MRP2 among registered drugs. *Pharm Res* **2009,** *26* (8), 1816-31.

336. Zhang, S. L.; Yue, Z.; Arnold, D. M.; Artiushin, G.; Sehgal, A., A Circadian Clock in the Blood-Brain Barrier Regulates Xenobiotic Efflux. *Cell* **2018,** *173* (1), 130-139 e10.

337. Berlin, R. D.; Oliver, J. M., Surface functions during mitosis. II. Quantitation of pinocytosis and kinetic characterization of the mitotic cycle with a new fluorescence technique. *J Cell Biol* **1980,** *85* (3), 660-71.

338. Cole, L.; Coleman, J.; Evans, D.; Hawes, C., Internalisation of fluorescein isothiocyanate and fluorescein isothiocyanatedextran by suspension-cultured plant cells. *J Cell Sci* **1990,** *96* (4).

339. Wright, H. M.; Clish, C. B.; Mikami, T.; Hauser, S.; Yanagi, K.; Hiramatsu, R.; Serhan, C. N.; Spiegelman, B. M., A synthetic antagonist for the peroxisome proliferator-activated receptor gamma inhibits adipocyte differentiation. *J Biol Chem* **2000,** *275* (3), 1873-7.

340. Liu, L. P.; Hong, H.; Liao, J. M.; Wang, T. S.; Wu, J.; Chen, S. S.; Li, Y. Q.; Long, Y.; Xia, Y. Z., Upregulation of RAGE at the blood-brain barrier in streptozotocin-induced diabetic mice. *Synapse* **2009,** *63* (8), 636-42.

341. Hong, H.; Liu, L. P.; Liao, J. M.; Wang, T. S.; Ye, F. Y.; Wu, J.; Wang, Y. Y.; Wang, Y.; Li, Y. Q.; Long, Y.; Xia, Y. Z., Downregulation of LRP1 [correction of LPR1] at the blood-

brain barrier in streptozotocin-induced diabetic mice. *Neuropharmacology* **2009,** *56* (6-7), 1054-9.

342. Koopman, W. J.; Beyrath, J.; Fung, C. W.; Koene, S.; Rodenburg, R. J.; Willems, P. H.; Smeitink, J. A., Mitochondrial disorders in children: toward development of small-molecule treatment strategies. *EMBO Mol Med* **2016,** *8* (4), 311-27.

343. Parikh, S.; Goldstein, A.; Karaa, A.; Koenig, M. K.; Anselm, I.; Brunel-Guitton, C.; Christodoulou, J.; Cohen, B. H.; Dimmock, D.; Enns, G. M.; Falk, M. J.; Feigenbaum, A.; Frye, R. E.; Ganesh, J.; Griesemer, D.; Haas, R.; Horvath, R.; Korson, M.; Kruer, M. C.; Mancuso, M.; McCormack, S.; Raboisson, M. J.; Reimschisel, T.; Salvarinova, R.; Saneto, R. P.; Scaglia, F.; Shoffner, J.; Stacpoole, P. W.; Sue, C. M.; Tarnopolsky, M.; Van Karnebeek, C.; Wolfe, L. A.; Cunningham, Z. Z.; Rahman, S.; Chinnery, P. F., Patient care standards for primary mitochondrial disease: a consensus statement from the Mitochondrial Medicine Society. *Genet Med* **2017,** *19* (12).

344. El-Hattab, A. W.; Zarante, A. M.; Almannai, M.; Scaglia, F., Therapies for mitochondrial diseases and current clinical trials. *Mol Genet Metab* **2017,** *122* (3), 1-9.

345. Rahman, S., Emerging aspects of treatment in mitochondrial disorders. *J Inherit Metab Dis* **2015,** *38* (4), 641-53.

346. Gorman, G. S.; Chinnery, P. F.; DiMauro, S.; Hirano, M.; Koga, Y.; McFarland, R.; Suomalainen, A.; Thorburn, D. R.; Zeviani, M.; Turnbull, D. M., Mitochondrial diseases. *Nat Rev Dis Primers* **2016,** *2*, 16080.

347. Pfeffer, G.; Majamaa, K.; Turnbull, D. M.; Thorburn, D. R.; Chinnery, P. F., Treatment for mitochondrial disorders. Chinnery, P. F., Ed. John Wiley & Sons, Ltd: Chichester, UK, 2012.

348. Enns, G. M., Treatment of mitochondrial disorders: antioxidants and beyond. *J Child Neurol* **2014,** *29* (9), 1235-40.

349. Ulatowski, L. M.; Manor, D., Vitamin E and neurodegeneration. *Neurobiol Dis* **2015,** *84*, 78-83.

350. Strawser, C.; Schadt, K.; Hauser, L.; McCormick, A.; Wells, M.; Larkindale, J.; Lin, H.; Lynch, D. R., Pharmacological therapeutics in Friedreich ataxia: the present state. *Expert Rev Neurother* **2017,** *17* (9), 895-907.

351. Cooper, J. M.; Korlipara, L. V.; Hart, P. E.; Bradley, J. L.; Schapira, A. H., Coenzyme Q10 and vitamin E deficiency in Friedreich's ataxia: predictor of efficacy of vitamin E and coenzyme Q10 therapy. *Eur J Neurol* **2008,** *15* (12), 1371-9.

352. Wilkins, H. M.; Morris, J. K., New Therapeutics to Modulate Mitochondrial Function in Neurodegenerative Disorders. *Curr Pharm Des* **2017,** *23* (5), 731-752.

353. Ibrahim, W. H.; Bhagavan, H. N.; Chopra, R. K.; Chow, C. K., Dietary coenzyme Q10 and vitamin E alter the status of these compounds in rat tissues and mitochondria. *J Nutr* **2000,** *130* (9), 2343-8.

354. Tarnopolsky, M. A., The mitochondrial cocktail: rationale for combined nutraceutical therapy in mitochondrial cytopathies. *Adv Drug Deliv Rev* **2008,** *60* (13-14), 1561-7.

355. Bergamasco, B.; Scarzella, L.; La Commare, P., Idebenone, a new drug in the treatment of cognitive impairment in patients with dementia of the Alzheimer type. *Funct Neurol* **1994,** *9* (3), 161-8.

356. Carelli, V.; Carbonelli, M.; de Coo, I. F.; Kawasaki, A.; Klopstock, T.; Lagreze, W. A.; La Morgia, C.; Newman, N. J.; Orssaud, C.; Pott, J. W. R.; Sadun, A. A.; van Everdingen, J.; Vignal-Clermont, C.; Votruba, M.; Yu-Wai-Man, P.; Barboni, P., International Consensus Statement on the Clinical and Therapeutic Management of Leber Hereditary Optic Neuropathy. *Journal of neuro-ophthalmology : the official journal of the North American Neuro-Ophthalmology Society* **2017,** *37* (4), 371-381.

357. Llòria, X.; Catarino, C.; Silva, M.; Klopstock, T., Idebenone is effective and well tolerated in Leber's hereditary optic neuropathy (LHON): Long-term results of real world clinical practice. *Acta Ophthalmologica* **2017,** *95* (S259).

358. McDonald, C. M.; Meier, T.; Voit, T.; Schara, U.; Straathof, C. S.; D'Angelo, M. G.; Bernert, G.; Cuisset, J. M.; Finkel, R. S.; Goemans, N.; Rummey, C.; Leinonen, M.; Spagnolo, P.; Buyse, G. M.; Group, D. S., Idebenone reduces respiratory complications in patients with Duchenne muscular dystrophy. *Neuromuscul Disord* **2016,** *26* (8), 473-80.

359. Ikejiri, Y.; Mori, E.; Ishii, K.; Nishimoto, K.; Yasuda, M.; Sasaki, M., Idebenone improves cerebral mitochondrial oxidative metabolism in a patient with MELAS. *Neurology* **1996,** *47* (2), 583-5.

360. Shirani, A.; Okuda, D. T.; Stuve, O., Therapeutic Advances and Future Prospects in Progressive Forms of Multiple Sclerosis. *Neurotherapeutics : the journal of the American Society for Experimental NeuroTherapeutics* **2016,** *13* (1), 58-69.

361. Rustin, P.; von Kleist-Retzow, J. C.; Chantrel-Groussard, K.; Sidi, D.; Munnich, A.; Rotig, A., Effect of idebenone on cardiomyopathy in Friedreich's ataxia: a preliminary study. *Lancet* **1999,** *354* (9177), 477-9.

362. Hausse, A. O.; Aggoun, Y.; Bonnet, D.; Sidi, D.; Munnich, A.; Rotig, A.; Rustin, P., Idebenone and reduced cardiac hypertrophy in Friedreich's ataxia. *Heart* **2002,** *87* (4), 346-9.

363. Artuch, R.; Aracil, A.; Mas, A.; Colome, C.; Rissech, M.; Monros, E.; Pineda, M., Friedreich's ataxia: idebenone treatment in early stage patients. *Neuropediatrics* **2002,** *33* (4), 190-3.

364. Pineda, M.; Arpa, J.; Montero, R.; Aracil, A.; Dominguez, F.; Galvan, M.; Mas, A.; Martorell, L.; Sierra, C.; Brandi, N.; Garcia-Arumi, E.; Rissech, M.; Velasco, D.; Costa, J. A.; Artuch, R., Idebenone treatment in paediatric and adult patients with Friedreich ataxia: long-term follow-up. *Eur J Paediatr Neurol* **2008,** *12* (6), 470-5.

365. Jaber, S.; Polster, B. M., Idebenone and neuroprotection: antioxidant, pro-oxidant, or electron carrier? *J Bioenerg Biomembr* **2015,** *47* (1-2), 111-8.

366. Erb, M.; Hoffmann-Enger, B.; Deppe, H.; Soeberdt, M.; Haefeli, R. H.; Rummey, C.; Feurer, A.; Gueven, N., Features of idebenone and related short-chain quinones that rescue ATP levels under conditions of impaired mitochondrial complex I. *PLoS One* **2012,** *7* (4), e36153.

367. Lind, C.; Hochstein, P.; Ernster, L., DT-diaphorase as a quinone reductase: a cellular control device against semiquinone and superoxide radical formation. *Arch Biochem Biophys* **1982,** *216* (1), 178-85.

368. Suno, M.; Nagaoka, A., Inhibition of lipid peroxidation by a novel compound, idebenone (CV-2619). *Jpn J Pharmacol* **1984,** *35* (2), 196-8.

369. Giorgio, V.; Petronilli, V.; Ghelli, A.; Carelli, V.; Rugolo, M.; Lenaz, G.; Bernardi, P., The effects of idebenone on mitochondrial bioenergetics. *Biochim Biophys Acta* **2012,** *1817* (2), 363-9.

370. Briere, J. J.; Schlemmer, D.; Chretien, D.; Rustin, P., Quinone analogues regulate mitochondrial substrate competitive oxidation. *Biochem Biophys Res Commun* **2004,** *316* (4), 1138-42.

371. Genova, M. L.; Pich, M. M.; Biondi, A.; Bernacchia, A.; Falasca, A.; Bovina, C.; Formiggini, G.; Castelli, G. P.; Lenaz, G., Mitochondrial Production of Oxygen Radical Species and the Role of Coenzyme Q as an Antioxidant. *Exp Biol Med* **2016,** *228* (5), 506-513.

372. Imada, I.; Sato, E. F.; Kira, Y.; Inoue, M., Effect of CoQ homologues on reactive oxygen generation by mitochondria. *Biofactors* **2008,** *32* (1-4), 41-8.

373. Ohnishi, S. T.; Ohnishi, T.; Muranaka, S.; Fujita, H.; Kimura, H.; Uemura, K.; Yoshida, K.; Utsumi, K., A possible site of superoxide generation in the complex I segment of rat heart mitochondria. *J Bioenerg Biomembr* **2005,** *37* (1), 1-15.

374. Fato, R.; Bergamini, C.; Leoni, S.; Lenaz, G., Mitochondrial production of reactive oxygen species: role of complex I and quinone analogues. *Biofactors* **2008,** *32* (1-4), 31-9.

375. Tai, K. K.; Pham, L.; Truong, D. D., Idebenone induces apoptotic cell death in the human dopaminergic neuroblastoma SHSY-5Y cells. *Neurotox Res* **2011,** *20* (4), 321-8.

376. King, M. S.; Sharpley, M. S.; Hirst, J., Reduction of hydrophilic ubiquinones by the flavin in mitochondrial NADH:ubiquinone oxidoreductase (Complex I) and production of reactive oxygen species. *Biochemistry* **2009,** *48* (9), 2053-62.

377. Murad, L. B.; Guimaraes, M. R.; Vianna, L. M., Effects of decylubiquinone (coenzyme Q10 analog) supplementation on SHRSP. *Biofactors* **2007,** *30* (1), 13-8.

378. Kelso, G. F.; Porteous, C. M.; Coulter, C. V.; Hughes, G.; Porteous, W. K.; Ledgerwood, E. C.; Smith, R. A.; Murphy, M. P., Selective targeting of a redox-active ubiquinone to mitochondria within cells: antioxidant and antiapoptotic properties. *J Biol Chem* **2001,** *276* (7), 4588-96.

379. Ross, M. F.; Kelso, G. F.; Blaikie, F. H.; James, A. M.; Cochemé, H. M.; Filipovska, A.; Da Ros, T.; Hurd, T. R.; Smith, R. A. J.; Murphy, M. P., Lipophilic triphenylphosphonium cations as tools in mitochondrial bioenergetics and free radical biology. *Biochemistry (Moscow)* **2005,** *70* (2), 222-230.

380. Rich, P. R., Chemiosmotic Theory. In *Encyclopedia of Biological Chemistry*, Second ed.; Lennarz, W. J.; Lane, M. D., Eds. Elsevier: 2013; pp 467-472.

381. Grinius, L. L.; Jasaitis, A. A.; Kadziauskas, Y. P.; Liberman, E. A.; Skulachev, V. P.; Topali, V. P.; Tsofina, L. M.; Vladimirova, M. A., Conversion of biomembrane-produced energy into electric form. I. Submitochondrial particles. *Biochim Biophys Acta* **1970,** *216* (1), 1-12.

382. Mitchell, P.; Moyle, J., Estimation of membrane potential and pH difference across the cristae membrane of rat liver mitochondria. *Eur J Biochem* **1969,** *7* (4), 471-84.

383. Murphy, M. P., Targeting lipophilic cations to mitochondria. *Biochim Biophys Acta* **2008,** *1777* (7-8), 1028-31.

384. Murphy, M. P., Understanding and preventing mitochondrial oxidative damage. *Biochem Soc Trans* **2016,** *44* (5), 1219-1226.

385. James, A. M.; Cocheme, H. M.; Murphy, M. P., Mitochondria-targeted redox probes as tools in the study of oxidative damage and ageing. *Mech Ageing Dev* **2005,** *126* (9), 982-6.

386. James, A. M.; Sharpley, M. S.; Manas, A. R.; Frerman, F. E.; Hirst, J.; Smith, R. A.; Murphy, M. P., Interaction of the mitochondria-targeted antioxidant MitoQ with phospholipid bilayers and ubiquinone oxidoreductases. *J Biol Chem* **2007,** *282* (20), 14708-18.

387. McManus, M. J.; Murphy, M. P.; Franklin, J. L., The mitochondria-targeted antioxidant MitoQ prevents loss of spatial memory retention and early neuropathology in a transgenic mouse model of Alzheimer's disease. *J Neurosci* **2011,** *31* (44), 15703-15.

388. Manczak, M.; Mao, P.; Calkins, M. J.; Cornea, A.; Reddy, A. P.; Murphy, M. P.; Szeto, H. H.; Park, B.; Reddy, P. H., Mitochondria-targeted antioxidants protect against amyloid-beta toxicity in Alzheimer's disease neurons. *J Alzheimers Dis* **2010,** *20 Suppl 2* (s2), S609-31.

389. Solesio, M. E.; Prime, T. A.; Logan, A.; Murphy, M. P.; Del Mar Arroyo-Jimenez, M.; Jordan, J.; Galindo, M. F., The mitochondria-targeted anti-oxidant MitoQ reduces aspects of mitochondrial fission in the 6-OHDA cell model of Parkinson's disease. *Biochim Biophys Acta* **2013,** *1832* (1), 174-82.

390. Snow, B. J.; Rolfe, F. L.; Lockhart, M. M.; Frampton, C. M.; O'Sullivan, J. D.; Fung, V.; Smith, R. A.; Murphy, M. P.; Taylor, K. M.; Protect Study, G., A double-blind, placebo-controlled study to assess the mitochondria-targeted antioxidant MitoQ as a disease-modifying therapy in Parkinson's disease. *Mov Disord* **2010,** *25* (11), 1670-4.

391. Jackson-Lewis, V.; Przedborski, S., Protocol for the MPTP mouse model of Parkinson's disease. *Nat Protoc* **2007,** *2* (1), 141-51.

392. Langston, J. W., The MPTP Story. In *J Parkinsons Dis*, 2017; Vol. 7, pp S11-9.

393. Mizuno, Y.; Suzuki, K.; Sone, N.; Saitoh, T., Inhibition of mitochondrial respiration by 1-methyl-4-phenyl-1,2,3,6-tetrahydropyridine (MPTP) in mouse brain in vivo. *Neurosci Lett* **1988,** *91* (3), 349-53.

394. Smith, R. A.; Murphy, M. P., Animal and human studies with the mitochondria-targeted antioxidant MitoQ. *Ann N Y Acad Sci* **2010,** *1201* (1), 96-103.

395. Stucki, D. M.; Ruegsegger, C.; Steiner, S.; Radecke, J.; Murphy, M. P.; Zuber, B.; Saxena, S., Mitochondrial impairments contribute to Spinocerebellar ataxia type 1 progression and can be ameliorated by the mitochondria-targeted antioxidant MitoQ. *Free Radic Biol Med* **2016,** *97*, 427-440.

396. Shrader, W. D.; Amagata, A.; Barnes, A.; Enns, G. M.; Hinman, A.; Jankowski, O.; Kheifets, V.; Komatsuzaki, R.; Lee, E.; Mollard, P.; Murase, K.; Sadun, A. A.; Thoolen, M.; Wesson, K.; Miller, G., alpha-Tocotrienol quinone modulates oxidative stress response and the biochemistry of aging. *Bioorg Med Chem Lett* **2011,** *21* (12), 3693-8.

397. Enns, G. M.; Kinsman, S. L.; Perlman, S. L.; Spicer, K. M.; Abdenur, J. E.; Cohen, B. H.; Amagata, A.; Barnes, A.; Kheifets, V.; Shrader, W. D.; Thoolen, M.; Blankenberg, F.; Miller, G., Initial experience in the treatment of inherited mitochondrial disease with EPI-743. *Mol Genet Metab* **2012,** *105* (1), 91-102.

398. Holmstrom, K. M.; Baird, L.; Zhang, Y.; Hargreaves, I.; Chalasani, A.; Land, J. M.; Stanyer, L.; Yamamoto, M.; Dinkova-Kostova, A. T.; Abramov, A. Y., Nrf2 impacts cellular bioenergetics by controlling substrate availability for mitochondrial respiration. *Biol Open* **2013,** *2* (8), 761-70.

399. Enns, G. M.; Cohen, B. H., Clinical Trials in Mitochondrial Disease. *JIEMS* **2017,** *5*.

400. Montenegro, L.; Turnaturi, R.; Parenti, C.; Pasquinucci, L., Idebenone: Novel Strategies to Improve Its Systemic and Local Efficacy. In *Nanomaterials (Basel)*, 2018; Vol. 8.

401. Torii, H.; Yoshida, K.; Kobayashi, T.; Tsukamoto, T.; Tanayama, S., Disposition of idebenone (CV-2619), a new cerebral metabolism improving agent, in rats and dogs. *J Pharmacobiodyn* **1985,** *8* (6), 457-67.

402. Nagai, Y.; Yoshida, K.; Narumi, S.; Tanayama, S.; Nagaoka, A., Brain distribution of idebenone and its effect on local cerebral glucose utilization in rats. *Arch Gerontol Geriatr* **1989,** *8* (3), 257-72.

403. Smith, R. A.; Porteous, C. M.; Gane, A. M.; Murphy, M. P., Delivery of bioactive molecules to mitochondria in vivo. *PNAS* **2003,** *100* (9), 5407-12.

404. Bodmer, M.; Vankan, P.; Dreier, M.; Kutz, K. W.; Drewe, J., Pharmacokinetics and metabolism of idebenone in healthy male subjects. *Eur J Clin Pharmacol* **2009,** *65* (5), 493-501.

405. Winklhofer-Roob, B. M.; van't Hof, M. A.; Shmerling, D. H., Reference values for plasma concentrations of vitamin E and A and carotenoids in a Swiss population from infancy to adulthood, adjusted for seasonal influences. *Clin Chem* **1997,** *43* (1), 146-53.

406. Mottier, P.; Gremaud, E.; Guy, P. A.; Turesky, R. J., Comparison of gas chromatography-mass spectrometry and liquid chromatography-tandem mass spectrometry methods to quantify alpha-tocopherol and alpha-tocopherolquinone levels in human plasma. *Anal Biochem* **2002,** *301* (1), 128-35.

407. Mardones, P.; Strobel, P.; Miranda, S.; Leighton, F.; Quinones, V.; Amigo, L.; Rozowski, J.; Krieger, M.; Rigotti, A., Alpha-tocopherol metabolism is abnormal in scavenger receptor class B type I (SR-BI)-deficient mice. *J Nutr* **2002,** *132* (3), 443-9.

408. Spector, R.; Johanson, C. E., Vitamin transport and homeostasis in mammalian brain: focus on Vitamins B and E. *J Neurochem* **2007,** *103* (2), 425-38.

409. Martin, A.; Janigian, D.; Shukitt-Hale, B.; Prior, R. L.; Joseph, J. A., Effect of vitamin E intake on levels of vitamins E and C in the central nervous system and peripheral tissues: implications for health recommendations. *Brain Research* **1999,** *845* (1), 50-59.

410. Haorah, J.; Ramirez, S. H.; Schall, K.; Smith, D.; Pandya, R.; Persidsky, Y., Oxidative stress activates protein tyrosine kinase and matrix metalloproteinases leading to blood-brain barrier dysfunction. *J Neurochem* **2007,** *101* (2), 566-76.

411. Rao, R. K., Oxidative stress-induced disruption of epithelial and endothelial tight junctions. *Frontiers in bioscience : a journal and virtual library* **2008,** *13*, 7210-26.

412. Rao, R. K.; Baker, R. D.; Baker, S. S., Inhibition of oxidant-induced barrier disruption and protein tyrosine phosphorylation in Caco-2 cell monolayers by epidermal growth factor. *Biochemical pharmacology* **1999,** *57* (6), 685-95.

413. Rao, R. K.; Baker, R. D.; Baker, S. S.; Gupta, A.; Holycross, M., Oxidant-induced disruption of intestinal epithelial barrier function: role of protein tyrosine phosphorylation. *The American journal of physiology* **1997,** *273* (4 Pt 1), G812-23.

414. Rao, R. K.; Basuroy, S.; Rao, V. U.; Karnaky, K. J., Jr.; Gupta, A., Tyrosine phosphorylation and dissociation of occludin-ZO-1 and E-cadherin-beta-catenin complexes from the cytoskeleton by oxidative stress. *Biochem J* **2002,** *368* (Pt 2), 471-81.

415. Vergauwen, H.; Tambuyzer, B.; Jennes, K.; Degroote, J.; Wang, W.; De Smet, S.; Michiels, J.; Van Ginneken, C., Trolox and Ascorbic Acid Reduce Direct and Indirect Oxidative Stress in the IPEC-J2 Cells, an In Vitro Model for the Porcine Gastrointestinal Tract. In *PLoS One*, 2015; Vol. 10.

416. Giulivi, C.; Cadenas, E., Inhibition of Protein Radical Reactions of Ferrylmyoglobin by the Water-Soluble Analog of Vitamin E, Trolox C. *Arch Biochem Biophys* **1993,** *303* (1), 152-158.

417. Sagach, V. F.; Scrosati, M.; Fielding, J.; Rossoni, G.; Galli, C.; Visioli, F., The water-soluble vitamin E analogue Trolox protects against ischaemia/reperfusion damage in vitro and ex vivo. A comparison with vitamin E. *Pharmacol Res* **2002,** *45* (6), 435-9.

418. Daffu, G.; del Pozo, C. H.; O'Shea, K. M.; Ananthakrishnan, R.; Ramasamy, R.; Schmidt, A. M., Radical roles for RAGE in the pathogenesis of oxidative stress in cardiovascular diseases and beyond. *Int J Mol Sci* **2013,** *14* (10), 19891-910.

419. Kutz, K.; Drewe, J.; Vankan, P., Pharmacokinetic properties and metabolism of idebenone. *J Neurol* **2009,** *256 Suppl 1*, 31-5.

420. Di Prospero, N. A.; Sumner, C. J.; Penzak, S. R.; Ravina, B.; Fischbeck, K. H.; Taylor, J. P., Safety, tolerability, and pharmacokinetics of high-dose idebenone in patients with Friedreich ataxia. *Arch Neurol* **2007,** *64* (6), 803-8.

421. Pignatello, R.; Intravaia, V. D.; Puglisi, G., A calorimetric evaluation of the interaction of amphiphilic prodrugs of idebenone with a biomembrane model. *J Colloid Interface Sci* **2006,** *299* (2), 626-35.

422. Sarangarajan, R.; Meera, S.; Rukkumani, R.; Sankar, P.; Anuradha, G., Antioxidants: Friend or foe? *Asian Pac J Trop Med* **2017,** *10* (12), 1111-1116.

423. Bouayed, J.; Bohn, T., Exogenous antioxidants--Double-edged swords in cellular redox state: Health beneficial effects at physiologic doses versus deleterious effects at high doses. *Oxid Med Cell Longev* **2010,** *3* (4), 228-37.

424. Pedersen, T. R.; Berg, K.; Cook, T. J.; Faergeman, O.; Haghfelt, T.; Kjekshus, J.; Miettinen, T.; Musliner, T. A.; Olsson, A. G.; Pyorala, K.; Thorgeirsson, G.; Tobert, J. A.; Wedel, H.; Wilhelmsen, L., Safety and tolerability of cholesterol lowering with simvastatin during 5 years in the Scandinavian Simvastatin Survival Study. *Arch Intern Med* **1996,** *156* (18), 2085-92.

425. Endo, A.; Kuroda, M.; Tsujita, Y., ML-236A, ML-236B, and ML-236C, new inhibitors of cholesterogensis produced by Penicillium citrinum. *J Antibiot* **1976,** *29* (12), 1346-1348.

426. Hovingh, G. K.; Gandra, S. R.; McKendrick, J.; Dent, R.; Wieffer, H.; Catapano, A. L.; Oh, P.; Rosenson, R. S.; Stroes, E. S., Identification and management of patients with statin-associated symptoms in clinical practice: A clinician survey. *Atherosclerosis* **2016,** *245*, 111-7.

427. Rosenson, R. S.; Baker, S. K.; Jacobson, T. A.; Kopecky, S. L.; Parker, B. A.; The National Lipid Association's Muscle Safety Expert, P., An assessment by the Statin Muscle Safety Task Force: 2014 update. *J Clin Lipidol* **2014,** *8* (3 Suppl), S58-71.

428. Sewright, K. A.; Clarkson, P. M.; Thompson, P. D., Statin myopathy: incidence, risk factors, and pathophysiology. *Curr Atheroscler Rep* **2007,** *9* (5), 389-96.

429. Stroes, E. S.; Thompson, P. D.; Corsini, A.; Vladutiu, G. D.; Raal, F. J.; Ray, K. K.; Roden, M.; Stein, E.; Tokgozoglu, L.; Nordestgaard, B. G.; Bruckert, E.; De Backer, G.; Krauss, R. M.; Laufs, U.; Santos, R. D.; Hegele, R. A.; Hovingh, G. K.; Leiter, L. A.; Mach,

F.; Marz, W.; Newman, C. B.; Wiklund, O.; Jacobson, T. A.; Catapano, A. L.; Chapman, M. J.; Ginsberg, H. N.; European Atherosclerosis Society Consensus, P., Statin-associated muscle symptoms: impact on statin therapy-European Atherosclerosis Society Consensus Panel Statement on Assessment, Aetiology and Management. *Eur Heart J* **2015,** *36* (17), 1012-22.

430. Ahmad, Z., Statin intolerance. *Am J Cardiol* **2014,** *113* (10), 1765-71.

431. Nurses, P. C., 2013 ACC / AHA Guideline on the Treatment of Blood Cholesterol to Reduce Atherosclerotic Cardiovascular Risk in Adults. *J Am Coll Cardiol* **2014,** *63* (25), 2889-934.

432. Keaney, J. F., Jr.; Curfman, G. D.; Jarcho, J. A., A pragmatic view of the new cholesterol treatment guidelines. *N Engl J Med* **2014,** *370* (3), 275-8.

433. Lamperti, C.; Naini, A. B.; Lucchini, V.; Prelle, A.; Bresolin, N.; Moggio, M.; Sciacco, M.; Kaufmann, P.; DiMauro, S., Muscle Coenzyme Q 10 Level in Statin-Related Myopathy. *Arch Neurol* **2005,** *62*, 8-11.

434. Paiva, H.; Thelen, K. M.; Van Coster, R.; Smet, J.; De Paepe, B.; Mattila, K. M.; Laakso, J.; Lehtimaki, T.; von Bergmann, K.; Lutjohann, D.; Laaksonen, R., High-dose statins and skeletal muscle metabolism in humans: a randomized, controlled trial. *Clin Pharmacol Ther* **2005,** *78* (1), 60-8.

435. Laaksonen, R.; Jokelainen, K.; Laakso, J.; Sahi, T.; Harkonen, M.; Tikkanen, M. J.; Himberg, J. J., The effect of simvastatin treatment on natural antioxidants in low-density lipoproteins and high-energy phosphates and ubiquinone in skeletal muscle. *Am J Cardiol* **1996,** *77* (10), 851-4.

436. Larsen, S.; Stride, N.; Hey-Mogensen, M.; Hansen, C. N.; Bang, L. E.; Bundgaard, H.; Nielsen, L. B.; Helge, J. W.; Dela, F., Simvastatin effects on skeletal muscle: relation to decreased mitochondrial function and glucose intolerance. *J Am Coll Cardiol* **2013,** *61* (1), 44-53.

437. Avis, H. J.; Hargreaves, I. P.; Ruiter, J. P.; Land, J. M.; Wanders, R. J.; Wijburg, F. A., Rosuvastatin lowers coenzyme Q10 levels, but not mitochondrial adenosine triphosphate synthesis, in children with familial hypercholesterolemia. *J Pediatr* **2011,** *158* (3), 458-62.

438. Okuyama, H.; Langsjoen, P. H.; Hamazaki, T.; Ogushi, Y.; Hama, R.; Kobayashi, T.; Uchino, H., Statins stimulate atherosclerosis and heart failure: pharmacological mechanisms. *Expert Rev Clin Pharmacol* **2015,** *8* (2), 189-99.

439. Moosmann, B.; Behl, C., Selenoprotein synthesis and side-effects of statins. *Lancet* **2004,** *363* (9412), 892-4.

440. Golomb, B. A.; Evans, M. A.; Dimsdale, J. E.; White, H. L., Effects of statins on energy and fatigue with exertion: results from a randomized controlled trial. *Arch Intern Med* **2012,** *172* (15), 1180-2.

441. Parker, B. A.; Thompson, P. D., Effect of statins on skeletal muscle: exercise, myopathy, and muscle outcomes. *Exerc Sport Sci Rev* **2012,** *40* (4), 188-94.

442. Eckel, R. H., Approach to the patient who is intolerant of statin therapy. *J Clin Endocrinol Metab* **2010,** *95* (5), 2015-22.

443. Antons, K. A.; Williams, C. D.; Baker, S. K.; Phillips, P. S., Clinical perspectives of statin-induced rhabdomyolysis. *Am J Med* **2006,** *119* (5), 400-9.

444. Feng, Q.; Wilke, R. A.; Baye, T. M., Individualized risk for statin-induced myopathy: current knowledge, emerging challenges and potential solutions. *Pharmacogenomics* **2012,** *13* (5), 579-94.

445. Oh, J.; Ban, M. R.; Miskie, B. A.; Pollex, R. L.; Hegele, R. A., Genetic determinants of statin intolerance. *Lipids Health Dis* **2007,** *6* (7), 7.

446. Laufs, U.; Filipiak, K. J.; Gouni-Berthold, I.; Catapano, A. L.; group, S. e. w., Practical aspects in the management of statin-associated muscle symptoms (SAMS). *Atheroscler Suppl* **2017,** *26*, 45-55.

447. Backes, J. M.; Ruisinger, J. F.; Gibson, C. A.; Moriarty, P. M., Statin-associated muscle symptoms-Managing the highly intolerant. *J Clin Lipidol* **2017,** *11* (1), 24-33.

448. Brown, M. S. Coenzyme Q10 with HMG-CoA reductase inhibitors. 1989.

449. Teive, H. A.; Moro, A.; Moscovich, M.; Arruda, W. O.; Munhoz, R. P., Statin-associated cerebellar ataxia. A Brazilian case series. *Parkinsonism Relat Disord* **2016,** *25*, 97-9.

450. Berner, J. E., Statins can produce ataxia in bipolar disorder: two case reports. *J Clin Psychiatry* **2010,** *71* (3), 359.

451. Tuccori, M.; Lapi, F.; Testi, A.; Coli, D.; Moretti, U.; Vannacci, A.; Motola, D.; Salvo, F.; Rivolta, A. L.; Blandizzi, C.; Mugelli, A.; Del Tacca, M., Statin-associated psychiatric adverse events: a case/non-case evaluation of an Italian database of spontaneous adverse drug reaction reporting. *Drug Saf* **2008,** *31* (12), 1115-23.

452. Ng, A. S. L.; Tan, E. K., Linking statins and lipids in Parkinson's disease. *Mov Disord* **2017,** *32* (6), 807-809.

453. Huang, X.; Alonso, A.; Guo, X.; Umbach, D. M.; Lichtenstein, M. L.; Ballantyne, C. M.; Mailman, R. B.; Mosley, T. H.; Chen, H., Statins, plasma cholesterol, and risk of Parkinson's disease: a prospective study. *Mov Disord* **2015,** *30* (4), 552-9.

454. Liu, G.; Sterling, N. W.; Kong, L.; Lewis, M. M.; Mailman, R. B.; Chen, H.; Leslie, D.; Huang, X., Statins may facilitate Parkinson's disease: Insight gained from a large, national claims database. *Mov Disord* **2017,** *32* (6), 913-917.

455. Evans, M. A.; Golomb, B. A., Statin-associated adverse cognitive effects: survey results from 171 patients. *Pharmacotherapy* **2009,** *29* (7), 800-11.

456. Kelley, B. J.; Glasser, S., Cognitive effects of statin medications. *CNS Drugs* **2014,** *28* (5), 411-9.

457. Gauthier, J. M.; Massicotte, A., Statins and their effect on cognition: Let's clear up the confusion. *Can Pharm J (Ott)* **2015,** *148* (3), 150-5.

458. Hippisley-Cox, J.; Coupland, C., Unintended effects of statins in men and women in England and Wales: population based cohort study using the QResearch database. *BMJ* **2010,** *340*, c2197.

459. Mancuso, M.; Orsucci, D.; Volpi, L.; Calsolaro, V.; Siciliano, G., Coenzyme Q10 in neuromuscular and neurodegenerative disorders. *Current drug targets* **2010,** *11* (1), 111-21.

460. Taylor, B. A., Does Coenzyme Q10 Supplementation Mitigate Statin-Associated Muscle Symptoms? Pharmacological and Methodological Considerations. *Am J Cardiovasc Drugs* **2018,** *18* (2), 75-82.

461. Medina, R. J.; O'Neill, C. L.; Devine, A. B.; Gardiner, T. A.; Stitt, A. W., The pleiotropic effects of simvastatin on retinal microvascular endothelium has important implications for ischaemic retinopathies. *PLoS One* **2008,** *3* (7), e2584.

462. Bjorkhem-Bergman, L.; Lindh, J. D.; Bergman, P., What is a relevant statin concentration in cell experiments claiming pleiotropic effects? *Br J Clin Pharmacol* **2011,** *72* (1), 164-5.

463. Najib, N. M.; Idkaidek, N.; Adel, A.; Admour, I.; Astigarraga, R. E.; Nucci, G. D.; Alam, S. M.; Dham, R.; Qumaruzaman, Pharmacokinetics and bioequivalence evaluation of two simvastatin 40 mg tablets (Simvast and Zocor) in healthy human volunteers. *Biopharmaceutics & drug disposition* **2003,** *24* (5), 183-9.

464. Alakhali, K. M., Method Validation for Analysis of Simvastatin in Human Plasma Using Liquid Chromatography Tandem Mass Spectrometry (LC-MS-MS). *J Clin Diagn Res* **2013,** *7* (12), 2739-43.

465. Hargreaves, I. P.; Sheena, Y.; Land, J. M.; Heales, S. J., Glutathione deficiency in patients with mitochondrial disease: implications for pathogenesis and treatment. *J Inherit Metab Dis* **2005,** *28* (1), 81-8.

466. Enns, G. M.; Cowan, T. M., Glutathione as a Redox Biomarker in Mitochondrial Disease—Implications for Therapy. In *J Clin Med*, 2017; Vol. 6.

467. Riederer, P.; Sofic, E.; Rausch, W. D.; Schmidt, B.; Reynolds, G. P.; Jellinger, K.; Youdim, M. B., Transition metals, ferritin, glutathione, and ascorbic acid in parkinsonian brains. *J Neurochem* **1989,** *52* (2), 515-20.

468. Garcia, M. J.; Reinoso, R. F.; Sanchez Navarro, A.; Prous, J. R., Clinical pharmacokinetics of statins. *Methods Find Exp Clin Pharmacol* **2003,** *25* (6), 457-81.

469. Saheki, A.; Terasaki, T.; Tamai, I.; Tsuji, A., In vivo and in vitro blood-brain barrier transport of 3-hydroxy-3-methylglutaryl coenzyme A (HMG-CoA) reductase inhibitors. *Pharm Res* **1994,** *11* (2), 305-11.

470. Sierra, S.; Ramos, M. C.; Molina, P.; Esteo, C.; Vazquez, J. A.; Burgos, J. S., Statins as neuroprotectants: a comparative in vitro study of lipophilicity, blood-brain-barrier penetration, lowering of brain cholesterol, and decrease of neuron cell death. *J Alzheimers Dis* **2011,** *23* (2), 307-18.

471. Wood, W. G.; Eckert, G. P.; Igbavboa, U.; Muller, W. E., Statins and neuroprotection: a prescription to move the field forward. *Ann N Y Acad Sci* **2010,** *1199* (1), 69-76.

472. Nicotera, P.; Lipton, S. A., Excitotoxins in neuronal apoptosis and necrosis. *J Cereb Blood Flow Metab* **1999,** *19* (6), 583-91.

473. Yang, D.; Knight, R. A.; Han, Y.; Karki, K.; Zhang, J.; Chopp, M.; Seyfried, D. M., Statins Protect the Blood Brain Barrier Acutely after Experimental Intracerebral Hemorrhage. *J Behav Brain Sci* **2013,** *3* (1), 100-106.

474. Wu, H.; Lu, D.; Jiang, H.; Xiong, Y.; Qu, C.; Li, B.; Mahmood, A.; Zhou, D.; Chopp, M., Simvastatin-mediated upregulation of VEGF and BDNF, activation of the PI3K/Akt pathway, and increase of neurogenesis are associated with therapeutic improvement after traumatic brain injury. *J Neurotrauma* **2008,** *25* (2), 130-9.

475. Greenwood, J.; Mason, J. C., Statins and the vascular endothelial inflammatory response. *Trends Immunol* **2007,** *28* (2), 88-98.

476. Jain, M. K.; Ridker, P. M., Anti-inflammatory effects of statins: clinical evidence and basic mechanisms. *Nat Rev Drug Discov* **2005,** *4* (12), 977-87.

477. Floris, S.; Blezer, E. L.; Schreibelt, G.; Dopp, E.; van der Pol, S. M.; Schadee-Eestermans, I. L.; Nicolay, K.; Dijkstra, C. D.; de Vries, H. E., Blood-brain barrier permeability and monocyte infiltration in experimental allergic encephalomyelitis: a quantitative MRI study. *Brain* **2004,** *127* (Pt 3), 616-27.

478. Ifergan, I.; Wosik, K.; Cayrol, R.; Kebir, H.; Auger, C.; Bernard, M.; Bouthillier, A.; Moumdjian, R.; Duquette, P.; Prat, A., Statins reduce human blood-brain barrier permeability and restrict leukocyte migration: relevance to multiple sclerosis. *Ann Neurol* **2006,** *60* (1), 45-55.

479. Pinzon-Daza, M.; Garzon, R.; Couraud, P.; Romero, I.; Weksler, B.; Ghigo, D.; Bosia, A.; Riganti, C., The association of statins plus LDL receptor-targeted liposome-encapsulated doxorubicin increases in vitro drug delivery across blood-brain barrier cells. *Br J Pharmacol* **2012,** *167* (7), 1431-47.

480. Tsujinaka, H.; Itaya-Hironaka, A.; Yamauchi, A.; Sakuramoto-Tsuchida, S.; Shobatake, R.; Makino, M.; Masuda, N.; Hirai, H.; Takasawa, S.; Ogata, N., Statins decrease vascular epithelial growth factor expression via down-regulation of receptor for advanced glycation end-products. *Heliyon* **2017,** *3* (9), e00401.

481. Bogman, K.; Peyer, A. K.; Török, M.; Küsters, E.; Drewe, J., HMG-CoA reductase inhibitors and P-glycoprotein modulation. *British Journal of Pharmacology* **2001,** *132* (6), 1183-1192.

482. Shah, G. N.; Mooradian, A. D., Age-related changes in the blood-brain barrier. *Exp Gerontol* **1997,** *32* (4-5), 501-19.

483. Popescu, B. O.; Toescu, E. C.; Popescu, L. M.; Bajenaru, O.; Muresanu, D. F.; Schultzberg, M.; Bogdanovic, N., Blood-brain barrier alterations in ageing and dementia. *J Neurol Sci* **2009,** *283* (1-2), 99-106.

484. Lass, A.; Agarwal, S.; Sohal, R. S., Mitochondrial ubiquinone homologues, superoxide radical generation, and longevity in different mammalian species. *J Biol Chem* **1997,** *272* (31), 19199-204.

485. Sohal, R. S.; Forster, M. J., Coenzyme Q, oxidative stress and aging. *Mitochondrion* **2007,** *7 Suppl*, S103-11.

486. Dai, Y. L.; Luk, T. H.; Siu, C. W.; Yiu, K. H.; Chan, H. T.; Lee, S. W.; Li, S. W.; Tam, S.; Fong, B.; Lau, C. P.; Tse, H. F., Mitochondrial dysfunction induced by statin contributes to endothelial dysfunction in patients with coronary artery disease. *Cardiovasc Toxicol* **2010,** *10* (2), 130-8.

487. Lass, A.; Forster, M. J.; Sohal, R. S., Effects of coenzyme Q10 and α-tocopherol administration on their tissue levels in the mouse: elevation of mitochondrial α-tocopherol by coenzyme Q10. *Free Radic Biol Med* **1999,** *26* (11-12), 1375-1382.

488. Brand, M. D., The sites and topology of mitochondrial superoxide production. *Exp Gerontol* **2010,** *45* (7-8), 466-72.

489. Sohal, R. S.; Brunk, U. T., Mitochondrial production of pro-oxidants and cellular senescence. *Mutat Res* **1992,** *275* (3-6), 295-304.

490. Turrens, J. F., Mitochondrial formation of reactive oxygen species. *J Physiol* **2003,** *552* (Pt 2), 335-44.

491. Bayot, A.; Santos, R.; Camadro, J. M.; Rustin, P., Friedreich's ataxia: the vicious circle hypothesis revisited. *BMC Med* **2011,** *9* (1), 112.

492. Ozkok, E.; Yorulmaz, H.; Ates, G.; Serdaroglu-Oflazer, P.; Tamer, A. S., Effects of prior treatment with simvastatin on skeletal muscle structure and mitochondrial enzyme activities during early phases of sepsis. *Int J Clin Exp Pathol* **2014,** *7* (12), 8356-65.

493. Ahmadi, Y.; Ghorbanihaghjo, A.; Naghi-Zadeh, M.; Yagin, N. L., Oxidative stress as a possible mechanism of statin-induced myopathy. *Inflammopharmacology* **2018,** *26* (3), 667-674.

494. Venturi, E.; Lindsay, C.; Lotteau, S.; Yang, Z.; Steer, E.; Witschas, K.; Wilson, A. D.; Wickens, J. R.; Russell, A. J.; Steele, D.; Calaghan, S.; Sitsapesan, R., Simvastatin activates single skeletal RyR1 channels but exerts more complex regulation of the cardiac RyR2 isoform. *Br J Pharmacol* **2018,** *175* (6), 938-952.

495. Rizzuto, R.; De Stefani, D.; Raffaello, A.; Mammucari, C., Mitochondria as sensors and regulators of calcium signalling. *Nat Rev Mol Cell Biol* **2012,** *13* (9), 566-78.

496. Griffiths, E. J.; Rutter, G. A., Mitochondrial calcium as a key regulator of mitochondrial ATP production in mammalian cells. *Biochim Biophys Acta* **2009,** *1787* (11), 1324-33.

497. Sirvent, P.; Mercier, J.; Lacampagne, A., New insights into mechanisms of statin-associated myotoxicity. *Curr Opin Pharmacol* **2008,** *8* (3), 333-8.

498. Velho, J. A.; Okanobo, H.; Degasperi, G. R.; Matsumoto, M. Y.; Alberici, L. C.; Cosso, R. G.; Oliveira, H. C.; Vercesi, A. E., Statins induce calcium-dependent mitochondrial permeability transition. *Toxicology* **2006,** *219* (1-3), 124-32.

499. Busanello, E. N. B.; Marques, A. C.; Lander, N.; de Oliveira, D. N.; Catharino, R. R.; Oliveira, H. C. F.; Vercesi, A. E., Pravastatin Chronic Treatment Sensitizes Hypercholesterolemic Mice Muscle to Mitochondrial Permeability Transition: Protection by Creatine or Coenzyme Q10. *Front Pharmacol* **2017,** *8*, 185.

500. Hunter, D. R.; Haworth, R. A.; Southard, J. H., Relationship between configuration, function, and permeability in calcium-treated mitochondria. *J Biol Chem* **1976,** *251* (16), 5069-77.

501. Sinzinger, H.; Mayr, F.; Schmid, P.; Granegger, S.; O'Grady, J.; Peskar, B. A., Sleep disturbance and appetite loss after lovastatin. *Lancet* **1994,** *343* (8903), 973.

502. Gomes, L. C.; Di Benedetto, G.; Scorrano, L., During autophagy mitochondria elongate, are spared from degradation and sustain cell viability. *Nat Cell Biol* **2011,** *13* (5), 589-98.

503. Rambold, A. S.; Kostelecky, B.; Lippincott-Schwartz, J., Together we are stronger. *Autophagy* **2014,** *7* (12), 1568-1569.

504. Liesa, M.; Shirihai, O. S., Mitochondrial dynamics in the regulation of nutrient utilization and energy expenditure. *Cell Metab* **2013,** *17* (4), 491-506.

505. Parrado-Fernandez, C.; Lopez-Lluch, G.; Rodriguez-Bies, E.; Santa-Cruz, S.; Navas, P.; Ramsey, J. J.; Villalba, J. M., Calorie restriction modifies ubiquinone and COQ transcript levels in mouse tissues. *Free Radic Biol Med* **2011,** *50* (12), 1728-36.

506. Rajarathnam, K.; Hochman, J.; Schindler, M.; Ferguson-Miller, S., Synthesis, location, and lateral mobility of fluorescently labeled ubiquinone 10 in mitochondrial and artificial membranes. *Biochemistry* **1989,** *28* (8), 3168-76.

507. Tyzack, G.; Lakatos, A.; Patani, R., Human Stem Cell-Derived Astrocytes: Specification and Relevance for Neurological Disorders. *Current stem cell reports* **2016,** *2*, 236-247.

508. Mahley, R. W., Central Nervous System Lipoproteins: ApoE and Regulation of Cholesterol Metabolism. *Arterioscler Thromb Vasc Biol* **2016,** *36* (7), 1305-15.

509. Appelt-Menzel, A.; Cubukova, A.; Gunther, K.; Edenhofer, F.; Piontek, J.; Krause, G.; Stuber, T.; Walles, H.; Neuhaus, W.; Metzger, M., Establishment of a Human Blood-Brain Barrier Co-culture Model Mimicking the Neurovascular Unit Using Induced Pluri- and Multipotent Stem Cells. *Stem Cell Rep* **2017,** *8* (4), 894-906.

510. Lippmann, E. S.; Azarin, S. M.; Kay, J. E.; Nessler, R. A.; Wilson, H. K.; Al-Ahmad, A.; Palecek, S. P.; Shusta, E. V., Derivation of blood-brain barrier endothelial cells from human pluripotent stem cells. *Nat Biotechnol* **2012,** *30* (8), 783.

511. Marchi, N.; Rasmussen, P.; Kapural, M.; Fazio, V.; Kight, K.; Mayberg, M. R.; Kanner, A.; Ayumar, B.; Albensi, B.; Cavaglia, M.; Janigro, D., Peripheral markers of brain damage and blood-brain barrier dysfunction. *Restor Neurol Neurosci* **2003,** *21* (0), 109-21.

512. Kanner, A. A.; Marchi, N.; Fazio, V.; Mayberg, M. R.; Koltz, M. T.; Siomin, V.; Stevens, G. H.; Masaryk, T.; Aumayr, B.; Vogelbaum, M. A.; Barnett, G. H.; Janigro, D., Serum S100beta: a noninvasive marker of blood-brain barrier function and brain lesions. *Cancer* **2003,** *97* (11), 2806-13.

Appendices

Appendix A – PBEC/astrocyte co-culture timeline

Non-contact (NC) co-culture of PBECs with primary rat astrocytes required considerable planning and coordination to ensure each component of the co-culture was in the optimal stage of growth to produce the desired BBB phenotype (Figure 91).

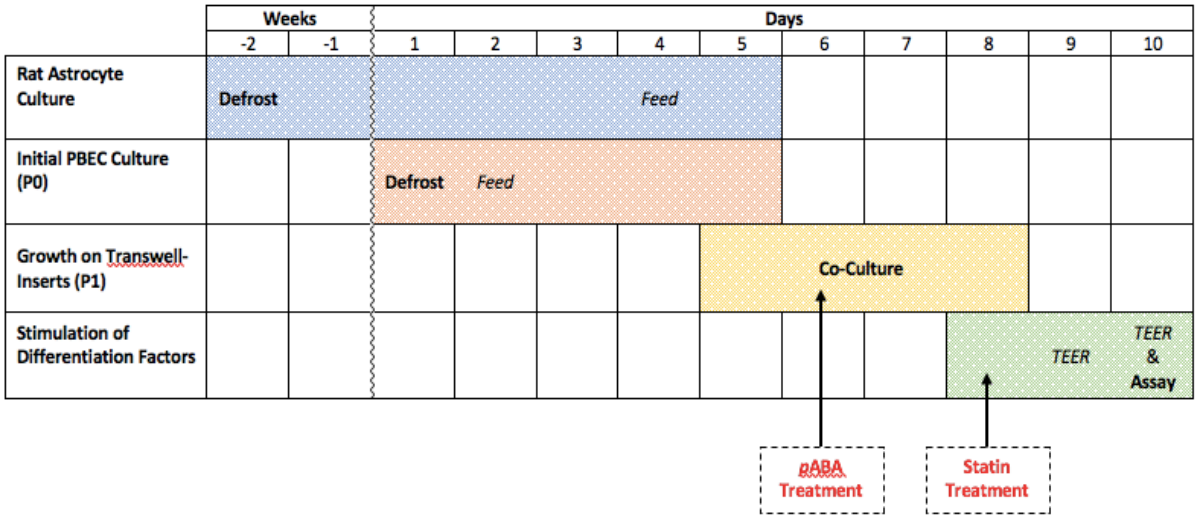

Figure 91: Timeline for the non-contact (NC) co-culture of primary PBECs with primary rat astrocytes. Additional treatments are highlighted in red. Both *p*ABA and simvastatin were added directly to culture medium and in subsequent feeds. 1 vial of PBECs is split into 2 x T-75 flasks, which are in turn seeded into ~ 12-Tanswell®-inserts. i.e. 1 vial ≈ 1 x 12-well plate.

Appendix B – *p*CEL-X™ *in silico* assessment of CoQ_{10} apparent permeability

Evaluation of CoQ_{10} apparent permeability *in silico* highlighted a necessity for stirring within the experimental procedure as a means to reduce any confounding hindrance from the aqueous boundary layer (Figure 92) [167]. However, it should be noted that this was in reference to 'free' CoQ_{10} and not reflective of CoQ_{10} incorporated within lipoproteins – as is the case *in vivo*. In view of these *in silico* findings, the experimental procedure was amended so that all P_{app} and uptake studies were performed on an orbital plate-shaker at 100 rpm, a level compatible with the PBEC BBB cell model.

Since the method for stirring required the use of a temperature controlled plate-shaker outside the optimal culture conditions of a humidified incubator, an upper limit of 2 hours was imposed to ensure cell viability.

Simulations were performed by the architect of the *p*CEL-X™ software, Prof Alex Avdeef.

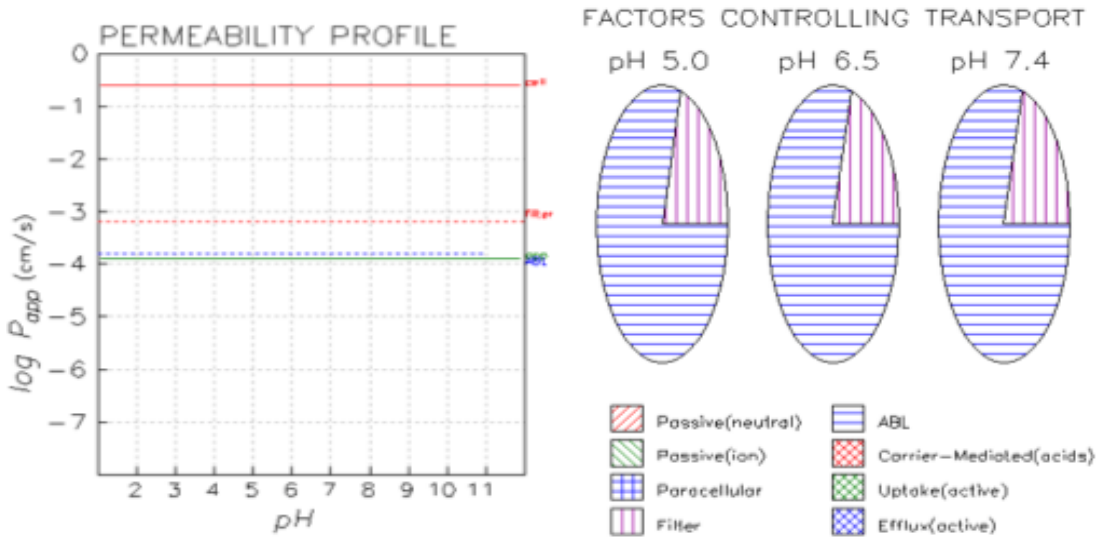

Figure 92: *in silico* *p*CEL-X™ analysis of the limiting factors that may influence CoQ_{10} apparent permeability; output suggests that the aqueous boundary layer (ABL) is the most prominent limiting factor for the permeability of 'free' CoQ_{10}, with the Transwell® filter showing a small degree of hindrance at a ratio of 4:1 respectively. *p*H showed no effect on CoQ_{10} apparent permeability.

Appendix C – comparative effect of vitamin E and trolox

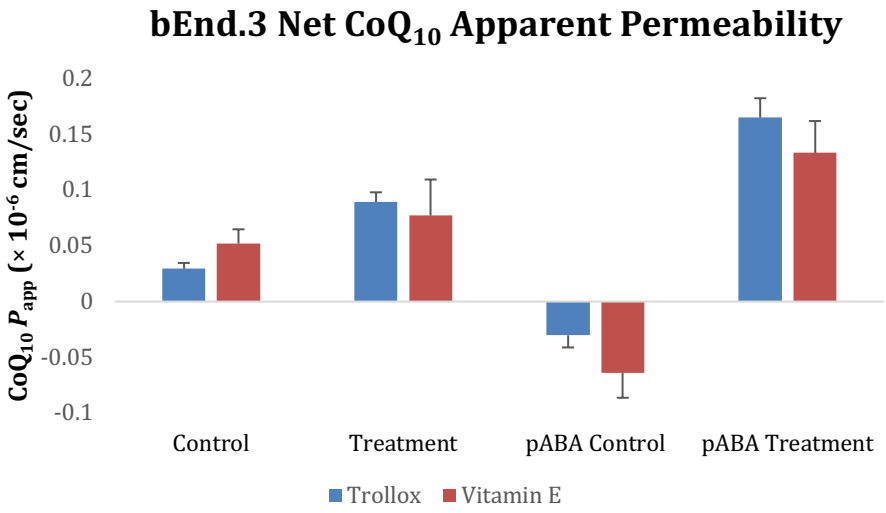

Figure 93: Net effect of co-administered vitamin E (50 µmol/L) or trolox (50 µmol/L) on CoQ_{10} apparent permeability in the bEnd.3 BBB. bEnd.3 controls (df = 11), vitamin E treated bEnd.3 (df = 11), trolox treated bEnd.3 (df = 9). *p*ABA bEnd.3 controls (df = 11), vitamin E treated *p*ABA bEnd.3 (df = 13), trolox treated *p*ABA bEnd.3 (df = 9). Error bars represent standard error of the mean (SEM).

Results (Figure 93) indicate a direct correlation between co-administered vitamin E and trolox on the apparent permeability of CoQ_{10} across the bEnd.3 BBB. This, therefore, suggests that the antioxidant function of vitamin E is likely to be the cause of any observed differences between control and treatment conditions.